Compact MIMO Terminals with Matching Networks

Yuanyuan Fei

A thesis submitted for the degree of Doctor of Philosophy.
The University of Edinburgh.
February 2008

Abstract

The development of wireless communications has significantly changed people's lifestyles in the last century. It can be shown that the use of multiple antennas, so called multiple-input multiple-output (MIMO) at both link ends can offer further improvement of spectral efficiency and link reliability of wireless systems, which has been studied in the past decade. With the maturity of theory, the practice of MIMO technology has become feasible, though several problems still need to be solved especially at the receive end. The inadequate antenna spacing limited by the small dimension of the receive terminal causes the mutual coupling (MC) effect, which may degrade MIMO system performance. This thesis focuses on the performance improvement of compact MIMO terminals by introducing matching networks between the receive antenna array and the load terminations. The investigation spans from practical implementation to data analysis, and theoretical derivation to system performance optimisation.

The contributions of this thesis are threefold. Firstly, three performance metrics signal correlation (SC), received power and capacity are well studied for compact MIMO terminals with matching networks. An overview of the existing methods to examine these metrics is presented. Especially for the received power, one proper approach is found and two methods are compared and unified analytically. The simulation results reveal that adding matching networks into compact MIMO terminals can significantly improve the system performance. However, SC and received power should be well balanced to achieve a good capacity performance.

The second contribution describes the experimental measurement of the analytical SC and received power study of the first contribution. A set-up of two quarter-wavelength monopoles and a ground plane with various matching networks are measured and the system design is aided by two simulation tools SEMCAD and FEKO. The measured results agree well with the analytical prediction though discrepancies exist. The implementation confirms that relatively high total receive power and low SC of the compact array can be achieved by choosing proper load impedance in practice. It also indicates that the load impedance to optimise the received power is different from the one for MIMO capacity maximisation.

Finally, inspired by the last finding of the second contribution, the optimal single-port matching (SPM) impedance for capacity maximisation in a two by two compact MIMO system is derived using an upper bound of the ergodic capacity for simplicity. A complete framework for MIMO systems with compact arrays at both link ends is deduced using Z-parameters for the analysis. A closed-form result for the optimal SPM impedance in high signal-to-noise ratio (SNR) regime is given and proved to be the input impedance of the receive antennas. The optimal SPM networks outperform other matching networks for small antenna spacings with any SNR. Moreover, the system performance sensitivity of a two by two MIMO system with coupled half-wavelength dipoles and SPM networks is evaluated versus antenna spacing and dipole length. It shows that MIMO capacity is not sensitive to the optimal impedance mismatch with fixed antenna spacing and dipole lengths. However, the MIMO system is relatively sensitive to antenna structure mismatch with a precise optimal matching network. Overall, the optimal single-port match is a feasible technique to improve the performance of the compact MIMO systems.

Declaration of originality

I hereby declare that the research recorded in this thesis and the thesis itself was composed and originated entirely by myself in the Department of Electronics and Electrical Engineering at The University of Edinburgh. The exception to this is the work reported in Chapter 4, which was carried out jointly with Dr. Buon Kiong Lau from Department of Electrical and Information Technology, Lund University, Sweden.

Yuanyuan Fei

February 2008

To my family
To my loved ones

Acknowledgements

I would like to first thank my supervisor Dr. John Thompson for offering me this PhD position, providing me with financial support and leading me to the end of the 3-year long journey. Without his continuous inspiration, patience, efficiency, encouragement, support, understanding and care to me on my study and life, I cannot achieve any page of this thesis. I am proud of being one of his students, and his charm of personality will influence all my life.

Secondly, I would like to express my appreciation to Dr. Buon Kiong Lau from Lund University, Sweden. Thanks for his invitation and trust on me to collaborate most of the work reported in Chapter 4. Many valuable discussions with him also inspire other parts of the thesis. I am also grateful to all the people I worked with in Lund.

My thanks also extended to my second supervisor Dr. Dave Laurensen, who examined my first year viva, helped me when John was offsite, and most important, offered me a postdoc job after my PhD.

I dedicated this thesis to my beloved family for their emotional and financial support. It is their understanding and encouragement make me obtain the strength of going through this tough journey.

Additionally, I would like to thank to my previous and present colleagues at IDCOM, my good friends Dan Hou, Sihong Chen and Yifan Li for many useful discussions on study and for sharing the ups and downs in PhD life. Their friendship warms me up and makes me feel I am not alone.

Last but not least, I would like to thank Dr. Yijia Fan, who is a model of my PhD study. Thanks for his great help on my research. Also his willpower and achievement give me confidence and courage to face and finish the challenge.

Contents

List of figures

List of tables

Acronyms and abbreviations

2D	two-dimensional
3D	three-dimensional
AF	array factor
AOA	angle-of-arrival
AOD	angle-of-departure
AS	angular spread
BLAST	Bell Labs Layered Space-Time
BS	base station
CDF	cumulative distribution function
CEM	computational electromagnetics
CSI	channel state information
EMF	electromotive force
FDTD	finite-difference time-domain
FF	far-field
i.i.d.	independent identically distributed
ISI	intersymbol interference
LOS	line-of-sight
MAOA	mean angle-of-arrival
MC	mutual coupling
MCM	multiport-conjugate match
MIMO	multiple-input multiple-output
MoM	the method of moments
MS	mobile station
NLOS	non-line-of-sight
OC	open-circuit
pdf	probability density function
PAS	power azimuth spectrum
SC	signal correlation
SIMO	single-input multiple-output

SNR	signal-to-noise ratio
SFC	spatial fading correlation
SPM	single-port match
SV	steering vector
SVD	singular value decomposition
ULA	uniform linear array
ZMCSCG	zero mean circularly symmetric complex Gaussian

Nomenclature

$\mathbf{a}$	steering vector of an antenna array
$\mathbf{a}_{mc}$	steering vector with MC
$\mathbf{a}_{nc}$	steering vector without MC
$\mathbf{a}_R$	normalized steering vector of the receiver
$\mathbf{a}_T$	normalized steering vector of the transmitter
A	array factor of an antenna array
c	average power gain of each channel branch
C	channel capacity
C_{ep}	equal-power capacity
C_{mc}	ergodic capacity of compact MIMO systems with MC at the receiver only
C_{wf}	waterfilling capacity
C_S	ergodic capacity of compact MIMO systems using scattering parameter approach
C_Z	ergodic capacity of compact MIMO systems using impedance parameter approach
d_i	antenna separation between the first and ith antenna elements
d_m	diameter of the monopole in measurement
$d(R_i, R_k)$	antenna spacing between the ith and kth receive antennas
d_R	antenna separation of the receiver
d_s	distance from the load impedance to the stub place
d_T	antenna separation of the transmitter
D	maximum dimension of an antenna
D_s	Doppler spread
$e_{T_j}(\vartheta)$	transmitted field per unit excited current of the jth transmit antenna in the direction of ϑ
$\mathbf{e}_{mc}$	vector of far-field patterns of a coupled array
$\mathbf{e}_{oc}$	vector of far-field patterns of a coupled array with elements of each antenna when all other elements are open-circuited
E_0	far-field pattern of a isolated reference antenna
E^i_{mc}	far-field pattern of the ith coupled antenna
$E_{R_i}(\vartheta, \varphi)$	far-field pattern of antenna element R_i in the direction φ and ϑ
F	Far-field pattern

F_{total}	far-field pattern of the array
h	channel of the SISO system
$h(R_i, T_j)$	channel branch between the jth transmitter and ith receiver
h_c	channel coefficient of a single tap in a discrete time complex baseband model
h_s	height of the substrate layer
h_I	imaginary part of h_c
h_R	real part of h_c
$\mathbf{H}$	channel matrix of MIMO systems
$\mathbf{H}_{cr}$	correlated channel matrix of Kronecker model
$\mathbf{H}_{i.i.d.}$	identically independent distributed channel matrix
$\mathbf{H}_{mc}$	channel transfer matrix between the source and the receiver load including MC
$\mathbf{H}_S$	channel matrix of compact MIMO systems using scattering parameter approach
$\mathbf{H}_V$	channel/voltage transfer matrix
$\mathbf{H}_Z$	channel matrix of compact MIMO systems using impedance parameter approach
$\hat{\mathbf{H}}_{mc}$	general MIMO system channel matrix including MC
$\tilde{\mathbf{H}}_{mc}$	MIMO system channel matrix when MC at the receiver only
$\mathbf{i}_R$	current vector at the receive end
$\mathbf{i}_T$	current vector at the transmit end
I_0	induced current of a single antenna with self-conjugate match
I_i	induced current of the ith antenna
I_{Ri}	current through the ith receive antenna
I_{Ti}	current through the ith transmit antenna
$\mathbf{I}$	identity matrix
J_0	zeroth Bessel function of the first kind
k	path loss exponent
k_r	normalization coupling ratio
k_{ij}	{i,j}th element of the MC matrix
$\mathbf{K}_{mc}$	mutual coupling matrix
l	total length of a dipole
l_0	length of the microstrip transmission line
l_c	length of the SMA connector
l_s	open stub length
M	number of transmit antennas

n	path loss exponent
N	number of transmit/receive antennas
N_P	number of channel paths
p	probability density function
p_L	Laplacian probability density function
p_U	uniform probability density function
$P_{2d,m}$	two-dimensional received power in measurement
$P_{3d,m}$	three-dimensional received power in measurement
P_{diff}	power difference of two receive antennas
P_i	received power of the ith coupled antenna in circuit theory
P_{total}	theoretical total received power of two receive antennas
P_R	total average received power
P_T	total average transmitted power
P_{TS}	transmit power with MC using scattering parameter approach
$\tilde{P}_i$	received power of the ith coupled antenna using steering vector
r	radius of the sphere coordinate
r_{11}	resistive part of the antenna self impedance
r_D	distance from an antenna
r_L	resistive part of the load impedance
r_{opt}	resistive part of the optimum load for MIMO capacity maximization
R_i	ith receiver
$\mathbf{R}_{mc}$	covariance matrix measured at the coupled antenna input ports
$\mathbf{R}_L$	covariance matrix after matching
$\mathbf{R}_{L,oc}$	covariance matrix of the open-circuit match
$\mathbf{R}_{L,z_0}$	covariance matrix of the characteristic impedance match
$\mathbf{R}_{\mathbf{xx}}$	covariance matrix of the input signal vector
$\mathbf{S}$	scattering parameter matrix
$\mathbf{S}_H$	scattering parameter matrix connecting the transmitter and receiver
$\mathbf{S}_M$	scattering parameter matrix of the matching network
$\mathbf{S}_{RR}$	scattering parameter matrix of the receive antennas
$\mathbf{S}_{RT}$	scattering parameter transfer matrix from transmitter to receiver
$\mathbf{S}_{TR}$	scattering parameter transfer matrix from receiver to transmitter
$\mathbf{S}_{TT}$	scattering parameter matrix of the transmit antennas

T_c	coherent time
T_d	time delay spread of the multipaths
T_i	ith transmitter
T_s	transmission symbol time
v	additive Gaussian noise
$\mathbf{v}_R$	voltage vector at the receive end
$\mathbf{v}_{RT}$	open-circuit voltage vector
$\mathbf{v}_S$	source voltage vector
$\mathbf{v}_T$	voltage vector at the transmit end
V_i	open-circuit voltage of the ith antenna
V_{Ri}	voltage across the ith receive antenna
V_{RT}	open-circuit voltage of the SISO system
V_{Si}	voltage across the ith source
V_{Ti}	voltage across the source connected to the ith transmit antenna
w_m	width of the microstrip line
W_c	coherence bandwidth
W_s	transmission symbol bandwidth
x	input signal
x_L	reactive part of the load impedance
x_{opt}	reactive part of the optimum load for MIMO capacity maximization
$\mathbf{X}_S$	covariance matrix of the transmit signals using scattering parameter approach
y	output signal
z_0	characteristic impedance
$z_{11,m}$	average self impedance of the monopole in the array in measurement
$z_{11,s}$	self impedance of the monopole in the array in simulation
$z_{12,m}$	average mutual impedance of the monopole in the array in measurement
$z_{12,s}$	mutual impedance of the monopole in the array in simulation
z_{ii}	self impedance of the ith antenna
z_{ij}	mutual impedance between the ith and the jth antenna
z_{in}	input impedance
z_L	load impedance added to each antenna port
$z_{mo,s}$	measured self impedance of a single monopole
$z_{mo,s}$	simulated self impedance of a single monopole

z_{oc}	open-circuit impedance
z_{opt}	optimum load for MIMO capacity maximization
z_{p1}	observed impedance from port 1 in Figure C.1
z_{RT}	transfer impedance from transmitter to receiver of the SISO system
z_{sc}	short-circuit impedance
$\mathbf{Z}$	antenna impedance matrix
$\mathbf{Z}_L$	load matching network impedance matrix
$\mathbf{Z}_S$	source matching network impedance matrix
$\mathbf{Z}_{RR}$	receive antenna impedance matrix
$\mathbf{Z}_{RT}$	impedance transfer matrix from transmitter to receiver
$\mathbf{Z}_{TR}$	impedance transfer matrix from receiver to transmitter
$\mathbf{Z}_{TT}$	transmit antenna impedance matrix
α	correlation coefficient between two receivers
β	complex channel gain of the path-based channel
β^a	path attenuation
δr	precision error of the resistive part of matching load
δx	precision error of the reactive part of matching load
Δ_φ	azimuth angular spread of the receiver
Δ_ϑ	azimuth angular spread of the transmitter
ε_c	relative permittivity of the SMA connector
ε_e	effective permittivity of the dielectric interface
ε_r	relative permittivity of the substrate layer
ε_{rg}	relative permittivity of the ground plane
ϕ	azimuth angle
φ	azimuth angle-of-arrival
φ_0	mean azimuth angle-of-arrival
γ	waterfilling coefficient
$\eta_{C_{mc}}$	performance efficiency of the ergodic capacity with mutual coupling
$\eta_{C_{up}}$	performance efficiency of the upper bound of the capacity with mutual coupling
λ	wavelength
λ_0	wavelength in free space
λ_s	wavelength in the substrate dielectric
μ	normalization constant of Laplacian probability density function

θ	elevation angle
ϑ	elevation angle-of-arrival
ϑ_p	phase shift of the transmission line
ρ	signal-to-noise ratio
ρ_{2d}	two-dimensional signal correlation
$\rho_{2d,m}$	two-dimensional signal correlation in measurement
ρ_{3d}	three-dimensional signal correlation
$\rho_{3d,m}$	three-dimensional signal correlation in measurement
ρ_h	signal correlation between channel branches
ρ_{mc}	signal correlation with mutual coupling
ρ_{oc}	open-circuit correlation coefficient
ρ_r	reference signal-to-noise ratio
ρ_s	signal correlation using scattering parameters
ρ_{xx}	real part of the open-circuit correlation coefficient
ρ_{xy}	imaginary part of the open-circuit correlation coefficient
$\tilde{\rho}_{2d}$	theoretical two-dimensional signal correlation
$\tilde{\rho}_{2d}^{ij}$	two-dimensional signal correlation between the ith and jth elements
$\tilde{\rho}_{2d}^{L}$	two-dimensional signal correlation with Laplacian angle-of-arrival distribution
$\tilde{\rho}_{2d}^{U}$	two-dimensional signal correlation with uniform angle-of-arrival distribution
$\tilde{\rho}_{mc}$	signal correlation with mutual coupling and matching impedances
σ	standard derivation of h_c
Ω_s	solid angle
$\mathbf{\Psi}$	simplified receive covariance matrix
$\mathbf{\Psi_{oc}}$	open-circuit correlation matrix
$\mathbf{\Psi}_R$	receive covariance matrix
$\mathbf{\Psi}_T$	transmit covariance matrix
$\mathbf{\Psi}_V$	covariance matrix of columnwise-vectorized matrix
$\mathbb{R}$	set of real numbers
$\mathbb{R}^+$	set of positive real numbers
$C_i(\cdot)$	cosine integral function
$\mathcal{F}_{Z-S}\{\cdot\}$	transfer function from impedance parameters to scattering parameters
$H(y)$	differential entropy of y
$I(x;y)$	mutual information between x and y

$S_i(\cdot)$	sine integral function
$(\cdot)^*$	conjugate operation of a complex number
$(\cdot)^T$	transpose operation of a matrix
$(\cdot)^H$	transpose conjugate operation of a matrix
$(\cdot)_{ij}$	the (i,j)-th element of a matrix
$\lvert\cdot\rvert$	absolute operation
$\lVert\cdot\rVert$	matrix norm
$\det(\cdot)$	determinant operation
$\mathrm{diag}\{\cdot\}$	diagonal matrix
$\mathrm{vec}(\cdot)$	columnwise vectorization operation
$\mathrm{Tr}(\cdot)$	trace of a matrix
$E\{\cdot\}$	expectation operation
j	the complex operator
$\mathrm{Re}\{\cdot\}$	real part of a complex number/vector/matrix
$\mathrm{Im}\{\cdot\}$	imaginary part of a complex number/vector/matrix
$\sin(\cdot)$	sine function
$\cos(\cdot)$	cosine function
$\tan(\cdot)$	tangent function
$\max(\cdot)$	maximization operation
$\min(\cdot)$	minimization operation
$\otimes$	Kronecker product

Chapter 1
Introduction

This thesis is devoted to the MIMO systems with compact terminals and matching networks. This chapter briefly introduces the origin and motivation of this work in Section 1.1. Then Section 1.2 addresses the objective and main contributions of the thesis. The organization of the remaining chapters is presented in Section 1.3.

1.1 Introduction and motivation

The comprehensively studied multiple-input multiple-output (MIMO) systems (Figure 1.1) promise significant gains in spectrum efficiency and link reliability by deploying multiple antennas at both ends of a wireless link [1–3]. The MIMO technique is an extension of *smart antennas* and the central idea of MIMO is *space-time* signal processing [4].

Two benefits of using MIMO systems over single-input single-output (SISO) systems draw our attention. One is called *diversity gain*, which is used to combat channel fading, i.e. the distortion that a carrier-modulated telecommunication signal experiences over certain propagation media, by multiple transmission of the same signal through multiple sub-channels and the combination of the information at the receiver. The representative schemes are *space-time coding* [4] and *transmit beamforming* [5]. The utilization of the diversity characteristic promises a significant improvement in link reliability. Another benefit is the *spatial multiplexing gain*, which is realized by transmitting different signals over different sub-channels simultaneously. A MIMO system (as in Figure 1.1) with M transmit and N receive antennas can achieve a support of $\min(M, N)$ data streams at most. A typical scheme for spatial multiplexing gain maximization is the BLAST [4, 6] technique.

As above discussion, the diversity performance is critical in MIMO system performance. Also sufficient antenna spacing (typically half of the wavelength or more) is an essential condition for a good MIMO system performance. However, the integration of multiple antennas into the subscriber end is affected by the limited design volume, which results in significant system performance degradation induced by the mutual coupling (MC) of compact arrays [2, 7, 8].

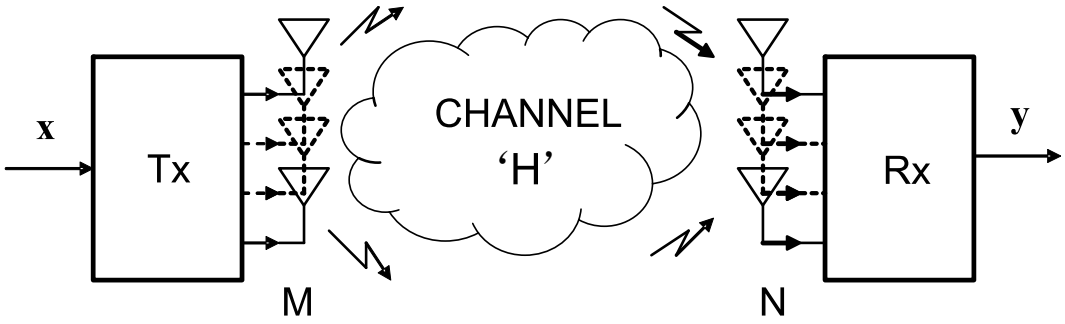

Figure 1.1: *A diagram of a typical MIMO system.*

The study of compact arrays at the receive end has drawn significant attention. In narrowband MIMO systems, it is widely agreed that the mutual coupling (MC) effect, which is induced by insufficient antenna element separation, can reduce the signal correlation by distorting the radiation patterns of each element [9–11]. However, it will also induce a mismatch between the characteristic impedance of the circuit and the antenna input, which is detrimental to the capacity performance [12]. This conflicting outcome of the MC effect is one important factor which contributes to different conclusions of its impact on MIMO capacity performance [10, 13–21]. Chapter 3 is presented to summarize and fairly compare the impact of MC on compact arrays using the contemporary methods in literature.

Besides MIMO capacity improvement, some advantages of using the *single-port match* have been described in [12, 22–24]. Received power maximization or zero output correlation can be achieved by selecting proper matching impedances [22] for very close antenna spacing ($d = 0.05\lambda$), but this has not been confirmed by experimental implementation. This is a motivation for the research in Chapter 4 and [25]. While the optimum received power and zero output correlation are very sensitive to load parameter variation [22], the maximum capacity is quite stable as the load changes [23]. However, it is observed in [23] that the optimum single-port matching impedance to maximize the capacity is different to the solutions that either maximize the received power or achieve zero correlation. This inspires part of the research in Chapter 5.

Two methods in *n*-port theory are usually adopted to study compact MIMO systems. One is S-parameter analysis which reflects the wave transmission in an *n*-port electrical network; the other is Z-parameter analysis which expresses the voltage and current relations among all ports. The capacity evaluation of compact MIMO systems with matching networks using Z-parameters has partially been carried out in [12–14, 23]. In [13] multiple antennas of a fixed length are studied without consideration of the matching networks. Although compact MIMO

receivers with various matching impedances are examined in [12,23], no complete Z-parameter model and analytical results for the optimal single-port match are given, which is a motivation of our study in Chapter 5. The author in [14] did present a Z-parameter MIMO system but with an inappropriate channel matrix expression, which will be further discussed in Chapter 5, and no matching network was included in the study. The S-parameter framework has been well examined in [11, 18, 19], and recently improved by introducing the effect of amplifier networks to the coupled receive end [26–28]. The authors of [18] introduce various matching networks to improve the system performance, while more varieties of antenna matching networks are examined in [29]. It is proved in [11, 18] that the so-called *multiport-conjugate match* can realize zero output correlation and lossless power transfer from the antennas to the loads for any antenna spacing, and can thus offer significant capacity improvement for very small antenna spacings. Nevertheless, when the investigation is extended to wideband compact MIMO systems, it turns out that the optimum multiport-conjugate match can only be achieved for a small bandwidth [30], which does not fulfill the requirement for large bandwidths in future broadband wireless communication networks. Apart from that, the multiport-conjugate match is not easy to implement as it involves multiple circuit components interconnected across the antenna ports [31]. Instead, the *single-port match* [12, 23, 29, 30] is a practical and suboptimal solution, as it provides capacity improvement compared to the non-matched case and has a larger bandwidth than the *multiport-conjugate match*. Thus, the investigation of the optimal single-port matching for capacity maximization is also studied in Chapter 5.

1.2 Objective and Contributions

1.2.1 Objective

The objective of the work reported in this thesis is:

> **This work is to study the system characteristics of compact MIMO terminals with various matching networks. It also aims to find out the proper matching impedances providing a low signal correlation and high received power performance theoretically and experimentally. Based on this, the next purpose is to seek the optimal single-port matching impedances for capacity maximization of compact MIMO systems. Finally, this work targets to give an insight of the advantage of using matching networks in compact MIMO systems through a two-by-two MIMO system demonstration.**

1.2.2 Contributions

The main contributions of this thesis can be summarized as follows:

- Two methods to evaluate the average received power of a two-element compact array with various matching loads are examined. The method based on circuit theory is proved to be appropriate for received power calculation. The two methods are united through analytical comparison. Simulation results are also presented to reflect the relation between the total average power and power difference between branches versus antenna separation with different matching networks [32].

- A model of two-element compact monopole array with various matching networks and ground plane at an antenna separation of 0.05 wavelength is constructed. The measured results of signal correlation and total received power as well as the system simulations in the computational electromagnetics (CEM) tools SEMCAD and FEKO are studied. The experimental results largely confirm the theoretical and simulation predictions though discrepancies are observed. The discrepancies are discussed from both theoretical and experimental points of view [25].

- A complete MIMO system framework with compact terminals and matching networks using Z-parameter is derived from the power transfer point of view. This model is suitable for any single-mode antennas in arbitrary channel models. A modified channel matrix including the MC effect and matching networks is presented. It is proved that when Kronecker channel model is chosen and MC is assumed at the receiver only, the system model used in [12, 23] are special cases of the general model presented here. The advantage of using matching networks at compact MIMO terminals can be studied for any MIMO configuration using this Z-parameter model [33, 34].

- The solution of the optimal single-port matching impedance is derived numerically for a two-by-two compact MIMO system with matching networks. Closed-form results in the high SNR regime are given and proved to equal the *input impedance* of the receive antennas. A perfect match between analytical and simulation results is demonstrated using ideal half-wavelength dipoles [33, 35].

- The capacity sensitivity of a two-by-two compact MIMO system with the optimal single-port matching networks is explored versus antenna separation and antenna dimensions.

Performance efficiency and precision error are defined to study the system sensitivity performance. The system improvement of using optimal single-port matching compared to other matching techniques has also been evaluated [24, 36].

1.3 Thesis structure

The remainder of this thesis is organized as follows.

Chapter 2 presents an overview of the background knowledge related to the topic of this thesis. It starts from the introduction of wireless propagation channels. Then a brief review of diversity techniques is offered. Important MIMO channel models and MIMO capacity concepts are discussed. After reviewing the basic antenna theories, the Z-parameters and S-parameters in port theory are also revisited.

Chapter 3 studies three characteristics of compact terminals in MIMO systems, i.e. signal correlation, average received power and capacity. Different methods for signal correlation calculation between coupled elements are reviewed and compared via simulation. Two approaches for average received power evaluation are examined and one appropriate method is selected through theoretical and simulation proof. In the end, the capacity of a MIMO system with a compact terminal and suitable matching networks is addressed.

Chapter 4 describes an experimental setup of a two-element compact receiver with various matching networks for the signal correlation and received power analysis. Besides the outcome from the implementation, the simulation results generated from the CEM tools SEMCAD and FEKO are also included. The load impedance selection for implementation and the measurement discrepancies are discussed. Finally, the MIMO capacity performance with chosen matching networks is examined.

Chapter 5 investigates the optimal single-port matching impedance for capacity maximization of compact MIMO systems. A network MIMO system model with compact terminals and matching networks is developed using the Z-parameter approach as a basis for further study. Then the numerical derivation of the optimal single-port matching for a two-by-two MIMO system is presented with closed-form expressions. Finally, the system improvement and sensitivity versus the optimal single-port matching are explored.

Chapter 6 concludes the whole thesis and further research directions are stated.

Chapter 2
Background

2.1 Introduction

MIMO systems and compact antenna arrays are two keywords of this thesis. This chapter offers an overview from basic wireless propagation channels to MIMO systems, fundamental antenna theory to brief port theory, which provides a good preparation for the rest of this thesis.

The remainder of this chapter is organized as follows. Section 2.2 introduces the background of wireless propagation channels. After a brief review of diversity techniques in Section 2.3, various MIMO channel models are presented in Section 2.4. Section 2.5 states the MIMO capacity and evaluation methods. Section 2.6 moves the angle to basic antenna theories. Port theory is focused in Section 2.7. Section 2.8 summarizes the chapter.

2.2 Wireless propagation channels

The understanding of wireless propagation channels is the fundation of any wireless system studies. The channel is the medium of the signal propagation between the source and destination in wireless communications. A channel can be referred as the variation of the electromagnetic propagation as a function of space and time. Because of the characteristic of the space, the transmitted signal is always attenuated versus distance; because of the structure of the space, i.e. the existence of various objects, the transmitted signal can be reflected, diffracted and scattered by different kinds of obstacles, which causes the energy to spread out in multiple paths. Hence, "fading" and "multipath" are two important characteristics of wireless propagation channels. For more details on material in this section please refer to [37–40].

Roughly speaking, the wireless fading channel effects can be divided into two groups: 1) *large scale fading*, which includes path loss and shadowing; 2) *small scale fading*, which can refer to Rayleigh fading [41].[1] Figure 2.1 manifests the classification of wireless fading channels, which is the main topic of this section.

[1] We note that some references introduce path loss independently from the large scale fading group, e.g. [40].

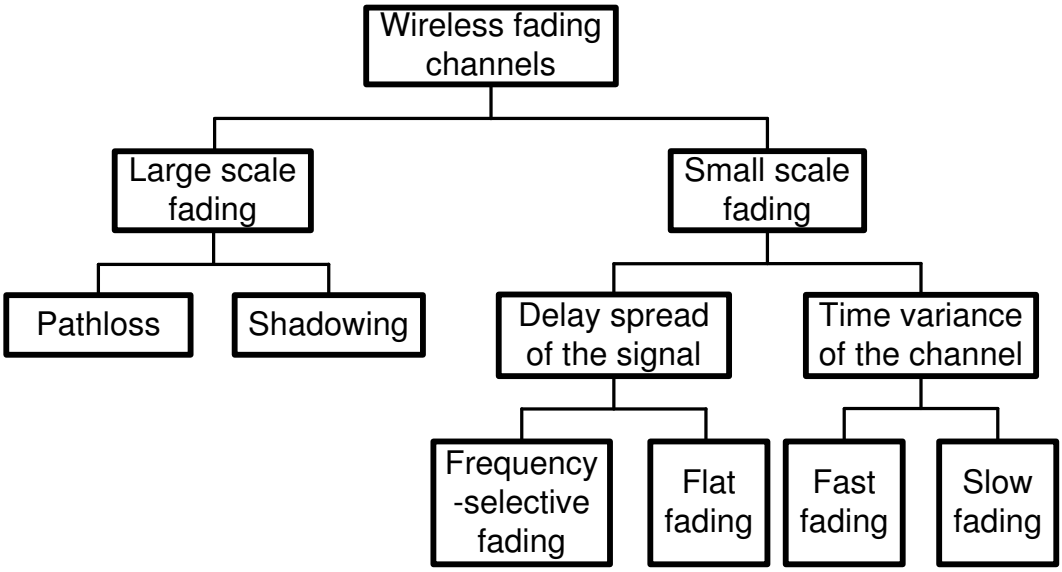

Figure 2.1: *A system block diagram of wireless fading channels.*

2.2.1 Large scale fading

The phenomenon of large scale fading occurs when the transmitted signal propagates over large distance (much larger than the wavelength of the electromagnetic waves) and is normally affected by prominent terrain and objects, e.g. hills, buildings etc.

- **Path loss**: The path loss is defined as the mean power attenuation of the transmitted signal as a function of distance. The effective mean path loss follows an inverse k-th power law, where k is the path loss exponent and varies from $2\sim6$. [40, 41].
- **Shadowing**: Shadowing effect is the variation of the mean path loss caused by large objects. It is found that the shadowing impact on the received power is approximately log-normally distributed [42].

2.2.2 Small scale fading

Small scale fading can be explained by the rapid fluctuations in signal amplitude and phase due to the changes of the the multipaths between the transmitter and receiver in space (as small as a half-wavelength), time and frequency. Small scale fading can be called Rayleigh fading (as shown in Figure 2.2) if there are a large number of independent multipaths and there is no

We follow the classification of fading channels here as in [37–39, 41]. Different fading channel classifications do not matter as the purpose of the classification is a good understanding of wireless fading channels.

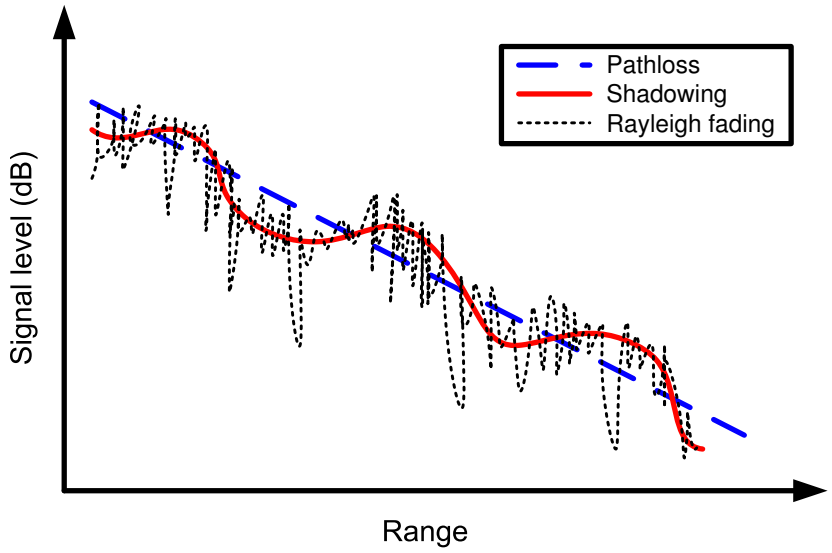

Figure 2.2: *Illustration of large scale and small scale fading.*

line-of-sight (LOS) signal component. In this case, the channel coefficient of a single tap in a discrete time complex baseband model can be denoted as

$$h_c = h_R + \mathrm{j}h_I \tag{2.1}$$

where h_R and h_I are independent identically distributed (i.i.d.) zero-mean Gaussian random variables with equal variance $\frac{\sigma^2}{2}$. The envelope of the received signal $|h_c|$ statistically follows the Rayleigh distribution with density

$$\frac{y}{\sigma^2} e^{-\frac{y^2}{2\sigma^2}}, \qquad x \geq 0. \tag{2.2}$$

Then h_c is called a zero mean circularly symmetric complex Gaussian (ZMCSCG) random variable. When there is a dominant LOS propagation path between the transmitter and the receiver, the small scale fading envelope becomes Rician distributed [39]. The illustration of the large scale and small scale fading of wireless channels is plotted in Figure 2.2.

2.2.2.1 Time delay of the signal

The time delay spread of the multipaths T_d is one parameter for small scale fading evaluation. It is defined as the propagation delay of any signal that exceeds the delay of the first signal arrival at the receiver, counting only the paths with significant energy [37]. In the frequency domain the

time delay spread of the channel dictates its *frequency coherence*. The *coherence bandwidth* W_c is a statistical measured frequency range over which the channel passes all spectral components with approximately equal gain and linear phase [41], which means the spectral components of the signal in that range are undergoing similar effect by the channel, i.e. exhibiting fading or no fading. We note that

$$W_c \propto 1/T_d \tag{2.3}$$

Next we define the transmission symbol time is T_s and the corresponding bandwidth is W_s.

- **Frequency-selective fading**: If $T_d \gg T_s$, i.e. $W_c \ll W_s$, the channel is said to be *frequency-selective*. In this case the channel-induced intersymbol interference (ISI) occurs as some of the signal components fall outside the coherence bandwith would be influenced by the channel differently.
- **Flat fading**: If $T_d \ll T_s$, i.e. $W_c \gg W_s$, the channel is referred to as *flat fading*, which indicates that all of the components of the signal are affected by the channel in a similar manner. The channel-induced ISI distortion will not happen in flat-fading. However, the performance degradation still exists due to the loss in SNR whenever the signal is fading.

2.2.2.2 Time variance of the channel

Another important parameter of small scale fading is the time-varying property of the channel caused by the movement of scatterers within the channel, or relative motion between the transmitter and receiver. In the time domain, the *coherence time* T_c is used to discribe this phenomenon. It is defined as a measurement of the expected time duration over which the channel's response is essentially the same [41]. In the frequency domain, the *time coherence* nature of the channel is expressed by the *Doppler spread* D_s. The relationship between T_c and D_s is

$$T_c \propto 1/D_s \tag{2.4}$$

- **Fast fading**: If $T_c \ll T_s$, i.e. $D_s \gg W_s$, the channel is referred to as *fast fading*. In this case the fading characteristic of the channel will change several times while a symbol is propagating, which induces distortion of the baseband signal. Moreover, if the channel

remains invariant over each T_c within one symbol period T_s and is i.i.d. across different coherence time intervals, it is called a *block fading* model. Each deterministic channel is also called one realization.

- **Slow fading**: If $T_c \gg T_s$, i.e. $D_s \ll W_s$, the channel is called *slow fading*, which implies that the channel stays invariant during the time in which a symbol is transmitted. The distortion of the baseband signal will not happen in slow fading. The performance degradation is the loss in SNR as with flat fading.

The channel models considered in this thesis are discrete-time, narrowband, complex, block fading, flat fading, baseband models.

2.3 Diversity

To reduce the multipath fading induced performance degradation, diversity techniques are usually used to provide independent fading paths. It improves the performance by ensuring that reliable communication is possible as long as one of the multipaths is strong. Two criteria must be fulfilled to achieve effective diversity performance [43]. One is sufficiently low correlation of the impairments of different paths to reduce the possibility of simultaneous signal degradation. The other is similar mean received power of each individual signal at the diversity systems to avoid the domination of the strongest receive branch. Three diversity techniques are popular in the literature [37, 40, 43]:

- **Time diversity**: Diversity can be realized over time by multiple retransmission of the same signal or interleaving in coding. Signal retransmission intervals should be larger than the signal fading period to guarantee sufficient decorrelation between successive transmissions for good diversity performance. A coded signal is interleaved over time in different coherence periods to make different parts of the codewords experience independent fades.

- **Frequency diversity**: If the channel is frequency-selective or wideband, the same signal can be transmitted over different carrier frequencies. This diversity is achieved by the ability of resolving multipaths at the receiver utilizing the wideband nature of the channel.

- **Spatial diversity**: Spatial diversity is obtained by locating multiple antennas at the transmitter and/or the receiver. The good diversity performance depends on adequate antenna

element separation. It is confirmed in practice that uncorrelated signals can be guaranteed when the antenna separation is larger than 10λ and 0.5λ at the base station (BS) and the mobile station (MS). Also, The element separation is determined by the placement of the scatterers and the carrier frequency. The multipaths decorrelate over shorter antenna separations when the MS is surrounded by sufficient scatterers.

Time and frequency diversity only requires single transmit and receive antennas, but they are not efficient as more transmission time or bandwidth are needed for each signal. Spatial diversity does not sacrifice time or bandwidth. However, more hardware and complex computational software have to be implemented, especially at the receive end. To take the most performance advantage of the spatial diversity at the receiver with compact dimension, we will investigate some metrics of spatial diversity performance, i.e. signal correlation (SC) and mean received power, of compact MIMO systems in the following chapters of this thesis.

2.4 MIMO channel models

We consider a $M \times N$ MIMO system (M is the number of the transmit antennas; N is the number of the receive antennas) with a linear array at both link ends as shown in Figure 2.3. The antenna separations of the transmitter and receiver are d_T and d_R, respectively. We note that from now on the channel of a sample realization is studied, i.e. the channel is deterministic and time-independent. Also our analysis focuses on the two-dimensional (2D) space only.

2.4.1 Physical channel model

The physical channel of MIMO systems can be constructed by the angle-of-departure (AOD) ϑ of the transmitter, angle-of-arrival (AOA) φ of the receiver, path attenuation β^a, d_T and d_R. If the AOD and AOA are associated with angle dispersion (as in Figure 2.3(a)), angular spread (AS) Δ should also be considered. We assume the transmitter and receiver are separated by a long distance (much larger than the carrier wavelength λ) and there is no line-of-sight (LOS) path. We assume there is an arbitrary number of multipaths between the transmitter and the receiver, then the physical channel of Figure 2.3(a) can be represented as

$$\mathbf{H} = \int_{\varphi_0-\Delta_\varphi}^{\varphi_0+\Delta_\varphi} \int_{\vartheta_0-\Delta_\vartheta}^{\vartheta_0+\Delta_\vartheta} \beta^a(\varphi)\, \mathbf{a}_R(\varphi)\, \mathbf{a}_T^H(\vartheta)\, d\vartheta d\varphi \tag{2.5}$$

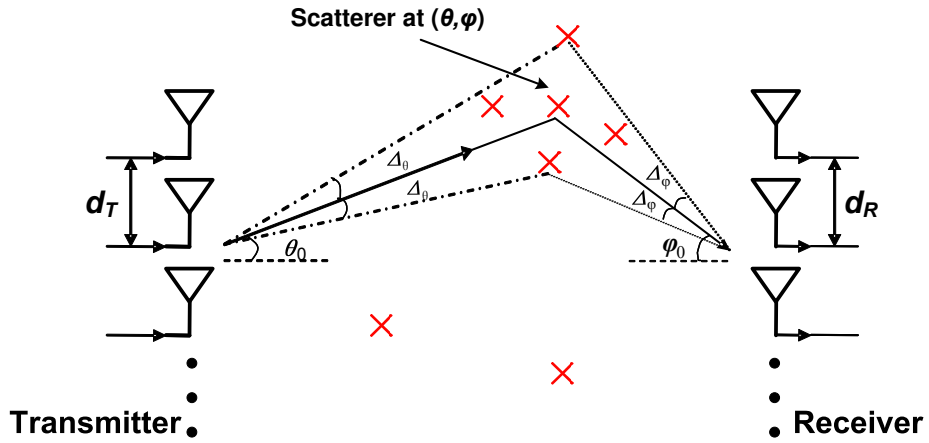

(a) Physical MIMO channel model

(b) i.i.d. scattering model

Figure 2.3: *MIMO channel models.*

where

$$\beta^a(\varphi) = \beta_{n,\varphi}\sqrt{MN},$$

$$\mathbf{a}_R(\varphi) = \frac{1}{\sqrt{N}}\left[\begin{array}{cccc} 1 & e^{j2\pi d_R \sin\varphi} & \cdots & e^{j2\pi(N-1)d_R\sin\varphi}\end{array}\right]^T,$$

$$\mathbf{a}_T(\vartheta) = \frac{1}{\sqrt{M}}\left[\begin{array}{cccc} 1 & e^{j2\pi d_T \sin\vartheta} & \cdots & e^{j2\pi(M-1)d_T\sin\vartheta}\end{array}\right]^T.$$

Also, ϑ_0 and φ_0 are the mean AOD and mean AOA, separately; Δ_ϑ and Δ_φ, respectively, are the AS of AOD and AOA; $\beta_{n,\varphi}$ is the path gain of the nth path with the AOA of φ. The vectors $\mathbf{a}_R(\varphi)$ and $\mathbf{a}_T(\vartheta)$ are the normalized steering vector (SV) of the receiver and transmitter, respectively. The notation $(\cdot)^H$ is the transpose conjugate operation, and $(\cdot)^T$ is the transpose operation. The channel model displayed in Figure 2.3(a) is called a single cluster model. For more complex physical models, please refer to Chapter 7 of [37].

2.4.2 Non-physical channel models

The MIMO channel models discussed in this subsection do not involve the physical path structure. Thus, they are known as non-physical models.

2.4.2.1 I.I.D. Rayleigh channel model

If a large number of scatterers are evenly distributed around both transmitter and receiver (Figure 2.3(b)), the energy of multipaths is equally spread out, and the antenna elements are either critically or sparsely spaced, the elements of $\mathbf{H}$ in (2.5) will become i.i.d. and circular symmetric complex Gaussian as in (2.1). Then $\mathbf{H} = \mathbf{H}_{i.i.d.}$ is called the i.i.d. Rayleigh fading model. It is the most often adopted model in the evaluation of MIMO system performance due to its analytical tractability. Some properties of $\mathbf{H}_{i.i.d.}$ are

$$E\left\{(\mathbf{H}_{i.i.d.})_{ij}\right\} = 0, \tag{2.6}$$

$$E\left\{\left|(\mathbf{H}_{i.i.d.})_{ij}\right|^2\right\} = 1, \tag{2.7}$$

$$E\left\{(\mathbf{H}_{i.i.d.})_{ij}\,(\mathbf{H}_{i.i.d.})^*_{kl}\right\} = 0 \quad \text{if } i \neq k \text{ or } j \neq l. \tag{2.8}$$

where $E\{\cdot\}$ is the expectation operation, $(\cdot)_{ij}$ is the (i,j)-th element of a matrix, and $(\cdot)^*$ is the conjugate operation of a complex number.

2.4.2.2 Kronecker model

The MIMO channel model cannot maintain the i.i.d. characteristic in real propagation environments due to the existence of LOS components and the gain imbalances between the channel elements [6]. Also in a NLOS scenario, it can become correlated by many physical factors, such as non-uniform-distributed scatterers, small angular spread (AS) and insufficient antenna separations [4, 20]. When individual channels are correlated, the channel can be expressed as [44]

$$\mathrm{vec}\,(\mathbf{H}) = \mathbf{\Psi}_V^{1/2}\mathrm{vec}\,(\mathbf{H}_{i.i.d.}) \tag{2.9}$$

where vec$(\cdot)$ is the columnwise vectorisation operation of a matrix, and $\mathbf{\Psi}_V$ is a $MN \times MN$ covariance matrix defined as $\mathbf{\Psi}_V = E\{\mathrm{vec}(\mathbf{H})\mathrm{vec}(\mathbf{H})^H\}$. If $\mathbf{\Psi} = \mathbf{I}_{MN}$, then $\mathbf{H} = \mathbf{H}_{i.i.d.}$.

If we further assume that the transmitter does not affect the spatial properties of the received signal at all, $\mathbf{\Psi}_V$ can be split to [40, 45]

$$\mathbf{\Psi}_V = \mathbf{\Psi}_T^T \otimes \mathbf{\Psi}_R \tag{2.10}$$

where $\mathbf{\Psi}_T$ and $\mathbf{\Psi}_R$ are the covariance matrix of the transmitter and receiver, respectively. The notation $\otimes$ is the Kronecker product. The equation (2.10) indicates that $\mathbf{H}$ is still a Rayleigh fading model with following covariance structure [13, 46]

$$E\left\{(\mathbf{H})_{ik}\,(\mathbf{H})_{jl}^{*}\right\} = (\mathbf{\Psi}_T)_{kl}\,(\mathbf{\Psi}_R)_{ij}\,. \tag{2.11}$$

Also $\mathbf{H}$ can be modified to

$$\mathbf{H} = \mathbf{H}_{cr} = \mathbf{\Psi}_R^{1/2}\mathbf{H}_{i.i.d.}\mathbf{\Psi}_T^{1/2}, \tag{2.12}$$

which is known as "Kronecker model" [47, 48]. This model is valid if the angular spread of the scatterers at the receive array are identical for signals arriving from any transmit antenna. Moreover, the transmit and receive antennas have identical radiation patterns and are closely placed [40]. Though the approximation of Kronecker model is deficient for large MIMO systems [49], it provides effective matching to the experimental results for up to four-element MIMO systems [5, 48, 50]. This channel model will be used in some parts of this thesis.

2.5 MIMO Capacity

To evaluate the performance upper bound in communication, the concept of *capacity* has been defined by Claude Shannon in 1948 [51], which is the foundation of information theory. Capacity is defined as the maximal achievable error-negligible rate of communication. In this section the frequency flat deterministic/time-invariant channels with bandwidth of 1Hz are considered.

2.5.1 SISO capacity

In a discrete-time complex baseband model, the input-output relation of a single-input single-output (SISO) system is

$$y = \sqrt{P_T}hx + v \tag{2.13}$$

where y is the output signal, P_T is the total average transmit power, h is the SISO channel, x is the input signal and v is the additive Gaussian noise at the receiver. Then the SISO system Shannon capacity is given by

$$C = \log_2\left(\rho\left|h\right|^2 + 1\right) \text{ bits/s/Hz} \tag{2.14}$$

where ρ is the signal-to-noise ratio (SNR) and h is the channel of the SISO system.

2.5.2 MIMO capacity

Similar to the SISO case, the input-output relation of an $M \times N$ MIMO system can be expressed as [40]

$$\mathbf{y} = \sqrt{\frac{P_T}{M}}\mathbf{H}\mathbf{x} + \mathbf{v} \tag{2.15}$$

where $\mathbf{y} = [y_1, y_2, ..., y_N]^T$, $\mathbf{x} = [x_1, x_2, ..., x_M]^T$, $\mathbf{v} = [v_1, v_2, ..., v_N]^T$ are the received signal vector, transmitted signal vector and vector of additive Gaussian noise, respectively. Thus, we have $E\{\mathbf{v}\mathbf{v}^H\} = N_0\mathbf{I}_N$. The covariance matrix $\mathbf{R_{xx}} = E\{\mathbf{x}\mathbf{x}^H\}$ must be constrained as $\mathrm{Tr}(\mathbf{R_{xx}}) \leq M$ to fulfill the total transmitted power constraint. We further assume the channel $\mathbf{H}$ is known to the receiver in the following analysis. The capacity of one MIMO channel realization is defined as [3]

$$\begin{aligned} C &= \max_{f(\mathbf{x})} I\left(\mathbf{x};\mathbf{y}\right) = \max_{f(\mathbf{x})}\left(H\left(\mathbf{y}\right) - H\left(\mathbf{v}\right)\right) \\ &= \max_{\mathrm{Tr}(\mathbf{R_{xx}})=M} \log_2 \det\left(\frac{P_T}{N_0 M}\mathbf{H}\mathbf{R_{xx}}\mathbf{H}^H + \mathbf{I}_N\right) \text{ bits/s/Hz} \end{aligned} \tag{2.16}$$

where $I(\mathbf{x};\mathbf{y})$ is the mutual information between vectors $\mathbf{x}$ and $\mathbf{y}$, and $f(\mathbf{x})$ is the probability distribution of vector $\mathbf{x}$. Also $H(\mathbf{y})$ is the differential entropy of vector $\mathbf{y}$, and $\mathrm{Tr}(\cdot)$ is the trace of a matrix. The mutual information $I(\mathbf{x};\mathbf{y})$ is maximized to achieve capacity C when $\mathbf{x}$ is a ZMCSCG vector.

2.5.2.1 Transmitter without knowledge of CSI

If the transmitter has no knowledge of the channel state information (CSI), the input signal/transmit power can be equally and independently distributed at the transmitter, i.e. $\mathbf{R_{xx}} =$

$\mathbf{I}_M$. The corresponding equal-power [3, 40] capacity is

$$C_{ep} = \log_2 \det\left(\frac{P_T}{N_0 M}\mathbf{H}\mathbf{H}^H + \mathbf{I}_M\right) = \sum_{i=1}^{\min(M,N)} \log_2\left(\frac{\rho}{M}\lambda_{\mathrm{i}} + 1\right) \text{ bits/s/Hz}. \quad (2.17)$$

The $\mathbf{H}\mathbf{H}^H$ in (2.17) is an $M \times M$ positive semi-definite Hermitian matrix. It can be expressed as $\mathbf{H}\mathbf{H}^H = \mathbf{D}\mathbf{\Lambda}\mathbf{D}^H$ by performing a singular value decomposition (SVD) [52], where $\mathbf{D}$ is a unitary matrix and

$$\mathbf{\Lambda} = \text{diag}\left\{\lambda_1, \lambda_2, ..., \lambda_{\min(M,N)}\right\}, \quad \lambda_i \geq 0 \quad (2.18)$$

where diag$\{\cdot\}$ in (2.18) is to form a diagonal matrix using λ_i as the diagonal entries. Considering a full rank channel and $M = N$, and the elements of $\mathbf{H}$ satisfy $|(\mathbf{H})_{ij}|^2 = 1$, $\mathbf{H}\mathbf{H}^{\mathbf{H}} = \mathbf{H}^{\mathbf{H}}\mathbf{H} = \mathbf{I}$, then (2.17) can be represented as

$$C_{ep} = M \log_2(1 + \rho) \text{ bits/s/Hz}. \quad (2.19)$$

where $\|\cdot\|$ is the matrix norm. Also The corresponding SISO channel $|h|^2 = 1$ in (2.14). Therefore, the capacity of a MIMO system with orthogonal channel matrix is M times of the SISO system.

2.5.2.2 Transmitter with knowledge of CSI

When the transmitter knows the CSI, the MIMO capacity in (2.17) can be further increased by optimising the power allocation of $\mathbf{R}_{\mathbf{xx}}$ in (2.16). We still assume $\mathbf{H}$ is full rank, then $\mathbf{R}_{\mathbf{xx}}$ can be properly chosen

$$\mathbf{R}_{\mathbf{xx}} = \mathbf{D}\mathbf{\Gamma}\mathbf{D}^H \quad (2.20)$$

where $\mathbf{\Gamma} = \text{diag}\left\{\gamma_1, \gamma_2, ..., \gamma_{\min(M,N)}\right\}$. The element γ_i should also satisfy

$$\gamma_i = \left(\mu - \frac{M}{\rho\lambda_i}\right)_+, \qquad \sum_{i=1}^{M} \gamma_i = M. \quad (2.21)$$

where $+$ denotes that only the positive terms are counted. Equation (2.21) is called the water-filling solution [3, 46, 53]. The MIMO capacity of (2.16) can be reformed to

$$C_{wf} = \sum_{i=1}^{\min(M,N)} \log_2 \left(\frac{\rho}{M} \gamma_i \lambda_i + 1 \right) \text{ bits/s/Hz} \tag{2.22}$$

The waterfilling method in (2.22) only outperforms equal-power solution in (2.17) at low SNR but the gain vanishes at high SNR [46] due to an asymptotically equal power allocation along the diagonal of $\mathbf{R_{xx}}$ [4, 54]. Furthermore, the MIMO diversity or multiplexing gain can be benefited using space-time coding or V-BLAST without knowledge of CSI at the transmitter. Hence, (2.17) is used in this thesis to evaluate the MIMO system performance.

2.5.3 Statistical characterisation

The MIMO capacity with deterministic channels are introduced in previous sections. However, the information rate is a random variable since $\mathbf{H}$ is random. Two notions are commonly used in studying the statical characterisation of MIMO capacity. They are *ergodic capacity* and *outage capacity* [3].

- **Ergodic capacity**: It is defined as the ensemble average of the information rate over the distribution of the elements of $\mathbf{H}$ [40]. It represents the optimal information rate (upper bound) when each signal $\mathbf{x}$ is transmitted over an independent channel realization. For (2.17), the ergodic capacity is

$$\overline{C_{ep}} = E \left\{ \sum_{i=1}^{\min(M,N)} \log_2 \left(\frac{\rho}{M} \lambda_{\mathrm{i}} + 1 \right) \right\} \text{ bits/s/Hz.} \tag{2.23}$$

- **Outage capacity**: The outage capacity implies the reliability of the system performance. The $q\%$ outage capacity is defined as the maximum information rate below which error free transmission can be maintained for $(100 - q)\%$ of the channel realizations.

Figure 2.4 is an example of both statistics. It is apparent that the MIMO systems outperforms the SISO system significantly considering both ergodic capacity and outage capacity. The advantage of a MIMO system increases with larger configurations.

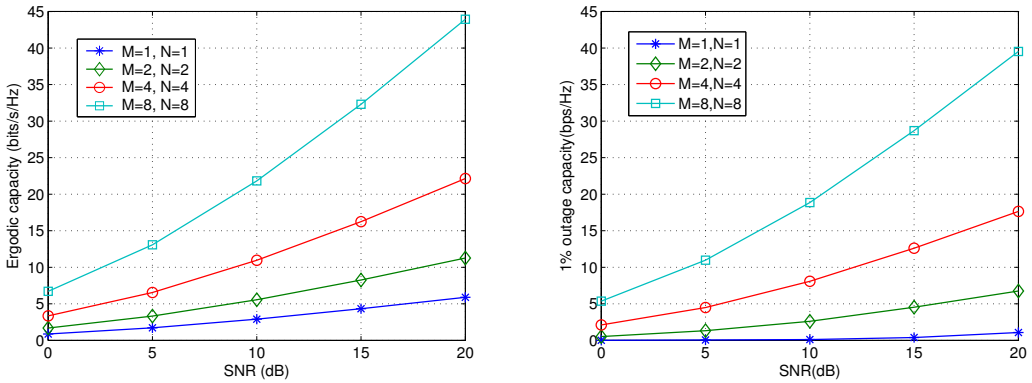

(a) Ergodic capacity

(b) 1% outage capacity

Figure 2.4: *The ergodic and outage capacity with an i.i.d. channel of different MIMO configurations as a function of SNR.*

We note that the MIMO capacity in other complex (non i.i.d.) channels can deviate from the i.i.d. performance largely due to the existence of correlation, insufficient antenna spacing, etc. These effects will be discussed in other chapters of this thesis. Also ergodic capacity is usually simulated for the system evaluation in the following analysis.

2.6 Antenna theory preliminaries

Antennas are essential components of the wireless communication systems. The performance of the MIMO systems is even more influenced by antennas as antenna arrays are involved. Therefore, some preliminaries of antenna theory are introduced in this section.

2.6.1 Antenna parameters

The antenna is a complex subject with a number of parameters to quantify its performance. We note that only parameters which will be used in the remainder of this thesis are reviewed here.

2.6.1.1 Radiation patterns

An *antenna radiation pattern* is defined as a mathematical function or a graphical representation of the radiation properties of the antenna as a function of space coordinates. In most cases, the radiation pattern is determined in the far-field (FF) region and is represented as a function of

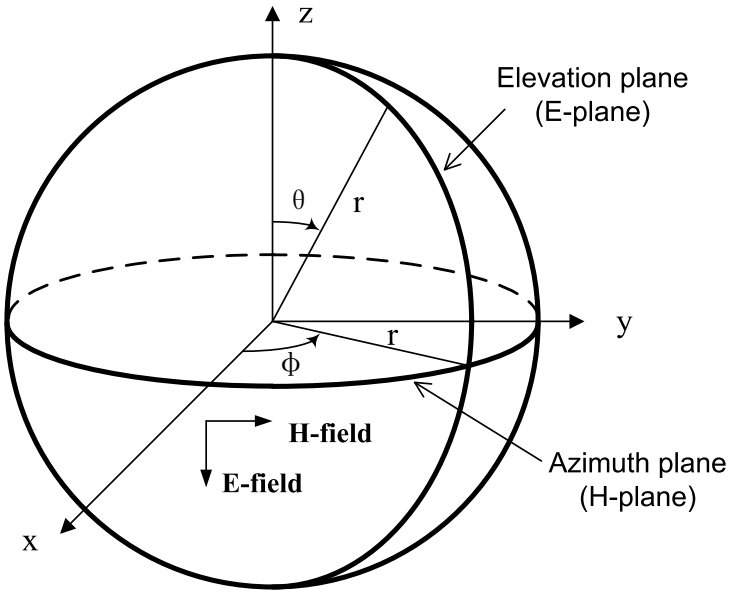

Figure 2.5: *The field components and coordinate system for antenna radiation pattern analysis.*

the directional coordinates [55]. The radiation property of most concern is the 2D or 3D spatial distribution of the radiated energy as a function of the observation spot along a path or surface of constant radius [7]. Figure 2.5 gives a visual example of the field components and sphere coordinate system for antenna analysis, where ϕ, θ and r are the azimuth angle, elevation angle and radius, respectively. A graph of the spatial variation of the electric (*E*-) or magnetic (*H*-) field along r is defined an amplitude *field pattern*. If a linear polarized antenna, e.g. ideal dipole, is put along z-axis in Figure 2.5, the azimuth plane (xy-plane in Figure 2.5) pattern is called *H-plane pattern* as it contains the magnetic vector only. Therefore, the elevation plane (every plane containing the z-axis in Figure 2.5) pattern is *E-plane pattern* as it contains the electric vector only. In this case, the *E*- and *H-plane patterns* are referred to as *principal plane patterns*. Most antennas can be oriented so that at least one of the principal plane patterns coincide with one of the geometrical principal planes [7]. For example in Figure 2.6, the yz-plane is selected as *E*-plane in Figure 2.6(b), and the xy-plane is chosen as *H*-plane in Figure 2.6(c).

- **Far-field (FF) patterns**: At large distances from an antenna, where the angular distribution around the antenna, i.e. the radiation pattern is independent of distance from the antenna, is called the *FF region*. All power is radiated power in the FF region. If the

maximum dimension of an antenna is D, the distance from the antenna is r_D, then the FF conditions are

$$r_D > \frac{2D^2}{\lambda}, \qquad r_D \gg D, \qquad r_D \gg \lambda. \tag{2.24}$$

where λ is the wave length. The distance to the FF is $2D^2/\lambda$, and the radiation pattern in the FF region is *FF pattern*.

- **Isotropic and omni-directional patterns**: A hypothetical lossless radiator having equal radiation in all directions is called an *isotropic* antenna. Though it is not feasible in practice, the isotropic pattern is regularly taken as a reference for evaluating the directive properties of the real antennas. In Figure 2.6(c) the pattern is uniform in a given plane (in

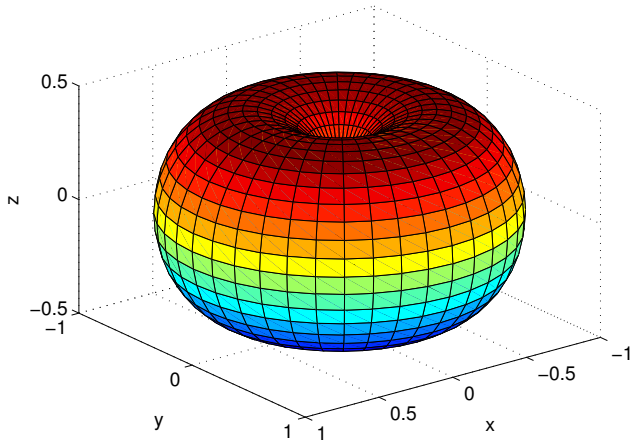

(a) 3D FF pattern

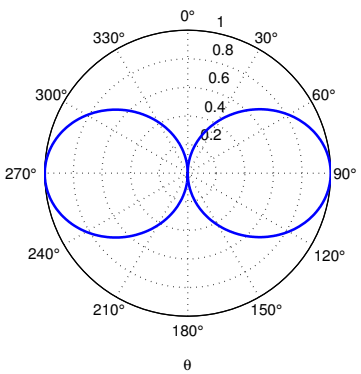

(b) $|E(\theta)|$, *E*-plane pattern

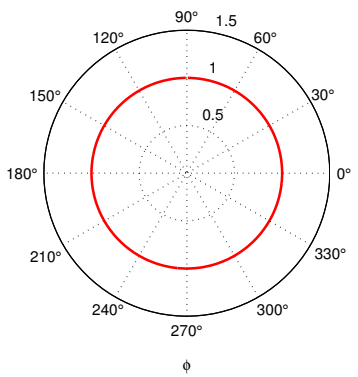

(c) $|H(\phi)|$, *H*-plane pattern

Figure 2.6: *The 3D and 2D principal plane patterns of an ideal dipole.*

this case the *xy*-plane), therefore it is called an *omni-directional pattern*. The antennas with omni-directional plane as azimuth plane are very popular in ground-based applications because only elevation plane has to be studied. The ideal dipole in Figure 2.6 is one such antenna.

The calculation of radiation patterns of any antenna can be achieved using radiation integrals and Maxwell's equations. Because the FF pattern equations of the antennas used in this thesis, i.e. dipoles and monopoles, are summarized in literature, the derivations will not be provided. More details can be found in many text books [7, 8, 56].

2.6.1.2 Polarization

The polarization of an antenna follows the polarization of the wave radiated by the antenna when transmitting [8]. Therefore, we focus on wave polarization. At any point in the FF region of an antenna the radiated wave can be recognized as a *plane wave* whose electric and magnetic fields lie in a plane. The *polarization* of a plane wave is the figure the instantaneous electric field traces out with time at a fixed observation spot. In Figure 2.7, a vertical linear polarized plane wave is shown as an example. The electric field at a fixed point oscillates back and forth with time varying along a vertical line. Meanwhile, the temporal and spatial variations of the magnetic field are perpendicular and similar to those of the electric field (Figure 2.7).

The polarization can be divided into three types, *linear*, *circular* and *elliptical* as displayed in

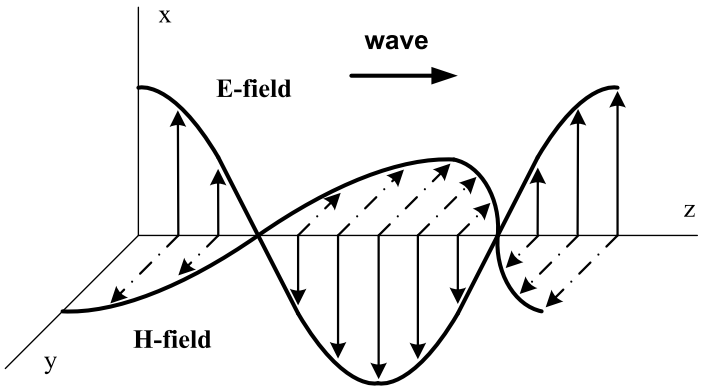

Figure 2.7: *The spatial behavior of the electric and magnetic fields of a vertical linear polarized wave for a fixed instant of time.*

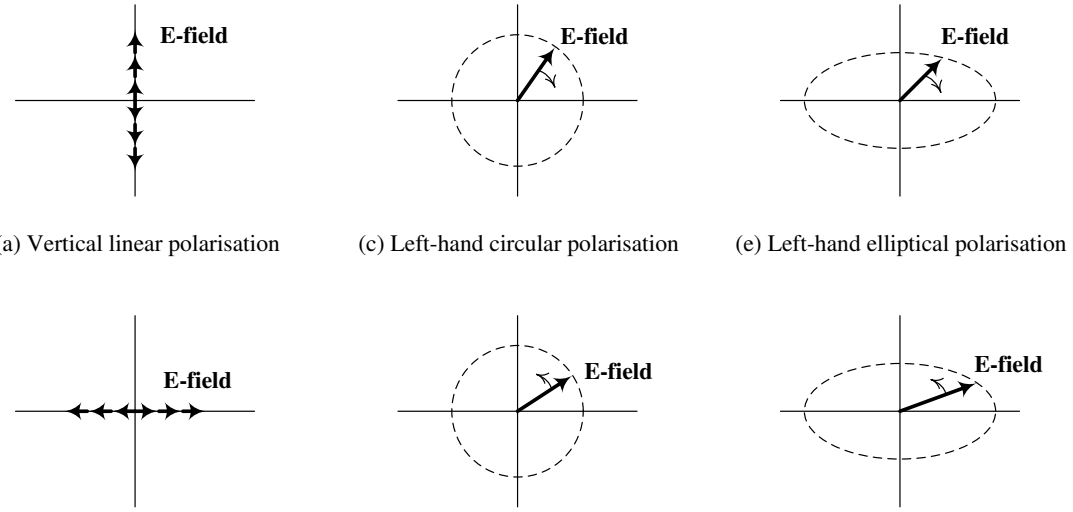

(a) Vertical linear polarisation (c) Left-hand circular polarisation (e) Left-hand elliptical polarisation

(b) Horizontal linear polarisation (d) Right-hand circular polarisation (f) Right-hand elliptical polarisation

Figure 2.8: *The classification of wave polarization.*

Figure 2.8. If the electric field vector moves back and forth along a line, the field is called *linearly polarized* (Figure 2.8(a) and 2.8(b)). Dipoles and monopoles are linear polarized antennas. The electric field remaining constant in length but rotating in a circular path is called *circularly polarized* (Figure 2.8(c) and 2.8(d)). A representative is helix antenna. If the electric field rotating with unequal lengths, an *elliptical polarization* is formed (Figure 2.8(e) and 2.8(f)). We note that only linear polarized antennas are considered in this thesis.

It is reported that polarization can be utilized to boost MIMO system performance by using multiple orthogonally-oriented antenna elements [57, 58]. However, the benefit is hard to achieve as strong MC and non-ideal pattern characteristics can reduce the number of independent channels [5]. Moreover, the imbalance of multiple polarizations also leads to performance degradation [59]. Thus, only single polarization antennas are used in this thesis.

2.6.1.3 Basic antenna models

We introduce some antenna models involved in this thesis.

- **Dipole**: The most commonly used antenna is the half-wavelength (λ/2) dipole and it is often taken as a reference in research. For an ideal (infinite thin) dipole the FF pattern is

$$F(\theta) = \frac{\cos((\pi/2)\cos\theta)}{\sin(\theta)}, \tag{2.25}$$

  which has been plotted in Figure 2.6. It is linearly polarized and its impedance is $73 + \mathrm{j}42.5\Omega$. In practice, the diameter of the wire affects dipole characteristics. If the wire is made thinner, the more the practical dipole approximates the ideal dipole [60]. If the wire is thicker, the dipole length must be shorter to achieve resonance [8, 61].

- **Monopole**: A monopole antenna (whip) is half of a dipole antenna placed on top of a ground plane. If the plane is infinite, planar and perfectly conducting, the monopole antenna will be equivalent to a dipole whose lower half is the *image* of the upper half [7, 8, 61]. The quarter-wavelength (λ/4) monopole is the most popular such antenna. For an ideal λ/4 monopole, its FF pattern (in the upper hemisphere) and impedance are identical to those of a λ/2 dipole. The performance of the monopole will deviate from the above discussion if infinite ground plane assumption is broken.

Some other types of antennas are also commonly used in wireless communications for different purposes. Helix antennas are circularly polarized antennas and often applied for broadband transmission. The planar inverted-F antenna is popular in small handhelds as it has compact size and relatively good bandwidth.

2.6.2 Antenna array

A number of antennas can be arranged in space to produce a combined directional radiation pattern, which is called an *antenna array*. The geometrical configuration, element separation, relative element pattern, excitation amplitudes and phases of the array elements are factors to determine the overall array pattern. The antenna array can *steer* from one focused direction to another by changing the relative phases of the array elements. The geometrical array configuration of an array can be linear, planer (rectangular), circular, etc. We only study the linear array characteristic in this thesis.

For simplicity, identical omni-directional antenna elements with identical excitation amplitudes and phases are assumed. Also the current in each element is assumed to be the same as that of

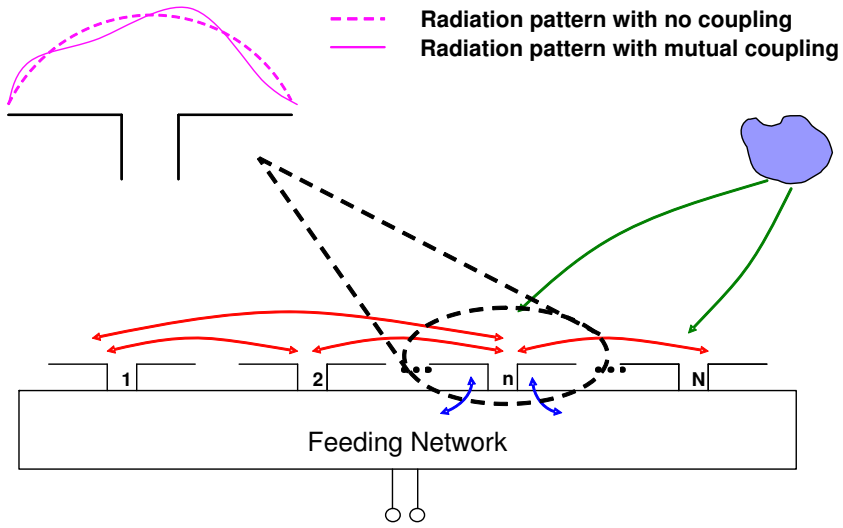

Figure 2.9: *Form of mutual coupling of an array.*

the isolated element. If the elements are placed with sufficient ($> \lambda/2$) identical separation in the azimuth plane in a 2D scenario, the steering vector (SV) $\mathbf{a}$ and array factor (AF) A of the linear array are

$$\mathbf{a}(\phi) = \left[\begin{array}{cccc} 1 & e^{\mathrm{j}\frac{2\pi}{\lambda}d_1\cos(\phi)} & e^{\mathrm{j}\frac{2\pi}{\lambda}d_2\cos(\phi)} & \cdots \quad e^{\mathrm{j}\frac{2\pi}{\lambda}d_{N-1}\cos(\phi)} \end{array} \right]^T \tag{2.26}$$

$$A(\phi) = 1 + e^{\mathrm{j}\frac{2\pi}{\lambda}d_1\cos(\phi)} + e^{\mathrm{j}\frac{2\pi}{\lambda}d_2\cos(\phi)} + \cdots + e^{\mathrm{j}\frac{2\pi}{\lambda}d_{N-1}\cos(\phi)}. \tag{2.27}$$

where d_i $(i = 2, ..., N)$ is the distance between the first and the ith antenna elements. Then the FF pattern of the array is

$$F_{\text{total}}(\phi) = F(\phi)A(\phi) \tag{2.28}$$

where $F(\phi)$ is the FF pattern of an isolated antenna element at the azimuth plane. Equation (2.28) is called *pattern multiplication*.

2.6.3 Mutual coupling

In previous analysis, the current distribution on each element is assumed to be identical in an array, and pattern multiplication is valid. However, in reality the elements interact with each other and change the currents (and thus impedances) from the isolated antennas, especially in a compact array ($d < \lambda/2$). This interaction is defined as mutual coupling (MC), which alters the total array pattern from the no-coupling case.

As shown in Figure 2.9, three factors are responsible for the MC effect. First is the direct MC interaction between elements. Second, the near-field conductor can induce MC to the adjacent elements. Third, the feeding network which connects to the elements provides a path for coupling.

The MC effect can be expressed by the way of the *mutual impedance* apart from the *self-impedance* of the isolated antenna element. In port theory, the antenna impedance matrix with MC $\mathbf{Z}$ is

$$\mathbf{Z} = \begin{bmatrix} z_{11} & z_{12} & z_{13} & \cdots \\ z_{21} & z_{22} & z_{23} & \cdots \\ z_{31} & z_{32} & z_{33} & \cdots \\ \vdots & \vdots & \vdots & \ddots \end{bmatrix} \tag{2.29}$$

where z_{ii} is the self-impedance of the ith element and z_{ij} means the mutual-impedance between the ith and jth elements. Also we have $z_{ij} = z_{ji}$ based on the reciprocity theorem [56]. In general, the mutual-impedance can be computed numerically using *E*-field integrals [7]. A set of closed-forms of mutual impedance for two side-by-side dipoles are obtained using the induced EMF (electromotive force) method [7, 56]

$$\begin{aligned} r_{21} &= r_{12} = 30\left[2C_i\left(u_0\right) - C_i\left(u_1\right) - C_i\left(u_2\right)\right] \\ x_{21} &= x_{12} = -30\left[2S_i\left(u_0\right) - S_i\left(u_1\right) - S_i\left(u_2\right)\right] \end{aligned} \tag{2.30}$$

where $C_i(\cdot)$ and $S_i(\cdot)$ are cosine and sine integral functions [62], and

$$\begin{aligned} u_0 &= 2\pi d_2/\lambda \\ u_1 &= 2\pi\left(\sqrt{d_2^2 + l^2} + l\right) \\ u_2 &= 2\pi\left(\sqrt{d_2^2 + l^2} - l\right) \end{aligned}$$

where l is the total length of the dipole. Equation (2.30) is only suitable for the ideal dipole antennas (with infinitely thin diameter). However, the ideal dipole assumption is not practical as the wire diameter is a factor which would affect the MC performance. Also the self-impedance of an antenna will change from the isolated antenna case in the existence of MC. Another more accurate approach to determine the mutual-impedance including the diameter impact is

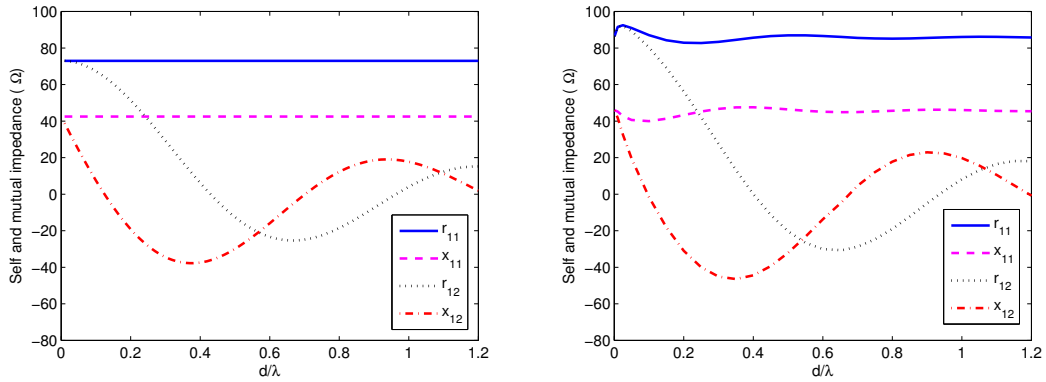

(a) Induced EMF method using ideal dipoles

(b) Simulation in FKEO using dipoles with $\lambda/400$ diameter

Figure 2.10: *The resistance and reactance components of self and mutual impedances of antenna 1 in a two $\lambda/2$ dipole array with various antenna spacings .*

to simulate/measure the open-circuit (OC) and short-circuit cases of the two dipole array [8]:

1. Open circuit/remove antenna element 2. Measure the OC impedance $z_{oc} = z_{11}$ at the port of antenna 1. For identical antennas we have $z_{22} = z_{11}$.
2. Short circuit antenna 2. Measure the short-circuit impedance z_{sc} at the port of antenna 1.
3. Then $z_{12} = \sqrt{z_{oc}(z_{oc} - z_{sc})}$.

The illustration of this method is shown in Figure 2.10(b). Comparing Figure 2.10(b) to Figure 2.10(a) using EMF method, it is obvious that the self-impedance of an antenna in a coupled array is different from that of isolated case and varies with element separations. The effect on the impedance of using a finite thickness of the antennas is also shown in Figure 2.10(b), where the self impedance of the half-wavelength dipole is larger than the ideal case in Figure 2.10(a).

The FF patterns can be distorted from the no-coupling case as well. We introduce the MC matrix to derive the calculation of FF from that without MC. In circuit theory, the MC matrix of a coupled array is given by[2]

$$\mathbf{K}_{mc} = z_L \cdot (\mathbf{Z} + z_L \cdot \mathbf{I})^{-1} = \begin{bmatrix} k_{11} & k_{12} \\ k_{12} & k_{11} \end{bmatrix} \tag{2.31}$$

[2]We note that in [10, 63] $\mathbf{K}_{mc} = (z_L + z_{11})(\mathbf{Z} + z_L\mathbf{I})^{-1}$ has been used. However, if we refer to [64], (2.31) is the correct expression for our model.

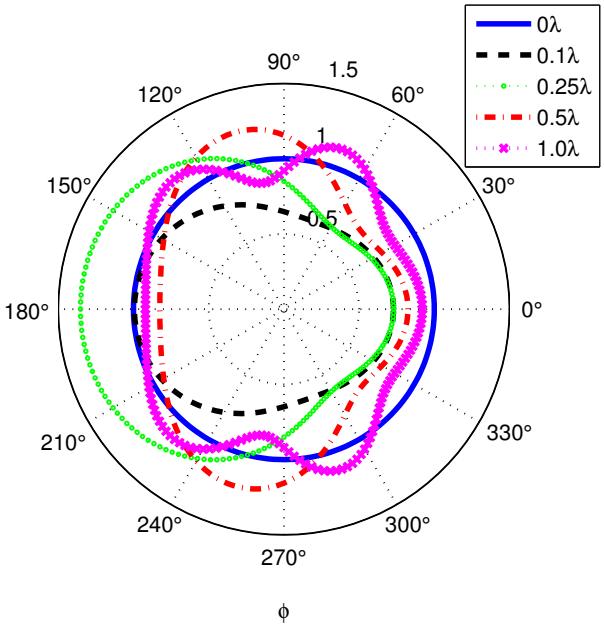

Figure 2.11: *FF patterns of antenna 1 in a two $\lambda/2$ dipole array with $\lambda/400$ diameter as a function of antenna spacings in FEKO.*

where z_L is the load impedance added to each antenna port. If no matching network is attached to the antennas, $z_L = 50\Omega$. Then the FF patterns of two ideal dipole array with MC are given [15]

$$F_1(\phi) = k_{11} + k_{12}e^{-\mathrm{j}\frac{2\pi}{\lambda}d_2\cos(\phi)},$$
$$F_2(\phi) = k_{11} + k_{12}e^{\mathrm{j}\frac{2\pi}{\lambda}d_2\cos(\phi)}. \tag{2.32}$$

The non-ideal FF pattern of compact arrays also can be simulated using electromagnetic tools as for impedances. The demonstration of the FF patterns with MC is displayed in Figure 2.11 using FEKO software [65]. Proper matching networks can be introduced to change z_L in (2.31) to change the impact of MC on MIMO system performance, which is a central idea of this thesis.

Experiment/Measurement is the ultimate way to obtain antenna/array parameters via field measurement. It is a good validation of theoretical/simulation results though it is costly to perform. Fortunately, the experimental study of compact MIMO terminals will be investigated in this thesis.

2.6.4 Simulation methods

Besides the induced EMF method, antenna design and analysis are usually based on the software using the numerical methods in computational electromagnetics (CEM). Two numerical methods are prominent in low frequency analysis: the method of moments (MoM) and finite-difference time-domain (FDTD). A brief introduction of these methods is presented.

- **Induced EMF**: The classical EMF method is limited to straight, parallel and linear arrays, and it does not include the radius of the wires as well as the gaps at the feeds [7]. However, closed-form solutions can be derived with very good design data.
- **MoM**: MoM is an integral-equation based CEM numerical method in the frequency domain. It works by constructing a "mesh" over the modeled surface, and only requires the calculation of the boundary values rather than values throughout the space. Therefore, it can be used to study more antenna configurations. However, the complexity of this method requires the necessary software to deal with the time- and storage-consuming mathematical equations, as well as software validation. Luckily, several commercial and freeware software packages are available, e.g. FEKO [65] and Sonnet Lite [66].
- **FDTD**: For problems with a range of frequencies, e.g. pulsed excitations and various transient phenomena, FDTD is a better choice than MoM because it is a differential-equation based method in the time domain [8]. Then all of the frequency domain data can be generated from one time domain calculation via the Fourier transform. FDTD directly solves Maxwell's curl equations at points on space grids in the time domain. It can achieve what MoM does and extends to broadband problems. One example of software using the FDTD method is SEMCAD [67].

In the remainder of this thesis, the analysis using FEKO and SEMCAD are utilized as simulation calibration of the measured results.

2.7 Port theory

Antenna array implementation is usually modeled as impedances connected to transmission lines to form a network [7, 8]. Hence, port theory is essential especially for investigating the MC effect in an array. Here we introduce the Z-parameters and S-parameters in port theory

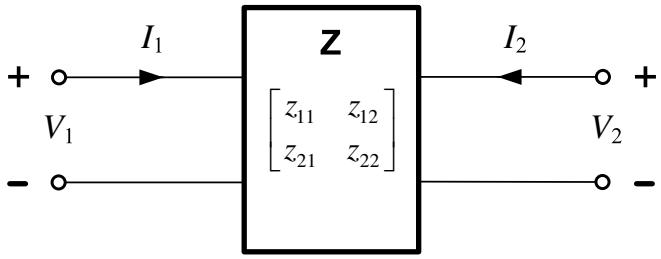

Figure 2.12: *Two port Z-parameter network.*

through a two-port network.

2.7.1 Z-parameter

The impedance parameter (Z-parameter) is the most intuitive way to represent the voltage-current relations of antenna elements in a array. As in Figure 2.12, the voltage-current relations of the two-port network are

$$\begin{bmatrix} V_1 \\ V_2 \end{bmatrix} = \mathbf{Z} \begin{bmatrix} I_1 \\ I_2 \end{bmatrix} = \begin{bmatrix} z_{11} & z_{12} \\ z_{21} & z_{22} \end{bmatrix} \begin{bmatrix} I_1 \\ I_2 \end{bmatrix} \tag{2.33}$$

where V_i and I_i are the voltage and current of the ith port, and $\mathbf{Z}$ is called the impedance matrix with elements

$$z_{ii} = \left.\frac{V_i}{I_i}\right|_{I_k=0 \text{ for } k\neq i}, \text{ and } z_{ij} = \left.\frac{V_i}{I_j}\right|_{I_k=0 \text{ for } k\neq j} (i \neq j). \tag{2.34}$$

We can see that (2.34) agrees with the second method for antenna self and mutual impedances determination in Section 2.6.3. If identical elements are assumed, we have $z_{11} = z_{22}$ and $z_{12} = z_{21}$. Furthermore, if the network is lossless, the condition Re$\{z_{ij}\}$ = 0 must be satisfied [68]. The network in Figure 2.12 can be extended by connecting with matching networks and loads, which will be discussed in this thesis. Also, the modeling of a complete MIMO system can be realized using Z-parameters, which is also one important contribution in this thesis and has been mentioned in many papers [12–14, 23].

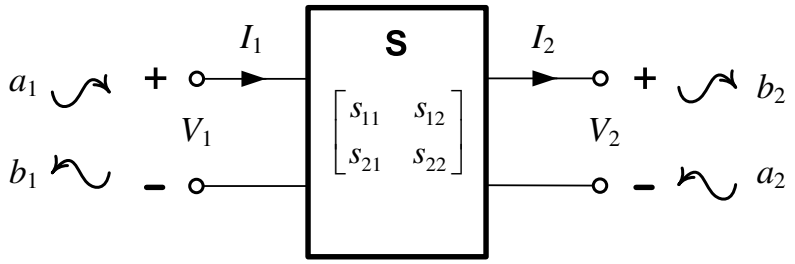

Figure 2.13: *Two port S-parameter network.*

2.7.2 S-parameter

To represent the wave flow of the network, the scattering parameter (S-parameter) is introduced. As the Z-parameter analysis, the S-parameter representations for Figure 2.13 are

$$\begin{bmatrix} b_1 \\ b_2 \end{bmatrix} = \mathbf{S} \begin{bmatrix} a_1 \\ a_2 \end{bmatrix} = \begin{bmatrix} s_{11} & s_{12} \\ s_{21} & s_{22} \end{bmatrix} \begin{bmatrix} a_1 \\ a_2 \end{bmatrix} \tag{2.35}$$

where

$$\begin{aligned} a_1 &= \frac{V_1 + z_0 I_1}{2\sqrt{z_0}}, \quad a_2 = \frac{V_2 - z_0 I_2}{2\sqrt{z_0}} \\ b_1 &= \frac{V_1 - z_0 I_1}{2\sqrt{z_0}}, \quad b_2 = \frac{V_2 + z_0 I_2}{2\sqrt{z_0}} \end{aligned} \tag{2.36}$$

are the traveling waves at the ports, and $\mathbf{S}$ is called scattering matrix. The measurement of S-parameters are made by connecting a matched load $z_L = z_0$ to one port and then another. Afterwards we have

$$s_{ii} = \left.\frac{b_i}{a_i}\right|_{z_L=z_0}, \text{ and } s_{ij} = \left.\frac{b_i}{a_j}\right|_{z_L=z_0} (i \neq j). \tag{2.37}$$

As for Z-parameters, if identical elements are assumed, we have $s_{11} = s_{22}$ and $s_{12} = s_{21}$. Furthermore, if the network is lossless, then [68]

$$\sum_{k=1}^{2} s_{ki} s_{ki}^* = 1, \text{ and } \sum_{k=1}^{2} s_{ki} s_{kj}^* = 0 \ (i \neq j). \tag{2.38}$$

The conversions between Z-parameters and S-parameters are [61]

$$\begin{aligned}\mathbf{S} &= \mathcal{F}_{Z-S}\{\mathbf{Z}\} = (\mathbf{Z} - z_0\mathbf{I})\,(\mathbf{Z}+z_0\mathbf{I})^{-1} \\ \mathbf{Z} &= \mathcal{F}_{S-Z}\{\mathbf{S}\} = (\mathbf{I} - \mathbf{S})^{-1}\,(\mathbf{I}+\mathbf{S})\,z_0.\end{aligned} \tag{2.39}$$

where z_0 is the characteristic impedance of the transmission line, usually $z_0 = 50\Omega$. The S-parameters can also be used to model MIMO systems. Some related works are discussed in Chapter 3 and more details can be found in [11, 18].

2.8 Summary

This chapter has reviewed the characteristics and classification of wireless propagation channels. To utilize space diversity, MIMO systems are introduced with various channel modeling and performance evaluation approaches. Basic antenna theory including antenna parameters, arrays, mutual coupling and simulation methods are discussed. The Z-parameters and S-parameters of port theory are briefly presented in the end. This chapter has covered all the outlined preliminaries, and will provide a good understanding for the remainder of this thesis.

As we can see MIMO systems offers significant improvement over SISO systems. Meanwhile, MC is an important effect in compact antenna arrays. How MC would affect MIMO system performance, and how to improve the performance of compact MIMO systems are really interesting. These two questions are the main topic of this thesis, while relevant measurement results will also be presented.

Chapter 3
Characteristics of compact arrays in MIMO systems

3.1 Introduction

This chapter investigates three commonly used parameters, signal correlation, received power and capacity in characterizing the performance of an antenna array in MIMO systems. When the antenna array becomes compact, the induced effect of MC will cause the system performance variation. Our research interest is focused on the compact receive end in MIMO systems.

The contributions of this chapter are:

- An overview of signal correlation is presented by classifying the calculation methods of the signal correlation into three groups. The consistency of different groups are proved by simulation. The advantage of using matching networks to reduce the signal correlation of a compact array is also discussed.
- The received power of a compact array is studied and two different methods are compared and unified through analytical comparison. Simulation results reveal the relation between the total array power, power difference of branches and the antenna separations of the compact array with matching networks in various scenarios.
- The MIMO capacity of a compact array with matching networks is investigated using S-parameter and Z-parameter approaches in circuit theory. The connection between the two methods are demonstrated in simulation. The capacity performance as a function of antenna separations in various scenarios is also examined.

The remainder of this chapter is organized as follows. Section 3.2 is focused on signal correlation. Section 3.3 discusses the received power. Section 3.4 studies the MIMO capacity. Section 3.5 summarizes the whole chapter.

Some key assumptions of the simulations in this chapter:

- a compact receiver with mutual coupling (MC) and matching networks is studied;
- if a MIMO system is studied, channel $\mathbf{H}$ is frequency-flat, rich scattering, and without a line-of-sight (LOS) propagation component;
- the receiver knows full channel state information (CSI) while transmitter has no CSI information;
- the transmit power is equally shared among the transmit antennas;
- transmitter and receiver arrays are linear;
- transmit antennas are sufficiently separated to avoid fading correlation or mutual coupling;
- the array elements are of identical polarization;
- the dimension of the arrays is negligible compared to the link distance.
- the results in this chapter are independent from the frequency as all the antenna separations are normalized to the wavelength. The modelling is suitable at frequencies from hundreds of MHz to several GHz.

3.2 Signal correlation

As mentioned in Chapter 2, the MIMO channel model can deviate from the i.i.d. model due to insufficient antenna separation or a non-ideal scattering model. As a result, the diversity advantage of the MIMO systems can be degraded by the correlation between the channel branches [4, 20, 60], which is called spatial fading correlation (SFC). Moreover, the insufficient antenna separation induced SFC can also be influenced by the introduction of matching networks [9, 11, 60, 69–71]. To unify the expression, we name both SFC and the correlation modified by the matching networks together as signal correlation (SC) in this thesis.

3.2.1 Definition of signal correlation

Two methods can be used to simulate the correlated MIMO channels [72]. One is the *non-theoretical* method according to the geometrical definition of the propagation environment us-

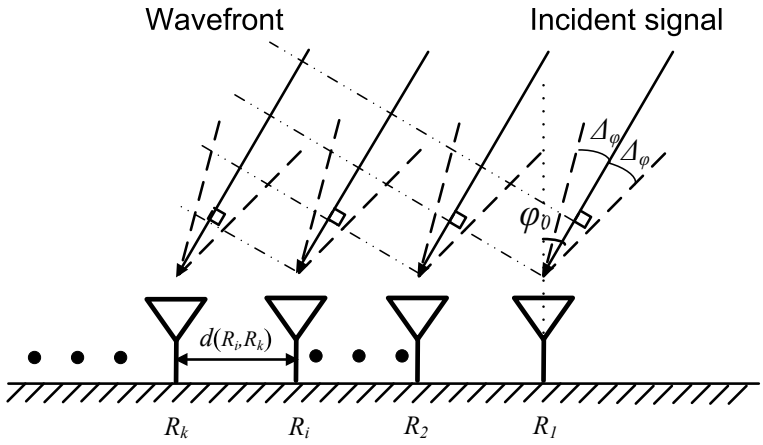

Figure 3.1: *Geometry of the linear receive subsystem in a MIMO system.*

ing ray-tracing techniques [73–78]. The other is the *theoretical* method using mathematical approximation with reduced numbers of channel parameters, e.g. mean angle-of-arrival (MAOA), mean angle-of-departure (MAOD), angular spread (AS). The most famous example of such a model is the Kronecker model [40, 45, 48]. The central idea of the ray tracing technique is to predict the realistic propagation environment including the effect of SC, while the Kronecker model allows one to separate the effect of SC from the classic i.i.d. channel matrix and it shows good consistency to the measured results for array dimension less than four [5, 48, 50].

Assuming the transmitters are sufficiently separated without SC at the transmit end. Also the omni-directional antenna pattern is considered for the antennas at both ends. We use the notation $h(R_i, T_j)$ to denote the channel branch between the jth transmitter and the ith receiver in an $M \times N$ MIMO system. From the definition, SC between the channel branches $h(R_i, T_j)$ and $h(R_k, T_l)$ can be expressed as [20]

$$\rho_h\left(R_iT_j, R_kT_l\right) = \frac{E\left\{h\left(R_i, T_j\right) h^*\left(R_k, T_l\right)\right\}}{\sqrt{E\left\{\left|h\left(R_i, T_j\right)\right|^2\right\} E\left\{\left|h\left(R_k, T_l\right)\right|^2\right\}}} \tag{3.1}$$

where $i, k = 1, 2, ..., N, j, l = 1, 2, ..., M$ and $|\cdot|$ is the absolute operation. The effect of SC between the channel branches is directly reflected by the voltage variation on the receive antennas. Moreover, the induced voltage on each element is intimately related to the far-field (FF) pattern of the array.

We consider the receive subsystem of a MIMO system as Figure 3.1. The notations φ_0 and Δ_φ are the MAOA and azimuth AS of the incident signal, respectively, and $d(R_i, R_k)$ denotes the

antenna spacing between the ith and the kth receivers. Thus, (3.1) can be modified to

$$\rho_{3d}\left(R_i, R_k\right) = \frac{\iint_{\Omega_s} E_{R_i}\left(\vartheta,\varphi\right) E^{*}_{R_k}\left(\vartheta,\varphi\right) p\left(\vartheta,\varphi\right) d\Omega_s}{\sqrt{\iint_{\Omega_s} \left|E_{R_i}\left(\vartheta,\varphi\right)\right|^2 p\left(\vartheta,\varphi\right) d\Omega_s} \cdot \sqrt{\iint_{\Omega_s} \left|E_{R_k}\left(\vartheta,\varphi\right)\right|^2 p\left(\vartheta,\varphi\right) d\Omega_s}} \tag{3.2}$$

where $E_{R_i}(\vartheta,\varphi)$ is the FF pattern of receive antenna R_i in the direction φ and ϑ, $p(\vartheta,\varphi)$ denotes the joint probability density function (pdf) of φ and ϑ, and Ω_s represents the solid angle with $d\Omega_s = \sin(\vartheta) d\vartheta d\varphi$ [7]. In addition, the integration limits are decided by the MAOA and AS in both azimuth and elevation directions. Equation (3.2) represents three-dimensional (3D) SC between elements R_i and R_k [20, 79]. Furthermore, it is proved in practical measurements that the transmitted energy is mainly distributed in the azimuth plane for outdoor scenarios [72, 80]. Then (3.2) can be reduced to two-dimensional (2D)

$$\rho_{2d}\left(R_i, R_k\right) = \frac{\int_{\varphi} E_{R_i}\left(\varphi\right) E^{*}_{R_k}\left(\varphi\right) p\left(\varphi\right) d\varphi}{\sqrt{\int_{\varphi} \left|E_{R_i}\left(\varphi\right)\right|^2 p\left(\varphi\right) d\varphi} \cdot \sqrt{\int_{\varphi} \left|E_{R_k}\left(\varphi\right)\right|^2 p\left(\varphi\right) d\varphi}} \tag{3.3}$$

where the integration limit is determined by the MAOA and AS in the azimuth direction, and other variables in (3.3) are related to the azimuth AOA φ only. Equation (3.3) will be used to analyze SC in the following discussion, and similar expressions to (3.3) can be found in [11, 60, 81]. No matter whether (3.2) or (3.3) is selected, it is apparent that the statistical distribution of the AOA $p(\varphi)$ is a critical parameter to determine the SC.

3.2.2 The impact of angle-of-arrival on signal correlation

Several kinds of statistical distributions have been reported to approximate the empirically measured distribution of AOA. In 2D scenario, the distribution of AOA can be recognized to follow a certain power azimuth spectrum (PAS). The three most widely adopted pdfs of PAS are uniform [18, 42, 82], Gaussian [83] and Laplacian [84–87]. It is verified by plenty of measurement results that the uniform distribution of AOA is a proper candidate in macrocell environment [88], and the truncated Laplacian distribution of AOA is widely accepted in micorcell environment [84–87]. These conclusions have also been cited by different standards bodies [80, 89, 90]. Thus, the uniform and truncated Laplacian pdfs are discussed.

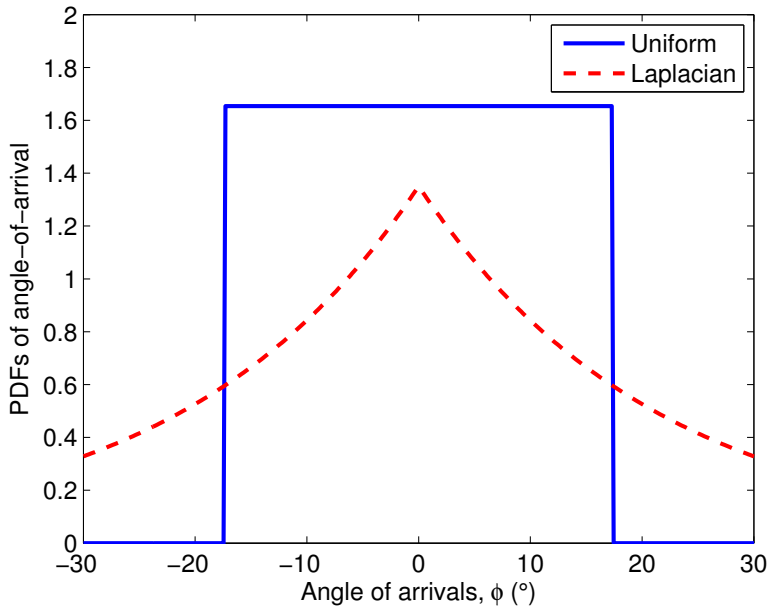

Figure 3.2: *The pdfs of the uniform and Laplacian AOA with AS = 30°.*

According to Figure 3.1, the uniform pdf of PAS is given by

$$p_U(\varphi) = \begin{cases} (2\Delta_\varphi^U)^{-1} & \text{for } \varphi \in \left[-\Delta_\varphi^U + \varphi_0, \Delta_\varphi^U + \varphi_0\right) \\ 0 & \text{otherwise} \end{cases} \tag{3.4}$$

where $\Delta_\varphi^U = \frac{\Delta_\varphi}{\sqrt{3}}$ is the standard deviation of $p_U(\varphi)$ [91]. The truncated Laplacian pdf can be expressed as

$$p_L(\varphi) = \begin{cases} \mu \left(\sqrt{2}\Delta_\varphi\right)^{-1} \cdot e^{-\sqrt{2}|\varphi/\Delta_\varphi|} & \text{for } \varphi \in [-\pi, \pi) \\ 0 & \text{otherwise} \end{cases} \tag{3.5}$$

where $\mu = 1/(1 - e^{-\sqrt{2}\pi/\Delta_\varphi})$ is the normalization constant to ensure that $p_L(\varphi)$ integrates to one and Δ_φ is equal to the standard deviation of $p_L(\varphi)$. The plot demonstration of the pdfs is shown in Figure 3.2. Besides the PAS distribution, the calculation of FF patterns of the array is the only factor which determines SC in (3.3).

3.2.3 Calculation approaches of signal correlation

According to the two methods evaluating the correlated MIMO channel, the calculation approaches of SC can be divided into three groups: *theoretical*, *semi-theoretical* and *non-theoreti-*

cal.

3.2.3.1 Calculation of signal correlation using array factor

We start from the *theoretical* method. As introduced in Chapter 2, without consideration of MC, the FF pattern of an array with identical elements can be generated from the same kind of isolated antenna pattern multiplying the array factor (AF). Furthermore, we assume the incident rays have uniform amplitudes and totally independent phases. Under these assumptions, (3.3) can be expressed according to Figure 3.1

$$\tilde{\rho}_{2d}\left(R_i, R_k\right) = \int_{-\pi+\varphi_0}^{\pi+\varphi_0} e^{\mathrm{j}\frac{2\pi}{\lambda}d(R_i,R_k)\sin(\varphi)} \cdot p\left(\varphi\right) d\varphi \tag{3.6}$$

where λ is the wavelength of the incident signal. To avoid time-consuming integrals, (3.6) can be further simplified in specific scenarios.

The so-called 'one-ring' model is an approximate example for the macrocell scenario in a suburban environment [4, 42]. The model assumes that the mobile station (MS) is surrounded by infinitely many, uniformly distributed scatters in azimuth while the base station (BS) is located far from the rich-scattered environment. In other words, we can recognize the PAS has the uniform pdf around the MS. In this scenario, Salz and Winters [82] conclude that (3.6) is asymptotic to

$$\tilde{\rho}_{2d}^{U}\left(R_i, R_k\right) \approx J_0\left(\frac{2\pi}{\lambda} d\left(R_i, R_k\right)\right) \tag{3.7}$$

where J_0 is the zeroth order Bessel function of the first kind. We note that (3.7) is only suitable for uniform linear array (ULA) with full AS case, i.e. $\Delta_\varphi = \pi$.

The approximate model for a microcell scenario has been reported recently in [72] with closed-form expression of Laplacian PAS for ULA,

$$\tilde{\rho}_{2d}^{L}\left(R_i, R_k\right) \approx \mu \cdot e^{\mathrm{j}\frac{2\pi}{\lambda}d(R_i,R_k)\sin(\varphi_0)} \cdot \left(1 + \frac{\Delta_\varphi^2}{2}\left(\frac{2\pi}{\lambda} d\left(R_i, R_k\right)\cos\varphi_0\right)^2\right)^{-1} \tag{3.8}$$

However, (3.8) only agrees well with (3.6) when AS is less than 10° [72]. As both (3.7) and (3.8) have their own limitations, (3.6) is still essential for calculating SC in scenarios with arbitrary AS.

When a compact receive array is considered, (3.6), (3.7) and (3.8) are not valid as the MC effect has not been included. The SC with MC can be calculated theoretically in two ways. One is combining the MC matrix (introduced in Chapter 2 on page 26) and steering vector (SV) [63]; the other is based on the circuit theory [22]. We note that unless specified, the following analysis is focused on a two-element single-mode compact receive array.

Combining SV of the array without MC $\mathbf{a}_{nc}(\varphi) = [\ 1 \quad e^{\mathrm{j}\tau}\ ]^T$, (2.31) on page 26 and (3.6), the SC expression with MC is given [63]

$$\rho_{mc} = \frac{2\mathrm{Re}\left\{k_r\right\} + \left(1+|k_r|^2\right)\mathrm{Re}\left\{\tilde{\rho}_{2d}^{12}\right\} + \mathrm{j}\left(1-|k_r|^2\right)\mathrm{Im}\left\{\tilde{\rho}_{2d}^{12}\right\}}{\sqrt{\left(1+|k_r|^2+2\mathrm{Re}\left\{k_r\right\}\mathrm{Re}\left\{\tilde{\rho}_{2d}^{12}\right\}\right)^2 - \left(2\mathrm{Im}\left\{\tilde{\rho}_{2d}^{12}\right\}\right)^2}} \tag{3.9}$$

where $\tilde{\rho}_{2d}^{12}$ is the abbreviated expression of $\tilde{\rho}_{2d}(R_1, R_2)$. Also $k_r = k_{12}/k_{11}$ is the normalized coupling ratio, where k_{11} and k_{12} are the elements of the MC matrix $\mathbf{K}_{mc}$ in (2.31) on page 26. Notations $\mathrm{Re}\{\cdot\}$ and $\mathrm{Im}\{\cdot\}$ denote the real and imaginary part of a complex number/vecter/matrix, respectively. Also $\tilde{\rho}_{2d}^{12}$ is equivalent to the so-called open-circuit (OC) correlation [11, 22, 60], which means the SC is calculated using the FF pattern (or voltage) of each element when other element(s) are open-circuited. Although (3.9) clearly includes the MC effect into the SC calculation of a compact array, it does not reflect the impact of matching impedances on SC performance. The following method covers this point.

Based on circuit theory, the SC between the two coupled elements with matching networks is [22]

$$\begin{aligned}\tilde{\rho}_{mc} \;=\; & \frac{\tilde{\rho}_{2d}^{12}\left|z_{11}+z_L\right|^2 + \left(\tilde{\rho}_{2d}^{12}\right)^*\left|z_{12}\right|^2 - 2\mathrm{Re}\left\{\left(z_{11}+z_L\right)z_{12}^*\right\}}{\sqrt{\left|z_{11}+z_L\right|^2+\left|z_{12}\right|^2-2\mathrm{Re}\left\{\tilde{\rho}_{2d}^{12}\left(z_{11}+z_L\right)z_{12}^*\right\}}} \\ & \cdot\frac{1}{\sqrt{\left|z_{11}+z_L\right|^2+\left|z_{12}\right|^2-2\mathrm{Re}\left\{\left(\tilde{\rho}_{2d}^{12}\right)^*\left(z_{11}+z_L\right)z_{12}^*\right\}}}\end{aligned} \tag{3.10}$$

utilizing the voltage-current relations. It is obvious that (3.10) contains both the MC effect and the impact of the matching networks on SC of the compact receive end. Nevertheless, one deficiency of (3.10) is that it is only capable of calculating SC for a single-port match (SPM). For multiport-conjugate matching techniques, we shall resort to the S-parameter approach.

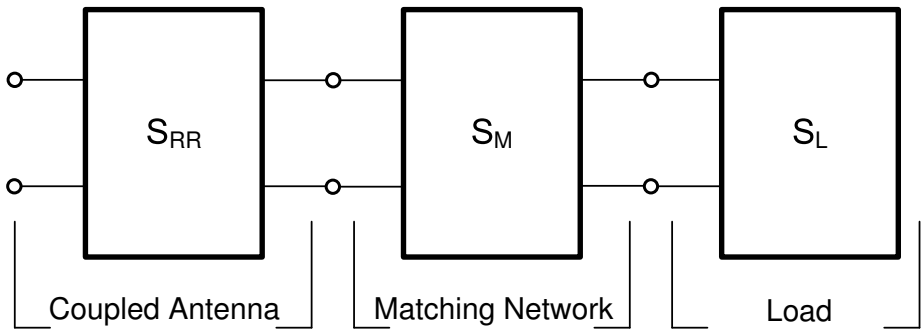

Figure 3.3: *Block diagram of a compact receive array with multiport matching network and loads.*

3.2.3.2 Calculation of signal correlation using scattering parameter

The network model of the compact receive end with matching networks is displayed in Figure 3.3, where $\mathbf{S}_{RR}$ is the S-parameter transform of $\mathbf{Z}_{RR}$, and the S-parameters of the matching network are defined as [11, 18]

$$\mathbf{S}_M = \begin{bmatrix} \mathbf{S}_{11} & \mathbf{S}_{12} \\ \mathbf{S}_{21} & \mathbf{S}_{22} \end{bmatrix}. \tag{3.11}$$

The 2D covariance matrix before the signal goes through the matching network block (measured at the coupled antenna input ports) is

$$\mathbf{R}_{mc} = \int_{\varphi} (\mathbf{I} - \mathbf{S}_{RR})\, \mathbf{e}_{oc}^{H}(\varphi)\, \mathbf{e}_{oc}(\varphi)\, (\mathbf{I} - \mathbf{S}_{RR})^{H} p(\varphi) d\varphi \tag{3.12}$$

where $\mathbf{e}_{oc}$ is the row vector of FF patterns of each antenna in the compact array when all other antenna elements are open-circuited. Instead of approximating the FF patterns of the array using AF as the *theoretical* method, we generate the antenna impedances and FF patterns of the compact array in an electromagnetic environment simulated by FEKO [65]. Some other related work also have done similar simulations using either Makarov code [60] or FDTD method [11], and both present very similar results. Compared to the *theoretical* method, data of antenna impedances and FF patterns obtained in this way are more appropriate to that in the real world. However, the total calculation of SC is still based on simulation. We call this method *semi-theoretical*.

If a uniformly distributed PAS with full AS, and identical antenna elements are assumed, using (3.11) and (3.12), we obtain the general covariance matrix including matching networks for

both SPM and multiport-conjugate match (MCM) as [11]

$$\mathbf{R}_L = \mathbf{S}_{21} \left(\mathbf{I} - \mathbf{S}_{RR}\mathbf{S}_{11}\right)^{-1} \mathbf{R}_{mc} \left(\mathbf{I} - \mathbf{S}_{RR}\mathbf{S}_{11}\right)^{H(-1)} \mathbf{S}_{21}^{H}. \tag{3.13}$$

Then the SC between the two antenna elements is

$$\rho_s = \frac{(\mathbf{R}_L)_{12}}{\sqrt{(\mathbf{R}_L)_{11} \cdot (\mathbf{R}_L)_{22}}}. \tag{3.14}$$

where $(\cdot)_{ij}$ denotes the (i, j)-th element of a matrix.

By choosing $\mathbf{S}_{11}$ appropriately in (3.13), we can get the desired ρ_s in (3.14).

$$\mathbf{S}_{11} = \begin{cases} \mathcal{F}_{Z-S}\left\{z_L \cdot \mathbf{I}\right\} & \text{for SPM} \\ \mathbf{S}_{RR}^{H} & \text{for MCM} \end{cases} \tag{3.15}$$

We assume the matching network is equipped with passive and reactive loads, thus the system obeys the lossless and reciprocal characteristic [11],

$$\begin{aligned} \mathbf{S}_{11}^{H}\mathbf{S}_{11} + \mathbf{S}_{21}^{H}\mathbf{S}_{21} &= \mathbf{I} \\ \mathbf{S}_{12}^{H}\mathbf{S}_{12} + \mathbf{S}_{22}^{H}\mathbf{S}_{22} &= \mathbf{I} \\ \mathbf{S}_{11}^{H}\mathbf{S}_{12} + \mathbf{S}_{21}^{H}\mathbf{S}_{22} &= 0. \end{aligned} \tag{3.16}$$

We note that the only difference between (3.16) and (2.38) on page 30 is that (3.16) concerns multiple antennas while in (2.38) only one antenna is involved. Substitution of the SVD of $\mathbf{S}_{ij} = \mathbf{D}_{ij}\mathbf{\Lambda}_{ij}^{1/2}\mathbf{V}_{ij}^{H}$ to (3.16) we have

$$\mathbf{V}_{21}\mathbf{\Theta}_{21} = \mathbf{V}_{11}, \qquad \mathbf{\Lambda}_{21} = \mathbf{I} - \mathbf{\Lambda}_{11} \tag{3.17}$$

$$\mathbf{V}_{12}\mathbf{\Theta}_{12} = \mathbf{V}_{22}, \qquad \mathbf{\Lambda}_{12} = \mathbf{I} - \mathbf{\Lambda}_{22} \tag{3.18}$$

where $\mathbf{D}_{ij}$ and $\mathbf{V}_{ij}$ are unitary matrices; $\mathbf{\Theta}_{ij}$ is diagonal phase shift matrix with arbitrary complex elements of unit magnitude [11]. From (3.17) we can see that with chosen $\mathbf{S}_{11}$, multiple values of $\mathbf{S}_{12}$ can be generated due to multiple selections of $\mathbf{D}_{ij}$. When $\mathbf{D}_{ij}$ is chosen as $\mathbf{I}$, $\mathbf{R}_L$ in (3.13) will be diagonal, otherwise $\mathbf{R}_L$ will not be diagonal.

Combining (3.15) with the input reflection expression, the covariance matrix equations for two

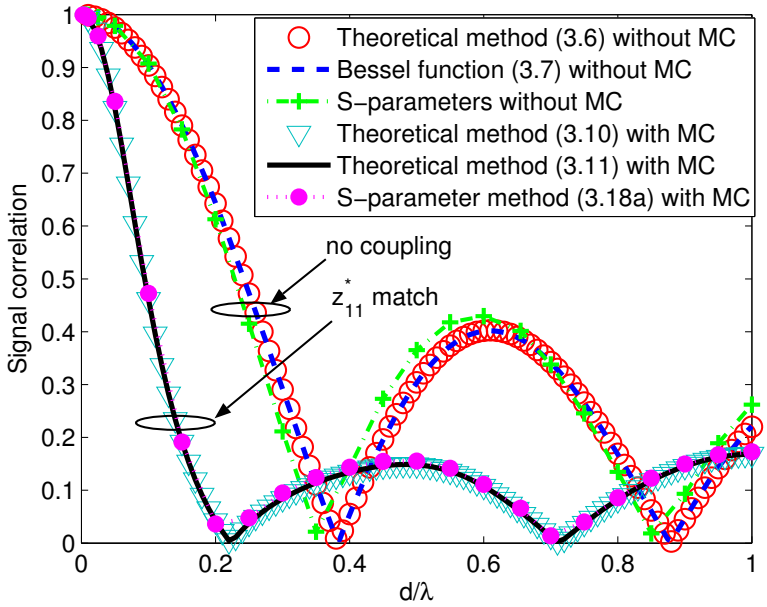

Figure 3.4: *The 2D SC of a two-dipole array with antenna spacing d using different methods with and without mutual coupling and z_{11}^* match.*

special matching networks can be found [11].

$$\mathbf{R}_{L,oc} = 4\left(\mathbf{I}-\mathbf{S}_{RR}\right)^{-1}\mathbf{R}_{mc}\left(\mathbf{I}-\mathbf{S}_{RR}^{H}\right)^{-1} \tag{3.19a}$$

$$\mathbf{R}_{L,z_0} = \mathbf{R}_{L} \tag{3.19b}$$

where $\mathbf{R}_{L,oc}$ and $\mathbf{R}_{L,z_0}$ are the covariance matrix for the OC match and characteristic impedance (z_0) match, respectively. We point out that the $\mathbf{R}_{L,oc}$ in (3.19a) is equivalent to the $\tilde{\rho}_{2d}^{12}$ in (3.9) and (3.10) of the *theoretical* method. Hence, the calculation of SC using S-parameters covers all the matching networks used to decouple the compact array.

3.2.3.3 Calculation of signal correlation in measurement

Both antenna impedances and FF patterns are able to be measured in practice. The measured data can be used to calculate 3D SC using (3.2), and 2D SC using (3.3), (3.9) or (3.10). This is what we call the *non-theoretical* method. Some implementation work related to SC can be found in [25, 92, 93]. However, not much work has been done in evaluation of SC for compact arrays with various matching networks except in [25], which is an important part of the novel contribution in Chapter 4.

3.2.4 Improvement of correlation performance using matching networks

To study the advantage of introducing matching networks into compact arrays, simulation results are presented. The 2D SC performance is focused, and identical half-wave length dipoles are illustrated. Also we assume that the signals are incident mainly from the broadside, i.e. MAOA $\varphi_0 = 0^\circ$ with full AS, and the distribution of PAS is uniform. Corresponding to the selected approaches for the calculation of SC, the self and mutual impedances of the dipoles are simulated using the theoretical EMF equations on page 25 for *theoretical* methods, and simulation results in FEKO [65] for *semi-theoretical* methods in Figure 3.4, 3.5 and 3.6. The diameter of the dipole in FEKO simulation is $\lambda/400$.

In Figure 3.4 the SC performance of two compact dipoles with no coupling is simulated using *theoretical* methods, 2D SC (3.6), approximated Bessel function (3.7) and *semi-theoretical* S-parameter approach in (3.19a). While the SC of the same array with the commonly used self-conjugate (z_{11}^*) match is generated using *theoretical* methods (3.9), (3.10), and *semi-theoretical* S-parameter approach (3.13). For the no coupling case, the two *theoretical* methods (theoretical 2D SC and Bessel function approximation) agree very well with each other, whereas the *semi-theoretical* S-parameter approach is slightly shifted from the *theoretical* methods due to the antenna impedances and FF pattern differences between the ideal and realistic dimensioned dipoles. However, the *theoretical* and *semi-theoretical* approaches for the z_{11}^* matched case are perfectly matched. The same consistency is found in simulations of the same coupled array with other matching networks not shown in Figure 3.4, which indicates that the *theoretical* and *semi-theoretical* methods are interchangeable for calculating the SC of coupled array with matching networks. Figure 3.4 also tells us that introducing proper matching networks into the compact arrays can efficiently reduce SC for small antenna spacings ($d < 0.3\lambda$) compared to the no coupling case.

Figure 3.5 demonstrates the SC performance of a compact two-dipole array with different matching networks using the *semi-theoretical* S-parameter approach as it covers both SPM and MCM cases. It can be seen that in general the compact array with any kind of matching networks outperforms that without MC (OC match) for $d < 0.3\lambda$. When $d \leq 0.2\lambda$, the z_0 match and z_{11}^* match provide similar performance, while the input impedance (z_{in}) match[1] and MCM give the lowest SC. The SC curves with z_{in} match and MCM overlap with each other over the whole range of antenna separations as they both involve the effect of the mutual

[1]The derivation of the z_{in} impedance match of two coupled antenna array is given in Appendix A.

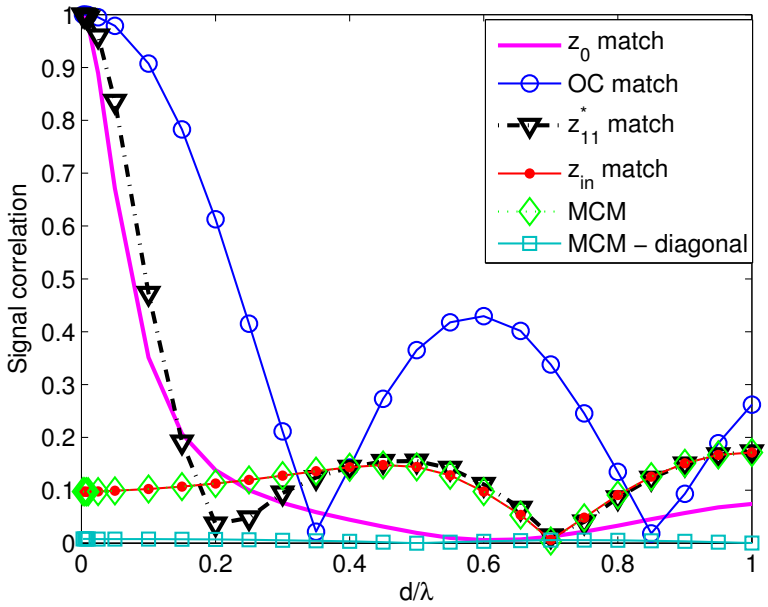

Figure 3.5: *The SC performance of a two-dipole array versus antenna spacing d with various matching networks using the S-parameter approach.*

impedances[2], and the z_{11}^* match performs nearly the same as them for $d > 0.3\lambda$, which implies that the advantage of the z_{in} match and MCM disappears for large antenna spacings. When $\mathbf{D}_{21}$ equals to $\mathbf{I}$, $\mathbf{R}_L$ for MCM is a diagonal matrix. Thus, in theory the coupled receiver with MCM can offer zero SC for the full range of antenna separations and with any AS values by choosing the appropriate MCM network [11].

Next we study the impact of the distributions of PAS and AS variation on the SC performance of the coupled array with matching networks. If the matrix $\mathbf{S}_{21}$ is not diagonal, MCM gives the same performance as z_{in} match in Figure 3.5. Hence, we plot the SC with various SPMs in scenarios of uniform and Laplacian distributed PAS with AS $15°$, $40°$, and $90°$ in Figure 3.6. For any coupled case, the SC decreases when AS increases with any PAS distribution. Furthermore, no matter which PAS distribution and what value of AS are chosen, the SC of the coupling array with any kind of matching network always outperforms the corresponding uncoupled case when $d < 0.4\lambda$. Meanwhile, the z_{in} match gives the best performance among all kinds of matching networks in each scenario at $d < 0.4\lambda$. We note that the severe jitter of z_{in} performance in each case at very small antenna spacing is due to the double effect of MC and decoupling of z_{in} at very close antenna separations. When $d > 0.4\lambda$, the SC curves with

[2]The results in Figure 3.5 and [60] are slightly different because the matrix $\mathbf{S}_{21}$ is not uniquely determined by (3.16).

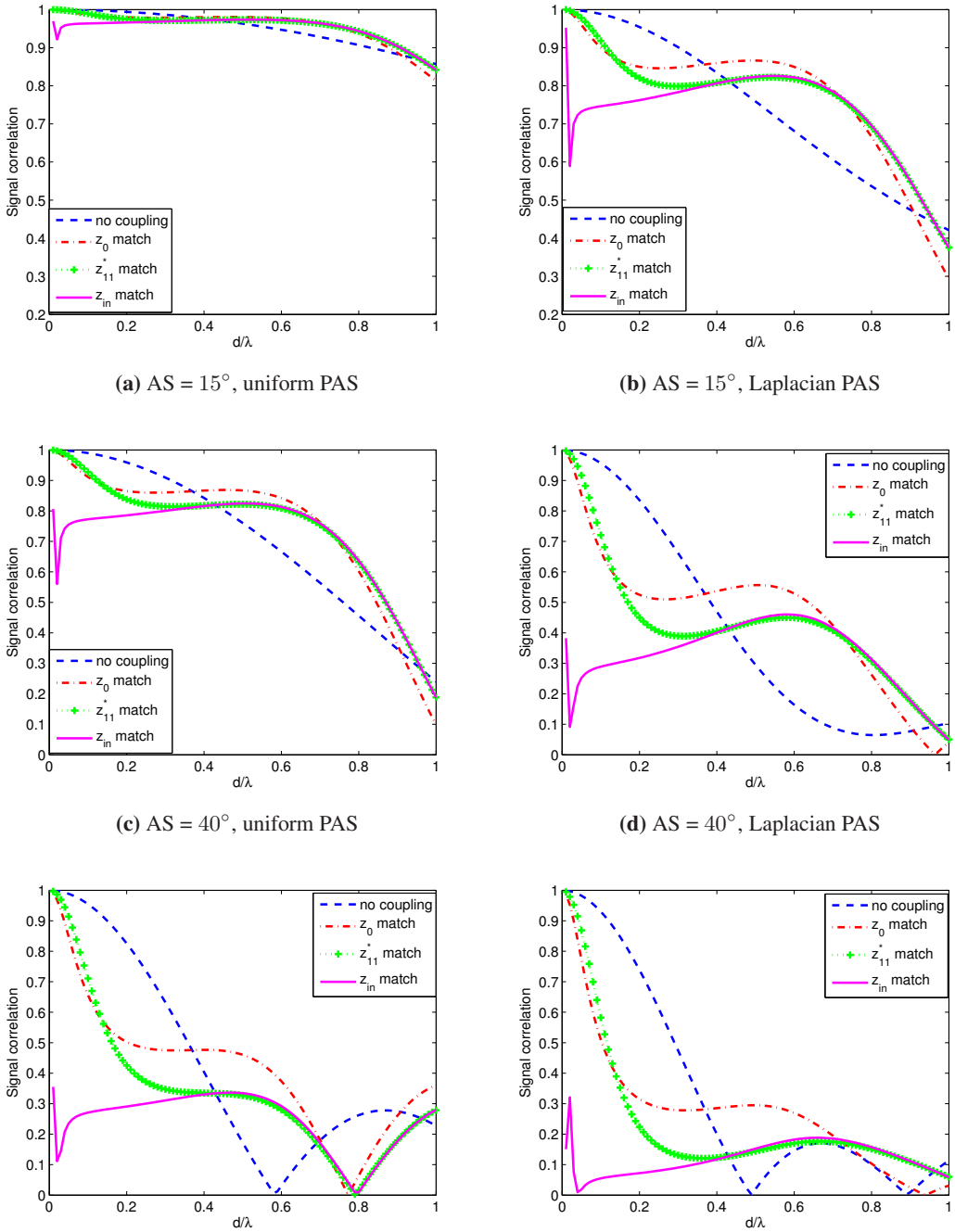

(a) AS = 15°, uniform PAS

(b) AS = 15°, Laplacian PAS

(c) AS = 40°, uniform PAS

(d) AS = 40°, Laplacian PAS

(e) AS = 90°, uniform PAS

(f) AS = 90°, Laplacian PAS

Figure 3.6: *The SC comparison with different matching networks in scenarios of uniform and Laplacian PAS with various AS values.*

z_{11}^* match and z_{in} match overlap with each other in any scenario, which extends our conclusion of Figure 3.5 that using special matching networks to improve the SC performance works efficiently for compact arrays, and it is not related to the changing of the environment. It is easy to understand that the MC effect decreases when d increases, thus the advantage of decoupling reduces for increasing d as well. Comparing the SC between uniform and Laplacian PAS with the same AS, the SC for the Laplacian PAS always performs better than that with the uniform PAS for identical matching network pairs at any antenna spacings. This is because that the arriving multipaths are only highly correlated within 10° in Laplacian distribution as in Figure 3.2, while they are evenly highly correlated in the whole AOA span in uniform distribution. The z_{in} match which provides the lowest SC among all the matching cases still performs better in the Laplacian PAS than in the uniform PAS when AS = 90° and $d < 0.4\lambda$. Hence, we can use the matching technique to reduce the SC effectively for compact arrays regardless of the PAS distributions and values of AS.

3.3 Received power

Since SC only partially reflects the diversity performance of a compact array, the absolute received power is also important. The total average received power of a compact array with MC and MCM has been investigated in [94], and it concludes that by introducing proper matching networks, the compact array can still provide the diversity advantage for a ULA with the number of elements less than four. However, the received power for each antenna branch has not been studied until recently in [22, 63, 79, 95]. All of the works confirm that the matching networks can be properly chosen to increase the received power of each antenna branch for a two-element half-wavelength dipole array.

3.3.1 Received power of compact array with matching networks

Analytical studies of the received power for each antenna branch are reported in both [63] and [22] with similar results though they are obtained from a different viewpoint. The discussion in [63] is based on the MC matrix combined with SV of the antenna array, while the derivation in [22] is presented from the circuit theory point of view. The result in [22] is more attractive than that in [63] because it also reveals the existence of the optimum impedances which maximize the received power, while [63] only assumes the receivers to be z_{11}^* matched. In theory [63] and

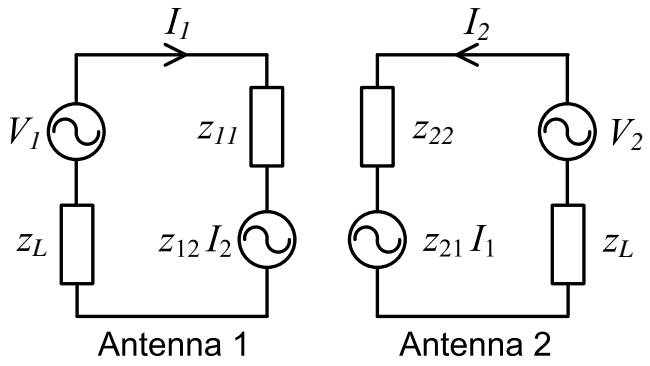

Figure 3.7: *Equivalent circuit of two mutual coupled antennas with matching impedances.*

[22] should present identical results of the impact of matching networks on the received power. Nevertheless, the simulation results are significantly different. In the following subsection we will look into the two methods and find out the cause of the divergence.

3.3.1.1 Received power from the circuit theory point of view

The analytical equivalent circuit for two coupled antennas is showed in Figure 3.7. Identical load impedances z_L are used for both elements. Notations z_{11}, z_{22} and z_{12}, z_{21} are the self and mutual impedances of antenna 1 and 2, respectively. Also V_1 and V_2 are OC voltages which are determined by the surrounding propagation environment, and they are correlated due to the insufficient antenna spacing. The induced current in the two circuits are denoted as I_1 and I_2. In *n*-port theory, the receive system in Figure 3.7 can be represented by the voltage-current relations [7]

$$V_1 = (z_{11} + z_L)I_1 + z_{12}I_2 \tag{3.20a}$$

$$V_2 = (z_{22} + z_L)I_2 + z_{21}I_1 \tag{3.20b}$$

We assume the antenna elements are identical and define a complex OC correlation coefficient

$$\rho_{oc} = \frac{E\{V_1 V_2^*\}}{E\{V_1 V_1^*\}}. \tag{3.21}$$

Actually the ρ_{oc} is equivalent to the $\tilde{\rho}_{2d}^{12}$ in (3.9) and (3.10). Then we have I_1 as

$$I_1 = \frac{V_1(z_{11} + z_L) - V_2 z_{12}}{(z_{11} + z_L)^2 - z_{12}^2}. \tag{3.22}$$

Normalizing the received power of one antenna branch to the power of single antenna with z_{11}^* match, i.e. $P_1 = E\{r_L|I_1|^2\}/E\{r_{11}|I_0|^2\}$ (where I_0 is the induced current of a single antenna) and combining (3.21), (3.22), the received power of antenna 1 is given [22]

$$P_1 = 4r_L r_{11} \cdot \frac{|z_{11}+z_L|^2 + |z_{12}|^2 \overbrace{-2\mathrm{Re}\left\{\rho_{oc}\left(z_{11}+z_L\right) z_{12}^*\right\}}^{\mathrm{D}_1}}{\left|\left(z_{11}+z_L\right)^2 - z_{12}^2\right|^2} \tag{3.23}$$

where r_L is the resistive part of z_L. We note that z_{11} is always larger than z_{12}, thus the denominator of (3.23) cannot be zero. Similar expressions for P_2 can be obtained by the same approach,

$$P_2 = 4r_L r_{11} \cdot \frac{|z_{11}+z_L|^2 + |z_{12}|^2 - 2\mathrm{Re}\left\{\rho_{oc}^*\left(z_{11}+z_L\right) z_{12}^*\right\}}{\left|\left(z_{11}+z_L\right)^2 - z_{12}^2\right|^2}. \tag{3.24}$$

Then the total received power and the power difference of the two antennas are

$$P_{\text{total}} = P_1 + P_2, \tag{3.25}$$

$$P_{\text{diff}} = |P_1 - P_2|. \tag{3.26}$$

3.3.1.2 Received power based on the mutual coupling matrix and array factor

According to Figure 3.1, the 2D SV of an antenna array with two identical and omni-directional elements and no MC is $\mathbf{a}_{nc}(\varphi) = [\ 1 \quad e^{\mathrm{j}\tau}\ ]^T$, where $\tau = \frac{2\pi}{\lambda} d(R_1, R_2)\sin(\varphi)$. Then the modified SV with MC of the same array can be represented as

$$\begin{aligned}\mathbf{a}_{mc}(\varphi) = \mathbf{K}_{mc} \times \mathbf{a}_{nc}(\varphi) &= \begin{bmatrix} k_{11} & k_{12} \\ k_{12} & k_{11} \end{bmatrix} \times \begin{bmatrix} 1 \\ e^{\mathrm{j}\tau} \end{bmatrix} \\ &= \begin{bmatrix} k_{11} + k_{12}\cdot e^{\mathrm{j}\tau} \\ k_{11}\cdot e^{\mathrm{j}\tau} + k_{12} \end{bmatrix} = \begin{bmatrix} k_{11} + k_{12}\cdot e^{\mathrm{j}\tau} \\ \left(k_{11} + k_{12}\cdot e^{-\mathrm{j}\tau}\right)\cdot e^{\mathrm{j}\tau} \end{bmatrix}\end{aligned} \tag{3.27}$$

Also (3.27) can be seen as a distortion of the array FF pattern with MC

$$\mathbf{e}_{mc}(\varphi) = \begin{bmatrix} E_{mc}^1(\varphi) \\ E_{mc}^2(\varphi) \end{bmatrix} = \begin{bmatrix} k_{11} + k_{12}\cdot e^{\mathrm{j}\tau} \\ k_{11} + k_{12}\cdot e^{-\mathrm{j}\tau} \end{bmatrix}. \tag{3.28}$$

where $E^i_{mc}(\varphi)$ is the FF pattern of the ith coupled antenna. Referring to [8], the mean received power of the ith antenna element is defined as

$$\tilde{P}_i = \int_{-\pi+\varphi_0}^{\pi+\varphi_0} |E_{R_i}(\varphi)|^2 \, p(\varphi) \, d\varphi. \tag{3.29}$$

We substitute (3.27) into (3.29), and the received power of the receive antenna 1 is given

$$\begin{aligned}
\tilde{P}_1 &= \int_{-\pi+\varphi_0}^{\pi+\varphi_0} \left|E^1_{mc}(\varphi)\right|^2 p(\varphi) \, d\varphi \\
&= \int_{-\pi+\varphi_0}^{\pi+\varphi_0} \left(|k_{11}|^2 + |k_{12}|^2 + k_{11} \cdot e^{-\mathrm{j}\tau} \cdot k^*_{12} + k^*_{11} \cdot k_{12} \cdot e^{\mathrm{j}\tau}\right) p(\varphi) \, d\varphi \\
&= |k_{11}|^2 \cdot \int_{-\pi+\varphi_0}^{\pi+\varphi_0} \left(1 + |k_r|^2 + k^*_r \cdot e^{-\mathrm{j}\tau} + k_r \cdot e^{\mathrm{j}\tau}\right) p(\varphi) \, d\varphi \\
&= |k_{11}|^2 \cdot \left(1 + |k_r|^2 + 2 \int_{-\pi+\varphi_0}^{\pi+\varphi_0} \mathrm{Re}\left\{k_r \cdot e^{\mathrm{j}\tau}\right\} p(\varphi) \, d\varphi\right) \\
&= |k_{11}|^2 \cdot \left(1 + |k_r|^2 + 2 \int_{-\pi+\varphi_0}^{\pi+\varphi_0} \left[\mathrm{Re}\{k_r\} \cos(\tau) - \mathrm{Im}\{k_r\} \sin(\tau)\right] p(\varphi) \, d\varphi\right)
\end{aligned} \tag{3.30}$$

where $k_r = k_{12}/k_{11}$ as defined in (3.9) on page 38. When the MC effect is ignored, ρ_{oc} can be further expanded from (3.6) as

$$\rho_{oc} = \int_{-\pi+\varphi_0}^{\pi+\varphi_0} e^{\mathrm{j}\tau} p(\varphi) \, d\varphi = \int_{-\pi+\varphi_0}^{\pi+\varphi_0} \left[\cos(\tau) + \mathrm{j}\sin(\tau)\right] p(\varphi) \, d\varphi = \rho_{xx} + \mathrm{j}\rho_{xy} \tag{3.31}$$

where ρ_{xx} and ρ_{xy} are the real and imaginary parts of ρ_{oc}. Rearranging (3.31) into (3.30), the received power of antenna 1 is given [63]

$$\tilde{P}_1 = |k_{11}|^2 \cdot [1 + |k_r|^2 + \underbrace{2 \cdot \mathrm{Re}\{k_r\} \cdot \rho_{xx} + 2 \cdot \mathrm{Im}\{k_r\} \cdot \rho_{xy}}_{\mathrm{D}_2}] \tag{3.32}$$

The received power $\tilde{P}_2$ can be derived in the similar way.

3.3.1.3 Derivation of the appropriate received power expression

Numerical results for equations (3.23) and (3.32) are plotted in Figure 3.8 and 3.9, respectively. For simplicity two ideal dipole antennas spaced by 0.05λ are chosen for the received power comparison. Moreover, uniform PAS is assumed with the MAOA from broadside and full AS.

The differences of the simulation results between (3.23) and (3.32) are obvious in Figure 3.8(a)

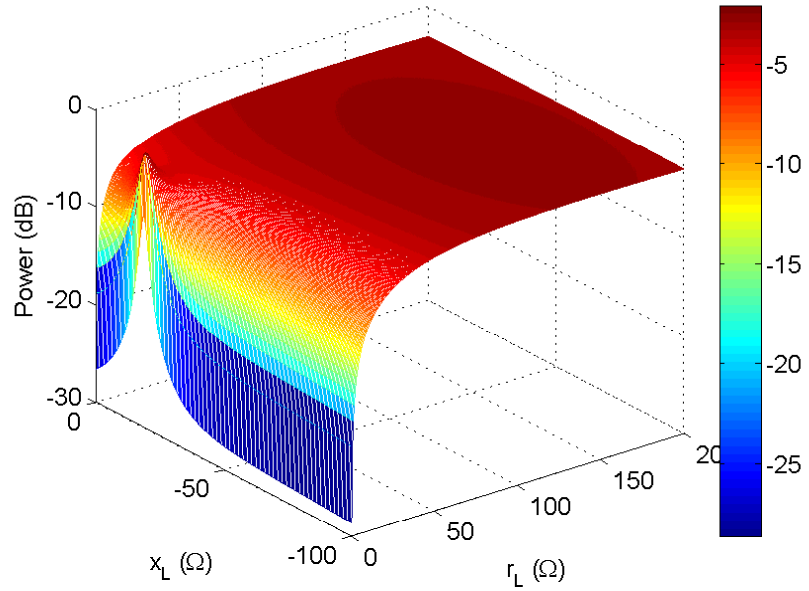

(a)

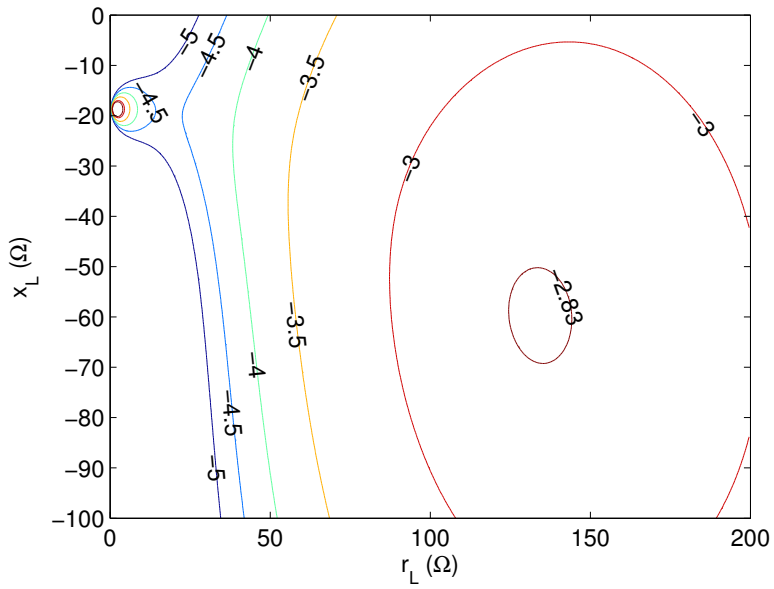

(b)

Figure 3.8: *The 3D and contour plots of P_1 in dB at one antenna as a function of the resistive (r_L) and reactive (x_L) parts of the load impedances.*

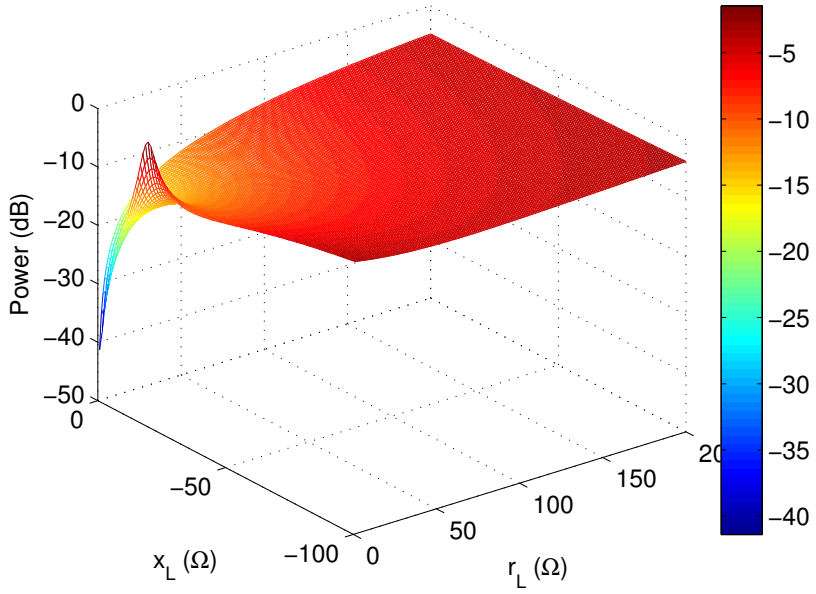

(a)

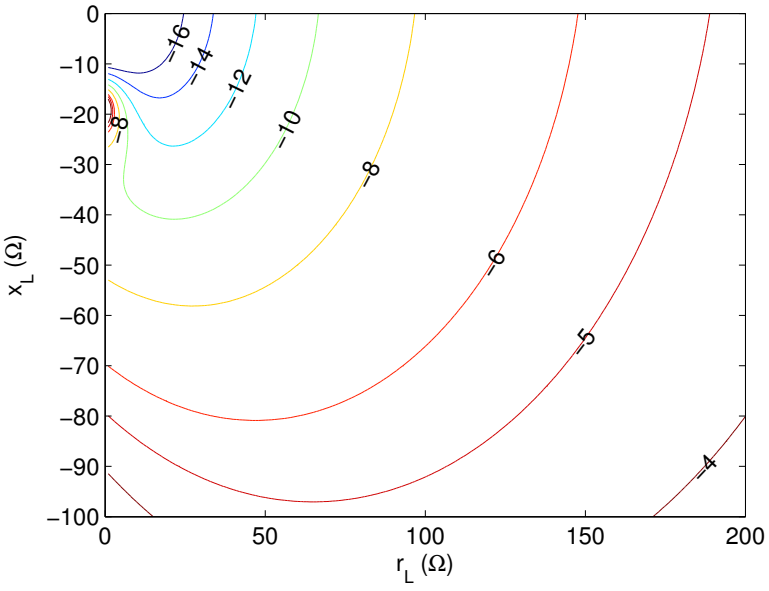

(b)

Figure 3.9: *The 3D and contour plots of $\tilde{P}_1$ in dB at one antenna as a function of the resistive (r_L) and reactive (x_L) parts of the load impedances.*

and 3.9(a), and even more clearly in Figure 3.8(b) and 3.9(b). In Figure 3.8 the two maxima phenomenon agrees well with the results in [22], which has also been reported earlier in [9] though only the resistive antenna and load are considered. The highest received power point of antenna 1 in Figure 3.8(b) is about -2.8dB. Hence, the total power received by both antennas should be around 0dB, which is equal to the isolated single antenna case in Figure 3.8. This is quite reasonable as the antenna spacing is so small that it looks like one single antenna element. However, in Figure 3.9 the double maxima characteristic in Figure 3.8 is substituted by only one maximum point around $(r_L, x_L) = (0, -18)\Omega$ (one of the maxima in Figure 3.8(b)). Another suspicious phenomenon in Figure 3.9 is that when r_L approaches zero and x_L deviates from the matching point at -20Ω, the received power should decrease as in Figure 3.8(b) rather than increase in Figure 3.9(b) because the power is stored not received from a circuit theory point of view.

To find the reason for the divergence between the two methods, we look back to (3.23) and (3.32). We express $\rho_{oc} = \rho_{xx} + \mathrm{j}\rho_{xy}$, $z_{11} = r_{11} + x_{11}$, $z_{12} = r_{12} + x_{12}$, and $z_L = r_L + x_L$. Then the part D_1 in (3.23) can be expanded as

$$\begin{aligned}
\mathrm{D}_1 &= -2\mathrm{Re}\left\{\rho_{oc}\left(z_{11}+z_L\right)z_{12}^*\right\} \\
&= -2\cdot\mathrm{Re}\left\{\left(\rho_{xx}+\mathrm{j}\rho_{xy}\right)\left[\left(r_{11}+r_L\right)+\mathrm{j}\left(x_{11}+x_L\right)\right]\left(r_{12}-\mathrm{j}x_{12}\right)\right\} \\
&= -2\cdot\mathrm{Re}\big\{\left(\rho_{xx}+\mathrm{j}\rho_{xy}\right)\left\{\left[r_{12}\left(r_{11}+r_L\right)+x_{12}\left(x_{11}+x_L\right)\right]\right. \\
&\quad \left.+\mathrm{j}\left[r_{12}\left(x_{11}+x_L\right)-x_{12}\left(r_{11}+r_L\right)\right]\right\}\big\} \\
&= -2\big\{\rho_{xx}\left[r_{12}\left(r_L+r_{11}\right)+x_{12}\left(x_L+x_{11}\right)\right] \\
&\quad +\rho_{xy}\left[x_{12}\left(r_L+r_{11}\right)-r_{12}\left(x_L+x_{11}\right)\right]\big\}.
\end{aligned} \tag{3.33}$$

Calculated in Maple [96], k_{11}, k_{12} and k_r can be expressed by the load and antenna impedances

$$k_{11} = \frac{z_L\left(z_L+z_{11}\right)}{\left(z_L+z_{11}\right)^2 - z_{12}^2}, k_{12} = \frac{-z_L z_{12}}{\left(z_L+z_{11}\right)^2 - z_{12}^2}, k_r = \frac{-z_{12}}{z_L+z_{11}} \tag{3.34}$$

where k_r can be further expanded as:

$$k_r = \frac{-z_{12}}{z_L+z_{11}} = \frac{-\left[r_{12}\left(r_L+r_{11}\right)+x_{12}\left(x_L+x_{11}\right)\right]+\mathrm{j}\left[x_{12}\left(r_L+r_{11}\right)-r_{12}\left(x_L+x_{11}\right)\right]}{\left(z_L+z_{11}\right)^2}. \tag{3.35}$$

We substitute (3.35) into the part D_2 of (3.32) and get

$$\begin{aligned}\mathrm{D}_2 &= 2 \cdot \mathrm{Re}\left\{k_r\right\} \cdot \rho_{xx} + 2 \cdot \mathrm{Im}\left\{k_r\right\} \cdot \rho_{xy} \\ &= -2 \cdot \frac{\rho_{xx} \cdot \left[r_{12}\left(r_L + r_{11}\right) + x_{12}\left(x_L + x_{11}\right)\right] + \rho_{xy} \cdot \left[x_{12}\left(r_L + r_{11}\right) - r_{12}\left(x_L + x_{11}\right)\right]}{\left(z_L + z_{11}\right)^2}.\end{aligned} \tag{3.36}$$

Comparing to (3.33), we have $\mathrm{D}_2 = \mathrm{D}_1 \cdot (z_L + z_{11})^2$. Then we substitute (3.34) and (3.36) into (3.32) we have

$$\begin{aligned}\tilde{P}_1 &= |k_r|^2 \cdot [1 + |k_{11}|^2 + 2 \cdot \mathrm{Re}\{k_{11}\} \cdot \rho_{xx} + \mathrm{Im}\{k_{11}\} \cdot \rho_{xy}] \\ &= \left|\frac{z_L(z_L + z_{11})}{(z_L + z_{11})^2 - z_{12}^2}\right|^2 \cdot \Big\{\Big\{1 + \left|\frac{z_{12}}{z_L + z_{11}}\right|^2 \\ &\quad - 2 \cdot \frac{\rho_{xx} \cdot [r_{12}(r_L + r_{11}) + x_{12}(x_L + x_{11})] + \rho_{xy} \cdot [x_{12}(r_L + r_{11}) - r_{12}(x_L + x_{11})]}{z_L + z_{11}}\Big\}\Big\} \\ &= |z_L|^2 \cdot \frac{|z_L + z_{11}|^2 + |z_{12}|^2 - 2 \cdot \mathrm{Re}\{\alpha(z_L + z_{11})\mathrm{z}_{12}^*\}}{\left|(z_L + z_{11})^2 - z_{12}^2\right|}.\end{aligned} \tag{3.37}$$

The difference between (3.23) and (3.32) is only attributed to that (3.23) has a factor $4r_L r_{11}$, and it is substituted by $|z_L|^2$ in (3.37).

The explanation of the difference between the expressions is because when the matching networks are considered, the calculation of the received power should only count in the voltage across the resistance rather than that over the impedance. If we modify (3.37) by multiplying factor $|z_L|^2$ to the correction factor $\frac{4r_L r_{11}}{|z_L|^2}$, Figure 3.9 will display exactly as Figure 3.8.

3.3.2 Improvement of received power using matching networks

After proving the correct expression of the received power for compact array with matching networks, we are interested in the optimum matching impedance which maximizes the received power in Figure 3.8[3]. We simulate the total received power in (3.25) and the power difference in (3.26) of the two branches using the same array model as in Figure 3.8. In addition we introduce more antenna spacings, and consider the impact of AS, MAOA and the distribution of PAS on the received power performance.

Figure 3.10 displays the total received power of the defined array with chosen matching net-

[3]We note that (3.23) is not suitable for calculating the received power of MCM, as it assumes that SPM is used according to Figure 3.7 on page 46.

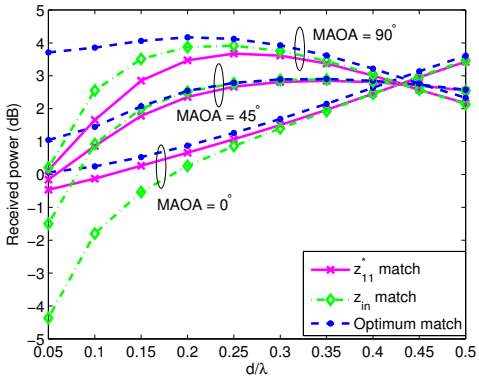

(a) AS = 15°,Laplacian PAS

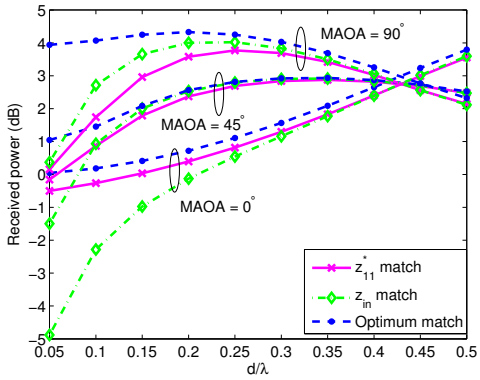

(b) AS = 15°, uniform PAS

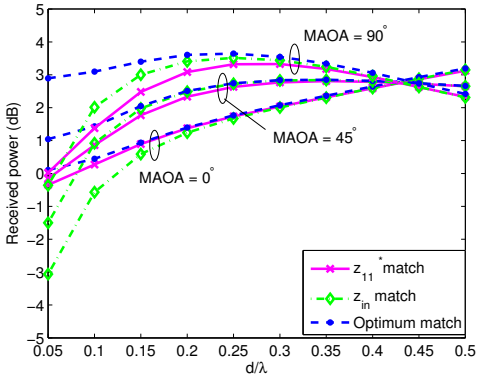

(c) AS = 40°, Laplacian PAS

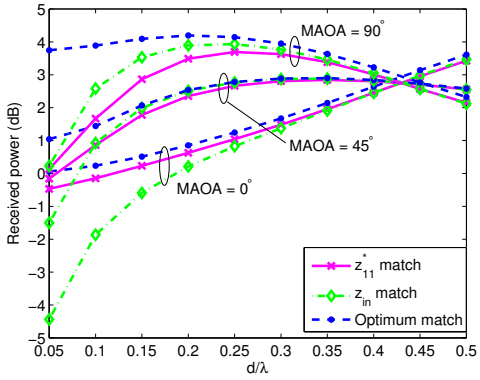

(d) AS = 40°, uniform PAS

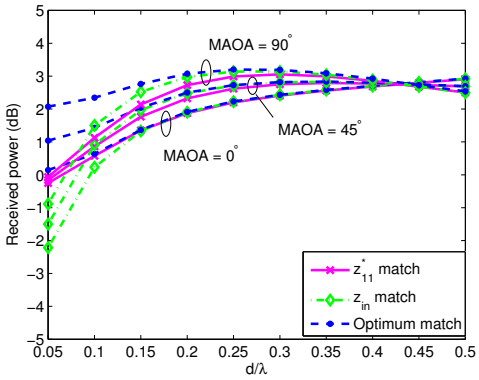

(e) AS = 90°, Laplacian PAS

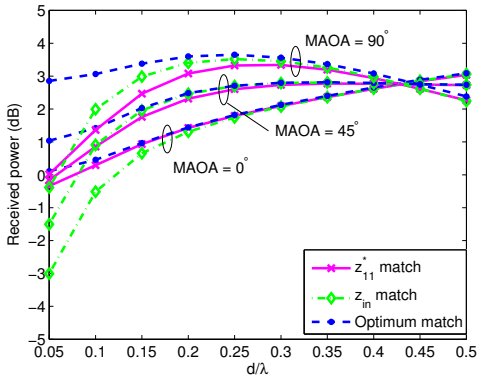

(f) AS = 90°, uniform PAS

Figure 3.10: *The total received power comparison with z_{11}^* and optimum matching networks in scenarios of uniform and Laplacian PAS with various AS values.*

works in different scenarios. We consider both uniform and Laplacian PAS as for the SC calculation as in Figure 3.6. The AS values are assumed to be 15°, 40° and 90°, and in each scenario three values of MAOA 0°, 45° and 90° are considered. For the matching networks, we select the z_{11}^* match and z_{in} match as comparisons to the optimum impedance match we found for each antenna spacing and scenario[4].

All the subfigures in Figure 3.10 look similar, which reveals that the variation of AS does not affect the received power performance greater than 1dB. Hence, we study Figure 3.10(a) as an example. In Figure 3.10(a), the total receive array with any kind of matching network obtains the highest received power at 90° MAOA and $d \leq 0.4\lambda$. Similar phenomena can be found in other subfigures of Figure 3.10. This interesting power gain can be explained by the super-directive characteristic of the antenna array at 90° MAOA [97, 98]. Because the MAOA is aligned with the direction of the maximum directivity, the received power is maximized. The total received power for 0° MAOA increases as d increases on account of the reduced MC effect. When the MAOA is 45°, the maximum received power occurs at $d = 0.3\lambda$ and starts to drop afterwards due to the smaller effect of MC compared to $d \leq 0.3\lambda$; for 90° MAOA and the maximum point is at $d = 0.2\lambda$ for the optimum impedance match and $d = 0.25\lambda$ for z_{11}^* and z_{in} matching. In all MAOA cases, the optimum impedance match always outperforms the other matching networks, and the z_{in} match provides the lowest power gain at small d values before approaching the others at $d = 0.3\lambda$. For example, when $d = 0.05\lambda$, the optimum impedance match offers a gain of 0.5dB at 0° MAOA, 1.1dB at 45° MAOA, 3.9dB at 90° MAOA compared to z_{11}^* match, and 4.2dB at 0° MAOA, 2.4dB at 45° MAOA, 3.9dB at 90° MAOA to the z_{in} match. All kinds of matching networks begin to approach each other at $d = 0.2\lambda$ and above in all MAOA scenarios. Other subfigures of Figure 3.10 can be investigated in the similar way.

Focusing on the column subfigures of Figure 3.10, we can see that the effect of super-directive characteristic decreases when AS increases. It is reasonable that the smaller AS has more impact on emphasizing the super-directive behavior [23]. Also when the AS increases, the difference in the total received power for of different MAOA becomes smaller for all matching cases, and in each MAOA scenario the performance gap between various matching networks decreases. With 90° AS, the performance of different matching networks approach each other at $d = 0.15\lambda$ for any MAOA in Figure 3.10(e). In each row of subfigures, the received power of Laplacian PAS is lower than that of the uniform PAS for the corresponding MAOA and

[4]We note that the optimum impedances for different antenna spacings and scenarios are indeed different.

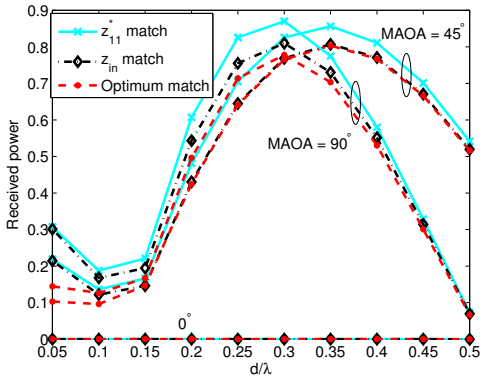

(a) AS = 15°,Laplacian PAS

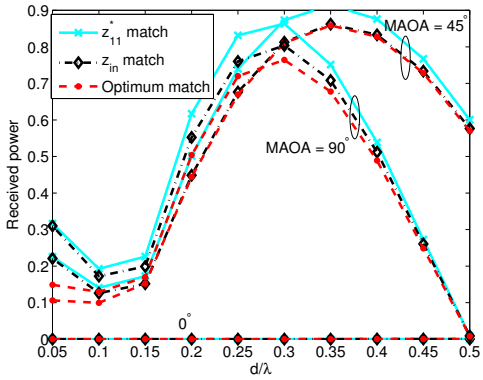

(b) AS = 15°, uniform PAS

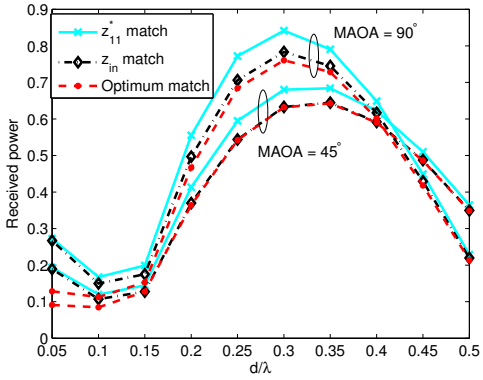

(c) AS = 40°, Laplacian PAS

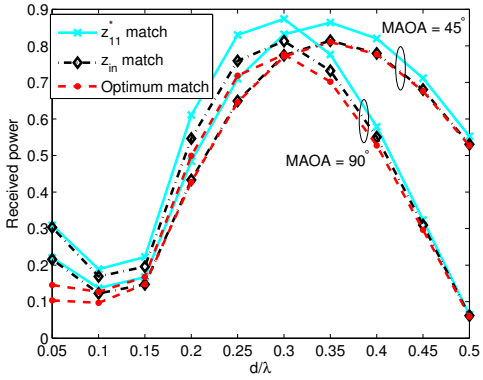

(d) AS = 40°, uniform PAS

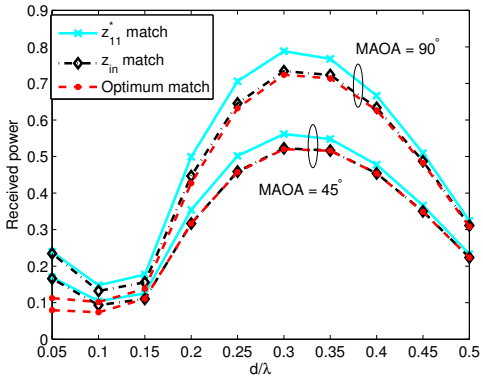

(e) AS = 90°, Laplacian PAS

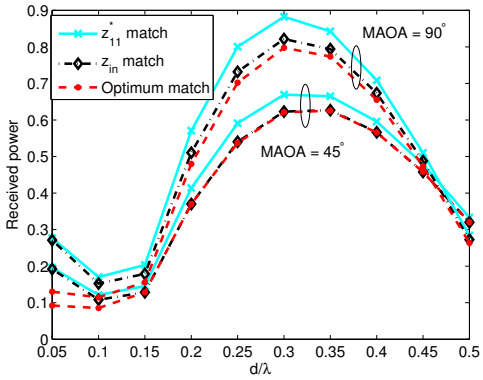

(f) AS = 90°, uniform PAS

Figure 3.11: *The power difference comparison with self-conjugate and optimum matching networks in scenarios of uniform and Laplacian PAS with various AS values.*

matching network pairs. However, the differences are not greater than 1dB, which reveals that the total received power is not strongly affected by the distribution of PAS.

Although the received power gain can be great improved by using matching networks, a good diversity performance in MIMO systems requires the received power to be distributed evenly at each receive branch. The absolute power differences between the two antennas with various matching networks are plotted in Figure 3.11 for the same scenarios as in Figure 3.10[5]. In general, the power difference is zero for any matching conditions and AS values at 0° MAOA because the receive model is symmetric. Hence, this case is only demonstrated in Figure 3.11(a) and 3.11(b). Again the performance of the power difference does not varying significantly with the PAS distributions. In Figure 3.11(a), the power difference with any matching network and in any scenario decreases at $d \leq 0.1\lambda$. After a slow growth till $d = 0.15\lambda$, it starts to increase dramatically for all matching cases and reaches the maximum point at $d = 0.35\lambda$ for 45° MAOA, and $d = 0.3\lambda$ for 90° MAOA. Interestingly, we find the power difference with all matching networks of 90° MAOA is much smaller than that of 45° MAOA when $0.35\lambda \leq d \leq 0.5\lambda$, which can also be explained by the super-directive theory. In any MAOA scenario, the optimum impedance matching outperforms other matching networks at the same d, and the second best match is the z_{in} match. In general, the performance of z_{in} match almost converges to the optimum impedance match at $d \geq 0.15\lambda$ in any scenario. For the column figures of Laplacian PAS, the power difference slightly decreases as AS increases in all corresponding cases.

To provide a comprehensive conclusion, we shall combine our observations from Figure 3.10 and 3.11. Although high total received power can be achieved at $0.15\lambda \leq d \leq 0.3\lambda$ in Figure 3.10, the power difference is large in that range, which does not fulfill the MIMO system requirement for equal power channels. On the other hand, the power difference is negligible for 0° MAOA in any case, whereas the received power is very low at small antenna spacings. However, when $0.1\lambda \leq d \leq 0.15\lambda$, the power difference is between 0.1 to 0.2 dB with any matching networks and in any scenarios in Figure 3.11. And the received power in any condition is acceptable within that range in Figure 3.10. Hence, $0.1\lambda \leq d \leq 0.15\lambda$ is desirable for compact array design considering the received power.

[5]The results are different from those in [24, 63] because we use absolute value for the calculation here.

3.4 MIMO capacity

The SC and received power are two important parameters for studying the performance of the compact array as one component of a MIMO system. However, it is important to carry out the system evaluation including the impact of the compact array. MIMO capacity is a widely used metric for such an evaluation. The impact of MC on MIMO capacity performance has been widely studied and different conclusions have been reached. Some work claims that MC is a benefit to MIMO systems [10,16,29], some [13,17,20] completely disagree with the first group, while the last [12, 14, 15, 18, 30, 99] has the opinion that the advantage of MC only happens in certain cases, e.g. a selected range of antenna spacings. There is also related work [19, 100] without direct comparison to the no MC cases. The divergence is caused by different channel normalization criteria, various assumptions of power allocation at the transmitter and the most significant point is whether the effect of matching networks is under consideration. Within these studies, only [18, 29] have included the matching network component into the MIMO system evaluation.

3.4.1 MIMO capacity in S-parameters and Z-parameters

The integration of MC and matching networks into MIMO systems requires proper modification of the traditional MIMO capacity expression. Two methods in *n*-port theory are usually adopted to study compact MIMO systems. One is the S-parameter approach which reflects the wave transmission in a *n*-port electrical network [18,99]; the other is the Z-parameter approach which expresses the voltage and current relations among all ports [23].

3.4.1.1 S-parameter approach

First we substitute the block $\mathbf{S}_{RR}$ to $\mathbf{S}_H$ in Figure 3.3 on page 39. The matrix $\mathbf{S}_{RR}$ has been used there because for SC calculation the receiver should be separated from the system. Then the S-matrix which connects the transmitter and receiver is given by

$$\mathbf{S}_H = \begin{bmatrix} \mathbf{S}_{TT} & \mathbf{S}_{TR} \\ \mathbf{S}_{RT} & \mathbf{S}_{RR} \end{bmatrix} \tag{3.38}$$

where $\mathbf{S}_{TT}$ and $\mathbf{S}_{RR}$ are the S-parameter transforms of the transmit and receive antenna impedance matrices, respectively. We assume $\mathbf{S}_{TR}$ is a zero matrix, which indicates the two link ends

are sufficiently separated that there is no power from the receiver reflected to the transmitter. Similarly, $\mathbf{S}_{RT}$ contains the information from the transmitter to the receiver, and can be denoted as [18]

$$\mathbf{S}_{RT} = \left(\mathbf{I} + \frac{\mathbf{Z}_{RR}}{z_0}\right)^{-1} \frac{\mathbf{Z}_{RT}}{z_0} \left(\mathbf{I} - \mathbf{S}_{TT}\right) \tag{3.39}$$

where $\mathbf{Z}_{RT}$ is the Z-parameter transform of $\mathbf{S}_{RT}$. For a path-based channel model with full AS [18],

$$\left(\mathbf{Z}_{RT}\right)_{ij} = \sum_{n=1}^{N_P} E_{R_i}\left(\varphi_n\right) \beta_n e_{T_j}\left(\vartheta_n\right) \tag{3.40}$$

where N_P is the number of paths, $e_{T_j}\left(\vartheta\right)$ means the transmitted field per unit excited current of the jth transmit antenna in the direction of ϑ, and β_n, φ_n, ϑ_n denote the complex channel gain, the AOA and AOD of the nth path, respectively. Then the modified MIMO capacity expression of an $N \times N$ system is [18]

$$C_S = \log_2 \det\left(\mathbf{I} + \frac{\rho}{N} \mathbf{H}_S \mathbf{X}_\mathbf{S} \mathbf{H}_S^H\right) \tag{3.41}$$

where

$$\mathbf{H}_S = z_0^{1/2} \mathbf{S}_{21} \left(\mathbf{I} - \mathbf{S}_{RR}\mathbf{S}_{11}\right)^{-1} \mathbf{S}_{RT}, \tag{3.42}$$

and $\mathbf{X}_S$ = $\mathbf{I}_N$ for the equal power allocation at the transmitter. If waterfilling power allocation is considered with MC at the transmit end, the constraint for the transmit power should be modified to

$$P_{TS} = \mathrm{Tr}\left(\mathbf{X}_S \left(\mathbf{I} - \mathbf{S}_{TT}^H \mathbf{S}_{TT}\right)\right). \tag{3.43}$$

The determination of $\mathbf{S}_{11}$ and $\mathbf{S}_{21}$ in (3.42) is the same as in Section 3.2.3.2. The channel power is normalized to the z_0 matched SISO case for each calculation. The S-parameter approach offers a complete network model for MIMO capacity evaluation with the MC at both ends and matching network effects, including both SPM and MCM.

3.4.1.2 Z-parameter approach

The capacity evaluation of compact MIMO systems with matching networks using Z-parameters has partially been carried out in [12–14, 23]. However, no network model has been reported using an Z-parameter approach. Among these papers, the work in [12, 23] draw our attention.

The channel matrix with MC and matching network effects using Z-parameters is given by

$$\mathbf{H}_Z = (\mathbf{Z} + z_L \cdot \mathbf{I})^{-1} \mathbf{H}_{cr} \tag{3.44}$$

where $\mathbf{Z}$ and $\mathbf{H}_{cr}$ are defined in Chapter 2 on page 14. Here we only concern ourselves with the MC induced SC at the receiver, so $\mathbf{\Psi}_T = \mathbf{I}$. Then the equal power MIMO capacity expression with MC and matching network effects at the receiver for a 2×2 system is [23]

$$C_Z = \log_2 \det \left(\mathbf{I} + 2\rho_r r_{11} r_L \mathbf{H}_Z \mathbf{H}_Z^H \right) \tag{3.45}$$

where ρ_r is the reference SNR and r_{11} is the resistive component of z_{11}. The derivation of (3.45) is based on the circuit theory in Figure 3.7. The power normalization of the SISO with both antennas z_{11}^* matched[6] is used to restrict the SC in $[0, 1]$.

Although (3.45) is only a special case of the result in (3.41), it is a intuitive way to study the impact of z_L on the compact MIMO system performance. Also, it is much easier to calculate the MIMO capacity and much less time-consuming than the S-parameter approach. Attracting by these strongpoints, we will develop a complete framework for $N \times N$ MIMO systems including the MC effect at both link ends using Z-parameters from a novel power transfer point of view in Chapter 5, and we will prove there that (3.45) is a special case of our derivation.

3.4.2 Improvement of MIMO capacity using matching networks

To validate both S-parameter and Z-parameter methods, we examine a 2×2 MIMO system as (3.45) is limited to this case. We focus on the compact array at the receiver only, thus the transmitter is assumed sufficiently spaced without MC and to be located in a rich-scattering environment. Also the PAS at the receive end is assumed to be uniformly distributed. Identical dipole antennas are considered at both ends and the same model simulated in FEKO is used as for the *semi-theoretical* SC in Figure 3.4. For the S-parameter approach, we assume $N_P = 8$ paths for the path-based channel model and the channel gain β is a Rayleigh random variable. In both simulations SNR = 20dB and 7000 channel realizations are used to compute the ergodic MIMO capacity in each antenna spacing and matching network case.

Figure 3.12 displays the equal power ergodic capacity of the system with various matching

[6]The normalization used here is slightly different that used in (3.41) because the benchmarks are different. In (3.41) it is the z_0 match and in (3.45) it is the z_{11}^* match.

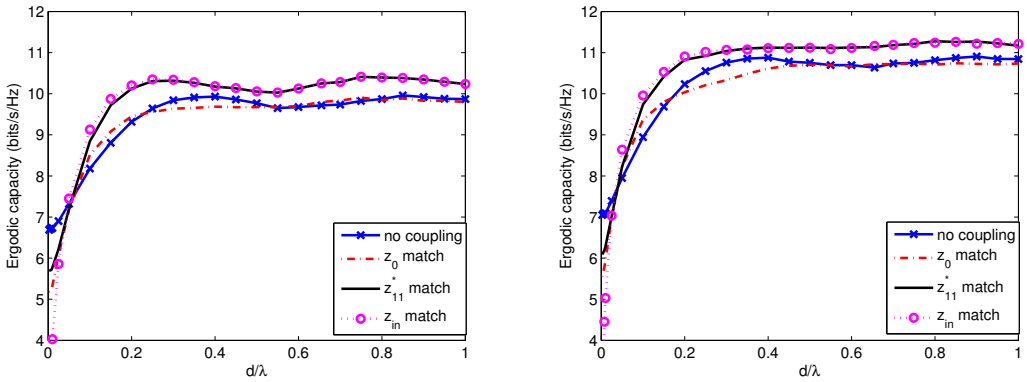

(a) S-parameter approach

(b) Z-parameter approach

Figure 3.12: *The equal power ergodic capacity of a compact MIMO system vs. antenna spacing and matching networks using both S-parameter and Z-parameter approaches.*

networks as a function of antenna spacing using both S-parameter and Z-parameter methods. The capacity of all cases increases with increasing d towards a stable value at about $d = 0.3\lambda$ and above. For the S-parameter approach in Figure 3.12(a), the system with MC and any matching networks except the z_0 match outperforms that with no coupling case when $d > 0.1\lambda$. At $d = 0.2\lambda$, the z_{in} match and z_{11}^* match outperform the z_0 match and no coupling case by 0.7bits/s/Hz and 0.5bit/s/Hz separately. Also the z_{in} match performs slightly better than z_{11}^* match when $0.1\lambda < d < 0.4\lambda$. The distribution of the curves can also be explained by combining the previous analysis of SC and received power. The no coupling case gives both worst SC in Figure 3.6(e) and received power in Figure 3.10(f), thus it has the worst capacity performance in Figure 3.12. Although the z_{in} match provides the lowest SC in Figure 3.6(e) at $d < 0.18\lambda$, its received power is the lowest within that range in Figure 3.10(f) as well. The capacity performance is ahead of other SPM in Figure 3.12 when $0.03\lambda < d < 0.15\lambda$. Meanwhile, the z_{11}^* match provides a lower SC than the z_{in} match for $0.18\lambda < d < 0.35\lambda$ in Figure 3.6(e) and the same SC and received power as z_{in} match in Figure 3.10(f). These comparisons are reflected in Figure 3.12 in that the z_{11}^* match performance equals the z_{in} match at $d = 0.15\lambda$, and they overlap each other in the following range of d. This analysis indicates that proper tradeoff has to be made between SC and received power for capacity maximization.

All the matching cases using the Z-parameter approach in Figure 3.12(b) are parallel to the corresponding matching cases using the S-parameter approach in Figure 3.12(a) with a upper shift about 1bit/s/Hz. This is because a large number of multipath components are assumed as the Kronecker model is included in (3.45), while only 8 paths are considered in Figure 3.12(b).

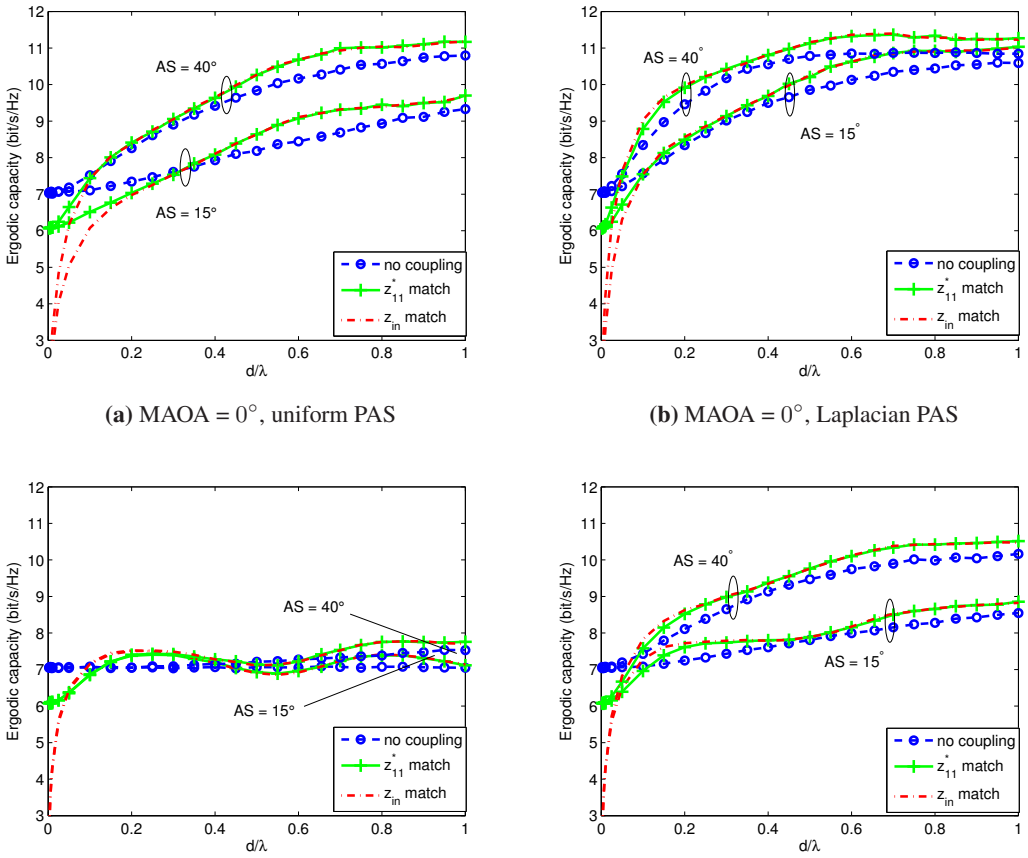

(a) MAOA = 0°, uniform PAS

(b) MAOA = 0°, Laplacian PAS

(c) MAOA = 90°, uniform PAS

(d) MAOA = 90°, Laplacian PAS

Figure 3.13: *The equal power capacity comparison of a compact MIMO system with various matching networks in scenarios of uniform and Laplacian PAS with various AS values.*

When the number of the paths in Figure 3.12(a) increases to infinity, the curves in Figure 3.12(a) will approach and overlap to the corresponding curves in Figure 3.12(b). In this sense, the Z-parameter approach provides as an upper bound for the S-parameter approach. We note that when $N_P \geq 8$, the ergodic capacity calculation in Figure 3.12(a) will become very time-consuming. In contrast, the Z-parameter approach showed in Figure 3.12(b) is much quicker to evaluate for a large number of Monte Carlo calculations. However, the flaw of the Z-parameter approach is that it limited to 2×2 case in (3.45). We will extend the possible array sizes of the Z-parameter approach in Chapter 5.[7]

Although the MCM gives a impressive performance in [18], it is not a feasible solution to

[7]The simulation results of the waterfilling capacity have not been presented here because all the curves follow the similar trend as in Figure 3.12 with a upper shift of 0.2bits/s/Hz. Similar results can be found in [60].

be implemented in practice. Multiple loads [31, 94] have to be added to each antenna port, which requires lots of space in the already congesting compact volume. Hence, we use the Z-parameter approach to study the MIMO capacity in different scenarios. Generally, the z_{in} match loses its advantage over the z_{11}^* match at any antenna separations with an insufficient AS for a broadside MAOA (Figure 3.13(a) and 3.13(b)). In Figure 3.13(a), the capacity of all cases suffers a degradation between $0.15\lambda < d < 0.6\lambda$ compared to Figure 3.12 when AS = 40°. When the AS decreases, the degradation range upper limit reaches 1λ and the advantage of matching networks to the no coupling case disappears when $0.2\lambda < d < 0.4\lambda$. With the Laplacian PAS the capacity results are similar to the uniform PAS for corresponding matching conditions at an AS = 40° in Figure 3.13(b). Meanwhile, the performance at AS = 15° is much better compared to that of the uniform case for any matching network. When the MAOA is from endfire (90° MAOA), all the capacity curves in Figure 3.13(c) suffer severe degradation at AS = 40°, and they even present a flat performance around 7bits/s/Hz in the whole antenna spacing range when AS = 15°. The same cases in Figure 3.13(d) have a relatively better performance than those in Figure 3.13(c). The super-directive merit in Figure 3.10 does not bring any boost to the capacity performance in Figure 3.13(c) and 3.13(d), as a very high SC is found in Figure 3.10 for the corresponding values of AS.

3.5 Summary

This chapter has investigated the SC, received power and MIMO capacity of a compact receiver in a MIMO system with various matching networks and in different scenarios. A two-element identical dipole array is chosen for characteristic studies. The same dipole array is adopted for the capacity evaluation of a 2×2 MIMO system. The conclusions of this chapter are:

- The *theoretical* and *semi-theoretical* calculation methods of SC is interchangeable. In theory the MCM can always provide zero SC between elements. Within the SPMs, the z_{in} match outperforms other SPM cases in all scenarios. Besides the full AS case, the SC of different matching network pairs performs better for the Laplacian PAS than for the uniform PAS.

- The received power expression based on the circuit theory is a proper method to study the MC effect with various SPM. There is a optimum impedance which always gives the best performance compared to other SPM networks in any scenario. Both total received

power and power difference are not sensitive to the changing of the scenarios. Antenna spacings within $[0.1, 0.2]\lambda$ are desirable for compact receive array design as all matching cases have the lowest power difference and relatively high power in any scenario within that range.

- Both S-parameters and Z-parameters are suitable for studying the capacity of a compact MIMO system and include the effect of matching networks. Moreover, the ergodic capacity calculated in Z-parameter can be recognized as an upper bound of the value generated by S-parameter analysis. The advantage of a compact MIMO system using matching networks degrades when AS decreases.

In a word, SC and received power should be jointly considered and well balanced in the system design to achieve a good capacity performance of a compact MIMO system. Also matching networks play an important role in the improvement of the capacity performance of a compact MIMO system.

Chapter 4
Experiments of closely coupled monopoles with load matching

4.1 Introduction

In this chapter we experimentally set up a compact receive array system to investigate the received power and SC performance with various load impedances in order to validate the results in Chapter 3. Besides practical implementation, electromagnetic simulation tools SEMCAD [67] and FEKO are also used to assist the experimental study.

The contributions of this chapter are:

- An experimental setup to investigate the received power and SC of closely coupled antennas with impedance matching is described. Specifically, a two-monopole array with a small antenna spacing of 0.05 wavelength and five different matching networks are constructed and measured for the first time.
- The system design has been carried out in simulation to support the experimental research. The antenna array and ground plane are modeled in SEMCAD, while various matching network designs are simulated in FEKO. The simulation and measured results of the characteristics of single monopole, coupled array and OC correlation are studied and show good consistency. Moreover, general rules for matching network design using transmission line tuning techniques are summarized for future research.
- The theoretical, simulation and measured results of the total received power and SC of the system with five selected matching impedances are presented and compared. Whereas the experimental results largely confirm the theoretical and simulation predictions, some discrepancies are observed. The discrepancies are investigated from both theoretical and experimental points of view. The MIMO system performance of the compact receive array with selected loads is also examined.

The remainder of this chapter is organized as follows. Section 4.2 presents the problem derivation and theoretical preparations. Section 4.3 describes the experimental setup of the system. Section 4.4 studies the characteristic of the system based on the measured results. Section 4.5 discusses the selection of the load impedances for implementation. Section 4.6 compares the theoretical, simulated and measured received power and SC results, while the discrepancy studies are also provided. Section 4.7 examines the MIMO capacity performance with selected load impedances. Section 4.8 summarizes the whole chapter.

4.2 Problem derivation and theoretical preliminaries

In Chapter 3 we showed that to improve the performance of compact MIMO systems, the SC and received power should be well balanced in the design of the compact array. In (3.10) on page 38 and (3.23) on page 47, it is obvious that the selection of matching networks is critical to the SC and received power evaluation for a compact array with fixed antenna spacing and chosen scenarios. Moreover, the optimum impedance which maximizes the total received power in Figure 3.10 apparently differs from z_{11}^* and z_{in}. Also it is reported in [22] that a series of matching impedances can be selected properly to achieve zero SC performance at $d = 0.05\lambda$. In order to confirm the analytical results in (3.10), (3.23) and to determine the matching impedance which optimizes both SC and received power, an implementation of a real compact array model has been carried out. We note that this experimental implementation was in collaboration with the authors of [22].

The analytical equivalent circuit of the measurement is identical to Figure 3.7. In order to choose the proper load impedances for measurement, the measured antenna impedances and ρ_{oc} are used to calculate the theoretical received power and SC. The theoretical SC is evaluated using (3.10), while the measured 2D SC is calculated using

$$\rho_{2d,m} = \frac{\int_0^{2\pi} E_{R_1}(\varphi)\, E_{R_2}^*(\varphi) d\varphi}{\sqrt{\int_0^{2\pi} |E_{R_1}(\varphi)|^2 d\varphi \cdot \int_0^{2\pi} |E_{R_2}(\varphi)|^2 d\varphi}}, \tag{4.1}$$

and the measured 3D SC is using

$$\rho_{3d,m} = \frac{\int_0^{2\pi}\int_0^{\pi} E_{R_1}(\vartheta,\varphi)\, E_{R_2}^*(\vartheta,\varphi) \sin(\vartheta) d\vartheta d\varphi}{\sqrt{\int_0^{2\pi}\int_0^{\pi} |E_{R_1}(\varphi)|^2 \sin(\vartheta) d\vartheta d\varphi \cdot \int_0^{2\pi}\int_0^{\pi} |E_{R_2}(\varphi)|^2 \sin(\vartheta) d\vartheta d\varphi}}. \tag{4.2}$$

It is obvious that (4.1) and (4.2) are modifications of (3.3) and (3.2), respectively.

In practice, it is very difficult to achieve perfectly identical antenna structures. As a result, the power allocation could be very different to each element even for small antenna spacings. Hence, the total mean received power of the compact array (3.25) on page 47 is considered. Meanwhile, the 2D measured total received power of an N-element array is

$$P_{2d,m} = \frac{\sum_{i=1}^{N} \int_0^{2\pi} |E_{R_i}(\varphi)|^2 d\varphi}{\int_0^{2\pi} |E_0(\varphi)|^2 d\varphi}. \tag{4.3}$$

Correspondingly, the 3D expression is given

$$P_{3d,m} = \frac{\sum_{i=1}^{N} \int_0^{2\pi} \int_0^{\pi} |E_{R_i}(\varphi,\vartheta)|^2 \sin(\vartheta) d\vartheta d\varphi}{\int_0^{2\pi} \int_0^{\pi} |E_0(\varphi,\vartheta)|^2 \sin(\vartheta) d\vartheta d\varphi} \tag{4.4}$$

where E_0 represents the FF patterns of the isolated reference monopole antenna.

4.3 Experimental setup

Half-wavelength dipoles are usually adopted in many related papers [11–13, 17–19, 22, 23, 29, 30, 79, 95, 100, 101] because they are able to be studied analytically and taken as references in the antenna field. Most of these references only used analytical or simulation results except for [79,95], where real dipoles with resonant lengths are implemented and tested in a reverberation chamber. However, as we can see in [102], the implementation of dipoles are not easy because special method is needed to fix the position of the dipoles. Thus, monopole antennas which are half the length of dipole antennas draw a lot of attention in practice [69, 103]. Monopole antennas are used in our measurements.

4.3.1 System configuration

The experimental setup of a compact receive array is shown in Figure 4.1. Two quarter-wavelength ($\lambda/4$) monopoles with antenna spacings of $d = 0.05\lambda, 0.1\lambda, 0.15\lambda$ and a center frequency of 900MHz are mounted on a 330mm $\times$ 250mm ground plane. Both brass antennas of identical dimensions (diameter of 2mm) are directly soldered onto 50Ω matching network boards with the output ports of SMA connectors soldered onto the opposite end of the boards.

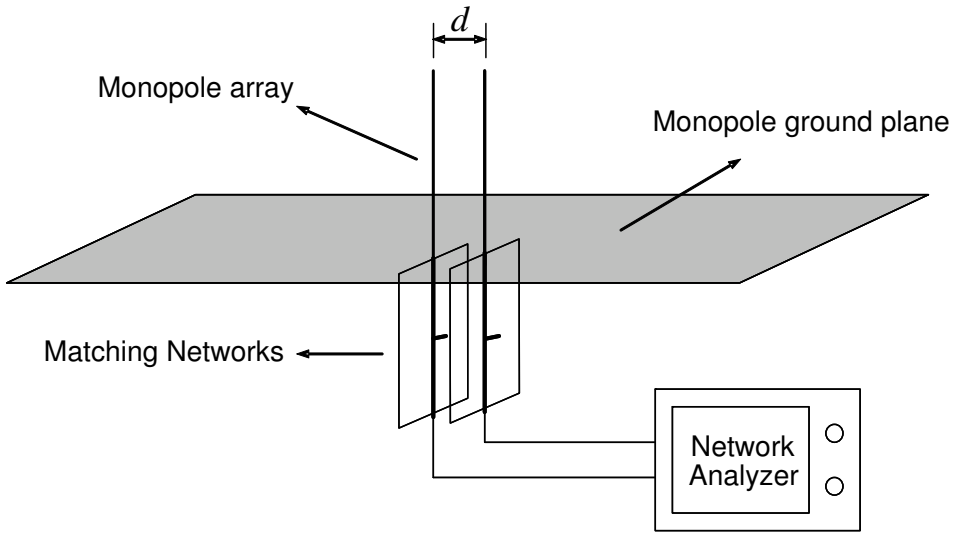

Figure 4.1: *Experimental setup of two $\lambda/4$ monopoles mounted on a ground plane and connected to matching networks.*

The self impedance of a single monopole and the self and mutual-impedances of the monopole array are measured using a network analyzer. To calculate the theoretical ρ_{oc}, 2D and 3D FF patterns of the monopole array with OC terminations are measured in an anechoic chamber at Perlos AB, Sweden[1]. Meanwhile, an identical system model is simulated in SEMCAD based on full-wave finite-difference time-domain (FDTD) analysis to calibrate the measured results.

4.3.2 Matching network design

The design of matching networks is the vital step in this measurement. We apply the well established single-stub matching technique [61, 68]. For simplicity, the configuration of a transmission line and parallel open-circuited stub based on a 50Ω transmission line is adopted. In this method, the matched impedance are determined by two parameters, which are the distance from the load impedance to the stub place d_s and the stub length l_s which can generate various susceptance or reactance values. Figure 4.2 gives the general concept of this structure. In

[1]Although the channel in the chamber is line-of-sight, the FF patterns are measured uniformly over 2π radians. This is consistent with the MIMO non-line-of-sight channel with uniformly distributed PAS and full angular spread. Thus the measured correlation can be used for the MIMO capacity evaluation.

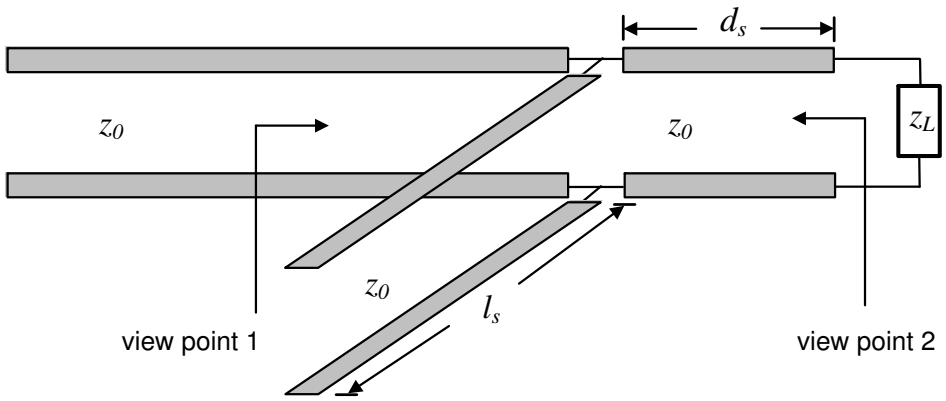

Figure 4.2: *Open-shunt connection of a single stub tuner.*

transmission line theory, the relation between $z_L = r_L + \mathrm{j}x_L$ and d_s, l_s is given by

$$\frac{d_s}{\lambda_s} = \begin{cases} \frac{1}{2\pi}\tan^{-1} t & \text{for } t \geq 0 \\ \frac{1}{2\pi}\left(\pi + \tan^{-1} t\right) & \text{for } t < 0 \end{cases} \tag{4.5a}$$

$$\frac{l_s}{\lambda_s} = -\frac{1}{2\pi}\tan^{-1}\left(\frac{r_L^2 t - (z_0 - x_L t)(x_L + z_0 t)}{z_0[r_L^2 + (x_L + z_0 t)^2]} \cdot z_0\right), \tag{4.5b}$$

where

$$t = \begin{cases} \frac{x_L \pm \sqrt{r_L\left[(z_0 - r_L)^2 + x_L^2\right]/z_0}}{r_L - z_0} & \text{for } r_L \neq z_0 \\ -x_L/2z_0 & \text{for } r_L = z_0 \end{cases}.$$

and λ_s is the wavelength in the substrate dielectric of the transmission line. Double sets of solutions can be generated for d_s and l_s, and usually only the solution set with shorter lengths is chosen to achieve a better bandwidth. The selection also depends on the dimension limit of the circuit design.

If we measure the network from view point 1 in Figure 4.2, z_{in} of the network should be equal to z_0 after tuning. On the contrary, if we observe the network from view point 2, z_{in} will become the conjugate of z_L, which implies that arbitrary impedances can be produced by adjusting the position and length of l_s. The stub tuning design can be measured and calculated directly using a Smith Chart [68]. However, the solutions are not as accurate as the ones calculated using (4.5).

In practice, the matching networks are realized by making proper microstrip transmission lines on double-sided PCB boards. The width (w_m) of the microstrip line is determined by the

relative permittivity (ε_r) and the height (h_s) of the substrate layer, while the design of d_s and l_s depends on $\lambda_s = \lambda_0/\sqrt{\varepsilon_e}$, where λ_0 is the wavelength in free space and ε_e is the effective permittivity of the dielectric interface, which can be deduced from ε_r and the ratio w_m/h_s. There are a couple of empirical formulas to calculate w_m and ε_e. In our implementation, both methods in [68] and [61] have been used. We prove that the formulas in [61] are much more accurate than the other presented in [68] from the measured and simulation results using FEKO following both methods. Hence, we adopt the formulas in [61] to design the practical matching networks and they are

$$\frac{w_m}{h_s} = \begin{cases} \frac{8}{e^{\mathrm{A}}-2e^{-\mathrm{A}}} & \text{for } \frac{w_m}{h_s} \leq 2 \\ \frac{\varepsilon_r - 1}{\pi\varepsilon_r}\left[\ln(\mathrm{B}-1) + 0.39 - \frac{0.61}{\varepsilon_r}\right] + \frac{2}{\pi}[\mathrm{B} - 1 - \ln(2\mathrm{B}-1)] & \text{for } \frac{w_m}{h_s} > 2 \end{cases} \tag{4.6}$$

where

$$\mathrm{A} = \pi\sqrt{2(\varepsilon_r+1)}\frac{z_0}{377} + \frac{\varepsilon_r - 1}{\varepsilon_r + 1}\left(0.23 + \frac{0.11}{\varepsilon_r}\right)$$
$$\mathrm{B} = \frac{\pi}{2\sqrt{\varepsilon_r}}\frac{377}{z_0}.$$

The accuracy of (4.6) is 1% [61]. Then ε_e is computed as

$$\varepsilon_e = \frac{\varepsilon_r + 1}{2} + \frac{\varepsilon_r - 1}{2}\left(1 + \frac{10}{w_m/h_s}\right)^{-ab} \tag{4.7}$$

where a, b are defined by

$$a = 1 + 49\ln\left[\frac{(w_m/h_s)^4 + (w_m/h_s/52)^2}{(w_m/h_s)^4 + 0.432}\right] + \frac{1}{18.7}\ln\left[1 + \left(\frac{w_m/h_s}{18.1}\right)^3\right]$$
$$b = 0.564\left(\frac{\varepsilon_r - 0.9}{\varepsilon_r + 3}\right)^{0.053}.$$

The accuracy of (4.7) is 0.01% for $w_m/h_s < 1$ and 0.03% for $w_m/h_s < 1000$.

We now summarize our procedure for designing matching networks. First, we choose a PCB board with known h_s and ε_r. Then w_m and ε_e can be calculated using (4.6) and (4.7), respectively. Utilizing ε_e we can obtain λ_s. Two sets of values d_s and l_s can be generated by substituting λ_s into (4.5). Finally the set of d_s, l_s with the smaller dimension and fitting to the size of the PCD board is integrated into our matching network design.

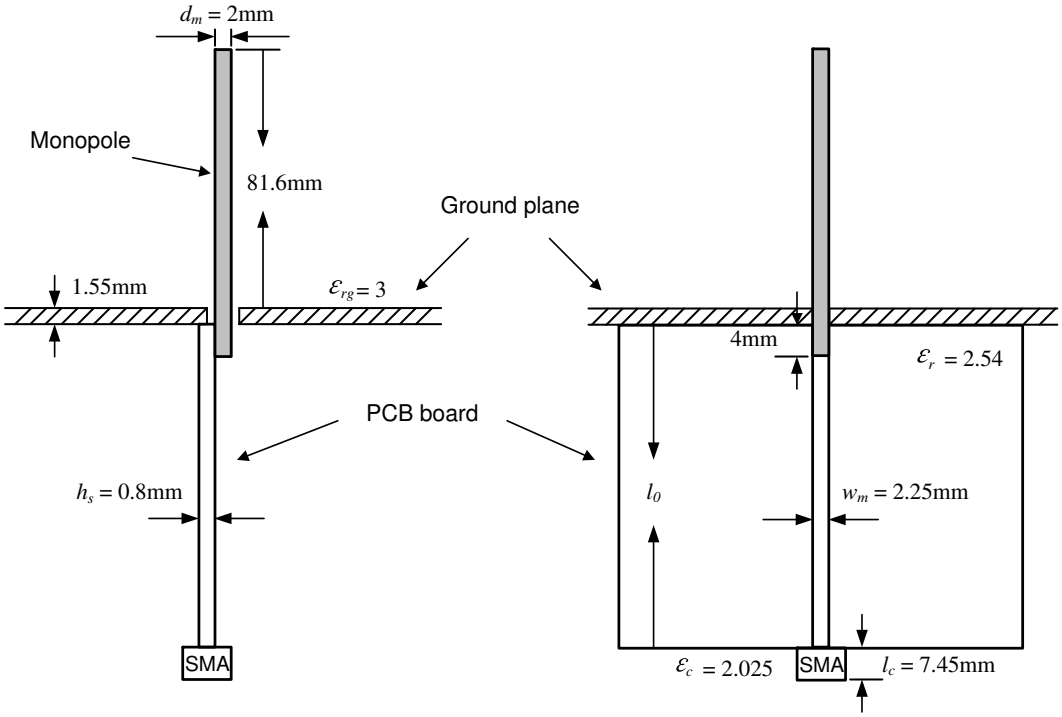

Figure 4.3: *The side and front views of the monopole soldered with matching PCB board and connected to the ground plane.*

4.3.3 Phase shift of the transmission line

The side and front views of the matched monopole design are depicted in Figure 4.3, where ε_{rg} and ε_c are the relative permittivity of the ground plane and the SMA connector, respectively. The notation l_0 is the length of the microstrip transmission line, and l_c represents the length of the SMA connector. The diameter of the monopole d_m in our model is as thin as 2mm, and the length above the ground plane is shorter than $\lambda/4$ as the ground plane of the model is made from a single-sided PCB board, and λ_0 would change when traveling into the dielectric substrate. The monopole has an extra 4mm length under the ground plane to be soldered to the matching networks, which can cause some unexpected interference to the system. Experimentally, the measured point where the impedance or S-parameter can be read from the network analyzer is at the end of the SMA connector. In order to get the actual impedance of the $\lambda/4$ monopole, a phase shift has to be included to transfer the observed impedance from the SMA connector to the bottom of the ground plane through the microstrip transmission line. The formula to compute the phase shift is

$$\vartheta_p = \frac{l_0 \times \sqrt{\varepsilon_e} + l_c \times \sqrt{\varepsilon_c}}{\lambda_0} \times \frac{180^\circ}{0.25} \tag{4.8}$$

The left part of the multiplication in (4.8) is to transform the length of the microstrip line and the SMA connector into the relative length over λ_0. Because in a Smith Chart half of the circle is corresponding to $0.25\lambda_0$ and 180° [68], the right part of the multiplication in (4.8) is to further transform the relative length into the phase shift. For example, if the impedance observed at the SMA connector is $z_m = |z_m|e^{\mathrm{j}\vartheta_m}$, then the impedance at the bottom of the ground plane should be $\tilde{z}_m = |z_m|e^{\mathrm{j}(\vartheta_m+\vartheta_p)}$.

4.4 System characteristic

Because there are no analytical or empirical equations available for computing the impedance matrix and FF patterns of the monopole array in our measurement[2], a simulation approach is essential to calibrate the measured results. Hence, the measured model of monopoles and ground plane are simulated using SEMCAD [67] based on full-wave FDTD analysis in our work. The total system model with matching networks has not been constructed in SEMCAD because the PCB board for matching network design is too thin compared to the dimension of other parts of the model, which requires extremely dense grids for FDTD calculation and causes system memory overflow. The demonstration of system model design in SEMCAD can be found in Appendix B.1. Also the related measured pictures are presented in Appendix B.2.

4.4.1 Single monopole characteristic

The 2D FF patterns of a single monopole in azimuth and elevation planes simulated in SEMCAD are shown in Figure 4.4. The FF patterns of the azimuth plane is almost omnidirectional, which matches the analytical predictions [7]. Referring to the elevation plane, a small backlobe appears under the ground plane, which is induced by the existence of the small hole and the dielectric layer. However, since only the pattern above the ground plane is important, the backlobe has a negligible impact on antenna performance. The simulated self impedance of a single monopole $z_{mo,s}$ = 45.6 + j20.5Ω agrees well with the measured result $z_{mo,m}$ = 45.5 + j19.22Ω.

To confirm the single-stub matching technique, the z_{11}^* match for a single monopole has been attempted. Details of the matching network design is described in Appendix C. From the

[2]In theory, if the $\lambda/4$ monopoles are mounted on a infinite ground plane, the antenna impedances should be half of the $\lambda/2$ dipoles. However, the ground plane cannot be infinite in practice.

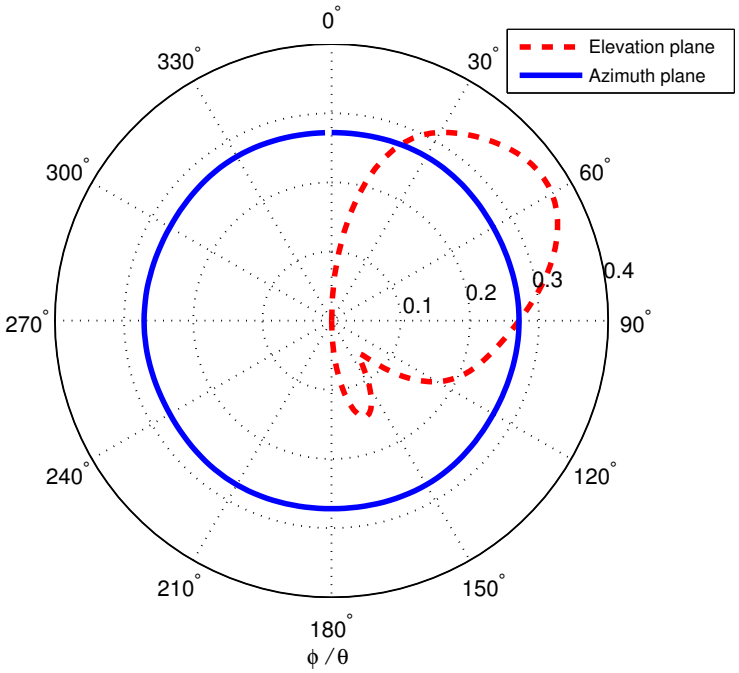

Figure 4.4: *2D FF patterns of the single monopole case simulated in SEMCAD in dB.*

impedance matching point of view, the impedance of the matched monopole observed at the network analyzer (view point 1 in Figure 4.2) should be exactly 50Ω at 900MHz, i.e. the resonant frequency is tuned to 900MHz. The impedance (in Smith chart) and reflection coefficient read from the network analyzer are displayed in Figure 4.5. It is clear that the monopole is well z_{11}^* matched as the impedance observed from the SMA point is about 50Ω in Figure 4.5(a). In Figure 4.5(b), the designed network has a resonant frequency of 900MHz and the bandwidth is about 350MHz at -3dB reflection coefficient (or 39% fractional bandwidth).

4.4.2 Coupled array characteristic

Figure 4.6 displays the self and mutual impedances of the two-element monopole array from both SEMCAD simulation and measurement. The simulation results are derived from the open and short-circuited impedances [8] and identical elements are assumed. The experimental results are transferred from the S-parameter data observed at the network analyzer. As in practice the monopoles cannot be fully identical, the average values of the measured results are shown in Figure 4.6 as well. The close match of the measured impedances of both monopole antennas ensures the validity of further experiment. Meanwhile, the simulation and average measured results are also consistent. It is clear that when the antenna spacing d increases, the difference

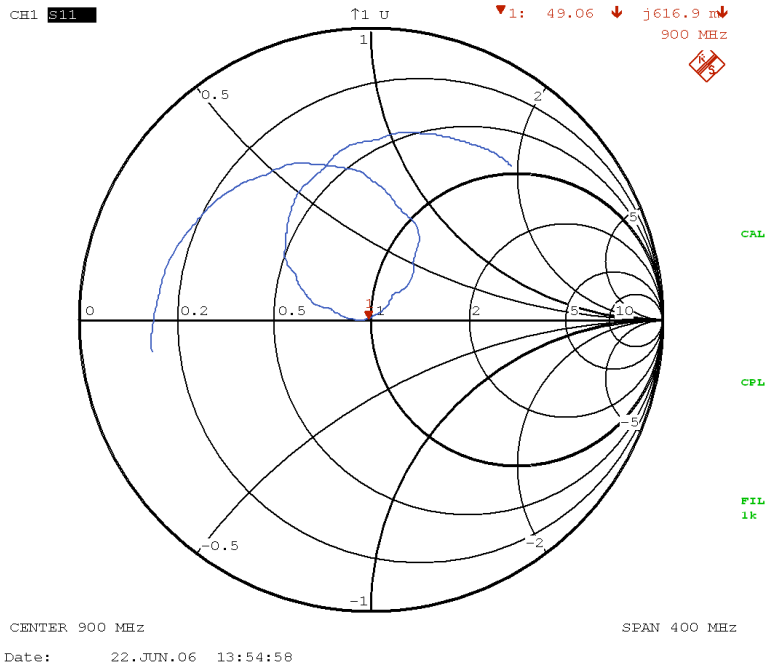

(a) The matched monopole in Smith Chart.

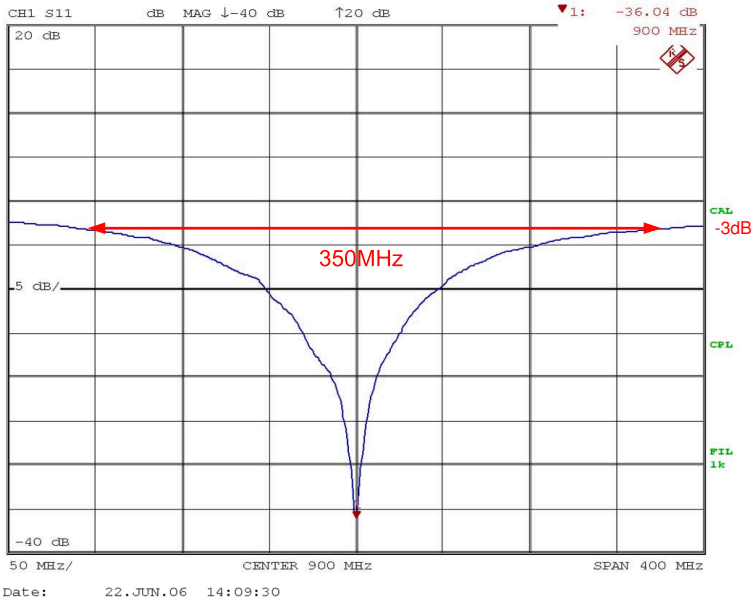

(b) The reflection coefficient of the z_{11}^* matched monopole.(The x-axis is from 700-1100MHz.)

Figure 4.5: *The original data of the matched monopole copied from the network analyzer.*

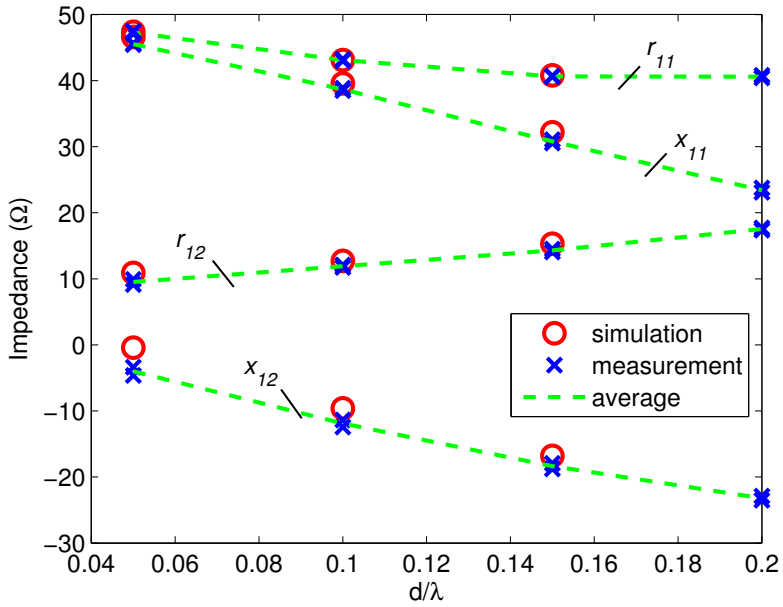

Figure 4.6: *Simulation and measured results of the self and mutual impedances for the monopole array with various antenna spacings.*

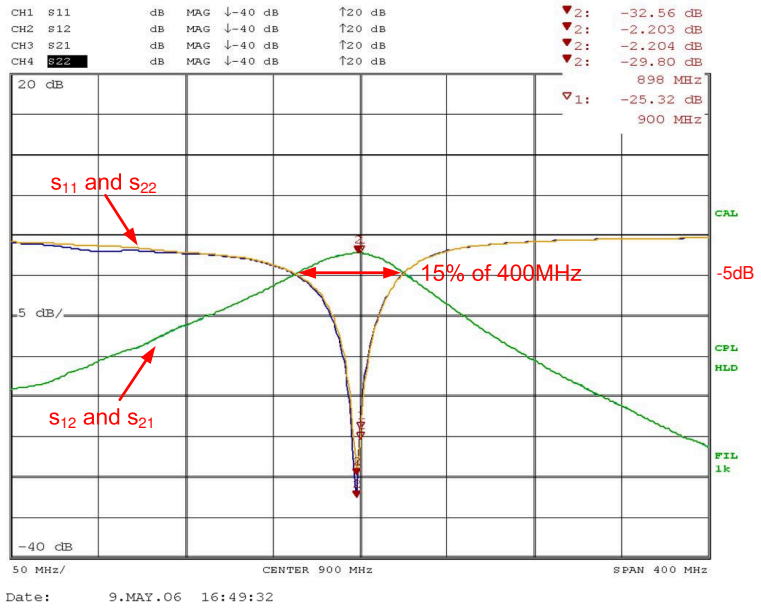

Figure 4.7: *The united S-parameters of two z_{in} matched monopoles observed from the network analyzer. (The x-axis is from 700-1100MHz.)*

between the simulation and the average measured results decreases. In the following measurement, we focus on $d = 0.05\lambda$, where the self and mutual impedances of the monopoles are $z_{11,s}$ = 47.5 + j10.9Ω, $z_{12,s}$ = 46.77 - j0.57Ω in simulation, and $z_{11,m}$ = 46.72 + j9.39Ω, $z_{12,m}$ = 45.31 - j2.57Ω on average in measurement.

Referred to the advanced matching network design in Appendix C, the z_{in} match is implemented for the coupled antennas. Both monopoles are equipped with z_{in}^*, which partially includes the effect of both self and mutual impedances when coupling occurs. Calculated as in [30, 60], the z_{in} of the system is z_{in} = 11.41 + j11.88Ω. If the monopole array is perfectly matched, the S-parameter matrix of the array should be tuned to 900MHz.

Figure 4.7 displays the observed S-parameter of the matched array. First, it shows that both monopoles are well tuned with a resonate frequency very close to 900MHz. Second, it indicates

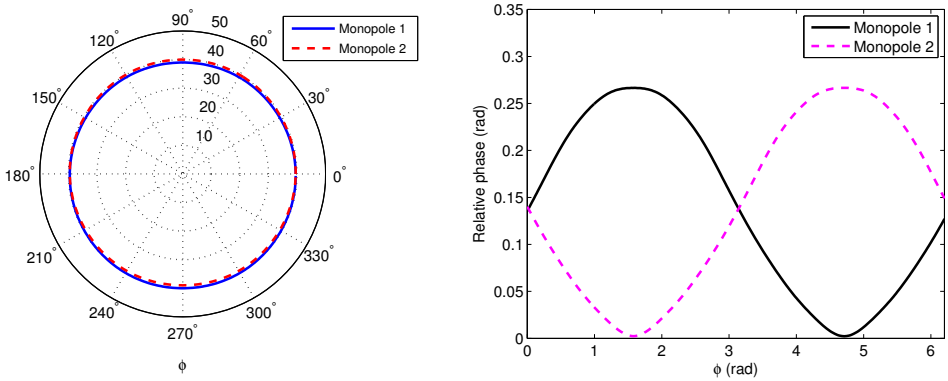

(a) $\left|E_{R_{1,2}}(\varphi)\right|$ in SEMCAD **(b)** Phase of $E_{R_{1,2}}(\varphi)$ in SEMCAD

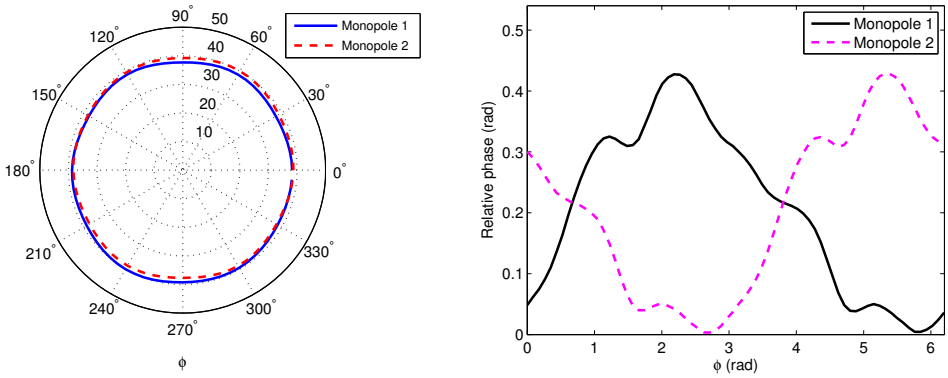

(c) $\left|E_{R_{1,2}}(\varphi)\right|$ in measurement **(d)** Phase of $E_{R_{1,2}}(\varphi)$ in measurement

Figure 4.8: *The simulation and measured results of 2D FF patterns of the monopole array at* $d = 0.05\lambda$.

that the design of the two monopoles and the corresponding z_{in} matching networks are almost symmetric, as the peak of s_{12} and s_{21} of the two branches overlap at 900MHz. Meanwhile, the reflection coefficient of the two monopoles (s_{11} and s_{22} in Figure 4.7) follow each other and both reduce significantly at 900MHz though with different magnitudes. We note that the cross range of s_{11}, s_{12}, s_{21} and s_{22} is the well tuned frequency range of the array. The wider the range is, the larger bandwidth can be achieved after the matching. The designed monopole array gives a 15% bandwidth over 400MHz frequency span as shown in Figure 4.7), which is quite reasonable at the close antenna spacing of $d = 0.05\lambda$.

4.4.3 Open-circuit correlation

Besides the array impedance matrix, ρ_{oc} is another parameter which determines the SC and received power expressions of (3.10) and (3.25). The 3D FF patterns of the array model have been simulated in SEMCAD and measured in experiment for $d = 0.05\lambda$. The 2D FF patterns are generated by slicing the 3D data in the azimuth plane ($\vartheta = 90^\circ$). Then the corresponding simulation and measured 2D and 3D ρ_{oc}s are evaluated using (4.1) and (4.2). According to the experimental scenario, theoretical 2D ρ_{oc} are calculated using (3.7), and the theoretical 3D ρ_{oc} can also be calculated as in [79]. Table 4.1 lists the 2D and 3D theoretical, simulation and measured ρ_{oc}. The measured 2D ρ_{oc} = 0.9473 + j0.0033 will be used for the load impedance selection.

	2D		3D	
	ρ_{oc}	$\lvert\rho_{oc}\rvert$	ρ_{oc}	$\lvert\rho_{oc}\rvert$
Theoretical	0.9755	0.9755	0.9798	0.9798
Simulation	0.9796 + j5.46e-06	0.9796	0.9823 + j2.22e-07	0.9823
Measured	0.9473 + j0.0033	0.9473	0.9658-j0.0009	0.9658

Table 4.1: *Comparison of 2D and 3D theoretical, simulation and measured open-circuit correlation of the two-element monopole array with* 0.05λ *spacing.*

Figure 4.8 depicts the 2D FF patterns of the monopole array generated in both simulation and measurement at $d = 0.05\lambda$. As is shown, the simulation and measured results of the magnitude are well matched in Figure 4.8(a) and 4.8(c). Whereas, the phase of the measured FF patterns in Figure 4.8(d) differs somewhat from the simulation result in Figure 4.8(b). The result in Figure 4.8(d) is slightly right-shifted along the abscissas compared to Figure 4.8(b), which can be explained by the fact that the system is not perfectly centered along direction $\varphi = 0^\circ$ when

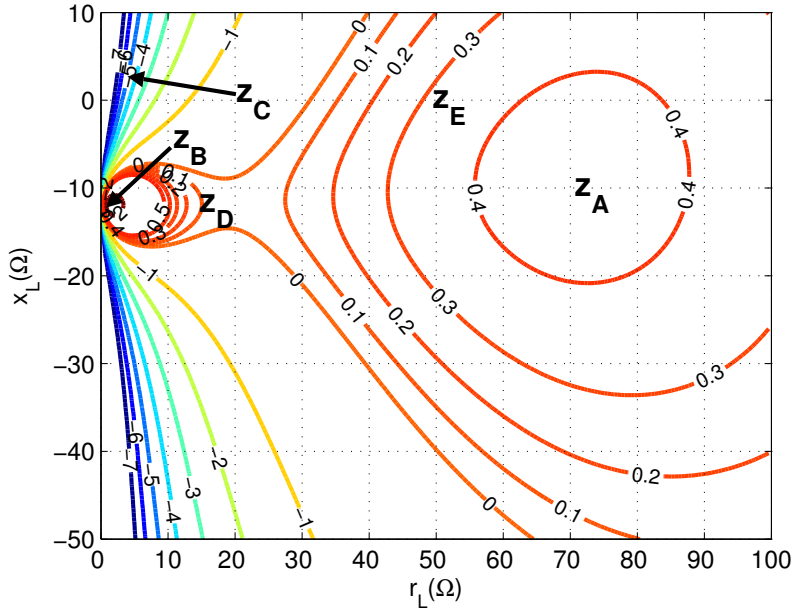

(a) P_{total} in dB

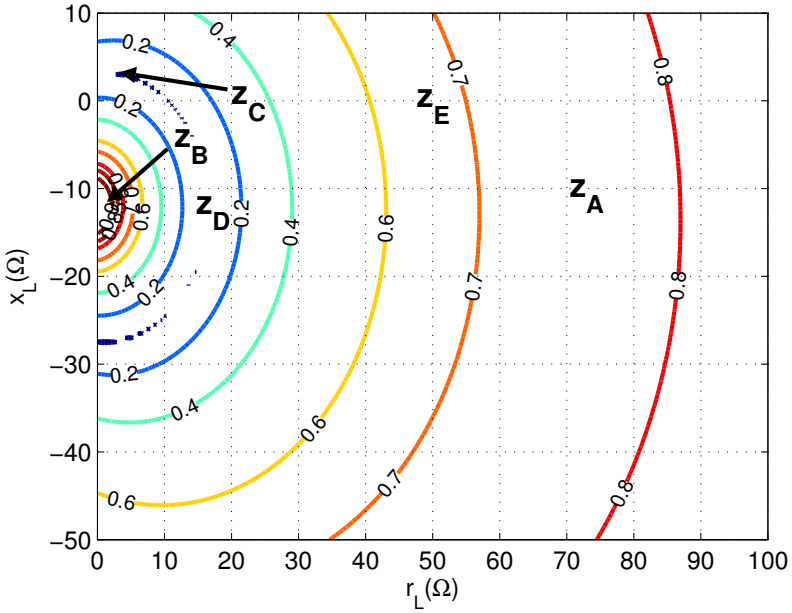

(b) Signal correlation $\tilde{\rho}_{mc}$

Figure 4.9: *The total received power and signal correlation results of the experimental monopole array at* $d = 0.05\lambda$ *with* ρ_{oc} *= 0.9473 + j0.0033.*

measured in the chamber. Meanwhile, the phase curves in Figure 4.8(d) are not as smooth and symmetric as those in Figure 4.8(b). Moreover, they have a higher peak-to-peak difference than the curves in Figure 4.8(b). Many factors can account for these discrepancies, such as the system model is not placed exactly vertical to the ground, the asymmetric design of the two monopoles, etc.

4.5 Selection of the load impedances

The measured array impedances $z_{11,m}$ = 46.72 + j9.39Ω, $z_{12,m}$ = 45.31 - j2.57Ω and ρ_{oc} = 0.9590 - j0.001 are used for the calculation of the total received power in (3.25) on page 47 and SC in (3.10) on page 38 for load selection. We note that a more accurate 2D OC correlation ρ_{oc} = 0.9590 - j0.001 is obtained after the load impedance selection as it will be involved in the following analysis. It will not affect the load selection because the loads are randomly picked from Figure 4.9. Figure 4.9(a) illustrates that the total received power of the monopole array still maintains the 'two maxima' property (in the vicinity of z_A and z_B) of the branch received power from equation (3.23). Also the concentric zero SC contour [22] of the monopole array is still visible in Figure 4.9(b) (along the circle where z_C and z_D locate).

To experimentally verify the P_{total} and $\tilde{\rho}_{mc}$ results of (3.25) and (3.10), five load impedances are selected from Figure 4.9 to be implemented and measured in the anechoic chamber.[3] The value of selected impedances and the reason of selection is summarized in Table 4.2.

	Impedance (Ω)	Reason of selection
z_A	70.69 - j9	local maximum of P_{total} in Figure 4.9(a)
z_B	1.5 - j12.8	local maximum of P_{total} in Figure 4.9(a)
z_C	4.06 + j3	zero $\tilde{\rho}_{mc}$ with relatively low P_{total} in Figure 4.9(b)
z_D	16.5 - j12	zero $\tilde{\rho}_{mc}$ with relatively high P_{total} in Figure 4.9(b)
z_E	50	characteristic impedance

Table 4.2: *Selected load impedances for measurement.*

[3] According to the ρ_{oc} data 'Measurement 2D (new)', the load points $z_A \sim z_D$ will not locate at the power peaks or zero-correlation circle any more, the following measurement is still valid to reflect the trend of P_{total} and $\tilde{\rho}_{mc}$.

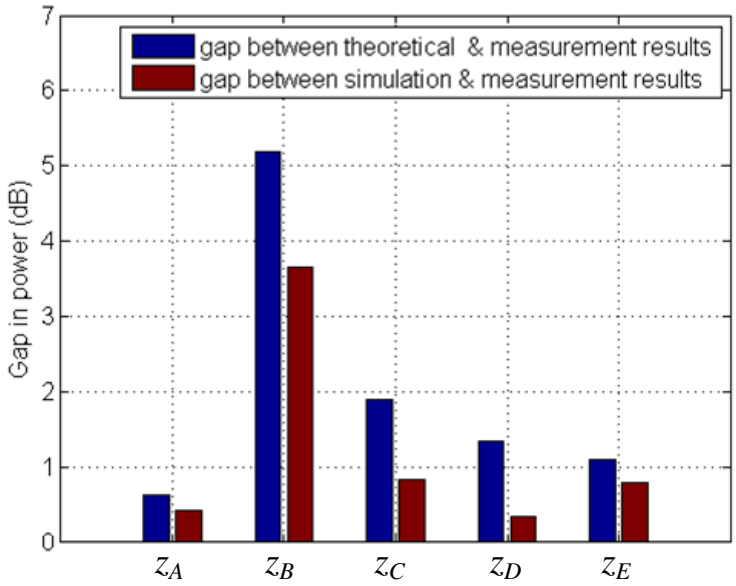

Figure 4.10: *The 2D total received power gap between the theoretical, simulation and measured results.*

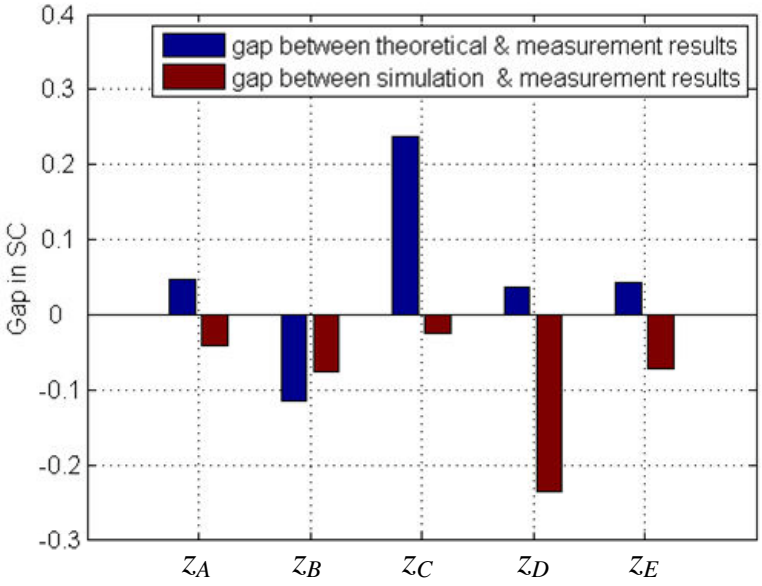

Figure 4.11: *The 2D SC gap between the theoretical, simulation and measured results.*

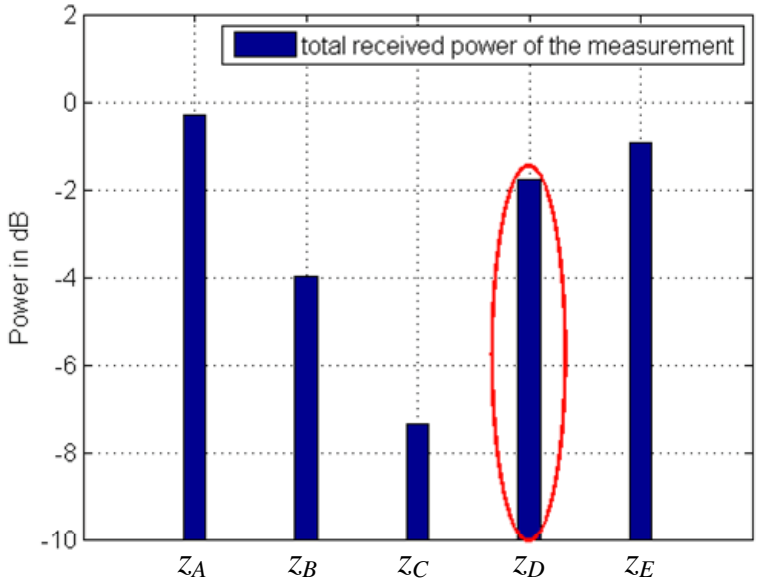

Figure 4.12: *The measured 2D total received power of the two-monopole array at $d = 0.05\lambda$.*

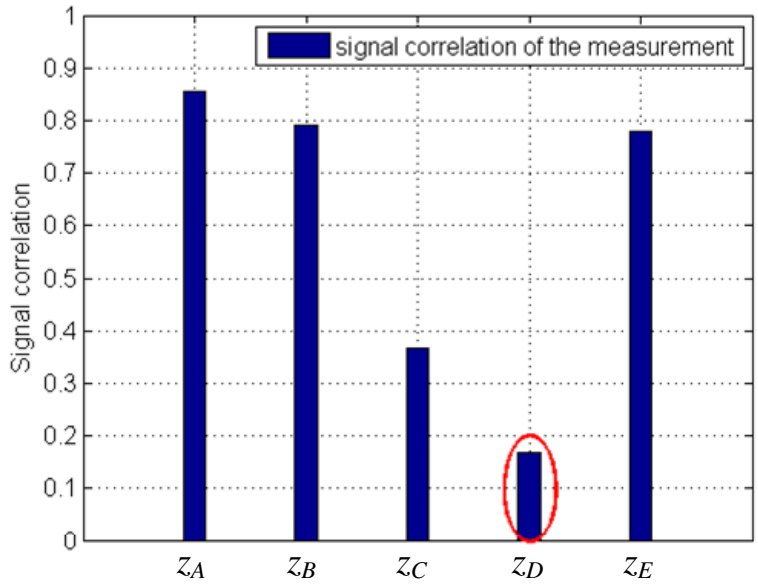

Figure 4.13: *The measured 2D SC of the two-monopole array at $d = 0.05\lambda$.*

	$Impedances$ (Ω)	Simulation*		Theoretical†		Measurement‡	
		P_{total} (dB)	$\tilde{\rho}_{mc}$	P_{total} (dB)	$\tilde{\rho}_{mc}$	$P_{2d,m}$ (dB)	$\rho_{2d,m}$
z_A	70.69 - j9	0.1310	0.8960	0.3393	0.8076	-0.2870	0.8541
z_B	1.5 - j12.8	-0.3479	0.8668	1.1898	0.9049	-3.9977	0.7910
z_C	4.06 + j3	-6.5213	0.3923	-5.4494	0.1304	-7.3498	0.3681
z_D	16.5 - j12	-1.4224	0.4032	-0.4298	0.1299	-1.7685	0.1674
z_E	50	-0.1300	0.8525	0.1822	0.7363	-0.9154	0.7800

*simulation results in SEMCAD with $z_{11,s}$ = 46.72 + j9.39Ω, $z_{12,s}$ = 45.31 - j2.57Ω, and ρ_{oc} = 0.959-j0.001

†theoretical results with $z_{11,m}$ = 46.72 + j9.39Ω, $z_{12,m}$ = 45.31 - j2.57Ω, and ρ_{oc} = 0.959-j0.001

‡measured results with $z_{11,m}$ = 46.72 + j9.39Ω, $z_{12,m}$ = 45.31 - j2.57Ω, and ρ_{oc} = 0.959-j0.001

Table 4.3: *Comparison of 2D theoretical, simulation and measured total received power and correlation of selected loads.*

4.6 Results comparison and analysis

4.6.1 Received power and signal correlation

The total received power and SC of the selected loads are measured in both 2D and 3D scenarios. The 2D theoretical, simulation and measured results are listed in Table 4.3. The theoretical and simulation total received power and SC are calculated using (3.25) and (3.10), while the corresponding measured results are computed using (4.3) and (4.1). To better understand Table 4.3, the received power and SC gap between the theoretical, simulation and measured results are plotted in Figure 4.10 and 4.11.

Comparing the theoretical and measured results in Table 4.3 (the left bar of each selected load in Figure 4.10), it is apparent that the measured total powers different matching cases generally suffer a degradation of 0.6$\sim$1.3dB except at point z_B where the gap is as large as 5.2dB. Regarding the measured SCs (the left bar of each selected load in Figure 4.11), they are 0.05 higher than the theoretical results for most cases: at point z_B 0.1 lower and point z_C 0.22 higher. Generally, the measured received power values agree better with the corresponding simulation results (the right bars of each selected load in Figure 4.10) than the theoretical results in Table 4.3; the gap between the measured and simulated SC (the right bars of each selected load in Figure 4.11) is also smaller compared to the theoretical cases except for the correlation of point z_D and z_E. The total received power and SC performance metrics (especially the trend) are in general consistent between the corresponding simulation and measured cases. The comparison of 3D theoretical, simulation and measured total received power and SC of selected loads is listed in Appendix B.3.

Contrasting among the measured results of the load points $z_A \sim z_E$ in Figure 4.12 and 4.13, it is shown that high received power and SC exist for both impedances z_A and z_B, while z_C has the lowest SC but also the lowest total received power. Only point z_D provides the lowest SC and relatively high received power simultaneously. It can be seen from Figure 4.12, 4.13 and the simulation results in Table 4.3 that load impedance z_D is the preferred matching impedance compared to points z_B and z_C which are located in the steep gradient region for the power in Figure 4.9(a).

4.6.2 Discrepancy study

To further study the discrepancies between the measured results and the predicted theoretical and simulation results, the contour plots of the total received power and SC in different scenarios of the two-monopole array are depicted in Figure 4.14. Figure 4.14(a) and 4.14(b) are generated using the measured $z_{11,m}$, $z_{12,m}$ and ρ_{oc} = 0.9473 + j0.0033 as in Figure 4.9, which was used to select the test load points $z_A \sim z_E$. Figure 4.14(c) and 4.14(d) are plotted using the same $z_{11,m}$, $z_{12,m}$ and the newly measured ρ_{oc} = 0.9590 - j0.0010 in Table 4.1. In Figure 4.14(e) and 4.14(f), the values for $z_{11,s}$, $z_{12,s}$ and ρ_{oc} = 0.9796 simulated in SEMCAD are adopted.

In Figure 4.14 it is clear that in any received power evaluation, the load z_B is located in the super high power gain area. However, in measurement this advantage has disappeared as shown in Figure 4.10. The additional power loss of the directly measured case in Figure 4.10 compared to the theoretical and simulation results can be partially accounted for by ohmic losses in the antennas and the matching networks. The ohmic loss is particularly severe in the case of the load z_B where the predicted super high gain is eliminated by high current flow.

The selected load z_D is around the zero ρ_{oc} circle in Figure 4.14(b) and 4.14(d), while it located at ρ_{oc} = 0.4 circle in Figure 4.14(f). This explains the disagreement between the simulation and measured SC at z_D in Figure 4.11. Meanwhile, the gap of simulation and measured SC of the impedance z_C should be different from each other as both z_C and z_D are selected from the zero ρ_{oc} circle in Figure 4.14(b). However, this predicted phenomenon has also been changed by the ohmic loss, because z_C is almost a capacitive load as z_B.

Comparing Figure 4.14(a) and 4.14(c), Figure 4.14(b) and 4.14(d), the received power and SC distribution have changed dramatically with the same array impedances but different ρ_{oc}

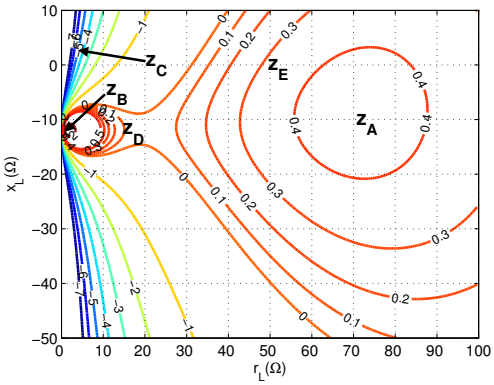

(a) Total power in measurement,ρ_{oc} = 0.9473 + j0.0033

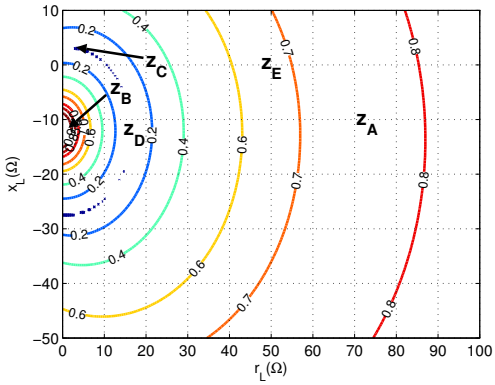

(b) SC in measurement, ρ_{oc} = 0.9473 + j0.0033

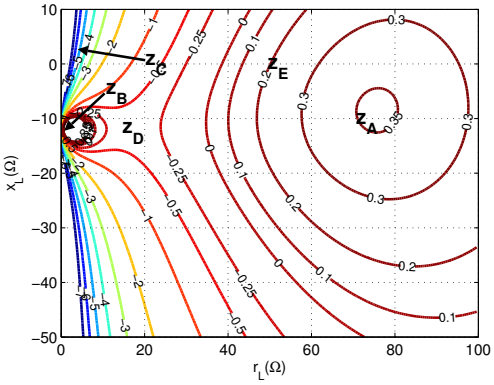

(c) Total power in measurement,ρ_{oc} = 0.9590 - j0.0010

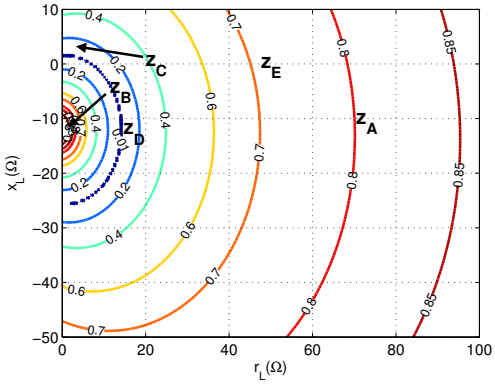

(d) SC in measurement, ρ_{oc} = 0.9590 - j0.0010

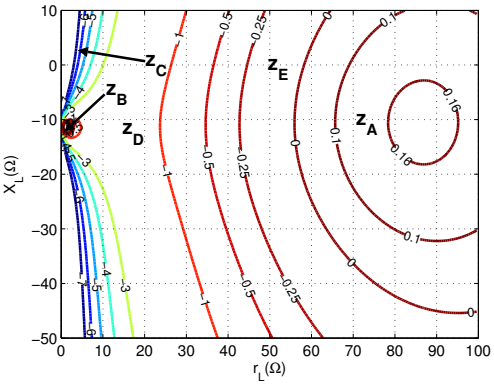

(e) Total power in SEMCAD, ρ_{oc} = 0.9796

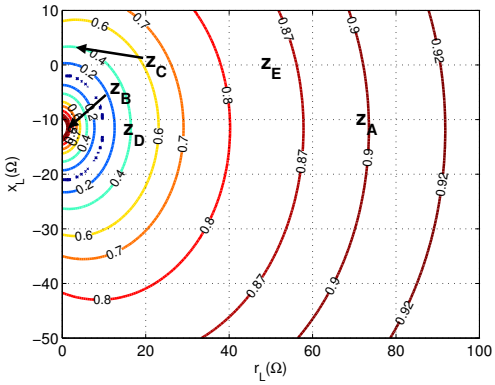

(f) SC in SEMCAD, ρ_{oc} = 0.9796

Figure 4.14: *The contour plots of the total received power (dB) and SC in different scenarios of the two-monopole array at $d = 0.05\lambda$.*

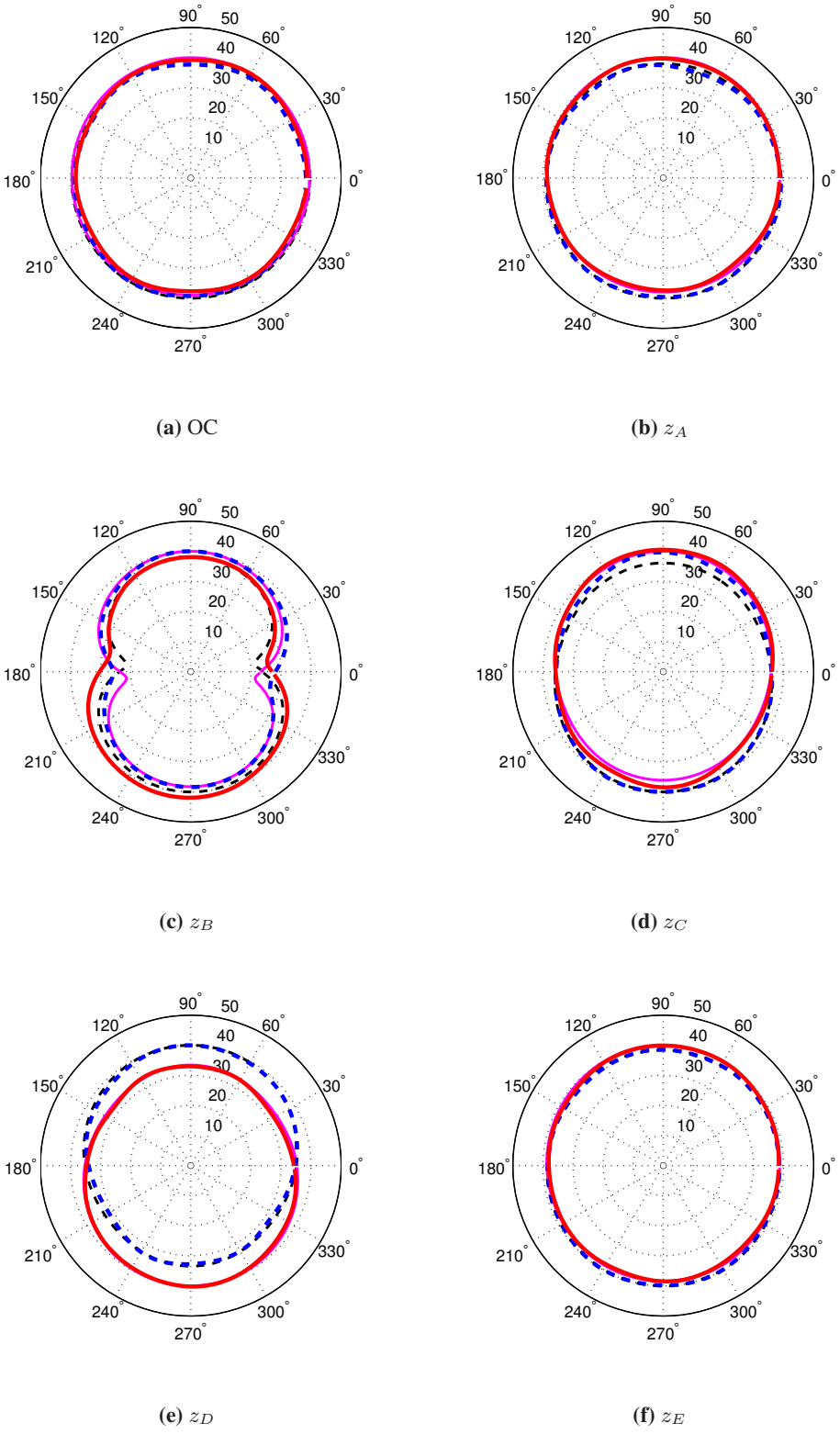

(a) OC **(b)** z_A

(c) z_B **(d)** z_C

(e) z_D **(f)** z_E

Figure 4.15: *Magnitude (dB) of the 2D FF patterns in SEMCAD and measurement of the selected cases as a function of φ. Legend of the curves is the same as in Figure 4.16.*

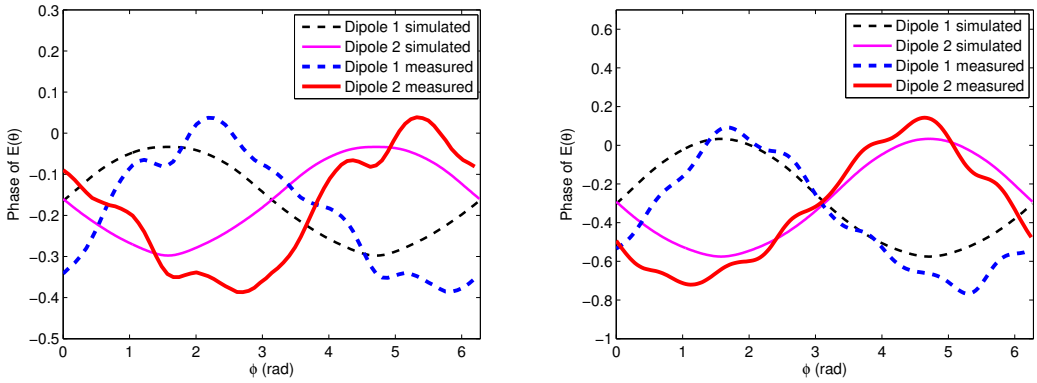

(a) OC **(b)** z_A

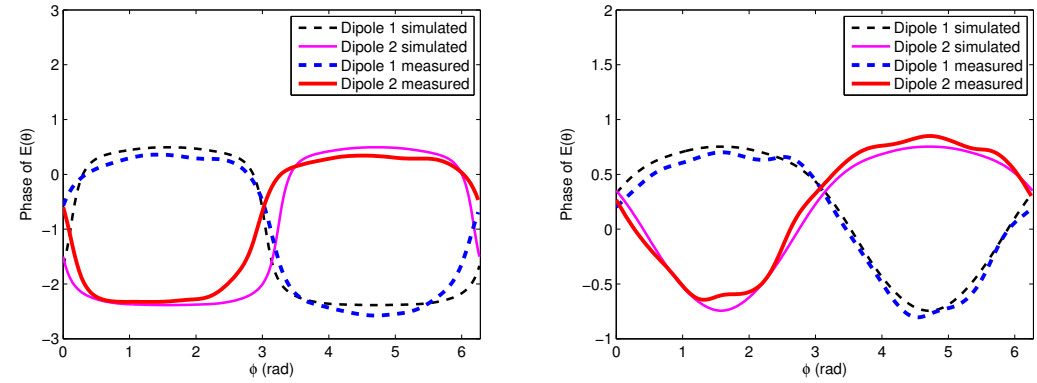

(c) z_B **(d)** z_C

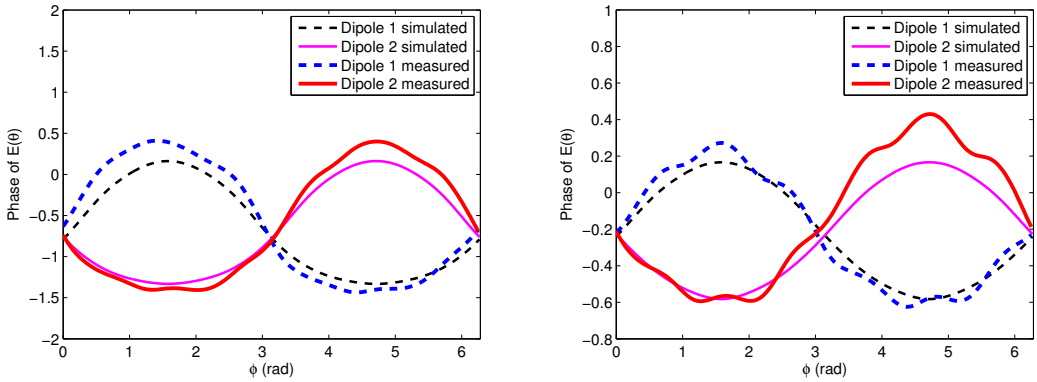

(e) z_D **(f)** z_E

Figure 4.16: *Phase of the 2D FF patterns in SEMCAD and measurement of the selected cases.*

values. Moreover, it is found that the simulation results in Table 4.3 remain almost unchanged if the measured antenna impedances $z_{11,m}$, $z_{12,m}$ (and simulated ρ_{oc}) are used instead of the simulated impedances $z_{11,s}$, $z_{12,s}$. Taking this into consideration, and the plot differences in Figure 4.14, we conclude that both received power and SC of the compact antenna array are sensitive to the variation of ρ_{oc}. It is difficult to measure ρ_{oc} accurately, so this will contribute significantly to the discrepancies in Figure 4.10, 4.11, and 4.14.

Figures 4.15 and 4.16 show the magnitude and phase of the 2D FF patterns of different selected load cases. Both simulation and measured results are plotted for comparison. The open-circuited termination case as in Section 4.4.3 is also displayed in Figure 4.15(a) and 4.16(a) with other matching terminations. We note that the simulation and measured FF patterns are normalized to the corresponding z_{11}^* matched single monopole case to achieve equal comparison. Interestingly, the experimental magnitude of the FF patterns of each matching case matches well to the simulation results except load z_B in Figure 4.15(c). Regarding to the phase of the FF patterns in Figure 4.16, the general trend of the simulation and measured results of the identical matching case agree well with each other. The asymmetric design of the two monopoles and/or matching networks is also clearly reflected by Figure 4.16. Thus, Figure 4.16 illustrates that the phase differences of the FF patterns mainly account for the ρ_{oc} discrepancies between the simulation and measured results. Although only the magnitude of the FF pattern has been considered in previous research, we show that the phase of the FF patterns becomes critical if the SC of the antenna array is studied.

4.7 MIMO capacity evaluation

The purpose of introducing matching networks into a compact receive array is to improve the MIMO system performance. We are curious to know if the impedance which maximizes the received power is related to the MIMO capacity maximization as well.

Table 4.4 lists the ergodic capacity C_Z calculated in (3.45) using antenna parameters generated from simulation and measurement of different selected loads. Each C_Z is averaged over 7000 realizations, and ρ_r = 20dB. For the z_{11}^* match, the $z_{\rm in}$ match and the optimum SPM for capacity maximization $z_{\rm opt}$, there are two sets of impedances shown based on the corresponding monopole impedances and OC correlations obtained in simulation and measurement,

	$Impedances\ (\Omega)$	$C_m\ (bits/s/Hz)$	
		sim†	mea‡
z_A	70.69 - j9	7.8572	8.4699
z_B	1.5 - j12.8	7.8150	8.3154
z_C	4.06 + j3	5.6516	6.2921
z_D	16.5 - j12	8.4068	9.1431
z_0	50	7.9810	8.6913
z_{11}^*	45.6 - j20.5 (sim)	8.0201	/
	45.5 - j19.22 (mea)	/	8.7579
z_{in}	8.29 - j11.46 (sim)	8.4517	/
	11.41 - j11.88 (mea)	/	9.2046
z_{opt}	8.67 - j11.85 (sim)	8.5313	/
	11.23 - j11.6 (mea)	/	9.2688

†results using $z_{11,s}$, $z_{12,s}$ and ρ_{oc} = 0.9796 from SEMCAD simulation.

‡results using $z_{11,m}$, $z_{12,m}$, and ρ_{oc} = 0.959-j0.001 from measurement.

Table 4.4: *Comparison of the ergodic capacity between chosen loads with antenna parameters from simulation and measurement & Contrast between numerical and simulation results of optimum single-port impedance.*

respectively.[4] The single monopole with z_{11}^* match (listed in Table 4.4) is used for power normalization of the corresponding cases. It is obvious that z_{11} for a single monopole differs from that in the array, because in traditional simulations an approximate method is used to simulate the MC effect, where identical values of z_{11} are assumed for both single antenna and antenna array cases. However, the value z_{11} of isolated antenna does change when it is put in the array [18, 60].

Generally, C_Z using the antenna parameters in measurement is about 0.5 bits/s/Hz higher than the corresponding results computed from the simulation of each load point. However, the even gap of the capacity results reveals the consistency between measurement and simulation. Apparently, none of the impedances either maximizing the received power or achieving zero output correlation maximize the capacity in Table 4.4, which illustrates that the impedance for power maximization cannot maximize the MIMO capacity [12, 23]. Among the selected impedances, z_D offers the best performance as it is chosen to be the load with the highest received power along the zero correlation circle, and also because it is close to z_{opt}. The commonly used matching impedances z_0 and z_{11}^* give inferior performance compared to the corresponding z_{in} match which provides an average capacity advantage of 0.5 bits/s/Hz. Another interesting phe-

[4]We note that z_{opt} of each case is found by searching from a certain area of z_L with calculated C_Z. The results for C_Z as a function of various z_L can be found in Appendix B.4.

nomenon is that the results of z_{opt} are very close to z_{in}, especially for the measured case. Is there a certain link between them? This question will be thoroughly investigated in Chapter 5.

4.8 Summary

In this chapter the normalized total received power and SC have been investigated theoretically and experimentally by constructing a highly compact (spaced by 0.05λ) two-element $\lambda/4$ monopole array with different matching terminations. The simulation tools SEMCAD and FEKO are also used to calibrate the implementation. The conclusions of this chapter are:

- The implementation confirms the theoretical predictions that a relatively high total received power and low SC of the compact array can be achieved by choosing the proper load impedance, for example z_D. However, the capacitive load z_B predicted to maximize the received power in theory performs poorly in practice.
- The matching network design can be realized using the microstrip transmission line single stub tuning technique. Apart from the empirical equations, some attention has to be paid in practice due to the real dimension of the transmission lines and physical structure based on the simulation in FEKO. Detailed design rules have been summarized in Appendix C.
- The received power and SC results of the selected matching cases in measurement agree better to the corresponding simulation results in SEMCAD than the theoretical predictions, which illustrates that the theoretical model simplification leads to system performance discrepancies. Other reasons for the discrepancies between the measurement and simulation results include:
  - The ohmic losses of the antennas and the matching networks.
  - The sensitivity of the high power gain location to the changing of ρ_{oc} (see Figure 4.14).
  - The error of ρ_{oc} caused by the inaccurately measured complex-valued FF patterns.
  - It is difficult to achieve ideal matching loads in implementation even though fine-tuning is performed.

- The matching loads for received power maximization or zero SC cannot maximize the MIMO capacity simultaneously. However, more research can be done to confirm that this is indeed true.

In general, the load values could be optimized to combat performance degradation due to MC effect in compact antenna arrays, which improves the feasibility of incorporating MIMO techniques into small handhelds.

Chapter 5
Optimal single-port matching impedance for capacity maximization in compact MIMO arrays

5.1 Introduction

This chapter investigates the optimal SPM impedance for capacity maximization of compact MIMO systems as a continuous study of Chapter 4. Before the investigation, a general description of the compact MIMO systems using the Z-parameter approach is prerequisite. Identification of the optimal SPM for capacity maximization will be presented from a mathematical point of view.

The contributions of this chapter are:

- A complete framework for $N \times N$ MIMO systems including the MC effect at both link ends using Z-parameters from a novel power transfer point of view is developed. This framework is suitable for any kind of single-mode antennas at the link ends. The analysis also embraces a transmit power constraint corresponding to the S-parameter approach [18]. Moreover, a modified channel matrix including the MC effect is presented. Then the model is simplified to consider the MC effect at the receivers only, which shows that the channel model used in equation (3.45) [12, 23] is a special case of the general MIMO channel matrix presented here. A number of simulation results show the convenience of our Z-parameter approach in the study of $N \times N$ compact MIMO systems.

- The derivation of the optimal SPM for capacity maximization of a 2×2 MIMO system with MC at the receivers only is given, utilizing an upper bound of the ergodic capacity. The deviation holds for all single-mode antennas. The optimal SPM for capacity maximization in high signal-to-noise ratio (SNR) and low SNR scenarios are also discussed. Closed-form results in high SNR regime are given and proved to equal the *input*

impedance (Appendix A) of the receive antennas. The derivation flow is illustrated using ideal dipole antennas. A perfect match is shown between analytical and simulation results.

- The performance sensitivity of a 2×2 MIMO system with coupled half-wavelength dipoles and SPM networks is explored versus antenna spacing and dipole length. The system sensitivity to the two joint parameters is also discussed. Performance efficiency and precision error are defined to study the MIMO system sensitivity to the SPM design. The advantage of using the optimal SPM compared to other SPM cases are evaluated by a number of simulation results.

The remainder of this chapter is organized as follows. Section 5.2 presents the analysis framework of the MIMO system model based on the Z-parameter approach. Simulation results are also shown to evaluate the system performance. Section 5.3 states the problem origin, provides the numerical derivation of the optimal SPM impedance for a 2×2 MIMO system and gives closed-form results in high SNR regime. Section 5.3 also applies the analytical results to ideal dipole antennas, and compares the numerical and simulation results. Section 5.4 studies the 2×2 MIMO system sensitivity as a function of antenna spacing, dipole length, and SPM networks. The superiority of the optimal SPM impedance for MIMO capacity maximization to other matching networks is also discussed. Section 5.5, summarizes the chapter.

5.2 MIMO System Analysis Based on Z-Parameters

As mentioned in Section 3.4.1.2, it is necessary to obtain the modified MIMO channel matrix expression utilizing Z-parameters to study the impact of the SPM impedance on MIMO system performance.

Some key assumptions of the simulations in this chapter:

- $N \times N$ MIMO systems with MC and SPM are at the receiver only;
- channel $\mathbf{H}$ is frequency-flat, rich scattering, and without a line-of-sight (LOS) propagation component;
- receiver knows full channel state information (CSI) while transmitter has no information of CSI;

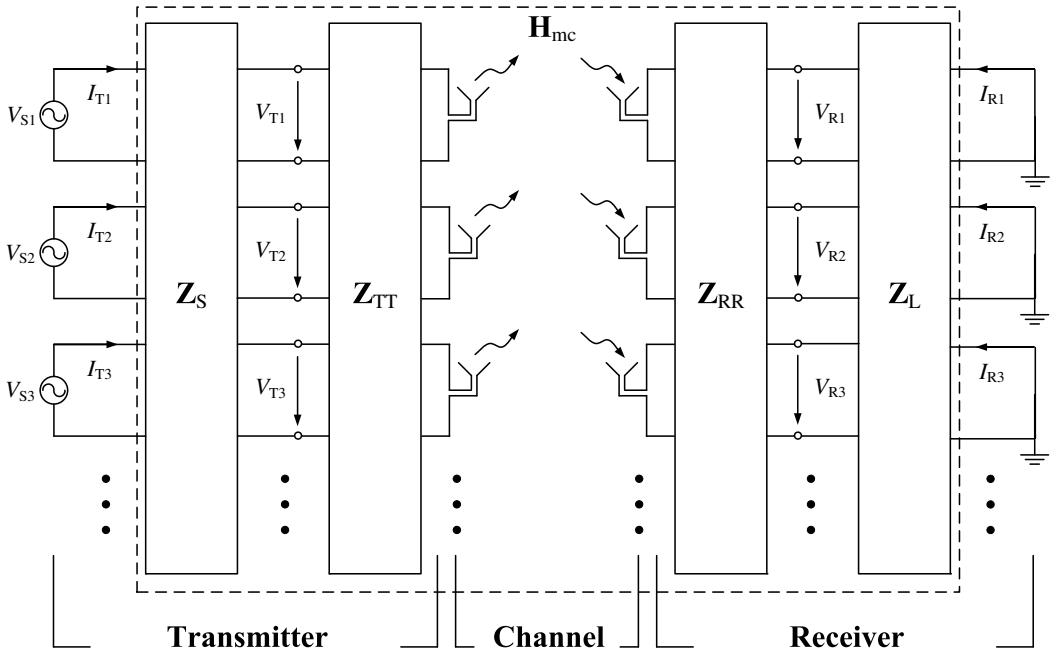

Figure 5.1: *Diagram of a MIMO system with antenna impedance matrices and matching networks at both link ends.*

- transmit power is equally distributed at each transmit antenna;
- the distribution of AOA is uniform PAS with full AS;
- transmitter and receiver arrays are linear;
- transmit antennas are sufficiently separated;
- transmitter does not affect the spatial properties of the received signal at all;
- the array elements are of identical polarization;
- the dimension of the arrays is negligible compared to the link distance;
- ideal $\lambda/2$ dipoles are utilized at both ends.

Under all the above assumptions, we start to investigate the impact of MC of the compact transmitter and/or receiver arrays on the original MIMO system excluding other possible factors which would affect the performance.

5.2.1 Framework development

According to the *n*-port theory, the channel transfer function between the transmit and the receive arrays in Figure 5.1 can be represented as [14]

$$\begin{bmatrix} \mathbf{v}_T \\ \mathbf{v}_R \end{bmatrix} = \begin{bmatrix} \mathbf{Z}_{TT} & \mathbf{Z}_{TR} \\ \mathbf{Z}_{RT} & \mathbf{Z}_{RR} \end{bmatrix} \begin{bmatrix} \mathbf{i}_T \\ \mathbf{i}_R \end{bmatrix} \tag{5.1}$$

where $\mathbf{v}_T = [V_{T1}, V_{T2}, ..., V_{TN}]^T$, $\mathbf{i}_T$ = $[I_{T1}, I_{T2}, ..., I_{TN}]^T$ are the voltage and current vectors at the transmit end, respectively. Similarly, $\mathbf{v}_R = [V_{R1}, V_{R2}, ..., V_{RN}]^T$, $\mathbf{i}_R = [I_{R1}, I_{R2}, ..., I_{RN}]^T$ denote the voltages and currents at the receive end. The diagonal sub-block matrices $\mathbf{Z}_{TT}$ and $\mathbf{Z}_{RR}$ are both antenna impedance matrices containing the self and mutual impedances with dimensions $N \times N$ for both the transmit end and receive end. The $N \times N$ matrix $\mathbf{Z}_{RT}$ can be translated as the impedance transfer matrix from transmitter to receiver [18] due to the impact of transmit end currents on the receive end voltages. We define $\mathbf{Z}_{TR} = 0$ to indicate that the transmitters are blind to the conditions (or currents) at the receivers.

In the compact receive subsystem of Figure 5.1, an $N \times N$ impedance matching network $\mathbf{Z}_L$ is added after the receive antennas to compensate for the MC induced power reduction. Utilizing circuit theory at the receive subsystem it is easy to obtain

$$\mathbf{v}_R = -\mathbf{Z}_L \mathbf{i}_R. \tag{5.2}$$

Substituting (5.2) into (5.1), the receive voltage $\mathbf{v}_R$ as a function of the transmit voltage $\mathbf{v}_T$

$$\mathbf{v}_R = \left(\mathbf{I} + \mathbf{Z}_{RR}\mathbf{Z}_L^{-1}\right)^{-1} \mathbf{Z}_{RT}\mathbf{Z}_{TT}^{-1}\mathbf{v}_T. \tag{5.3}$$

Now we look back to the transmit subsystem. Usually the transmit antennas are assumed to be spaced sufficiently far apart to ignore the impact of MC, but even then mismatches between antennas and corresponding sources still exists. As future wireless communication may involve peer-to-peer transmission between compact MIMO terminals (eg. mobile cooperation [104]), MC will be an issue for both link ends. Thus, a suitable source impedance network $\mathbf{Z}_S$ is inserted between the sources and transmit antennas to ensure efficient power transmission. Similar to the receive subsystem, the relation between the source voltage $\mathbf{v}_S$ and transmit voltage

$\mathbf{v}_T$ is

$$\mathbf{v}_T = \mathbf{Z}_{TT}\left(\mathbf{Z}_{TT} + \mathbf{Z}_S\right)^{-1}\mathbf{v}_S \tag{5.4}$$

where $\mathbf{v}_S = [V_{S1}, V_{S2}, ..., V_{SN}]^T$. Substituting (5.4) into (5.3) results in

$$\mathbf{v}_R = \overbrace{\mathbf{Z}_L \underbrace{\left(\mathbf{Z}_L + \mathbf{Z}_{RR}\right)^{-1}\mathbf{Z}_{RT}\left(\mathbf{Z}_{TT} + \mathbf{Z}_S\right)^{-1}}_{-\mathbf{i}_R}\mathbf{v}_S}^{\mathbf{H}_V} \tag{5.5}$$

where $\mathbf{H}_V$ is the channel/voltage transfer matrix [14]. However, because only the voltage across the resistance can be exploited by the receiver, $\mathbf{H}_V$ has to be modified to fulfill the power transfer requirement. We define $\mathbf{Z}_{L+R} = \mathbf{Z}_L + \mathbf{Z}_{RR}$, $\mathbf{Z}_{T+S} = \mathbf{Z}_{TT} + \mathbf{Z}_S$ and substitute $\mathbf{i}_R$ as defined in (5.5), then the total average received power of the MIMO system is given by

$$\begin{aligned} P_R &= E\left\{\mathrm{Tr}\left(\mathrm{Re}\left\{\mathbf{Z}_L\mathbf{i}_R\mathbf{i}_R^H\right\}\right)\right\} \\ &= E\left\{\mathrm{Tr}\left(\mathrm{Re}\left\{\mathbf{Z}_L\right\}\mathbf{Z}_{L+R}^{-1}\mathbf{Z}_{RT}\mathbf{Z}_{T+S}^{-1}\mathbf{v}_S\mathbf{v}_S^H\mathbf{Z}_{T+S}^{-H}\mathbf{Z}_{RT}^H\mathbf{Z}_{L+R}^{-H}\right)\right\} \\ &= E\left\{\mathrm{Tr}\left(\mathbf{R}_L^{1/2}\mathbf{Z}_{L+R}^{-1}\mathbf{Z}_{RT}\mathbf{Z}_{T+S}^{-1}\mathbf{v}_S\mathbf{v}_S^H\mathbf{Z}_{T+S}^{-H}\mathbf{Z}_{RT}^H\mathbf{Z}_{L+R}^{-H}\mathbf{R}_L^{1/2(H)}\right)\right\} \end{aligned} \tag{5.6}$$

where $\mathbf{R}_L = \mathrm{Re}\left\{\mathbf{Z}_L\right\}$.

At the transmit end, the total average transmitted power is

$$P_T = E\left\{\mathrm{Tr}\left(\mathrm{Re}\left\{\mathbf{Z}_{TT}\mathbf{i}_T\mathbf{i}_T^H\right\}\right)\right\} = E\left\{\mathrm{Tr}\left(\mathbf{R}_T^{1/2}\mathbf{Z}_{T+S}^{-1}\mathbf{v}_S\mathbf{v}_S^H\mathbf{Z}_{T+S}^{-H}\mathbf{R}_T^{1/2(H)}\right)\right\} \tag{5.7}$$

where $\mathbf{R}_T = \mathrm{Re}\left\{\mathbf{Z}_{TT}\right\}$. If only the receiver knows the channel conditions, P_T can be evenly distributed across the antennas at the transmit end. Then (5.6) becomes

$$P_R = E\left\{\mathrm{Tr}\left(\mathbf{H}_{mc}\frac{P_T}{N}\mathbf{I}\mathbf{H}_{mc}^H\right)\right\} \tag{5.8}$$

where $\mathbf{H}_{mc}$ is the channel transfer matrix between the source and the receiver load including the MC effect as represented in Figure 5.1. We assume identical antenna elements are used in the whole system model, as a result all the matrices in (5.7) are symmetric. Equation (5.7) can be substituted into (5.8) to give

$$P_R = \frac{1}{N}E\left\{\mathrm{Tr}\left(\mathbf{H}_{mc}\mathbf{R}_T^{1/2}\mathbf{Z}_{T+S}^{-1}\mathbf{v}_S\mathbf{v}_S^H\mathbf{Z}_{T+S}^{-H}\mathbf{R}_T^{(1/2)(H)}\mathbf{H}_{mc}^H\right)\right\}. \tag{5.9}$$

Comparing (5.6) and (5.9) we have

$$\mathbf{H}_{mc} = \mathbf{R}_L^{1/2}\mathbf{Z}_{L+R}^{-1}\mathbf{Z}_{RT}\mathbf{R}_T^{-1/2} = \mathbf{R}_L^{1/2}\mathbf{Z}_{L+R}^{-1}\mathbf{H}\mathbf{R}_T^{-1/2}. \tag{5.10}$$

The matrix $\mathbf{Z}_{RT}$ represents the ratio of the OC received voltages to the transmit currents as defined in (3.40) on page 58 in Chapter 3. Given a propagation channel $\mathbf{H}$ in (5.10) includes the effect of $\mathbf{Z}_{RT}$ [27]. Further we assumed that the transmitter does not affect the spatial properties of the received signal at all, channel $\mathbf{H}$ becomes the Kronecker model defined on page 14 in Chapter 2. We have

$$E\left\{(\mathbf{H})_{ik}(\mathbf{H})_{jl}^*\right\} = c\,(\mathbf{\Psi}_T)_{kl}\,(\mathbf{\Psi}_R)_{ij} \tag{5.11}$$

where c is the average power gain of each channel branch (assuming the power gain of each branch is the same), $\mathbf{\Psi}_T$ and $\mathbf{\Psi}_R$ are $N \times N$ transmit and receive covariance matrices, respectively [40] with $\left|(\mathbf{\Psi}_T)_{ij}\right|$, $\left|(\mathbf{\Psi}_R)_{ij}\right| \leq 1$ and $(\mathbf{\Psi}_T)_{ii}$, $(\mathbf{\Psi}_R)_{ii} = 1, i, j = 1, 2, ..., N$. We assume $c = 1$ in the following analysis. Also the MIMO channel should be normalized to the average channel gain of both link ends for the single antenna case. Consider a SISO system with both antennas z_{11}^* matched, i.e. $z_L = z_{11}^*$. Utilizing (5.6) and (5.9) we obtain

$$E\{hh^*\} = \frac{1}{4r_{11}^2}E\{z_{RT}z_{RT}^*\} \tag{5.12}$$

where h and z_{RT} are SISO channel and transfer impedance from transmitter to receiver, respectively, and $r_{11} = \mathrm{Re}\{z_{11}\}$. The general MIMO system channel transfer matrix including the MC effect at both link ends represented in Z-parameters is

$$\hat{\mathbf{H}}_{mc} = 2r_{11}\mathbf{R}_L^{1/2}\mathbf{Z}_{L+R}^{-1}\mathbf{\Psi}_R^{1/2}\mathbf{H}_{i.i.d.}\mathbf{\Psi}_T^{1/2}\mathbf{R}_T^{-1/2}. \tag{5.13}$$

Another method is available to prove (5.13) from the electromagnetic transmission point of view. We return to (5.5) and define

$$\mathbf{v}_{RT} = \mathbf{Z}_{RT}\mathbf{i}_T = \mathbf{Z}_{RT}(\mathbf{Z}_{TT} + \mathbf{Z}_S)^{-1}\mathbf{v}_S, \tag{5.14}$$

where the voltage vector $\mathbf{v}_{RT}$ is recognized as the received voltages induced by the transmitter currents without the MC effect at the receivers [14]. In other words, the elements of $\mathbf{v}_{RT}$ are the OC voltages caused by the incident electromagnetic field when other receive antennas are

open-circuited [11, 14]. Utilizing (5.5) and (5.14), (5.6) can be rewritten as

$$P_R = E\left\{\mathrm{Tr}\left(\mathrm{Re}\left\{\mathbf{Z}_L^{-1}\mathbf{v}_R\mathbf{v}_R^H\right\}\right)\right\} = E\left\{\mathrm{Tr}\left(\mathbf{R}_L\mathbf{Z}_{L+R}^{-1}\mathbf{v}_{RT}\mathbf{v}_{RT}^H\mathbf{Z}_{L+R}^{-H}\right)\right\}$$
$$= \mathrm{Tr}\left(\mathbf{R}_L\mathbf{Z}_{L+R}^{-1}E\left\{\mathbf{v}_{RT}\mathbf{v}_{RT}^H\right\}\mathbf{Z}_{L+R}^{-H}\right). \tag{5.15}$$

Normalizing the term $E\left\{\mathbf{v}_{RT}\mathbf{v}_{RT}^H\right\}$ to the SISO case described before, we have

$$\frac{E\left\{\mathbf{v}_{RT}\mathbf{v}_{RT}^H\right\}}{\frac{1}{4r_{11}^2}E\left\{V_{RT}V_{RT}^H\right\}} = 4r_{11}^2\boldsymbol{\Psi}_{\mathbf{oc}} \tag{5.16}$$

where V_{RT} is the OC voltage of the SISO system and $\boldsymbol{\Psi}_{\mathbf{oc}}$ is the so-called OC correlation matrix [22]. If both transmitters and receivers are coupled, $\boldsymbol{\Psi}_{\mathbf{oc}} = \boldsymbol{\Psi}_{\mathbf{R}}\boldsymbol{\Psi}_{\mathbf{T}}$; if the MC effect is assumed at the receivers only, $\boldsymbol{\Psi}_{\mathbf{oc}} = \boldsymbol{\Psi}_{\mathbf{R}}$. Combining (5.7), (5.8), (5.15) and (5.16), we find

$$E\left\{\hat{\mathbf{H}}_{mc}\hat{\mathbf{H}}_{mc}^H\right\} = 4r_{11}^2\mathbf{R}_L\mathrm{Re}\left\{\mathbf{Z}_{TT}^{-1}\right\}\mathbf{Z}_{L+R}^{-1}\boldsymbol{\Psi}_{oc}\mathbf{Z}_{L+R}^{-H}, \tag{5.17}$$

which is exactly the expectation of the total power gain of channel matrix in (5.13).

It is obvious in (5.13) that the source impedance network $\mathbf{Z}_S$ has no impact on the modified MIMO channel, as it has already affected the transmitted power in (5.7). If the transmitters are coupled, a new power constraint has to be defined for the channel-known-at-transmitter case, i.e. the waterfilling algorithm [18].

The maximum power transfer from the receive antennas to the load networks happens when $\mathbf{Z}_L = \mathbf{Z}_{RR}{}^H$, which is easily achieved in theory but difficult to implement in practice as an additional $N(N-1)/2$ load impedances are needed to decouple the MC among N receive antennas [31, 94]. Therefore, SPM is usually adopted where $\mathbf{Z}_L$ becomes diagonal. In the following sections we will concentrate on the compact receive end of the MIMO system with SPM. We further assume that the transmit antennas are sufficiently separated with no MC, rich scattering, i.e. $\boldsymbol{\Psi}_T = \mathbf{I}$, and z_{11}^* match is used. Also when the receive antennas are matched with identical load impedance z_L, then (5.13) can be simplified as

$$\tilde{\mathbf{H}}_{mc} = 2\sqrt{r_{11}}\mathbf{R}_L^{1/2}\mathbf{Z}_{L+R}^{-1}\boldsymbol{\Psi}_R^{1/2}\mathbf{H}_{i.i.d.}. \tag{5.18}$$

Under the equally distributed transmit power assumption, the narrowband MIMO capacity for

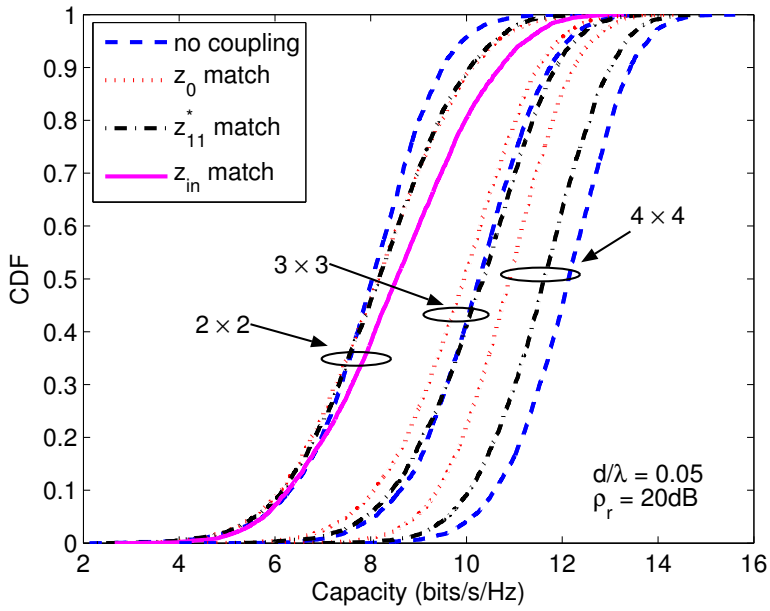

Figure 5.2: *The cumulative distribution function of MIMO capacity with different configurations and matching networks.*

the channel matrix given by (5.18) is denoted as

$$C_{mc} = \log_2 \det \left(\mathbf{I} + \frac{\rho_r}{N} \tilde{\mathbf{H}}_{mc} \tilde{\mathbf{H}}_{mc}^H \right). \tag{5.19}$$

Substituting (5.18) into (5.19) for a 2×2 MIMO case, (5.19) is equal to (3.45), which reveals that the assumed channel model in [12, 23] is a special case of our general MIMO channel matrix in (5.13).

5.2.2 System evaluation

To show the correctness of our Z-parameter framework derivation, several simulation results are prepared based on (5.19). MIMO systems with ideal half-wavelength ($\lambda/2$) dipoles equipped at both ends are evaluated. We note that ideal half-wavelength dipoles are adopted because their self and mutual impedances are easily computed numerically, as well as being a reference case in the antenna field. The impedance matrices of other kinds of antennas obtained either analytically or experimentally can be applied in the system model in Section 5.2.1 as well. Hence, the analysis in Section 5.2.1 is general. A uniform distributed PAS with full AS is assumed at the receive end. Thus, the correlation matrix $\mathbf{\Psi}$ can be calculated using (3.7). The

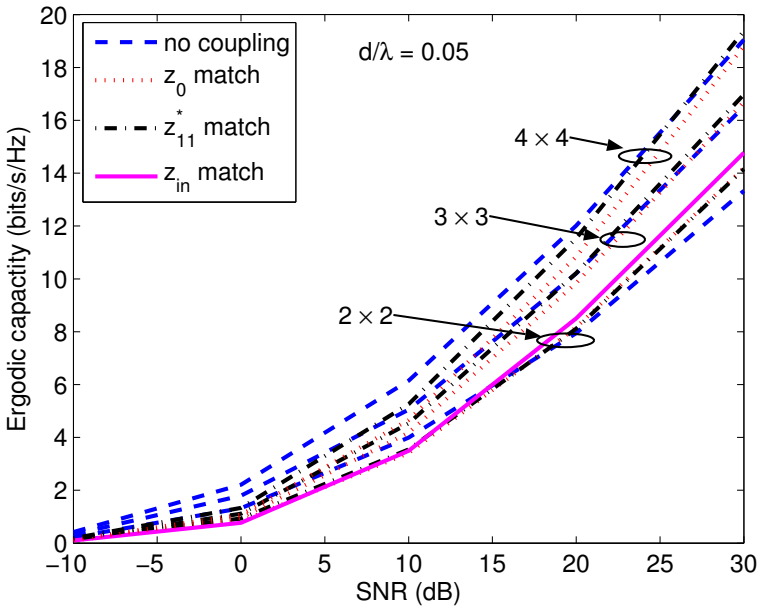

Figure 5.3: *Ergodic capacity as a function of ρ_r of different MIMO configurations with matching networks.*

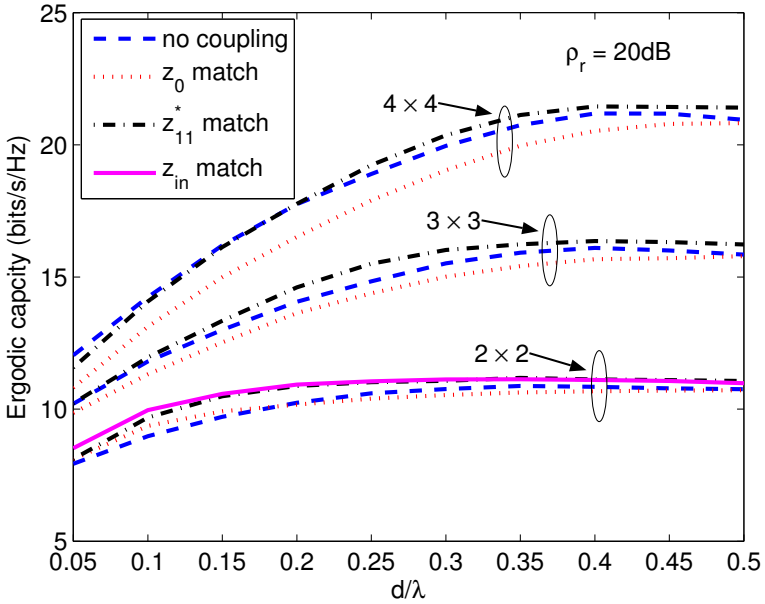

Figure 5.4: *Ergodic capacity of different MIMO configurations with matching networks vs. antenna spacings.*

ergodic capacity of 2×2, 3×3 and 4×4 (N = 2,3,4) MIMO configurations are simulated with different d, ρ_r and SPM networks. Each ergodic capacity is averaged over 7000 channel realizations.

Figure 5.2 plots the cumulative density function (CDF) of the ergodic MIMO capacity performance with different configurations when the antenna spacing $d = 0.05\lambda$ and reference SNR ρ_r = 20dB. For 2×2 and 3×3 MIMO systems in Figure 5.2, introducing matching networks into the compact receiver provides better system performance even than the no coupling case. The ergodic capacity dramatically increases for a 4×4 MIMO system by choosing proper matching networks (the z_{11}^* match). Under fixed d and ρ_r, a larger MIMO system will benefit more via an appropriate matching network selection. For example, using the z_{11}^* match rather than the z_0 match gives no improvement for the 2×2 MIMO system, offers 0.5bits/s/Hz capacity improvement for 3×3, and 1bits/s/Hz for 4×4 MIMO systems. The z_{in} match for the 2×2 MIMO configuration offers only 0.1bits/s/Hz for 10% outage capacity compared to other matching networks, but more than 0.5bits/s/Hz for 50% and above outage capacity, which means that the benefit of z_{in} match mainly occurs in long-term usage.[1]

The ergodic capacity of various MIMO systems for changing values of ρ_r at 0.05λ antenna spacing is depicted in Figure 5.3. It shows that the advantage of using matching networks at the compact receive end is more obvious in high SNR scenarios. The performance of a compact array with MC and proper matching network adoption surpasses the impractical no coupling case at 15dB SNR for 2×2, 20dB for 3×3, and approaches the no coupling case at 25dB for 4×4 MIMO configurations. Especially for 2×2 case, the z_{in} match outperforms the no coupling case and other matching networks by 2bits/s/Hz and 1bits/s/Hz, respectively. We note that at such close antenna spacing $d = 0.05\lambda$, the system benefits of different matching networks are not obvious in Figure 5.3 for any MIMO configurations. However, the system performance improvement is significant for larger antenna separations as we will see in Figure 5.4.

In Figure 5.4 we explore the MIMO system performance with changing d at ρ_r = 20dB. Generally, the antenna elements have to be separated further to achieve full capacity performance for larger system configuration, e.g. 0.2λ for 2×2, 0.35λ for 3×3, and 0.4λ for 4×4 cases. Utilizing the z_{11}^* match promises significant system improvement compared to the simple z_0 match over the whole spacing range of about 1bits/s/Hz for 2×2, 1.5bits/s/Hz for 3×3 and 2bits/s/Hz for 4×4 MIMO configurations. Moreover, the z_{in} match for 2×2 case outperforms the z_{11}^* match when $d \leq 0.2\lambda$ and overlaps with it afterwards.

Figures 5.2, 5.3 and 5.4 exhibit system improvement of different compact MIMO configurations by introducing proper SPM networks using the Z-parameter approach. Comparing to the S-

[1] We note that the analytical expression of z_{in} is only available for two-element array as derived in Appendix A.

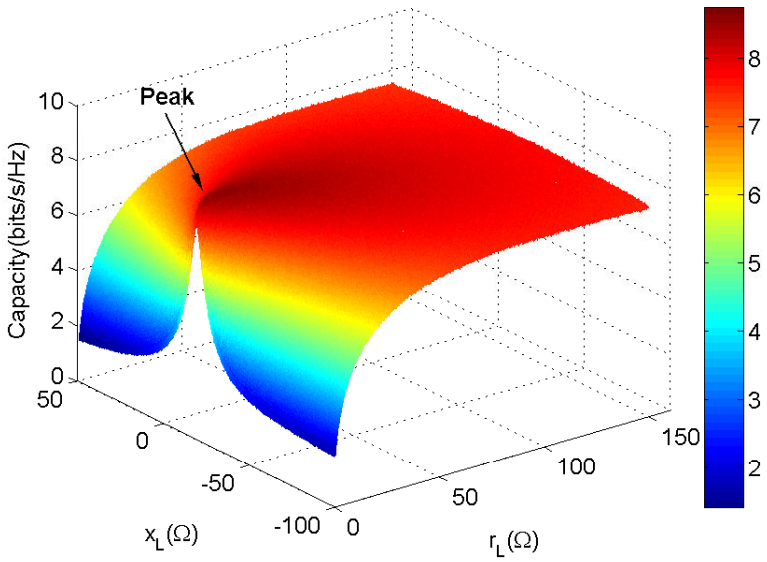

Figure 5.5: *Ergodic capacity vs. the resistive and reactive parts of z_L at $d = 0.05\lambda$, ρ_r = 20dB.*

parameter approach in Section 3.4.1.1, the Z-parameter approach avoids complex simulation of the receive end model to obtain the FF patterns of each antenna element, which makes it much easier and less time-consuming to study the impact of matching networks on compact MIMO systems with larger dimensions.

5.3 Optimal single-port matching impedance

Now we focus on the 2×2 ($N = 2$) MIMO system simulated under the assumptions presented in Section 5.2.2. For each load point z_L, 7000 random channel realizations are deployed to estimate the MIMO system performance using (5.19) at ρ_r = 20dB.

As shown in Figure 5.5, the 3D ergodic capacity surface is plotted with various matching impedance points. The range of impedance points is $\{z_L = r_L + \mathrm{j}x_L : r_L \in [0, 150]\Omega, x_L \in [-100, 50]\Omega\}$. We take $d = 0.05\lambda$ case as an example to demonstrate that the capacity performance is concave and resembles the received power characteristic in [22] except only one peak is observed with changes of the matching networks at the chosen d. For other antenna spacings less than 0.5λ, the surface of C_{mc} has the similar properties, which implies that there should be an optimal SPM for maximization of C_{mc} at each d.

5.3.1 Analytical derivation

In this section, we derive the optimal SPM impedance $z_{\text{opt}} = r_{\text{opt}} + \text{j}x_{\text{opt}}$ for the capacity maximization of the 2×2 MIMO system model.

As (5.19) contains a random channel matrix, it is difficult to carry out further analysis. Using Jensen's inequality and the concavity of $\log_2\det$ [51], for any fixed antenna spacing d, the upper bound C_{up} [105] of the MIMO capacity is

$$E\left\{C_{mc}\right\} \leq C_{up} = \log_2 \det\left(\mathbf{I} + \frac{4\rho_r r_{11} r_L}{N}\mathbf{Z}_{L+R}^{-H}\mathbf{Z}_{L+R}^{-1}\mathbf{\Psi}_R\right). \tag{5.20}$$

We define the antenna self-impedance $z_{11} = r_{11} + \text{j}x_{11}$, mutual-impedance $z_{12} = r_{12} + \text{j}x_{12}$, load impedance $z_L = r_L + \text{j}x_L$, where r_{11}, r_{12}, $r_L \in \mathbb{R}^+$ as they are resistance components and the reactance components x_{11}, x_{12}, $x_L \in \mathbb{R}$. For identical antenna elements, we have $(\mathbf{Z}_{RR})_{ij} = (\mathbf{Z}_{RR})_{ji}$ based on the reciprocity theorem [56]. Given an antenna spacing d and SNR ρ_r, (5.20) becomes a function of variables (r_L, x_L). As the matrix product $\mathbf{Z}_{L+R}^{-H}\mathbf{Z}_{L+R}^{-1}$ in (5.20) contains the variable pair (r_L, x_L), it has to be simplified.

$$\begin{aligned}\mathbf{Z}_{L+R}^{-H}\mathbf{Z}_{L+R}^{-1} &= \left(\left[\mathbf{Z}_{RR} + \mathbf{Z}_L\right]\left[\mathbf{Z}_{RR} + \mathbf{Z}_L\right]^H\right)^{-1} = \left(\left[\mathbf{Z}_{RR} + z_L\mathbf{I}\right]\left[\mathbf{Z}_{RR}^H + z_L^*\mathbf{I}\right]\right)^{-1} \\ &= \Big(\underbrace{|z_L|^2\mathbf{I}}_{\mathbf{Z}_1} + \underbrace{z_L\mathbf{Z}_{RR}^H + z_L^*\mathbf{Z}_{RR}}_{\mathbf{Z}_2} + \underbrace{\mathbf{Z}_{RR}\mathbf{Z}_{RR}^H}_{\mathbf{Z}_3}\Big)^{-1}.\end{aligned} \tag{5.21}$$

Expanding (5.21) we have

$$\begin{aligned}\mathbf{Z}_1 &= \begin{bmatrix} r_L^2 + x_L^2 & 0 \\ 0 & r_L^2 + x_L^2 \end{bmatrix} \\ \mathbf{Z}_2 &= 2\left(r_L \cdot \begin{bmatrix} r_{11} & r_{12} \\ r_{12} & r_{11} \end{bmatrix} + x_L \cdot \begin{bmatrix} x_{11} & x_{12} \\ x_{12} & x_{11} \end{bmatrix}\right) \\ \mathbf{Z}_3 &= \begin{bmatrix} r_{11}^2 + x_{11}^2 + r_{12}^2 + x_{12}^2 & 2(r_{11}r_{12} + x_{11}x_{12}) \\ 2(r_{11}r_{12} + x_{11}x_{12}) & r_{11}^2 + x_{11}^2 + r_{12}^2 + x_{12}^2 \end{bmatrix}\end{aligned} \tag{5.22}$$

Lemma 1: For any real symmetric Toeplitz matrix $\mathbf{A} = \begin{bmatrix} a_1 & a_2 \\ a_2 & a_1 \end{bmatrix}$, the singular value de-

composition (SVD) of $\mathbf{A}$ can be written as $\mathbf{A} = \mathbf{U}\mathbf{D}\mathbf{U}^{\mathbf{T}} = \mathbf{U}\mathbf{D}\mathbf{U}$, where

$$\mathbf{U} = \frac{1}{\sqrt{2}} \begin{bmatrix} 1 & 1 \\ 1 & -1 \end{bmatrix}, \mathbf{D} = \begin{bmatrix} a_1 + a_2 & 0 \\ 0 & a_1 - a_2 \end{bmatrix}.$$

Proof: $\mathbf{A}$ is a 2×2 circulant matrix. Following [106], the eigenvalue solution of $\mathbf{A}$ is $\lambda_k = a_1 + a_2 r_k$, $k = 1, 2$, and r_k is the kth complex root of $r^2 = 1$. The corresponding eigenvector $u_k = 2^{-1/2}[1, r_k]^T$. Then $\mathbf{U} = [u_1, u_2]$, and $\mathbf{U}$ is unitary. ■

Utilizing Lemma 1, the singular value decomposition (SVD) of (5.21) is given

$$\begin{aligned} \mathbf{Z}_{L+R}^{-H}\mathbf{Z}_{L+R}^{-1} =& \left(\mathbf{U} \left(\begin{bmatrix} r_L^2 + x_L^2 & 0 \\ 0 & r_L^2 + x_L^2 \end{bmatrix} + 2r_L \cdot \begin{bmatrix} \mathfrak{R}_1 & 0 \\ 0 & \mathfrak{R}_2 \end{bmatrix} \right.\right. \\ & \left.\left. + 2x_L \cdot \begin{bmatrix} \mathfrak{X}_1 & 0 \\ 0 & \mathfrak{X}_2 \end{bmatrix} + \begin{bmatrix} \mathfrak{R}_1^2 + \mathfrak{X}_1^2 & 0 \\ 0 & \mathfrak{R}_2^2 + \mathfrak{X}_2^2 \end{bmatrix} \right) \mathbf{U} \right)^{-1} \\ =& \mathbf{U} \begin{bmatrix} (r_L + \mathfrak{R}_1)^2 + (x_L + \mathfrak{X}_1)^2 & 0 \\ 0 & (r_L + \mathfrak{R}_2)^2 + (x_L + \mathfrak{X}_2)^2 \end{bmatrix}^{-1} \mathbf{U} \\ =& \mathbf{U}\mathbf{\Lambda}^{-\mathbf{1}}\mathbf{U} \end{aligned} \tag{5.23}$$

where $\mathfrak{R}_1 = r_{11} + r_{12}$, $\mathfrak{X}_1 = x_{11} + x_{12}$, $\mathfrak{R}_2 = r_{11} - r_{12}$, $\mathfrak{X}_2 = x_{11} - x_{12}$. Using the property $\det(\mathbf{I} + \mathbf{A}\mathbf{B}) = \det(\mathbf{I} + \mathbf{B}\mathbf{A})$ [3], (5.20) can be rewritten as

$$C_{up} = \log_2 \det(\mathbf{I} + \kappa r_L \cdot \mathbf{U}\mathbf{\Lambda}^{-\mathbf{1}}\mathbf{U}\mathbf{\Psi}_R) = \log_2 \det(\mathbf{I} + \kappa \mathbf{U}\mathbf{\Psi}_R\mathbf{U} r_L \mathbf{\Lambda}^{-\mathbf{1}}) = \log_2 \det(\mathbf{Y}) \tag{5.24}$$

where $\kappa = \rho_r \cdot 4r_{11}/N$. According to the monotonically increasing characteristic of $\log_2(\cdot)$, the maximum point of $\det(\cdot)$ is the maximum point of $\log_2\det(\cdot)$. To derive the maximum point $(r_{\text{opt}}, x_{\text{opt}})$ of $\det(\mathbf{Y})$, we evaluate the following derivatives for the 2×2 case

$$\frac{\partial \det(\mathbf{Y})}{\partial r_L} = \kappa \cdot \frac{\left(\mathfrak{R}_1^2 - r_L^2 + (x_L + \mathfrak{X}_1)^2\right) \cdot \Sigma_2 + \left(\mathfrak{R}_2^2 - r_L^2 + (x_L + \mathfrak{X}_2)^2\right) \cdot \Sigma_1}{\left(\left((r_L + \mathfrak{R}_1)^2 + (x_L + \mathfrak{X}_1)^2\right)\left((r_L + \mathfrak{R}_2)^2 + (x_L + \mathfrak{X}_2)^2\right)\right)^2} \tag{5.25a}$$

$$\frac{\partial \det(\mathbf{Y})}{\partial x_L} = -2\kappa r_L \cdot \frac{(x_L + \mathfrak{X}_1) \cdot \Sigma_2 + (x_L + \mathfrak{X}_2) \cdot \Sigma_1}{\left(\left((r_L + \mathfrak{R}_1)^2 + (x_L + \mathfrak{X}_1)^2\right)\left((r_L + \mathfrak{R}_2)^2 + (x_L + \mathfrak{X}_2)^2\right)\right)^2} \tag{5.25b}$$

where

$$\begin{aligned}\Sigma_1 &= \big((r_L+\mathfrak{R}_1)^2+(x_L+\mathfrak{X}_1)^2\big)\\ &\quad\cdot\big((1-\mathrm{Re}\{\alpha\})\big((r_L+\mathfrak{R}_1)^2+(x_L+\mathfrak{X}_1)^2\big)+(1-|\alpha|^2)\kappa r_L\big),\\ \Sigma_2 &= \big((r_L+\mathfrak{R}_2)^2+(x_L+\mathfrak{X}_2)^2\big)\\ &\quad\cdot\big((1+\mathrm{Re}\{\alpha\})\big((r_L+\mathfrak{R}_2)^2+(x_L+\mathfrak{X}_2)^2\big)+(1-|\alpha|^2)\kappa r_L\big),\end{aligned} \tag{5.26}$$

and $\alpha = (\mathbf{\Psi}_R)_{12} = (\mathbf{\Psi}_R)_{21}$ is the correlation coefficient between the two receivers. In (5.26) it can be shown that $\forall\Sigma_{1,2} > 0$. As the maximum point $(r_{\mathrm{opt}}, x_{\mathrm{opt}})$ makes (5.25) equal to zero, then from (5.25b) we can deduce

$$x_{\mathrm{opt}} \in [\min(-\mathfrak{X}_1, -\mathfrak{X}_2), \max(-\mathfrak{X}_1, -\mathfrak{X}_2)]. \tag{5.27}$$

Substituting (5.27) into (5.25a) we have

$$r_{\mathrm{opt}} \in [\min(\mathfrak{R}_1, \mathfrak{R}_2), \max(\sqrt{\mathfrak{R}_1^2+(\mathfrak{X}_1-\mathfrak{X}_2)^2}, \sqrt{\mathfrak{R}_2^2+(\mathfrak{X}_1-\mathfrak{X}_2)^2})]. \tag{5.28}$$

Solving (5.25a) and (5.25b) the simple relation between r_L and x_L can be obtained

$$r_L^2 + (x_L+\sigma)^2 = \Gamma. \tag{5.29}$$

Geometrically, $(r_{\mathrm{opt}}, x_{\mathrm{opt}})$ is a point on the circumference of a circle with the center at $(0, -\sigma)$ and radius $\sqrt{\Gamma}$, where $\sigma = x_{11} + \frac{r_{11}r_{12}}{x_{12}}, \Gamma = r_{11}^2 + r_{12}^2 + x_{12}^2 + \frac{r_{11}^2 r_{12}^2}{x_{12}^2}$. Combined with (5.27) and (5.28), $(r_{\mathrm{opt}}, x_{\mathrm{opt}})$ can be restricted to be located in an arc of the circle.

Substituting (5.29) into (5.25b), we can deduce a polynomial in x_L

$$\sum_{m=0}^{8} p_m x_L^m = \sum_{m=0}^{8} f_m(\mathfrak{R}_1, \mathfrak{X}_1, \mathfrak{R}_2, \mathfrak{X}_2, \sigma, \Gamma, \kappa) x_L^m = \sum_{m=0}^{8} g_m(r_{11}, x_{11}, r_{12}, x_{12}, \rho_r) x_L^m = 0 \tag{5.30}$$

where the coefficients p_m are determined by the high order polynomials

$$f_m(\mathfrak{R}_1, \mathfrak{X}_1, \mathfrak{R}_2, \mathfrak{X}_2, \sigma, \Gamma, \kappa) = g_m(r_{11}, x_{11}, r_{12}, x_{12}, \rho_r).$$

For details of (5.30) please refer to Appendix D. With fixed antenna spacing d and SNR ρ_r, the numerical result for the optimal SPM impedance $z_{\rm opt}$ for capacity maximization of a 2×2 MIMO system with compact receivers can be found as:

Step 1. Solving (5.30) to find all the roots of x_L;

Step 2. Filtering the results of **Step 1** by (5.27);

Step 3. Substituting the results of **Step 2** into (5.29) to get the corresponding roots of r_L;

Step 4. Filtering the results of **Step 3** by (5.28).

5.3.1.1 High SNR regime

In high SNR regime, (5.24) can be simplified as

$$C_{up} = \log_2 \det(\kappa \mathbf{U}\mathbf{\Psi}\mathbf{U} r_L \mathbf{\Lambda^{-1}}) = \log_2 \det(\mathbf{Y}) \tag{5.31}$$

where $\det(\mathbf{Y}) = \frac{(\mathbf{1}-\alpha^{\mathbf{2}})}{\det(\mathbf{\Lambda})}$. The derivatives in (5.25) are modified by simplifying (5.26) as

$$\Sigma_i = (r_L + \mathfrak{R}_i)^2 + (x_L + \mathfrak{X}_i)^2, \qquad i = 1, 2. \tag{5.32}$$

Solving the equations we derive the closed-form of $z_{\rm opt} = r_{\rm opt} + {\rm j}x_{\rm opt}$, where

$$r_{\rm opt} = \sqrt{\mathfrak{R}_1\mathfrak{R}_2\left(1 + \frac{(\mathfrak{X}_1 - \mathfrak{X}_2)^2}{(\mathfrak{R}_1 + \mathfrak{R}_2)^2}\right)} = \sqrt{r_{11}^2 - r_{12}^2 + x_{12}^2 - \frac{r_{12}^2 x_{12}^2}{r_{11}^2}} \tag{5.33a}$$

$$x_{\rm opt} = -\frac{\mathfrak{R}_1\mathfrak{X}_2 + \mathfrak{R}_2\mathfrak{X}_1}{\mathfrak{R}_1 + \mathfrak{R}_2} = \frac{r_{12}x_{12}}{r_{11}} - x_{11} \tag{5.33b}$$

This solution of $z_{\rm opt}$ is exactly the input impedance ($z_{\rm in}$) match in Appendix A[2]. Equations (5.33) prove that the closed-form solution of the optimal SPM impedance $z_{\rm opt}$ for capacity maximization of a 2×2 MIMO system with compact receivers is the input impedance of the receiver.

The significance of this result is that for a high SNR scenario, $z_{\rm opt}$ is an exact solution only related to the array impedances and independent from the correlation α, which provides the possibility of practical implementation. It is not surprising to find out that $z_{\rm in}$ is the $z_{\rm opt}$ in the

[2]Similar derivation of the input impedance can be found in [30]

high SNR case as we already commented on this in Section 4.7 on page 87 of Chapter 4. Also from circuit theory considerations $z_{\rm in}$ includes the MC effect into the matching network [101], which realizes the maximum power transfer between the corresponding source and receiver. Furthermore, it gives low correlation for any antenna separation in Figure 3.6 and a similar property is reported in [30]. Although it is not the optimal SPM impedance for received power maximization in Section 3.3.2, it is the best candidate for capacity maximization in high SNR scenarios.

5.3.1.2 Low SNR regime

In low SNR regime, utilizing the approximation $\log_2(1+x) \approx x\log_2 e$ for x small [37] we have (5.24) modified to

$$C_{up} = \kappa r_L \cdot \left(\frac{1 + \mathrm{Re}\{\alpha\}}{(r_L + \mathfrak{R}_1)^2 + (x_L + \mathfrak{X}_1)^2} + \frac{1 - \mathrm{Re}\{\alpha\}}{(r_L + \mathfrak{R}_2)^2 + (x_L + \mathfrak{X}_2)^2} \right) \cdot \log_2 e. \quad (5.34)$$

Then (5.25) can be substituted with the modification of (5.26) as

$$\begin{aligned} \Sigma_1 =& \log_2 e(1 - \mathrm{Re}\{\alpha\}) \left((r_L + \mathfrak{R}_1)^2 + (x_L + \mathfrak{X}_1)^2 \right)^2, \\ \Sigma_2 =& \log_2 e(1 + \mathrm{Re}\{\alpha\}) \left((r_L + \mathfrak{R}_2)^2 + (x_L + \mathfrak{X}_2)^2 \right)^2. \end{aligned} \quad (5.35)$$

Equations (5.27), (5.28) and (5.29) are all valid in the low SNR case except (5.30) is correspondingly changed to a six-order polynomial instead of eight-order. Generation of the optimal SPM impedances in this case still refers to the steps summarized on page 104. One conclusion can be deduced from this that the optimal SPM impedances in the low SNR regime are independent of SNR. The evaluation of the low SNR derivation can be found in following analysis.

5.3.2 Simulation examples

We use ideal $\lambda/2$ dipole antennas to numerically evaluate the analysis in Section 5.3.1. The optimal SPM impedance $z_{\rm opt}$ generated by Monte Carlo simulations of the same MIMO system model for both ergodic capacity C_{mc} and upper bound of capacity C_{up} are compared to the numerical results.

The self and mutual impedances of the ideal $\lambda/2$ dipoles are calculated numerically using the

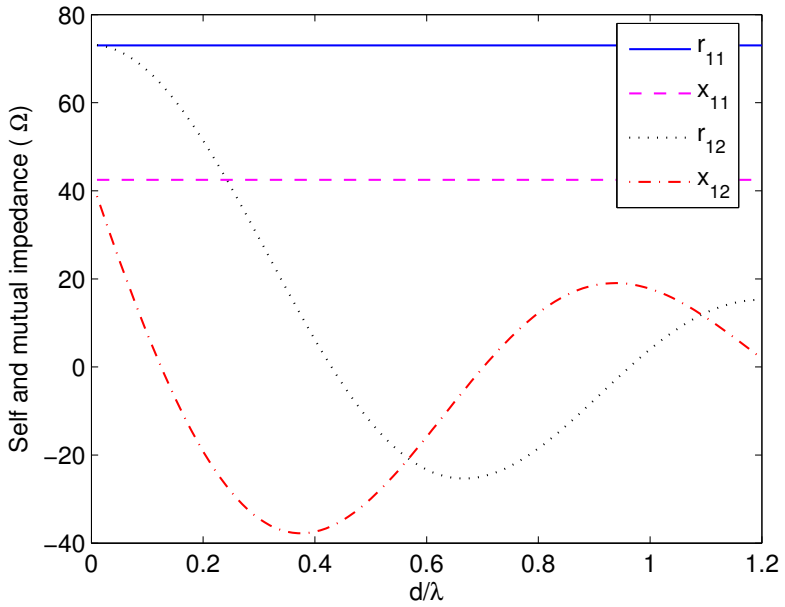

Figure 5.6: *The resistance and reactance components of self and mutual impedances with various antenna spacings.*

modified EMF method in Figure 5.6.[3] Choosing a specific reference SNR ρ_r and substituting the computed impedances data z_{11}, z_{12} into pre-calculated analytical polynomials g_m in (5.30), we can get multiple solutions of x_L for a given antenna spacing d. Then the selected values of x_L(s) are filtered by the range (5.27) which is also displayed in Figure 5.7(a). Next the corresponding r_L(s) can be computed by (5.29). Figure 5.8 depicts the arc of possible locations for $(r_{\text{opt}}, x_{\text{opt}})$ following from (5.29) of antenna spacing $d = 0.05\lambda$. The abscissa of Figure 5.8 is determined by r_{Lmin} = min($\Re_2$) and r_{Lmax} = max($\sqrt{\Re_1^2 + (\mathfrak{X}_1 - \mathfrak{X}_2)^2}$) according to Figure 5.7(b). In Figure 5.8 it is obvious that $x_{Lmax} = -\mathfrak{X}_2 = -17.9\ \Omega$ and thus x_L(s) can not reach zero as shown in Figure 5.7(a). Then the lower bound of x_L in Figure 5.8 is accordingly modified to $x_{Lmin} = \min(-\mathfrak{X}_1)|_{-\mathfrak{X}_2 \leq -17.9}$ from Figure 5.7(a). Then using (5.28) corresponding to Figure 5.7(b), the correct solution pair $(r_{\text{opt}}, x_{\text{opt}})$ can be obtained. Our method will find the unique solution of $(r_{\text{opt}}, x_{\text{opt}})$ for each fixed d and ρ_r.

To verify the accuracy of our numerical results $(r_{\text{opt}}, x_{\text{opt}})$, Monte Carlo simulations for the ergodic capacity and the simulation of upper bound are used. If the uniformly distributed arrivals scattering model is assumed, α can be calculated using (3.7) on page 37. We concentrate on

[3] Infinite thin dipoles are assumed for the EMF calculations using (2.30) on page 25. Usually the dipole diameter is much less than its length, thus the EMF values are stille usable. Similar self and mutual impedance results can be found for practical dipole cases in [18, 60]. As our focus is on the relative ratio of the self and mutual impedances and not the absolute values, ideal dipoles are selected for simplicity.

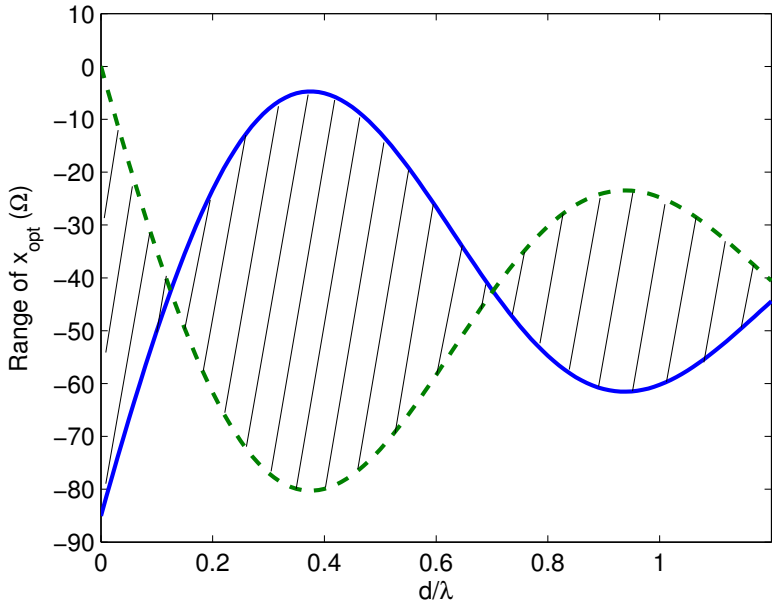

(a) x_{opt} varies between $-\mathfrak{X}_1$ (solid line) and $-\mathfrak{X}_2$ (dash line)

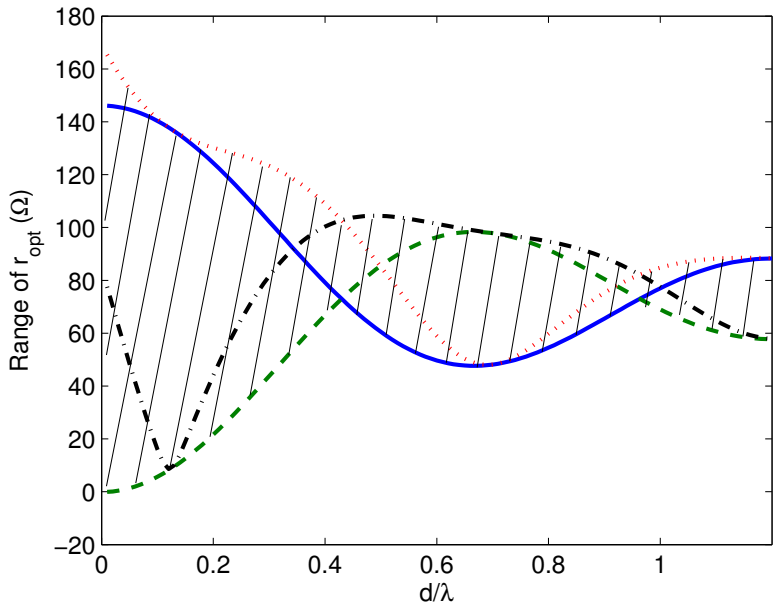

(b) r_{opt} moves among $\mathfrak{R}_1$ (solid line), $\mathfrak{R}_2$ (dash line), $\sqrt{\mathfrak{R}_1^2 + (\mathfrak{X}_1 - \mathfrak{X}_2)^2}$ (dot line) and $\sqrt{\mathfrak{R}_2^2 + (\mathfrak{X}_1 - \mathfrak{X}_2)^2}$ (dash-dot line).

Figure 5.7: *The possible range (shadow areas) of* $(r_{\mathrm{opt}}, x_{\mathrm{opt}})$ *of ideal* $\lambda/2$ *dipoles as a function of antenna spacing.*

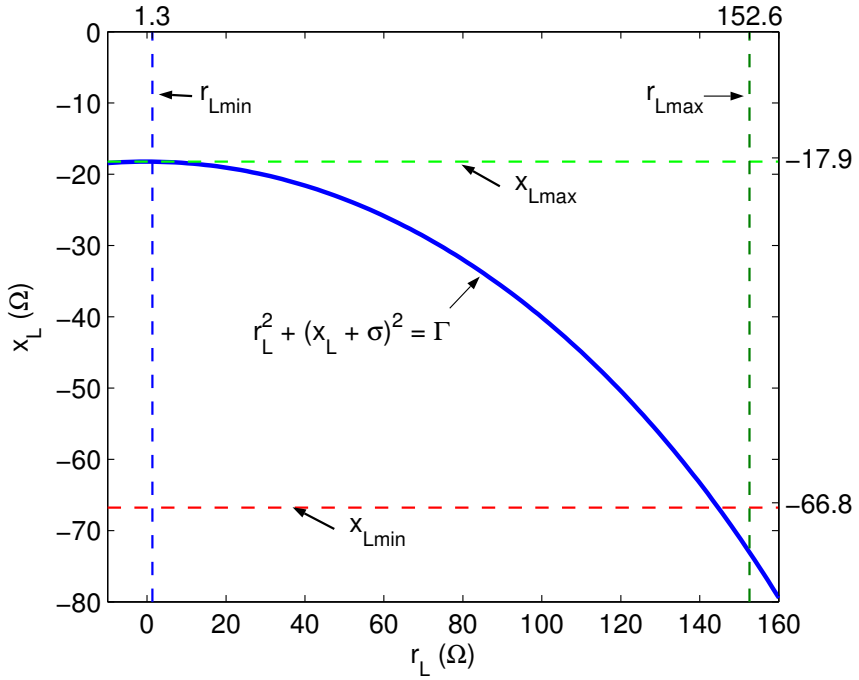

Figure 5.8: *Arc of the possible values of* $(r_{\text{opt}}, x_{\text{opt}})$ *for two compact ideal* $\lambda/2$ *dipoles of* $d = 0.05\lambda$.

the system performance with $d < 0.5\lambda$ when the MC effect becomes severe. As the numerical z_{opt} is the maximum point of the upper bound C_{up} rather than the ergodic capacity C_{mc}, the corresponding maximum points obtained by simulation for both cases are plotted in Figure 5.9. We note that the numerical results of z_{opt} (z_{opt} (num) in Figure 5.9) are calulated using the derivations of Section 5.3.1.2 for $\rho_r = -20$dB, Section 5.3.1.1 for $\rho_r = 20$dB, and Section 5.3.1 for $\rho_r = 5$dB. The range of impedance points $\{z_L = r_L + \mathrm{j}x_L : r_L \in [0, 150]\Omega, x_L \in [-100, 50]\Omega\}$ are chosen to get the maximum point of each C_{up}. The ergodic capacity C_{mc} is simulated over 10000 random channel realizations for each impedance point at each selected antenna spacing d, thereby the range of z_L has to be shrunk to a few ohms around the maximum point of C_{up} in the same case to save computing time. In Figure 5.9 it is apparent that the numerically derived z_{opt} agrees well with the corresponding results generated from simulations of C_{up}, and it matches the impedance where C_{mc} reaches the maximum value as well. It is also clear that z_{opt} approaches z_{in} when the SNR increases, which is perfectly in accordance with our derivation in Section 5.3.1. Another observation is that when SNR is increasing, the reactance of z_{opt} is hardly affected and overlaps with the reactive part of z_{in} for medium SNR; the resistive part of z_{opt} approaches and then equals the resistive part of z_{in} at $d = 0.4\lambda$ for ρ_r = -20dB, $d = 0.15\lambda$ for ρ_r = 5dB.

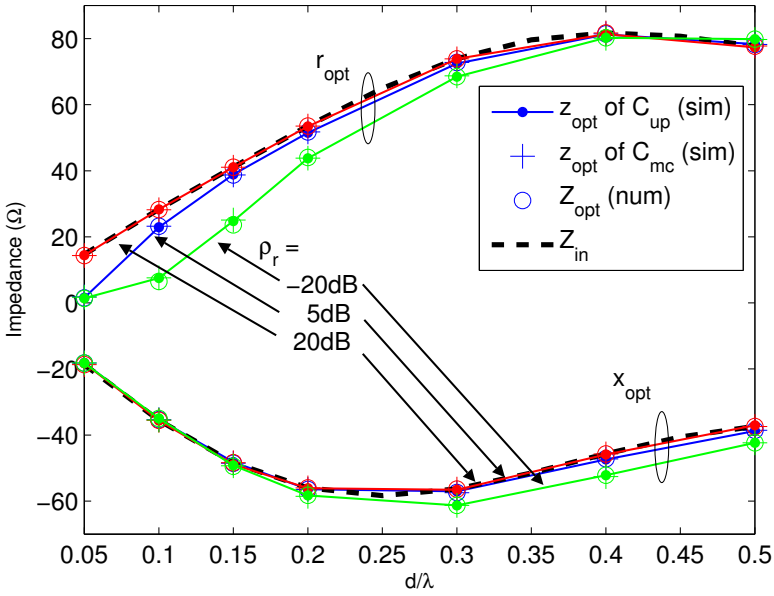

Figure 5.9: *The real and imaginary parts of numerical and simulation optimal single-port impedances compared to input impedance matching as a function of various antenna spacings with different ρ_r.*

In the high SNR regime, r_{11}, x_{11} are constant in Figure 5.6, then (5.33b) is dominated by $r_{12}x_{12}$. As r_{12} is monotonically decreasing and x_{12} is convex over $d \in [0.05, 0.5]\lambda$ in Figure 5.6, the convexity of x_{opt} can be well explained in Figure 5.9. (5.33a) can be further written as

$$r_{\text{opt}} = \frac{\sqrt{r_{11}^4 - r_{11}^2 r_{12}^2 + r_{11}^2 x_{12}^2 - r_{12}^2 x_{12}^2}}{r_{11}}.$$

Figure 5.6 shows that $-r_{12}^2$ is monotonically increasing over $d \in [0.05, 0.4]\lambda$, and x_{12}^2 is monotonically increasing over $d \in [0.1, 0.5]\lambda$. Thus r_{opt} should be monotonically increasing over $d \in [0.1, 0.4]\lambda$, which agrees well with the r_{opt} curve in Figure 5.9.

Because the numerical values of z_{opt} match very well to the simulation results of z_{opt} for both C_{up} and C_{mc} cases, we present the precise data of z_{opt} in Table 5.1. For the resistive component r_{opt}, the numerical and both sets of simulation results differ from each other slightly for $d \leq 0.2\lambda$ with the maximum error of around 1Ω. The errors decrease while ρ_r increases. When $d \geq 0.3\lambda$, the numerical and simulation r_{opt} of C_{up} are equal to each other with nearly no error and there is a maximum error of 0.4Ω compared to the simulation r_{opt} of C_{mc} for any value of ρ_r. For the reactive component x_{opt}, the numerical x_{opt} is equal to the simulation x_{opt} of C_{up} with nearly no error for all values of ρ_r. The x_{opt} of C_{mc} has an maximum error of 0.4Ω

compared to the other two cases due to the limited number of realizations used for the Monte Carlo simulation. Both Figure 5.9 and Table 5.1 confirm that our analytical study in Section 5.3 can yield $z_{\rm opt}$ corresponding to the maximum C_{up} accurately, and can further predict $z_{\rm opt}$ of the maximum C_{mc} correctly and more efficiently than the Monte Carlo method. Values of $z_{\rm in}$ of various d are also presented in Table 5.1, and they agree well with the corresponding values of $z_{\rm opt}$ at $\rho = 20$dB. This again confirms our analytical finding of high SNR regime in Section 5.3.1.1.

5.4 MIMO system sensitivity and coupled array design

In practice, the MIMO system performance relies on the design of the compact receiver. The impact of the variation of antenna spacing, matching impedance and antenna dimension on compact MIMO system will be examined in this section.

d/λ	$r_{\rm opt}(\Omega)$									$r_{in}(\Omega)$
	$\rho_r = -20$dB			$\rho_r = 5$dB			$\rho_r = 20$dB			
	num*	$\text{sim}^{\dagger}_{up}$	$\text{sim}^{\ddagger}_{m}$	num	sim_{up}	sim_{m}	num	sim_{up}	sim_{m}	
0.05	1.38	1.41	1.74	1.53	1.81	1.56	14.36	14.33	14.44	14.69
0.10	6.47	7.54	7.61	23.23	23.22	22.92	28.23	28.22	28.29	28.35
0.20	44.01	43.78	43.83	51.78	51.76	51.49	53.53	53.53	53.45	53.60
0.30	68.47	68.46	68.76	72.77	72.77	72.48	73.90	73.90	73.89	73.95
0.40	80.25	80.25	80.11	81.44	81.44	81.27	81.73	81.73	81.37	81.74
0.50	79.84	79.84	79.75	78.26	78.26	78.36	77.75	77.75	77.35	77.73
	$x_{\rm opt}(\Omega)$									$x_{in}(\Omega)$
0.05	-18.23	-18.23	-18.18	-18.23	-18.23	-18.16	-18.66	-18.66	-18.26	-18.68
0.10	-34.97	-34.98	-35.47	-35.35	-35.35	-35.30	-35.54	-35.54	-35.62	-35.55
0.20	-58.22	-58.27	-58.53	-56.46	-56.46	-56.44	-56.02	-56.02	-56.12	-56.00
0.30	-61.29	-61.29	-61.32	-57.44	-57.44	-57.05	-56.35	-56.35	-56.57	-56.30
0.40	-52.17	-51.18	-52.60	-47.21	-47.21	-47.39	-45.75	-45.75	-45.88	-45.69
0.50	-42.37	-42.37	-42.35	-38.54	-38.55	-38.77	-37.41	-37.41	-37.07	-37.36

*numerical results †simulation results based on C_{up} ‡simulation results based on C_m

Table 5.1: *Comparison of the numerical and simulation resistance and reactance components of the optimal single-port match impedances with various antenna spacings and reference SNRs*

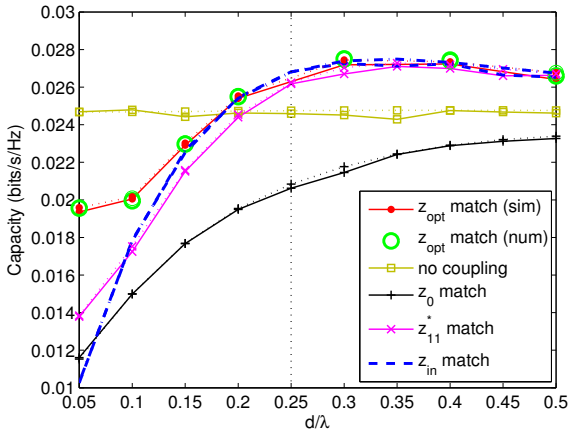

(a) $\rho_r = -20dB$

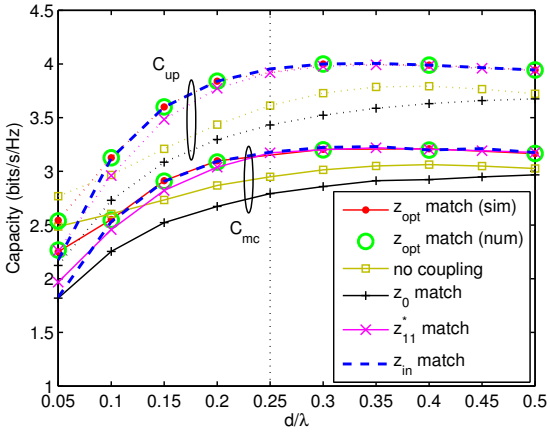

(b) $\rho_r = 5dB$

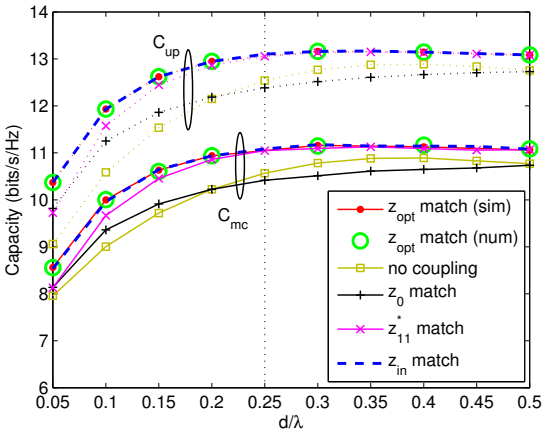

(c) $\rho_r = 20dB$

Figure 5.10: *The ergodic capacity (solid line) and upper bound (dash line) with various matching networks as a function of d with different* ρ_r.

5.4.1 Capacity sensitivity and antenna spacing

Introducing various matching networks into compact MIMO terminals will improve the system performance. To illustrate how much we can benefit from the $z_{\rm opt}$ match, the ergodic capacity C_{mc} and capacity upper bound C_{up} computed for antennas with no coupling[4] and z_0 cases, self-conjugate match ($z_{11}{}^*$), input impedance match ($z_{\rm in}$) and maximum capacity ($z_{\rm opt}$) matching are depicted with different values of ρ_r in Figure 5.10. Both C_{up} and C_{mc} results are plotted to show the validity of using the capacity upper bound C_{up} to predict matching values for C_{mc}. As illustrated in Figure 5.10, using a matching network to optimize C_{up} also optimizes the value of C_{mc}. In Figure 5.10(a) both C_{up} and C_{mc} results overlap with each other for every SPM pair when $\rho_r = -20$dB. The no coupling case gives flat performance at such low SNRs. The $z_{\rm opt}$ match outperforms other SPM networks before it is matched by $z_{\rm in}$ match at $d = 0.15\lambda$. When $\rho_r = 5$dB (Figure 5.10(b)), the performance of the receivers without MC is always better than with MC. Also in Figure 5.10(b) the performance of the $z_{\rm opt}$ match deviates from that of the $z_{\rm in}$ match with better capacity results only at extremely close antenna spacings for $d < 0.1\lambda$. However, for $\rho_r = 20$dB case (Figure 5.10(c)), the coupled compact array with any kind of matching networks outperforms that without MC at small spacing ($d < 0.2\lambda$). Meanwhile, the $z_{\rm opt}$ match surpasses other matching schemes when $d < 0.25\lambda$ and overlaps with the z_{11}^* match and the $z_{\rm in}$ match as $d \geq 0.25\lambda$ in all SNR scenarios. Figure 5.10(c) also shows that C_{mc} has an advantage of around 1bit/s/Hz for $d < 0.25\lambda$ compared to the z_0 match at the system. Moreover, a capacity benefit of 0.5bits/s/Hz can be achieved over the commonly used z_{11}^* match at $d = 0.05\lambda$. With increasing SNR, the performance of $z_{\rm opt}$ and $z_{\rm in}$ overlap with each other for all antenna spacings in Figure 5.10(c), which again verifies our analysis in Section 5.3.1.1. The relation between the trend of C_{up} and $x_{\rm opt}$ for the high SNR case can not be explained clearly from the analytical results. However, it is obvious that $r_{\rm opt}$ is the dominant factor that determines the value of C_{up} as in Figure 5.10 as C_{up} follows the monotonically increasing property of $r_{\rm opt}$ in Figure 5.9 with all spacings. It can be understood physically that it is because $r_{\rm opt}$ is the load receiving the power which contains the MC information.

[4]No coupling case is usually adopted when MC effect is not considered. This case is unrealistic when a compact array is studied. We add this curve in the simulation results to show that how different the performance of a compact array would be if the MC effect is not considered.

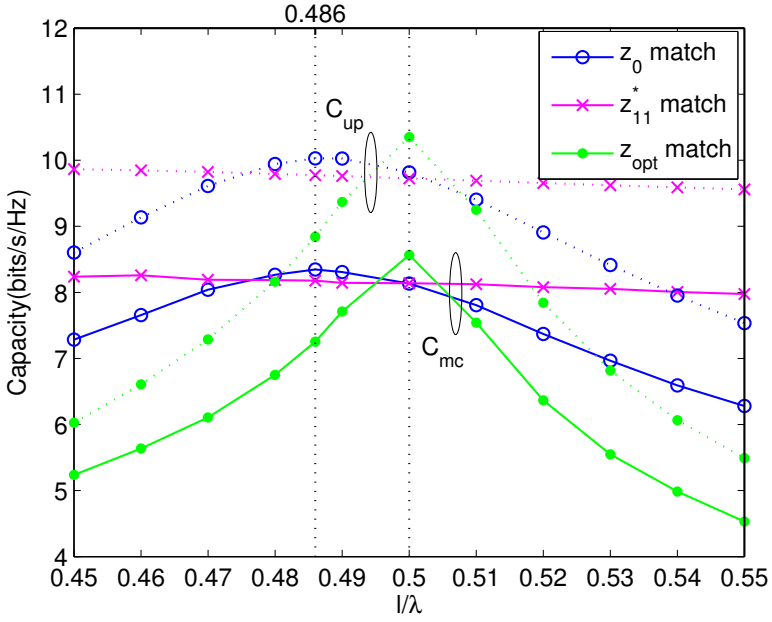

(a) $d = 0.05\lambda$

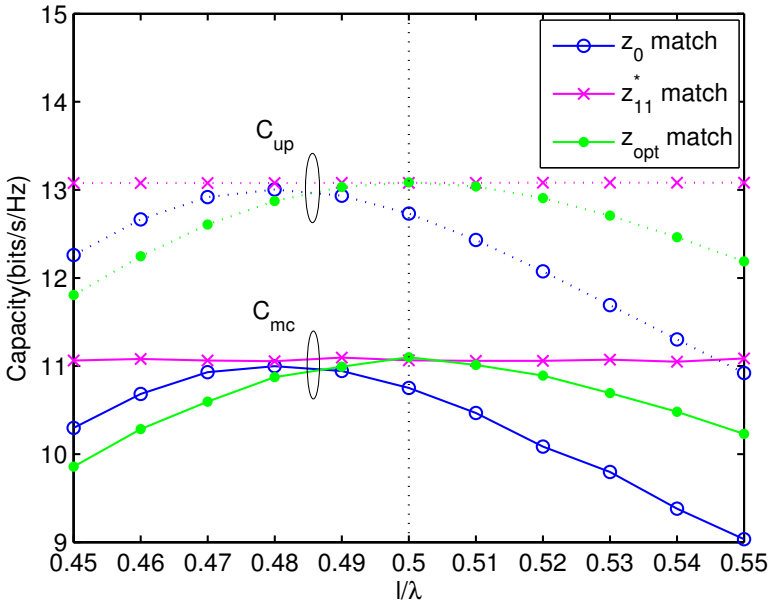

(b) $d = 0.5\lambda$

Figure 5.11: *The ergodic capacity (solid line) and upper bound (dash line) with various matching networks as a function of dipole lengths.*

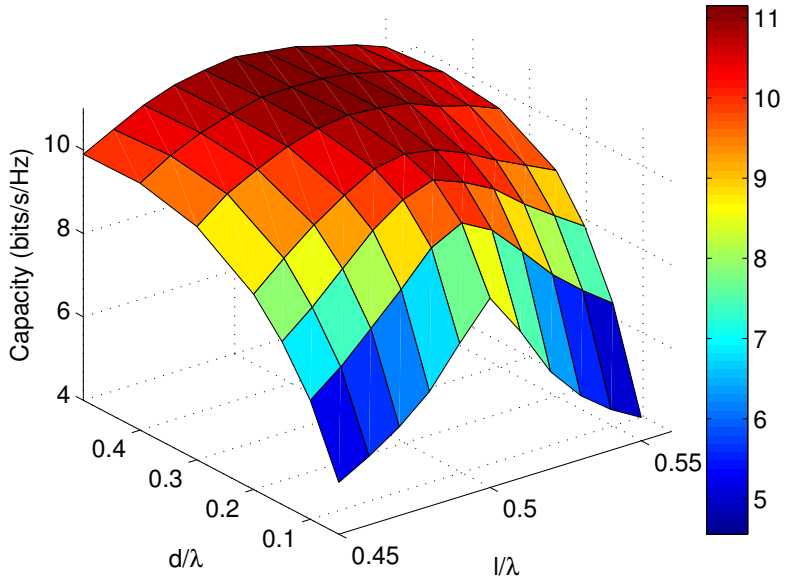

Figure 5.12: *MIMO system sensitivity as a function of both antenna spacing and dipole length.*

5.4.2 Capacity sensitivity and antenna structure

Besides antenna spacing, the accuracy of the antenna structure is another factor which can affect the MIMO systems performance directly by changing the self and mutual impedances. The self and mutual impedances are simulated based on the approach in [61]. As in Figure 5.11(a), with a very close antenna spacing, although z_{opt} matching provides 0.5bits/s/Hz benefit compared to other matching networks at half-wavelength dipole length ($l = 0.5\lambda$), its performance drops quickly if l is not precisely 0.5λ. The highest capacity of z_0 matching is attained at $l = 0.486\lambda$, which is the first resonant length ($z_{11} = r_{11}$) of a dipole antenna. In Figure 5.11, the ${z_{11}}^*$ match gives the most stable performance among three SPM methods. When d increases to 0.5λ (Figure 5.11(b)), the curve of the z_{opt} match becomes flatter than that in Figure 5.11(a), and the performance of the ${z_{11}}^*$ match surpasses the z_{opt} match except for $l = 0.5\lambda$ case. Therefore, the ${z_{11}}^*$ match is the best SPM network for large antenna spacings with imprecisely known dipole length. The 3D Figure 5.12 clearly shows that with the $z_{\rm opt}$ match the MIMO system performance is more sensitive to dipole length for smaller antenna spacing ($d \leq 0.2\lambda$). If the dipole length is exactly $\lambda/2$, good capacity performance can be guaranteed even for $d = 0.1\lambda$.

5.4.3 Capacity sensitivity and impedance matching

The sensitivity of the matching network is important as it varies easily with the environment (temperature, humidity, etc.) besides the design accuracy. To evaluate the sensitivity reasonably, we define the performance efficiency of C_{mc} and C_{up} with each single d as

$$\eta_{C_{mc}}|_{z_L=z_{L_0}} = \frac{C_{mc}|_{z_L=z_{L_0}}}{\max(C_{mc}|_{z_L=z_{L_0}})} = \frac{C_{mc}|_{z_L=z_{L_0}}}{C_{mc}|_{z_L=z_{opt}}} \tag{5.36a}$$

$$\eta_{C_{up}}\big|_{z_L=z_{L_0}} = \frac{C_{up}|_{z_L=z_{L_0}}}{\max(C_{up}|_{z_L=z_{L_0}})} = \frac{C_{up}|_{z_L=z_{L_0}}}{C_{up}|_{z_L=z_{opt}}}. \tag{5.36b}$$

Next, the precision error of the matching network is defined as

$$\Delta r = \frac{r_L - r_{\text{opt}}}{z_0}, \Delta x = \frac{x_L - x_{\text{opt}}}{z_0} \tag{5.37}$$

where $z_0 = 50\Omega$ is the reference of calibration. It is obvious that z_{opt} is located at the origin of the Cartesian coordinates under the definition of (5.37). Also, we assume that the matching networks of both receivers have the same precision error simultaneously. In Figure 5.13 the smooth solid curve is the contour plot of $\eta_{c_{up}}$, while the clusters of dots are the distribution of $\eta_{C_{mc}}$. It is coarse because of the random channels to generate C_{mc}. However, Figure 5.13 also

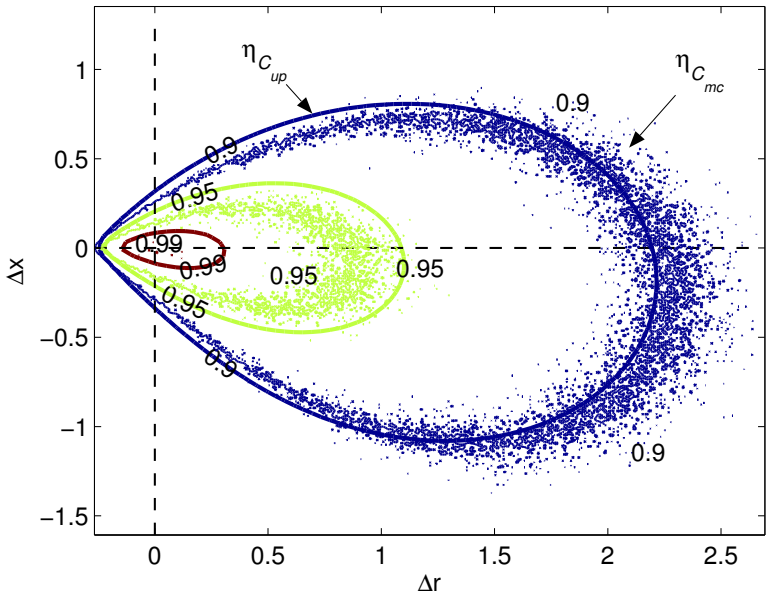

Figure 5.13: *The capacity efficiency* $\eta_{c_{mc}}, \eta_{c_{up}} = 0.9, 0.95, 0.99$ *as a function of* $(\Delta r, \Delta x)$ *with* $d = 0.05\lambda$.

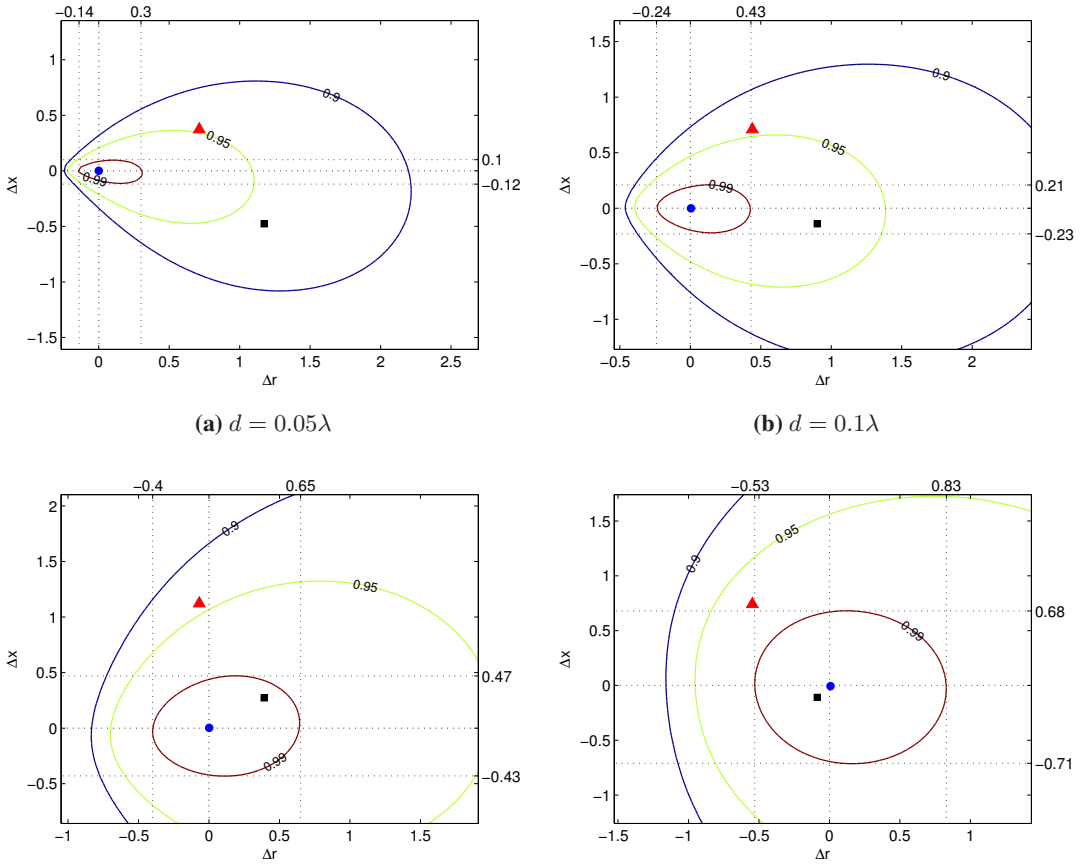

(a) $d = 0.05\lambda$ **(b)** $d = 0.1\lambda$

(c) $d = 0.2\lambda$ **(d)** $d = 0.5\lambda$

Figure 5.14: *The upper bound capacity efficiency* $\eta_{c_{up}} = 0.9, 0.95, 0.99$ *as a function of* $(\Delta r, \Delta x)$ *with various* d*. Special impedances* z_{opt} *(dots),* z_0 *(triangles), and* ${z_{11}}^*$ *(squares) are also marked in different cases.*

shows that

$$E\left\{(\Delta r, \Delta x)\right\}|_{\eta_{C_{mc}}=\eta_0} \approx (\Delta r_0, \Delta x_0)|_{\eta_{C_{up}}=\eta_0} \tag{5.38}$$

where $\eta_0 \in [0.9, 1]$. Figure 5.13 indicates that $\eta_{c_{up}}$ can be recognized as an upper bound of $\eta_{C_{mc}}$ especially when $\eta_0 \in [0.99, 1]$. Therefore, $\eta_{c_{up}}$ is generated for different d to estimate the capacity sensitivity, which avoids extensive Monte Carlo simulations of $\eta_{C_{mc}}$.

Figure 5.14 give us a clear demonstration of the MIMO performance disturbance due to the z_{opt} deviation and its trend with increasing antenna spacing. For example, Figure 5.14(a) tells us that the system has to sacrifice 1% performance degradation if the matching impedances in the system were offset from z_{opt} with a maximal range of $\Delta r \in [-0.14, 0.3]$, $\Delta x \in [-0.12, 0.1]$.

It also shows that both z_0 and ${z_{11}}^*$ matching can offer about 95% of the maximum capacity at $d = 0.05\lambda$, which is consistent with Figure 5.10(c).

When d is fixed, the maximal range of Δx is always smaller than the range of Δr at $\eta_{C_{up}} = 0.99$, which indicates that the system's performance is more sensitive to the matching reactance error x_L. When d is increasing, the maximal precision error area for 99% capacity efficiency gets larger, which is an encouraging phenomenon for practical implementation. Meanwhile, the z_{opt} point is approaching ${z_{11}}^*$ with increasing d, which explains why the system performance of both matching networks converges in Figure 5.10(c) when d increases. Generally, the MIMO system performance is not sensitive to z_{opt} mismatch even at very small antenna spacings such as $d = 0.05\lambda$, which makes SPM a promising approach to improve the performance of compact arrays.

5.5 Summary

This chapter has investigated a complete MIMO system network model with compact arrays at both link ends containing arbitrary matching networks based on the Z-parameter approach. This model is used to derive the optimal single-port matching impedance ($z_{\rm opt}$) for capacity maximization of a 2×2 MIMO system with coupled antenna elements at the receive end only. The MIMO system sensitivity and couple receive array design have also been studied. The conclusions of this chapter are:

- A compact MIMO system with MC and SPM networks can be formulated using the Z-parameter approach. A general channel matrix including the MC effect expressed in Z-parameter form can also be obtained. Utilizing the Z-parameter model to examine the $N \times N$ MIMO systems we can show:
  - The system will benefit more by choosing the appropriate SPM for larger N.
  - With fixed antenna spacing, the system performs better for higher SNR when the appropriate SPM is chosen.
  - With fixed SNR, the system is optimized with proper SPM selection for any antenna spacing, and larger configurations will provide more performance advantages.
- Unlike the optimal SPM for power maximization in Chapter 3, the optimal SPM for MIMO capacity maximization ($z_{\rm opt}$) can be derived numerically. Moreover, the input

impedance is proved to be z_{opt} in the high SNR scenario and a precise closed-form is available, which confirms the conjecture in the end of Chapter 4. The ergodic capacity upper bound can substitute the ergodic capacity to simplify the derivation of z_{opt}. The derivation of z_{opt} is valid for any 2×2 single-mode antenna array.

- The compact MIMO system performance depends on various parameters of the system design. Generally, the system performs better with larger antenna spacing (d) with any SPM, and achieves full capacity performance around 0.25λ in any SNR regime. The system takes good advantage of introducing z_{opt}, and the z_{opt} match outperforms any other SPM networks when $d \leq 0.15\lambda$ for any SNR cases. With accurately designed SPM networks, the system with the z_{opt} match is very sensitive to the dipole length variation, and the advantage of z_{opt} match disappears when d increases. With accurately designed dipole length and d, MIMO capacity is not sensitive to the z_{opt} mismatch. The upper bound can be used to study the system sensitivity instead of the ergodic capacity, which will reduce significantly the time cost of Monte Carlo simulation.

Generally speaking, the performance of compact MIMO systems can be greatly improved by introducing the optimal SPM impedance to the couple receive end for small antenna spacings ($d \leq 0.15\lambda$). For a 2×2 compact MIMO system, the optimal SPM impedance is the input impedance in a high SNR scenario. When antenna spacing and dipole lengths are fixed, MIMO capacity is not sensitive to the optimal impedance mismatch; when the optimal matching network is precise, the MIMO system is relatively sensitive to antenna structure mismatch. Hence, the optimal single-port match is a feasible technique to improve the performance of the compact MIMO systems.

Chapter 6
Conclusions and future work

This thesis has been concerned with the performance evaluation and improvement of MIMO systems with compact terminals and matching networks. This chapter will draw together the results of previous chapters and highlight the main conclusions and limitations of this thesis. Some suggestions for possible future research extensions are also discussed.

6.1 Conclusions and summary of results

Insufficient antenna separation ($\lambda/2$) induces mutual coupling (MC) and can significantly affect the performance of antenna arrays, especially at the receive end. Including proper matching networks between the receive antenna array and load terminations will compensate the performance degradation due to the MC effect. In Chapter 3, the array performance metrics of signal correlation (SC), received power and MIMO capacity for a two-element compact MIMO terminal with various matching networks are investigated. The simulation results show that the SC performance using *theoretical* methods without MC [82] and with MC [22, 63] agree well with the corresponding results generated in *semi-theoretical* method [11]. With full angular spread (AS), the multi-port conjugate match gives zero SC between antenna elements in theory. If single-port matching networks are considered, the input-impedance match outperforms other matching approaches. The average received power of the two-element array based on circuit theory [22] and the steering vector approach [63] are also examined. It is proved numerically in Chapter 3 that the method in [22] is appropriate for the received power calculation of compact receivers. There are optimal single-port matching impedances for received power maximization at each antenna separation. Antenna spacings within $[0.1, 0.2]$ wavelengths are desirable for compact receiver design as the lowest power difference and relatively high received power can be achieved for any matching conditions in any scenario. The capacity performance of compact MIMO systems with matching networks can be simulated using both Z-parameters and S-parameters. In general, the value of AS critically affects the SC, power and capacity performance and the distribution of the power azimuth spectrum (PAS) has a less impact on those

metrics apart from the matching network selection. However, the broadside angle-of-arrival with larger AS always lead to better SC, total received power and MIMO capacity performance. Moreover, the introduction of proper matching networks can improve the performance of compact MIMO systems.

To confirm the existence of an optimum load for received power maximization in Chapter 3, a compact (spaced by 0.05 wavelength) two-element quarter-wavelength monopole array with various matching networks has been set up experimentally. In Chapter 4, the construction and measured outcome of 2D and 3D SC and total received power are studied. Meanwhile, the measured model is simulated using computational electromagnetic simulation tools SEMCAD, FEKO to calibrate the experimental results. Microstrip transmission line with single-stub tuning is utilized for matching network design. Careful attention must be paid in experimental work because the dimension of the transmission lines has not been considered in the empirical equations. Therefore, proper simulation calibration is essential. There are discrepancies between the measured and theoretical, simulation results. The better consistency between the measured and simulation results reveals that theoretical simplification is the main reason of these differences. Ohmic losses of the antennas, the sensitivity of the high power gain location and errors in the measurements may all contribute to the discrepancies between the experimental and simulation results. The most important findings of Chapter 4 are as follows. First, the measurement confirms the theoretical predictions in Chapter 3 that there is a proper matching impedance to achieve a relatively high total received power and low SC for any specific antenna separation. Second, the capacitive load which is predicted to maximize the received power in Chapter 3 performs poorly in reality. Last but not the least, the matching impedance for power maximization or zero SC are not the same as the one maximizing the MIMO capacity.

The impedances for capacity maximization at the end of Chapter 4 draws our attention. To continue the investigation, a complete MIMO system network model with compact arrays at both link ends with matching networks has been developed using Z-parameters in Chapter 5. The study of Z-parameter network model shows that MIMO system will benefit more by choosing the proper single-port matching (SPM) with larger system configurations. Higher signal-to-noise ratio (SNR) will improve the system performance if an appropriate SPM is chosen at fixed antenna separation. The optimal single-port matching for capacity maximization of a 2×2 compact MIMO system with single-mode identical antennas are derived numerically utilizing the ergodic capacity upper bound. In high SNR regime, the input matching impedance

is proved to be the optimal SPM for capacity maximization. The optimal SPM outperforms any other SPM network considered in this thesis when the antenna separations are less than 0.15 wavelength with any SNR. The MIMO system sensitivity and compact receiver design are also studied. It turns out that the performance of the optimal SPM is very sensitive to the mismatch of the antenna structure, e.g. dipole length. With the accurate design of the antenna structure and separation, the system performance is not sensitive to the mismatch of the optimal SPM. Hence, the optimal SPM is a feasible solution to improve the performance of MIMO systems with compact terminals.

The conclusions of the whole thesis can be summarized as follows:

> **Matching networks can be used to improve the signal correlation and received power performance of a compact array, which has been proved theoretically and confirmed experimentally. The performance of MIMO systems with compact terminals can be significantly improved by proper matching network selection. For a 2×2 MIMO system, there is an optimal single-port matching impedance for capacity maximization at each antenna separation. The input impedance of the receive antennas (including the mutual coupling) is the optimal single-port match in high SNR region. The performance of compact MIMO systems is not very sensitive to the mismatch of the optimal single-port match. Therefore, the optimal single-port matching is a feasible approach to improve the performance of MIMO systems with compact terminals.**

6.2 Future work

Several directions can be extended around the topics involved in this thesis. Some suggestions are listed below:

- The biggest limitation of this thesis is that most of the theoretical analysis is confirmed by either two-element compact terminal or 2×2 MIMO systems. To study the compact arrays of more than two elements, the assistance of robust CEM simulation tools is inevitable. Most of the literature related to this topic [11, 12, 18, 22, 29, 30] is also limited to 2×2 MIMO configurations. Larger-sized compact MIMO configurations with matching networks has to be confirmed either by CEM simulations or practical implementation.
- As a extension work of Chapter 4, the experimental evaluation of MIMO capacity can be carried out to confirm the capacity improvement of matching networks on compact MIMO terminals. No contemporary literature has reported measured results on this topic.

- The noise assumption of the Z-parameter system analysis is simplistic. A more realistic amplifier noise model as in [27, 28] can be added into the system analysis. How this module would affect our optimal single-port impedance derivation in Chapter 5 is an interesting next step of research.

- The optimal single-port matching impedances for MIMO capacity maximization for larger compact MIMO configurations should be studied. We note that for higher dimensions of compact receivers, the input-impedance of each element is unlikely to be identical because the position of the antenna and the point of the incident angle results in unequal feeding current distribution on each element. This makes it difficult to study larger array sizes in MIMO systems. However, it is clearly worthwhile to find out the solutions for this case.

- More types of antennas besides dipoles and monopoles need to be simulated using CEM tools to examine the MIMO system sensitivities versus the parameters of the antenna structures. Even for dipole antennas, the wire diameter should be considered as a factor which would affect the MIMO system performance.

- The multiport-conjugate match introduced in Chapter 3 outperforms the single-port match. It has not been studied here because of its complexity of implementation [31] and poor performance in broadband scenarios [29]. However, if efforts can be made to conquer these two disadvantages of the multiport-conjugate match, it should be recognized as superior to the optimal single-port match because it can offer maximum power transfer and zero SC [11, 18] for the compact MIMO terminals.

Appendix A
Derivation of input impedance match

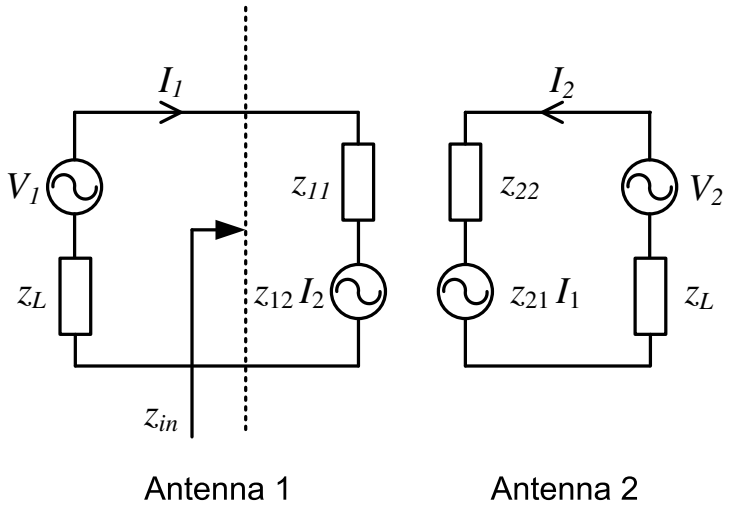

Figure A.1: *Equivalent circuit of two mutual coupled antennas with matching impedances for z_{in} calculation.*

In circuit theory, the voltage-current relations of antenna 1 can be expressed as

$$z_{in}I_1 = z_{12}I_2 + z_{11}I_1 \tag{A.1}$$

If the input impedance z_{in} is used for matching, we have $z_L = z_{in}^*$. In a similar way, the circuit of antenna 2 can be represented as

$$-z_{in}^*I_2 = z_{21}I_1 + z_{22}I_2 \tag{A.2}$$

According to the reciprocity theorem [56], $z_{12} = z_{21}$. Also we assume antenna 1 and 2 are identical elements, then $z_{11} = z_{22}$.

Combining (A.1) and (A.2), we have

$$z_{in} = z_{11} - \frac{z_{12}^2}{z_{11} + z_{in}^*} \tag{A.3}$$

Next we define z_{in} = r_{in} + jx_{in}, z_{11} = r_{11} + jx_{11} and z_{12} = r_{12} + jx_{12} in (A.3). Then equation (A.3) can be simplified to

$$x_{in} = -\frac{r_{12}x_{12}}{r_{11}} + x_{11} \tag{A.4a}$$

$$r_{in}^2 = r_{11}^2 - r_{12}^2 + x_{12}^2 - \frac{r_{12}^2 x_{12}^2}{r_{11}^2}. \tag{A.4b}$$

The square root of (A.4b) must be real by the definition of resistance. Equation (A.4b) can be further written as

$$r_{in}^2 = r_{11}^2 - r_{12}^2 + x_{12}^2 - \frac{r_{12}^2 x_{12}^2}{r_{11}^2} = \left(r_{11}^2 - r_{12}^2\right)\left(1 + \frac{x_{12}^2}{r_{11}^2}\right). \tag{A.5}$$

As is known, $r_{11} > r_{12}$ [30] for sure. Then the positive square root of r_{in}^2 is

$$r_{in} = \sqrt{r_{11}^2 - r_{12}^2 + x_{12}^2 - \frac{r_{12}^2 x_{12}^2}{r_{11}^2}}. \tag{A.6}$$

For z_{in} match, i.e. z_L = z_{in}^*, we have

$$z_L = r_{in} - jx_{in} = \sqrt{r_{11}^2 - r_{12}^2 + x_{12}^2 - \frac{r_{12}^2 x_{12}^2}{r_{11}^2}} + j\left(\frac{r_{12}x_{12}}{r_{11}} - x_{11}\right). \tag{A.7}$$

Appendix B
Supplementary data of the monopole array implementation

B.1 System design in SEMCAD

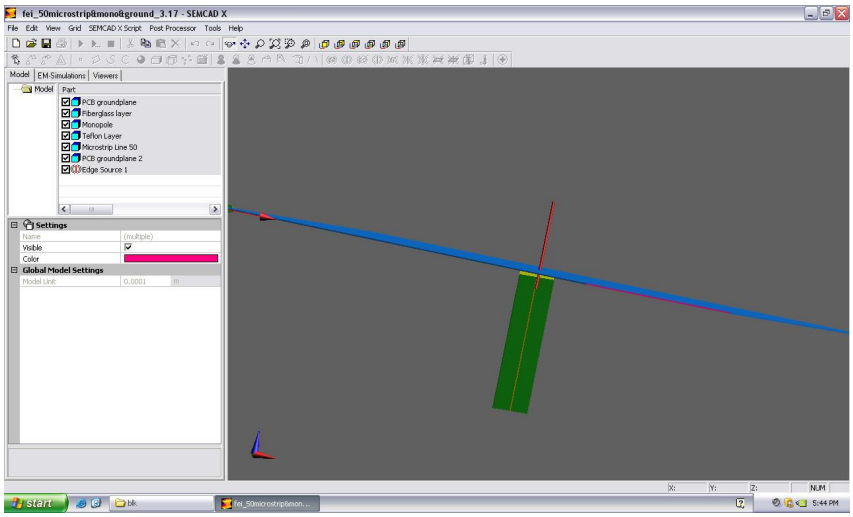

Figure B.1: *Overview of the system model in SEMCAD CAD window.*

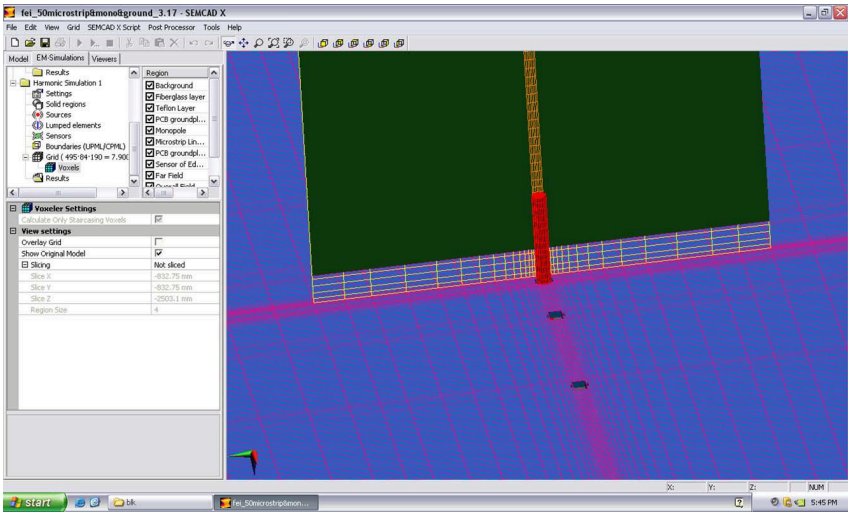

Figure B.2: *Mesh design at the junction of monopole, PCB board and the ground plane.*

In Figure B.1 the simulated system model using SEMCAD is shown. The system includes the ground plane, $4/\lambda$ monopole and the 50Ω transmission line designed on a PCB board as in Figure 4.3. Figure B.2 is zoomed to the connecting point between the monopole antenna with the transmission line and the bottom of the ground plane. The red cylinder is end part of the monopole. The blue surface and the magenta mesh represent the dielectric layer and the metal layer of the ground plane, respectively. Also the green surface is the dielectric layer of the PCB board; the yellow mesh represents the transmission line and the metal layer.

B.2 Pictures of the system measurement

Figure B.3: *The Electronic Lab I worked at in Lund University, Sweden.*

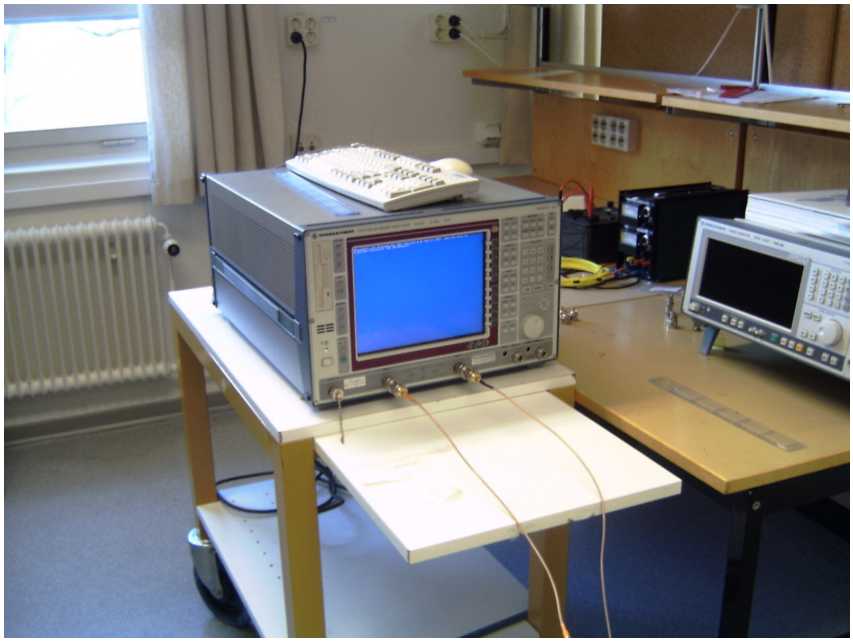

Figure B.4: *The network analyzer we used for measurement of matching impedances.*

Figure B.5: *The calibration kit used for measurement of the self and mutual impedances of the monopole array.*

Figure B.6: *The experimental model before tested in the anechoic chamber at Perlos AB, Sweden.*

B.3 Comparison of different 3D results of selected loads

Comparing the theoretical and measured results in Table B.1, we can see that the measured total powers different matching cases generally suffer a degradation of 0.1∼1.3dB except at point z_B where the gap is as large as 5.6dB. Regarding the measured SCs, they are 0.08∼0.2 higher than the theoretical results for most cases: at point z_B 0.3 lower and point z_C 0.33 higher. The measured received power values agree better with the corresponding simulation results than the

	$Impedances\ (\Omega)$	Simulation*		Theoretical†		Measurement‡	
		P_{total} (dB)	$\tilde{\rho}_{mc}$	P_{total} (dB)	$\tilde{\rho}_{mc}$	$P_{3d,m}$ (dB)	$\rho_{3d,m}$
z_A	70.69 - j9	0.1066	0.9093	0.2832	0.8374	0.1171	0.9096
z_B	1.5 - j12.8	-0.9207	0.8478	0.4439	0.8867	-5.2147	0.5809
z_C	4.06 + j3	-6.6955	0.4512	-5.8153	0.2199	-7.1293	0.5550
z_D	16.5 - j12	-1.5932	0.4615	-0.7459	0.2193	-1.4128	0.4488
z_0	50	-0.1671	0.8647	0.0995	0.7758	-0.3319	0.8647

*simulation results in SEMCAD with $z_{11,s} = 47.5 + j10.9\Omega$, $z_{12,s} = 46.77 - j0.57\Omega$, and ρ_{oc} = 0.9823

†theoretical results with $z_{11,m} = 46.72 + j9.39\Omega$, $z_{12,m} = 45.31 - j2.57\Omega$, and ρ_{oc} = 0.9658-j0.0009

‡measured results with $z_{11,m} = 46.72 + j9.39\Omega$, $z_{12,m} = 45.31 - j2.57\Omega$, and ρ_{oc} = 0.9658-j0.0009

Table B.1: *Comparison of 3D theoretical, simulation and measured total received power and correlation of selected loads.*

theoretical results in Table B.1; the gap between the measured and simulated SC is also smaller compared to the theoretical cases except for the correlation of point z_B. The total received power and SC performance metrics (especially the trend) are in general consistent between the corresponding simulation and measured cases.

In general the 3D results follow the trend of the corresponding 2D results in Table 4.3 on page 81. The 3D received power of each selected load is slightly increased compared to the corresponding 2D case.

B.4 Ergodic MIMO capacity as a function of matching impedances

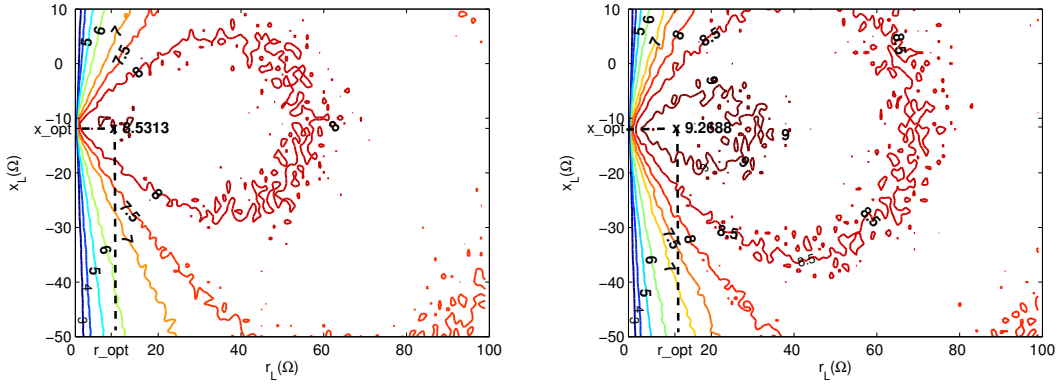

(a) Simulation **(b)** Measurement

Figure B.7: *The contour plots of the ergodic MIMO capacity of simulation and measured cases as a function of matching impedances of the monopole array at $d = 0.05\lambda$, ρ_r = 20dB. Both z_{opt} locations are marked, where $z_{opt} = r_{opt} + jx_{opt}$.*

The ergodic capacity results in Figure B.7 are computed using C_Z calculated in (3.45) on page 59. Figure B.7(a) shows the capacity results based on the antenna impedances and SC used for the 'Simulation' column listed in the comments of Table B.1, while Figure B.7(b) provides the results based on the 'Measured' antenna impedances and SC listed in Table B.1. The capacity contour looks similar to the received power in Figure 4.9(a) on page 77 in Chapter 3. Nevertheless, unlike the received power, the capacity has only one maximum in both cases. The maximum at the large matching impedance area (like impedance z_A) in Figure 4.9(a) disappeared in the capacity contour due to high correlation in that region as listed in Table 4.3 on page 81. The position of the narrow peak (like impedance z_B) in the received power in Figure 4.9(a) has been shifted to the right due to the contribution of low to zero correlation in Figure

4.9(b) to capacity improvement in this region. The maximum capacity using the measured results (9.2688bits/s/Hz) in Figure B.7(b) is slightly higher than that using the simulation results (8.5313bits/s/Hz) in Figure B.7(a). The z_{opt} of both cases are listed in Table 4.4 on page 87.

Appendix C
Advanced matching network design

The single-stub tuning technique introduced in Section 4.3.2 assumes the transmission line is infinitely thin. However, in practice the microstrip transmission line must have a finite width. Because the matching impedance design is determined by d_s and l_s shown in Figure C.1, choosing the optimum position and lengths of d_s and l_s are crucial to the design accuracy. To realize the correct implementation, the matching network configurations are simulated in software the FEKO [65] based on the MoM method. Various d_s and l_s combinations have been attempted for each matching impedance.

Firstly, the z_{11}^* match of the single monopole is simulated. The equivalent circuit of the design and in measurement is modeled as in Figure C.1. With measured self impedance of $z_{mo,m}$ = 45.5 + j19.22Ω at $d = 0.05\lambda$, we choose the suitable solution $d_s = 111.53$mm and $l_s = 14.34$mm for z_{11}^* match design. In Figure C.1 port 2 is equipped with the monopole antenna, and port 1 is the view point connected to the network analyzer. If the monopole is perfectly matched, a 50Ω load should be observed from port 1.

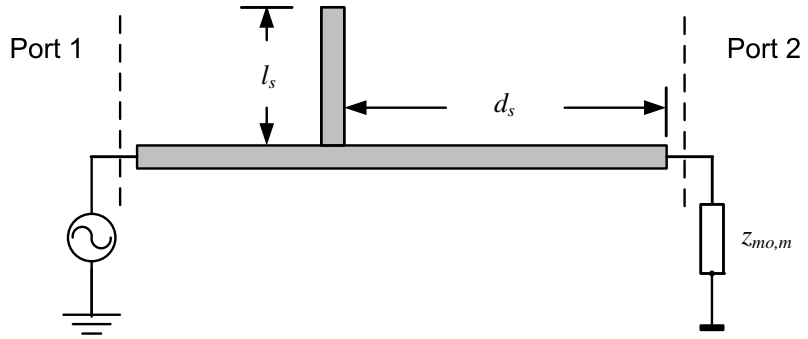

Figure C.1: *The equivalent circuit of z_{11}^* match for a monopole.*

To find the best combination of the position and lengths of d_s and l_s, ten sets of configurations as shown in Figure C.2 have been simulated in FEKO. Referring to [107], the length of l_s has to be extended between 0.1 to 1 times h_s depending on the ratio w_m/h_s due to the microstrip

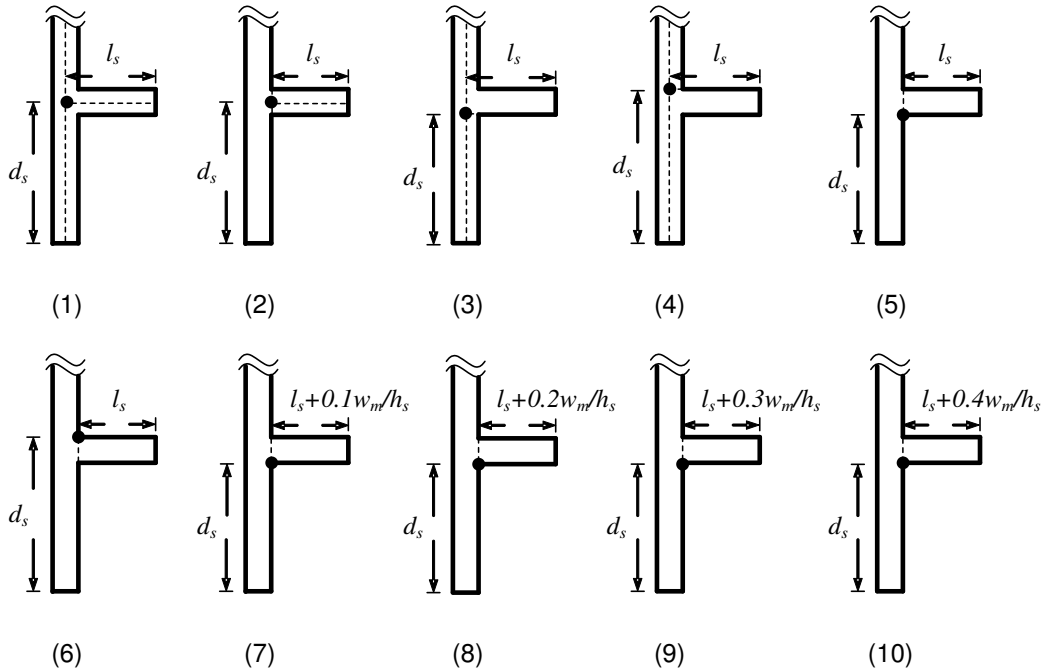

Figure C.2: *Various combinations of d_s and l_s for z_{11}^* match of a monopole.*

Case	Impedance at port 1 (Ω)	Reflection coefficient
1	53.94 - j0.165	0.03
2	52.37 + j0.78	0.0244
3	53 - j1.19	0.0313
4	55.05 + j0.74	0.0485
5	51.38 - j0.254	0.0139
6	53.58 + j1.863	0.0389
7	50.96 - j0.020	0.0095
8	50.52 - j0.216	0.0056
9	50.11 - j0.473	0.0048
10	49.66 + j0.73	0.008

Table C.1: *Impedance values and reflection coefficient observed from port 1 of various z_{11}^* matched cases for a monopole.*

discontinuities in practice. The corresponding impedance values and reflection coefficient for different cases are listed in Table C.1.

In Table C.1 case 9 gives the best matching result compared to other cases because its resistive part is the closest one to 50Ω and the reflection coefficient is the lowest among all cases. In case 9 the OC stub length is about $l_s + 0.3w_m/h_s$, which agrees well with [107]. The reflection coefficient of case 9 from 700MHz to 1.1GHz is showed in Figure C.3. It is clear that the impedance is tuned to 900MHz with reflection coefficient as low as -48dB.

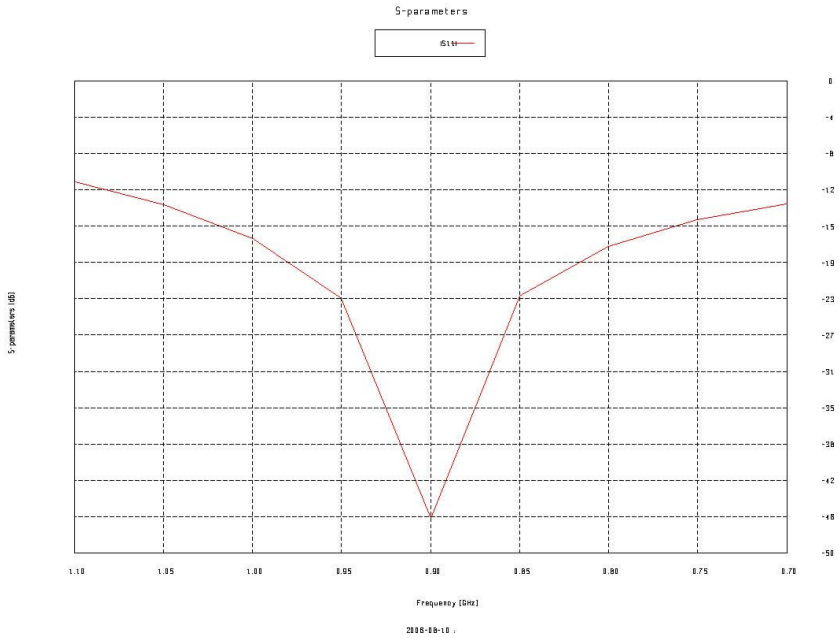

Figure C.3: *The reflection coefficient of case 9 in Figure C.2 of z_{11}^* match for a monopole simulated in FEKO. The abscissa is the frequency span from 700MHz to 1.1GHz. The ordinate is the reflection coefficient in dB.*

Secondly, the z_{in} match of the coupled monopole array is attempted. When $d = 0.05\lambda$, the input impedance of the monopole is z_{in} = 11.41 + j11.89Ω, and the corresponding design structure is d_s = 6.92mm, l_s = 37.81mm. Then the impedance measured from port 1 of Figure C.1 and computed in (4.8) is z_{p1} = 100.54 + j96.30Ω when port 2 is equipped with $z_{mo,m}$ = 45.5 + j19.22Ω in theory. Because the length of l_s in this design is too long to fit in our PCB board dimension and d_s is too short to connect to port 2 (the monopole), we have to rotate the OC stub with an angle (not perpendicular to the 50Ω transmission line). Hence, the optimum matching for z_{11}^* match (case 9 in Figure C.2) is not suitable for this model. More design combinations of d_s and l_s have been carried out in FEKO as displayed in Figure C.4. The OC stub has been

rotated with 30° angle away from port 1 with various lengths. The impedance values of case 1 to 15 observed from port 2 are listed in Table C.2.

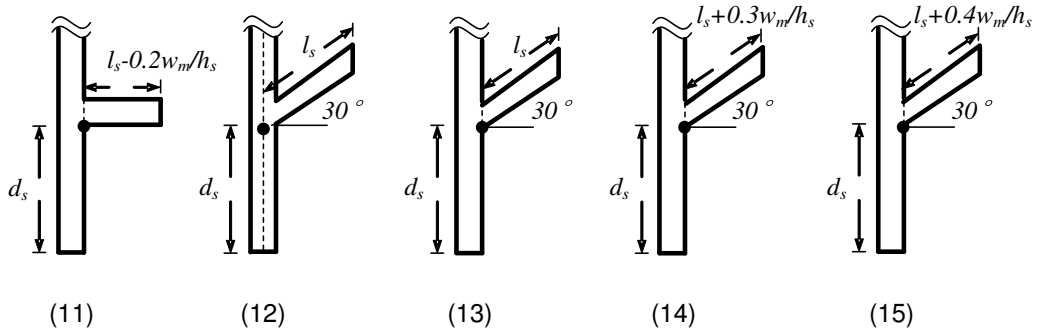

Figure C.4: *Extended combinations of d_s and l_s of Figure C.2 for z_{in} match of a monopole.*

Case	Impedance at port 1 (Ω)
1	122.52 + j85.76
2	137.17 + j95.81
3	110.20 + j90.20
4	113.20 + j79.30
5	112.33 + j101.34
6	150.20 + j87.40
7	125.40 + j104.69
8	129.38 + j108.10
9	134.44 + j111.75
10	138.36 + j115.33
11	115.42 + j95.23
12	91.06 + j76.06
13	98.62 + j84.82
14	105.87 + j93.45
15	108.43 + j96.28

Table C.2: *Impedance values observed from port 1 of various z_{in} matched cases for a monopole.*

We can see that case 15 outperforms other cases in Table C.2. The corresponding design structure of case 15 in FEKO is shown in Figure C.5. We note that the substrate layer of the PCB board can only be simulated with infinite area in FEKO. Hence, a potential error exists between simulation and measurement results. Though there are no empirical equations for matching network design considering the transmission line dimensions, some general rules can be summarized from our exploration.

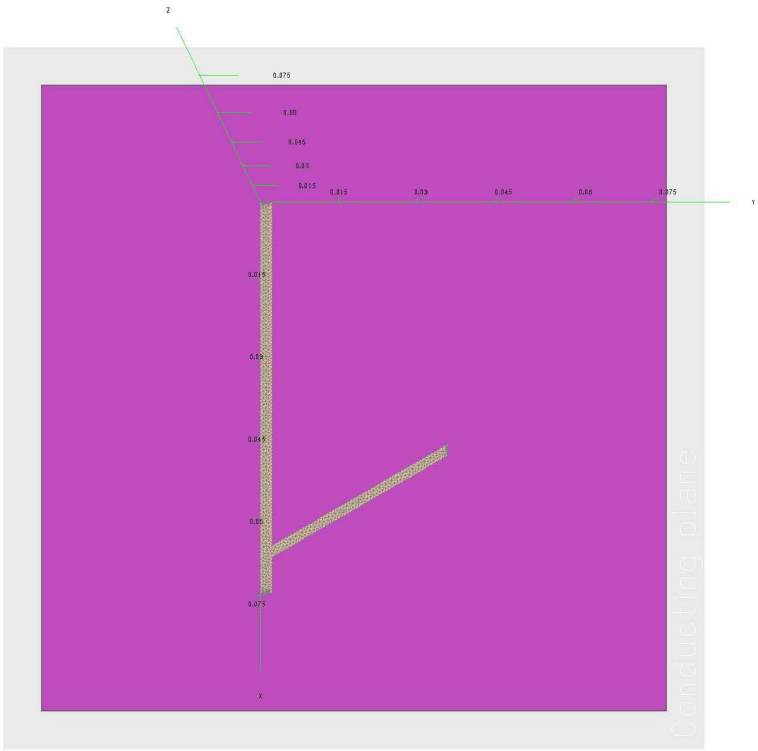

Figure C.5: *Design structure of case 15 in Figure C.4 for z_{in} match of a monopole simulated in FEKO.*

- The distance from the load to be matched to the matching stub place d_s should be designed first as calculated in Section 4.3.2.
- The OC stub should start from the end of d_s and be located beside one side of the transmission line.
- The length of the OC stub l_s is always longer than that calculated in Section 4.3.2, i.e. 0.1 to 1 times h_s depending on the w_m/h_s, due to the microstrip discontinuities characteristic.
- If d_s is too short and l_s is too long to fit into the PCB board, the OC stub can be designed with an angle to the transmission line, though new l_s should be simulated before implementation.

The matching networks of the five selected impedances in Section 4.5 have also been simulated in FEKO. The impedance values of z_{p1} calculated in (4.8) are compared to those generated using FEKO in Table C.3. The matching network structure of load points z_A and z_E is imple-

mented as case 9 in Figure C.2, while the impedances $z_B \sim z_D$ are tuned as case 15 in Figure C.4. In Table C.3 the theoretical and simulated z_{p1} values agree well for each selected load impedance. However, Table C.3 also tells us that the matched impedances can never be tuned precisely utilizing the transmission line with single shunt stub matching technique, which may cause error for future received power and SC measurement.

	Impedance (Ω)	d_s(mm)	l_s(mm)	z_{p1} in (4.8) (Ω)	z_{p1} in FEKO (Ω)
z_A	70.69 - j9	88.65	13.23	79.10 + j8.88	82.67 + j9.94
z_B	1.5 - j12.8	112.03	51.04	3.79 + j58.19	3.19 + j60.05
z_C	4.06 + j3	12.31	46.35	118.46 + j257.28	112.66 + j262.16
z_D	16.5 - j12	9.00	32.53	65.90 + j60.56	66.69 + j59.48
z_E	50	75	0	35.05 - j8.75	35.39 - j8.25

Table C.3: *Impedance values observed from port 1 for five selected load impedances z_A to z_E.*

Appendix D
Derivation of polynomial (5.30)

As known to all, generally there can be no general formula (involving only the arithmetical operations and radicals) for the roots of a polynomial of degree 5 or greater in terms of its coefficients [108]. However, numerical results can be solved on some extent.

Recalling (5.25) and (5.26), we have

$$\big(\mathfrak{R}_1^2 - r_L^2 + (x_L + \mathfrak{X}_1)^2\big) \cdot \Sigma_2 + \big(\mathfrak{R}_2^2 - r_L^2 + (x_L + \mathfrak{X}_2)^2\big) \cdot \Sigma_1 = 0; \tag{D.1a}$$

$$(x_L + \mathfrak{X}_1) \cdot \Sigma_2 + (x_L + \mathfrak{X}_2) \cdot \Sigma_1 = 0. \tag{D.1b}$$

where

$$\begin{aligned}
\Sigma_1 = &\big((r_L + \mathfrak{R}_1)^2 + (x_L + \mathfrak{X}_1)^2\big) \\
&\cdot \big((1 - \mathrm{Re}\{\alpha\})\big((r_L + \mathfrak{R}_1)^2 + (x_L + \mathfrak{X}_1)^2\big) + (1 - |\alpha|^2)\kappa r_L\big), \\
\Sigma_2 = &\big((r_L + \mathfrak{R}_2)^2 + (x_L + \mathfrak{X}_2)^2\big) \\
&\cdot \big((1 + \mathrm{Re}\{\alpha\})\big((r_L + \mathfrak{R}_2)^2 + (x_L + \mathfrak{X}_2)^2\big) + (1 - |\alpha|^2)\kappa r_L\big),
\end{aligned} \tag{D.2}$$

$\mathfrak{R}_1 = r_{11} + r_{12}$, $\mathfrak{X}_1 = x_{11} + x_{12}$, $\mathfrak{R}_2 = r_{11} - r_{12}$, $\mathfrak{X}_2 = x_{11} - x_{12}$ as defined in (5.23) on page 102, $\kappa = \rho_r \cdot 4r_{11}/N$ as defined in (5.24) on page 102, and $\alpha = (\mathbf{\Psi}_R)_{12} = (\mathbf{\Psi}_R)_{21}$ is the correlation coefficient between the two receivers.

Utilizing (5.29) on page 103, we have

$$r_L^2 = \Gamma - (x_L + \sigma)^2 \tag{D.3}$$

where $\sigma = x_{11} + \frac{r_{11}r_{12}}{x_{12}}$, $\Gamma = r_{11}^2 + r_{12}^2 + x_{12}^2 + \frac{r_{11}^2 r_{12}^2}{x_{12}^2}$. From (D.1b) and (D.2) we notice that the highest degree of r_L in (D.1b) is 4. First, we use the command `collect` in Matlab [109] to

rewrite (D.1b) in terms of the powers of r_L. Then we replace

$$\begin{aligned} r_L^2 &= \Gamma - (x_L + \sigma)^2; \\ r_L^3 &= (\Gamma - (x_L + \sigma)^2) r_L; \\ r_L^4 &= (\Gamma - (x_L + \sigma)^2)^2 \end{aligned} \tag{D.4}$$

in (D.1b) using command `subs` in Matlab. Now (D.1b) becomes a polynomial containing variables of r_L of degree 1 and x_L of various degrees. To eliminate variable r_L in (D.1b), we square (D.1b) and substitute r_L^2 using (D.3). Then a polynomial ((5.30) on page 103) with x_L of degrees 8 is obtained:

$$p_8 x_L^8 + p_7 x_L^7 + p_6 x_L^6 + p_5 x_L^5 + p_4 x_L^4 + p_3 x_L^3 + p_2 x_L^2 + p_1 x_L + p_0 = 0 \tag{D.5}$$

where x_L is the reactant part of the matching load z_L, and the coefficients p_ms can be expressed by r_{11}, x_{11}, r_{12}, x_{12} and ρ_r only. When antenna spacing and reference SNR are fixed, x_L can be solved numerically using `roots` command in Matlab.

Appendix E
Original publications

E.1 Book chapter

- †[1] **Y. Fei** and J. S. Thompson, "Design of Compact Antenna Arrays for MIMO Wireless Communications", *4G Mobile & Wireless Communications Technologies*, River Publishers, Nov., 2007.

E.2 Journal Paper

- †**Y. Fei**, Y. Fan, B. K. Lau and J. S. Thompson, "Optimal single-port impedance matching for capacity maximization in compact MIMO arrays,"*IEEE Transactions on Antennas and Propagation.*, under major revision.

E.3 Conference Papers

- †**Y. Fei**, Y. Fan and J. S. Thompson, "Optimal single-port impedance matching for compact MIMO arrays," submitted to *50th IEEE Globe Telecommunication Conference (GLOBECOM 07')*, 26-30 Nov., Washington D.C., USA.
- †**Y. Fei** and J. S. Thompson, "Continuous study of closely coupled dipoles with matching networks," to appear in *Proceedings of 2nd European Conference of Antennas and Propagation (EUCAP 07')*, 11-16 Nov., 2007, Edinburgh, UK.
- †**Y. Fei** and J. S. Thompson, "The capacity of matched compact linear antenna arrays," to appear in *Proceedings of 2nd Euroupen Conference of Antennas and Propagation (EUCAP 07')*, 11-16 Nov., 2007, Edinburgh, UK.
- †**Y. Fei** and J. S. Thompson, "MIMO system sensitivity and coupled array design," to appear in *Proceedings of 18th IEEE International Personal Indoor Mobile Radio Conference (PIMRC 07')*, 3-6 Sep., 2007, Athens, Greece.

[1]These publications are enclosed in this appendix.

- †**Y. Fei**, B. K. Lau, A. Sunesson, A. J. Johansson, J. B. Andersen and J. S. Thompson, "Experiments of closely coupled monopoles with load matching in a random field," in *Proceedings of 1st European Conference of Antennas and Propagation (EUCAP 06')*, 5-10 Nov., 2006, Nice, France.

- **Y. Fei** and J. S. Thompson, "MIMO system with dielectric resonator antennas," in *Proceedings of IEEE/IET/EPSRC Posgraduate Research Conference (PREP 05')*, 28 Mar.-1 Apr., 2005, Lancaster, UK. **(Best Presentation Prize)**

Design of Compact Antenna Arrays for MIMO Wireless Communications

Yuanyuan Fei[a,1] and John Thompson[a]
[a] *Institute for Digital Communications, University of Edinburgh, Kings Buildings, Edinburgh, United Kingdom.*

Abstract. – Theoretical analysis and measurements have indicated that closely spaced or compact antenna arrays (typically smaller than half the carrier wavelength) can achieve good performance in multiple input multiple output (MIMO) wireless communications. This is an important result which could lead to MIMO technology being deployed even on small wireless terminals. However, these results need to take into account the effect of mutual coupling which arises between closely spaced antenna elements. In this chapter, we discuss how mutual coupling can be properly modeled in a MIMO wireless system. We also discuss how simple matching networks that take into account the mutual coupling effect can be used to provide significant performance improvements in compact antenna array receivers. We provide simulation results for a 2×2 MIMO system to verify the effect of different matching networks and show results for the sensitivity of MIMO performance to errors in the matching network components and antenna element dimensions. Our results show that optimizing a single-port matching impedance is a simple but promising approach to improve the performance of compact arrays.
Keywords: Wireless Telecommunications, 4G, Multiple Input Multiple Output (MIMO), mutual coupling, matching networks, sensitivity analysis.

1. Introduction

The study of compact arrays in small wireless receivers has recently received significant attention from researchers. In narrowband multiple input multiple output (MIMO) systems, it is widely agreed that the mutual coupling (MC) effect, which arises between closely spaced antenna elements in an antenna array, can reduce the signal correlation by distorting the radiation patterns of each element [1,2,3]. However, it will also induce a mismatch between the characteristic impedance of the circuit and the antenna input, which is detrimental to the received signal power level [4]. These conflicting results from the MC effect are one important factor which contributes to differing conclusions concerning its impact on MIMO capacity performance. Some work claims that MC is a benefit to MIMO systems [3,5,6], some completely disagree with the first claim [7.8.9], while a third group [2,4,10,11] believe that the MC only leads to performance advantages in certain specific cases, e.g. a selected range of antenna spacings. This divergence of opinion is caused by different channel normalization criteria, various power allocation strategies at the transmitter and whether the effect of the receiver

[1] Corresponding Author: Yuanyuan Fei, Institute for Digital Communications, School of Engineering and Electronics, University of Edinburgh, Kings Buildings, Edinburgh, EH9 3JL, UK. Email: y.fei@ed.ac.uk

matching network is under consideration. Within these studies, only [2,6] included the matching network of the receiver in their MIMO system evaluations.

Two methods in *n*-port theory are usually adopted to study compact MIMO systems. One is S-parameter analysis which reflects the wave transmission in an *n*-port electrical network; the other is Z-parameter analysis which expresses the voltage and current relations among all ports. The S-parameter framework has been examined in detail in [2], and recently improved by analysing the effect of amplifier networks on the coupled receiver [12]. The authors of [2] introduce several matching networks to improve the system performance, while other types of antenna matching networks are examined in [6]. It is proved in [2] that the so-called *multiport-conjugate match* can realize zero output correlation and lossless power transfer from the antennas to the loads for any antenna spacing, thus offering significant capacity improvement for very small antenna spacings. However, it turns out that the optimum multiport-conjugate match can only be achieved for a small system bandwidth [13], which is in contrast to the desire to use large system bandwidths in future broadband wireless communication networks. Apart from this issue, the multiport-conjugate match is not easily implemented in practice as it requires multiple circuit components to be interconnected across the antenna ports. Instead, the *single-port match* [4,6,13] is a practical, if suboptimal solution, as it provides capacity improvement compared to the non-matched case and has a much broader bandwidth than the multiport-conjugate match.

The impact of the single-port match on the performance of MIMO systems can be studied using a Z-parameter approach, and this evaluation has been partially been carried out in [4,7,10,14,15]. In [4,14] the authors focus on the 2×2 MIMO system. The optimal single-port matching impedance for capacity maximization is first observed in [14] for certain antenna spacings, and then more antenna spacings are investigated in [4]. We have proved in [16] that the optimal single-port matching impedance for capacity maximization can be found analytically for any antenna spacing. Initial results for the study of matching with larger array sizes in compact MIMO systems can be found in [17]. However, the system sensitivity of the 2×2 MIMO system has not received a lot of attention as the capacity performance relies on the practical design of the compact receiver [15]. The importance of matching networks in compact array and their sensitivity to small parameter changes will be discussed in detail in this chapter.

The remainder of this chapter is organized as follows. Part 2 describes the system model and how the effect of mutual coupling and receiver matching networks can be included into the performance evaluation of MIMO systems using Z-parameters. Part 3 presents simulation results which investigate the performance and sensitivity of different coupling techniques on MIMO performance. Finally, Part 4 presents our conclusions.

2. MIMO System Model

A MIMO system with N transmit and N receive antennas is considered in this chapter. For simplicity it is assumed that the channel is frequency-flat fading, and the total average energy at the transmitter over one symbol period is P. The input-output relation for a symbol period is:

$$\mathbf{y} = \sqrt{P/N}\mathbf{H}\mathbf{x} + \mathbf{v}$$

where $\mathbf{y} = [y_1,...,y_N]^T$ is the received signal vector and $\mathbf{x} = [x_1,...,x_N]^T$ is the transmitted signal vector. $\mathbf{H}$ represents the MIMO channel with dimension $N \times N$, and the additive Gaussian noise vector is $\mathbf{v} = [v_1,...,v_N]^T$ with covariance matrix $E[\mathbf{v}\mathbf{v}^H] = N_0\mathbf{I}$. The superscripts T and H means transpose and conjugate transpose, while $E[\cdot]$ denotes the expectation operator. Finally, $\mathbf{I}$ is an $N \times N$ identity matrix.

2.1. Capacity of MIMO Channels

We assume that $\mathbf{H}$ has no preferred transmit direction, and is perfectly known at the receiver. This implies the optimum transmit signals to maximize capacity are independent and equal-power waveforms at the transmit antennas [18]. The narrowband MIMO Shannon capacity is given by:

$$C = \log_2 \det\left[\mathbf{I} + (\rho/N)\mathbf{H}\mathbf{H}^H\right]$$

where ρ is the signal-to-noise (SNR) ratio. Moreover, we assume the channel has rich-scattering at both ends, as well as the transmitter antennas being located far apart. Then the channel $\mathbf{H}$ can be expressed by the semicorrelated Kronecker model [19]:

$$\mathbf{H} = \mathbf{R}^{1/2}\mathbf{H}_{iid}$$

If the uniformly distributed arriving signal model in space is assumed, the receive end correlation matrix $\mathbf{R}$ has elements $\mathbf{R}_{ii} = 1$ and $\mathbf{R}_{ii} = J_0(2\pi d/\lambda)$ [20], where $J_0(\,)$ and d, and are the zero order Bessel function and the receiver antenna spacing. The matrix $\mathbf{H}_{iid}$ is an $N \times N$ independent and identically Rayleigh distributed (i.i.d.) channel matrix.

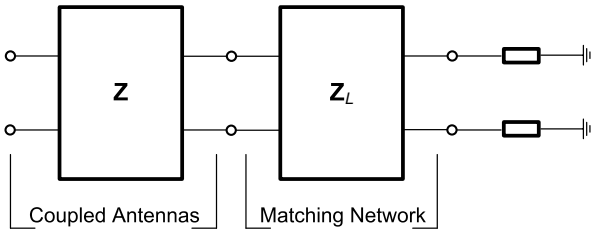

Figure 1: Block diagram of the coupled MIMO receivers with matching networks.

2.2. Effect of Mutual Coupling

As compact receive antennas are considered with spacings $d<0.5\lambda$, the MC effect becomes an important one to model properly. MC can be explained as an interaction caused by neighboring elements inducing extra voltages between each other. In port theory, the mutual impedance matrix $\mathbf{Z}$ is defined as

$$\mathbf{Z} = \begin{bmatrix} Z_{11} & Z_{12} & \cdots \\ Z_{21} & Z_{22} & \ddots \\ \vdots & \ddots & \ddots \end{bmatrix}$$

where Z_{ii} is the self-impedance of the ith element and Z_{ij} means the mutual-impedance between the ith and jth elements. Here the equality $Z_{ij} = Z_{ji}$ is based on the reciprocity

theorem [21]. In Figure 1, the matching-impedance matrix $\mathbf{Z}_L$ is a diagonal matrix whose ith diagonal entry is Z_{Li} which is the matching impedance in the ith antenna branch. Assuming there is no MC between the matching impedances, the non-diagonal elements of Z_L are zero. In this chapter, the antenna elements are considered identical and the load elements are assumed to be identical too, so that the diagonal entries of $\mathbf{Z}_L$ are all equal to Z_L. By utilizing the voltage-current relations [22], the MC coefficient matrix is:

$$\mathbf{\Omega}_{mc} = \left(\mathbf{Z} + \mathbf{Z}_L\right)^{-1} = \left(\mathbf{Z} + Z_L\mathbf{I}\right)^{-1}$$

2.3. MIMO Capacity with Mutual Coupling

The MC effect at the receiver can be easily included into the MIMO model [11] by using the relation $\mathbf{H}_{mc} = \mathbf{\Omega}_{mc}\mathbf{H}$ where $\mathbf{H}_{mc}$ is the modified MIMO channel with MC. Suppose that the matching networks are perfectly lossless and the each transmitter has self-conjugate Z_{11}^{*} match (* denotes the complex conjugate). Without the MC effect, the MIMO system will always have an antenna power gain of ($4R_{11}R_L$) when normalized to the self-conjugate matched single antenna case [14] for a 2×2 system, a point which should be included in the system evaluation. R_{11} and R_L are the resistances (real parts) of Z_{11} and Z_L, respectively. The modified MIMO capacity expression is thus:

$$C_m = \log_2 \det\left[\mathbf{I} + (\rho_r R_{11} R_L / N)\mathbf{H}_{mc}\mathbf{H}_{mc}^{H}\right]$$

where ρ_r is the reference SNR of the system which clearly depends on N_0. An identical result has been derived in [4], though obtained from a different perspective. Now define the ergodic capacity of the MIMO link as E[C_m]. Using Jensen's inequality and the concavity of the log det function [23], we can take the expectation inside the log det function and obtain an upper bound C_{up} at each impedance matching load point Z_{L0} as:

$$C_{up} = \log_2 \det\left[\mathbf{I} + (\rho_r R_{11} R_{L0} / N)\mathbf{\Omega R}\right] \geq \mathrm{E}[C_m]$$

where R_{L0} is the real part of Z_{L0}. As we will see in Section III, C_{up} is very helpful for simplifying the evaluation of the optimum impedance match and for measuring the sensitivity of MIMO capacity to impedance match imperfections.

3. Simulation and Analysis

To illustrate the impact of MC on MIMO systems, a basic 2×2 system configuration is simulated under the conditions presented in Part 2. Identical ideal half-wavelength dipoles with infinite thin wire diameter are used at both ends since they often taken as references in the antenna field. Now we focus on the coupled receive end. Under this ideal assumption, the self-impedance Z_{11} = 73 + j42.5 ohms is constant, and the mutual-impedance $Z_{12} = Z_{21}$ is calculated using the modified EMF method [22]. For each load point Z_{L0}, 10000 random channel realizations are deployed to estimate the MIMO system performance with ρ_r = 15dB.

3.1. Capacity of Different Impedance Matching Techniques

As shown in Figure 2, the 3-dimensional ergodic capacity surface is plotted with various matched impedances points $Z_{L0} = R_{L0} + jX_{L0}$. We take the $d = 0.05\lambda$ case as an example to

demonstrate that the capacity performance is concave and as in [14] one peak is observed with the changing of matching networks at one fixed value of d. For other antenna spacings less than 0.5λ, the surface of C_m has the similar properties.

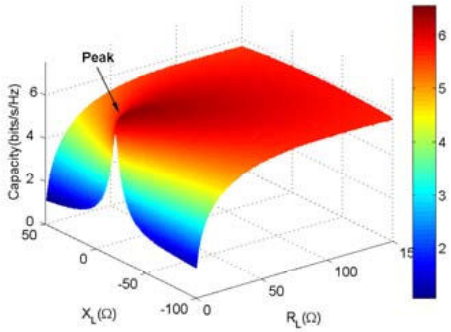

Figure 2: Ergodic capacity vs. the real and imaginary parts of Z_L for $d = 0.05\lambda$

(a) (b)

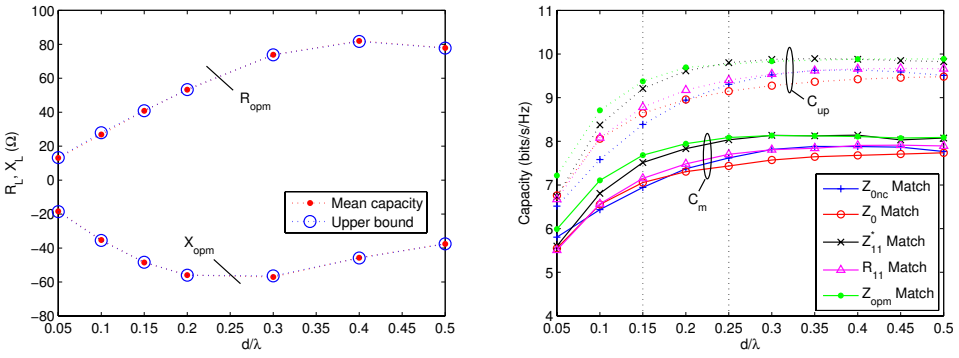

Figure 3: (a) The optimal matching impedances $Z_{opm} = R_{opm} + jX_{opm}$ versus antenna spacing for the mean capacity and upper bound capacity of the system (b) The mean capacity (solid line) and upper bound capacity (dash line) with various matching networks vs antenna spacing (SNR = 15dB)

Although the multiport-conjuate match is theoretically attractive to improve the compact array performance in MIMO systems [2], it is difficult to implement in practice given the current state of the art. Therefore, the optimum single-port impedance match, which gives the best MIMO performance for specific antenna spacing, should be investigated as a simpler alternative. Figure 3(a) plots the optimal matching impedances Z_{opm} (i.e. the peak co-ordinate of Figure 2) vs the antenna spacing d (<0.5λ for compact arrays) for both the mean and upper bound capacities of the system. It is clear that the simulation results agree very well as each dot (C_m) is almost in the centre of the circle (C_{up}) it corresponds to. This means we can use the capacity upper bound in place of the actual capacity result to determine the optimum impedance match very simply. To show how much we can benefit from the Z_{opm} matching, the mean capacity and upper bound capacity have been computed for ideal antennas with characteristic-impedance match

both with no coupling (Z_{0nc}) and with MC (Z_0), self-conjugate match (Z_{11}^*), and Z_{opm} match. The results for these comparisons are shown in Figure 3(b). The coupled compact array with matching networks outperforms the array without MC at small spacings (d<0.2λ). Meanwhile, Z_{opm} match surpasses other matching schemes when d<0.25λ. Another interesting phenomenon is the slope of the results for C_m and C_{up} are nearly the same for different matching pairs with d>0.15λ, which is very useful for investigating the sensitivity of MIMO capacity results. We look back to Figure 2. Despite of the superiority of Z_{opm} match, we need to consider how its sensitivity to small changes in receiver configuration will impact practical implementation.

3.2. Capacity Sensitivity Results

The sensitivity of the matching network is important as it will vary with the environment (temperature, humidity, etc.) as well as due to design accuracy limitations. We define the performance efficiency of C_m for given d and matching impedance Z_{L0} as:

$$\eta_m(Z_{L_0}) = \frac{C_m(Z_{L_0})}{\max\left[C_m(Z)\right]} = \frac{C_m(Z_{L_0})}{C_m(Z_{opm})}$$

The notation $C_m(Z_{L0})$ emphasizes the dependence of C_m on the matching impedance Z_{L0}. The specified precision error of the resistive and reactive components, ΔR and ΔX, relative to the optimum values in Z_{opm} for the matching impedance, are normalized to 50 ohms, so ΔR=2 implies a component error of 100 ohms in R_L. It should be clear that Z_{opm} defines the origin in a plot of ΔR and ΔX. We assume that the matching networks of both receivers have the same precision error simultaneously. The scalar η_{up} is defined in the same way for C_{up} and it turns out [15] that the load impedance that maximizes C_m also approximately maximizes C_{up}. Therefore η_{up} is used to generate results for the capacity sensitivity, which avoids the extensive Monte Carlo simulations needed to evaluate η_m.

(a) (b)

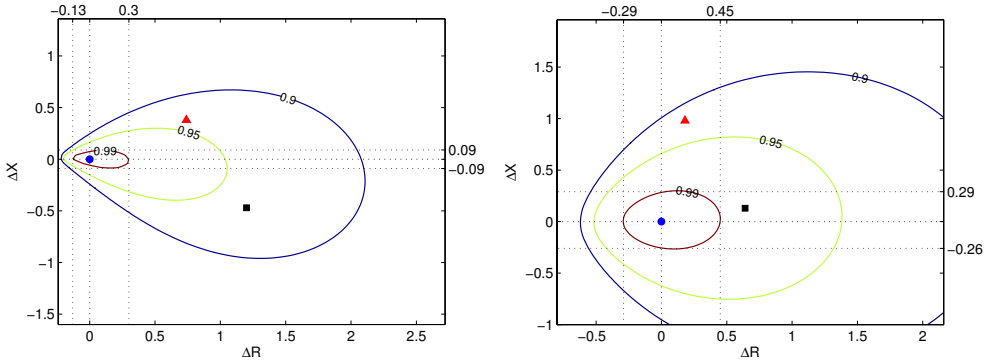

Figure 4: Upper bound capacity efficiency contours for η_{up} = 0.9, 0.95 and 0.99 as a function of ΔR and ΔX with (a) d= 0.05λ and (b) d = 0.15λ. Special matching impedances Z_{opm} (dots), Z_0 (triangles), and Z_{11}^* (squares) are also marked (SNR=15dB).

Figure 4 gives us a clear demonstration of the deterioration in MIMO performance due to mismatches in the optimal impedance for two different antenna spacings. For example, Figure 4(a) tells us that the system capacity reduces by 1% if the normalized error ΔR exceeds the range [-0.13,+0.3] or ΔX exceeds ±0.09. The results also show that Z_0 and

Z_{11}^* matching impedances achieve around 95% of the maximum system capacity, as would be expected from Figure 3(b). Increasing the antenna spacing from d=0.05 to 0.15λ significantly increases the 99% and 95% capacity regions in Figure 4(b), suggesting that the matching is somewhat less sensitive for larger antenna spacings. In addition, the Z_{opm} and Z_{11}^* matches are closer in value, again following the convergence of these two matching approaches as d increases in Figure 3(b). Even for d=0.05λ the MIMO capacity is not very sensitive to small errors in the matching values ΔR and ΔX.

Besides antenna spacing and matching networks, the accuracy of the antenna dimension is another factor which can degrade MIMO performance due to changes in the self and mutual impedances. The impedance values are simulated based on the approach in [24]. Figure 5(a) shows that for d=0.05λ the performance of Z_{opm} match is very sensitive to small errors in the antenna length. However Figure 5(b) shows that Z_{opm} match does not degrade so quickly for d=0.5λ. The highest capacity of Z_0 match is attained for an antenna length of 0.486λ, which is the first resonant length $Z_{11} = R_{11}$ of a dipole antenna. Figure 5 also shows that Z_{11}^* match gives the most stable performance of the three methods. The results demonstrate that MIMO capacity is not sensitive to antenna length at all for this form of matching. Therefore, Z_{11}^* match is probably the best matching network when the dipole length is not precisely known.

(a) (b)

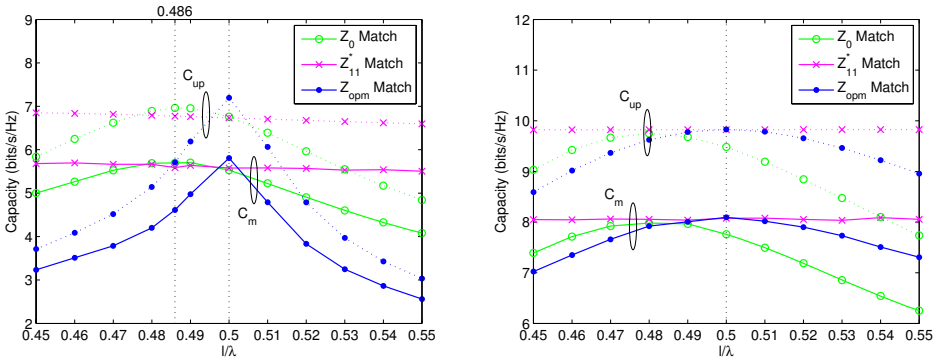

Figure 5: The mean capacity (dash line) and upper bound capacity (solid line) with various matching networks for (a) d= 0.05λ and (b) d = 0.15λ. (SNR=15dB)

4. Conclusion

The performance sensitivity of a *2×2* MIMO system with coupled half-wavelength dipoles and decoupling matching networks is presented in this paper. By utilizing MIMO capacity results and upper bounds which include the mutual coupling and matching networks effect, the optimal single-port matching impedances for various antenna spacing can be found from analysis or simulation. Optimum matching outperforms other matching networks, particularly for small antenna spacing (d < 0.25λ). When antenna spacing and dipole lengths are fixed, the MIMO capacity is not particularly sensitive to small mismatches in the optimal impedance. However, the optimal matching network is relatively sensitive to small changes in antenna size. Despite this limitation, optimal single-port match is a simple and effective technique to improve the performance of MIMO systems using compact antenna array receivers. Recent work has also derived

analytic techniques [16] to determine the optimum impedance value, simplifying the calculations required.

References

[1] R. G. Vaughan and J. B. Andersen, “Antenna diversity in mobile communications”, IEEE Trans Vehicular Technology, Vol 36, pp 149-172, Nov 1987.

[2] J. W. Wallace and M. A. Jensen, “Termination-dependent diversity performance of coupled antennas: Network theory analysis”, IEEE Trans Antennas and Propagation, Vol 52, pp 98-105, Jan 2004.

[3] T. Svantesson and A. Ranheim, ``Mutual coupling effects on the capacity of multielement antenna systems,'' in Proc IEEE Intl Conf on Acoustics Speech and Signal Processing (ICASSP), Vol 4, pp. 2485-2488, May 2001.

[4] B. K. Lau, J. B. Andersen. G. Kristensson and A. F. Molisch, “Antenna Matching for Capacity Maximization in Compact {MIMO} systems”, in Proceedings of 3rd International Symposium on Wireless Communications Systems (ISWCS), Sept 2006.

[5] V.Jungnickel, V.Pohl, and C.V. Helmolt, “Capacity of MIMO systems with closely spaced antennas,” IEEE Communication Letters, Vol. 7, No.8, pp. 361-363, Aug. 2003.

[6] B. K. Lau, S. M. S. Ow, G. Kristensson and A. F. Molisch, “Capacity analysis for compact {MIMO} systems”, in Proc IEEE Vehicular Technology Conf (VTC Spring), Vol 1, pp 165-170, May-June 2005.

[7] R. Janaswamy, “Effect of element mutual coupling on the capacity of fixed length linear arrays”, IEEE Antennas and Wireless Propagation Letters, Vol 1, pp 157-160, 2002.

[8] P. N. Fletcher, M. Dean and A. R. Nix, “Mutual coupling in multi-element array antennas and its influence on MIMO channel capacity”, IEE Electronics Letters, Vol 39, No 4, Feb 2003, pp 342-344.

[9] M. K. Özdemir, E. Arvas and H. Arslan, “Dynamics of spatial correlation and implications on MIMO systems”, IEEE Communications Magazine, pp S14-S19, June 2004.

[10] N. Chiurtu, B. Rimoldi, E. Telatar and V. Pauli, “Impact of correlation and coupling on the capacity of MIMO systems”, in Proc IEEE International Symposium on Signal Processing and Information Technology (ISSPIT'03)}, pp 154-157, Dec 2003.

[11] B. Clerckx, D. Vanhoenacker-Janvier, C. Oestges, and L. Vandendorpe, “Mutual coupling effects on the channel capacity and the space-time processing of MIMO communication systems,” in Proceedings of IEEE International Conference on Communications (ICC)}, Vol. 4, pp. 2638-2642, May 2003.

[12] M. L. Morris and Michael A. Jensen, “Improved network analysis of coupled antenna diversity performance”, IEEE Trans Wireless Communications, Vol 4, No 4, pp 1928-1934, July 2005.

[13] B.K. Lau, J. B. Andersen, G. Kristensson and A.F. Molisch, “Impact of Matching Network on Bandwidth of Compact Antenna Arrays”, IEEE Trans Antennas and Propagation, Vol. 54, No 11, pp 3225-3238, Nov 2006.

[14] B. K. Lau and J. B. Andersen, “On closely coupled dipoles with load matching in a random field”, in Proc IEEE Intl Symposium on Personal, Indoor and Mobile Radio Communications (PIMRC), Sept 2006.

[15] Y. Fei and J. S. Thompson, “MIMO system sensitivity and coupled array design”, in Proc IEEE Intl Symposium on Personal, Indoor and Mobile Radio Communications (PIMRC), Sept 2007

[16] Y. Fei, Y. Fan and J. S. Thompson, “Optimal single-port impedance matching for compact MIMO arrays”, In Proceedings of IEEE Global Communications Conference (GLOBECOM), Nov. 2007.

[17] Y. Fei and J. S. Thompson, “The capacity of matched compact linear antenna arrays,” Proceedings of 2nd European Conference of Antenna and Propagation (EUCAP), Nov 2007.

[18] A. Paulraj, R. Nabar and D. Gore, “Introduction to space-time wireless communications”, Cambridge University Press, 2003.

[19] P. J. Smith, S. Roy and M. Shafi, “Capacity of MIMO systems with semicorrelated flat fading”, IEEE Trans Information Theory, Vol 49, No 10, pp 2781-2788, Oct 2003.

[20] J.Salz and J.H. Winters, “Effect of fading correlation on adaptive arrays in digital mobile radio”, IEEE Trans. Vehicular Technology, Vol. 43, No. 4, pp. 1049-1057, Nov. 1994.

[21] J.D. Kraus, “Antennas”, 2nd edition, New York, McGraw-Hill, 1988.

[22] C.A. Balanis, “Antenna theory”, 2nd edition, USA, John Wiley & Sons, 1997.

[23] S. Loyka and G. Tsoulos, “Estimating MIMO system performance using the correlation matrix approach,” IEEE Communication Letters, Vol. 6, No. 1, pp. 19-21, Jan. 2002.

[24] S.J. Orfanidis, “Electromagnetic waves and antennas”, USA, 2004. Available online at the following web page: http://www.ece.rutgers.edu/\~orfanidi/ewa/

Optimal Single-Port Matching Impedance for Capacity Maximization in Compact MIMO Arrays

Yuanyuan Fei, Yijia Fan, Buon Kiong Lau, John S. Thompson

Abstract

A complete MIMO system model with compact arrays at both link ends containing arbitrary matching networks is presented based on a Z-parameter approach. The complete channel matrix including the coupling effect is also presented. Utilizing this system model, the optimum single-port matching impedance for capacity maximization is derived for a 2×2 MIMO system with coupling at the receivers only. A closed-form result for the optimum matching impedance in high signal-to-noise ratio scenarios is given and proved to be equal to the input impedance of the receive end. Simulation of ideal dipoles verifies our analytical results and demonstrates the superiority of the optimum matching to other matching conditions in improving MIMO system performance. Experimental data for monopoles is also presented to further confirm our numerical findings and validate the accuracy of our derivation.

I. Introduction

A. Background

The comprehensively studied multiple-input multiple-output (MIMO) systems promise significant gains in spectrum efficiency and link reliability by deploying multiple antennas at

Part of this work has been accepted for the IEEE Global Telecommunications Conference, Washington D.C., USA, November 2007.

Y. Fei and J. S. Thompson are with the Institute for Digital Communications, the University of Edinburgh, Edinburgh, EH9 3JL, UK (email: y.fei@ed.ac.uk, john.thompson@ed.ac.uk).

Y. Fan is with the Department of Electrical Engineering, Princeton University, Princeton, NJ, 08544, USA (e-mail: yijiafan@princeton.edu).

B. K. Lau is with the Department of Electrical and Information Technology, Lund University, SE-221 00 Lund, Sweden (e-mail: bklau@ieee.org).

both ends of a wireless link [1]–[3]. To achieve the maximum N times capacity benefit of MIMO systems over the traditional single-input single-output (SISO) system, it requires that an *N*-transmit antenna/*N*-receive antenna (or $N \times N$) MIMO system operates in an independent and identically-distributed (i.i.d.) channel [4]. Although in reality an i.i.d. channel is often not obtained due to certain reasons, e.g. high spatial fading correlation caused by a small number of dominant propagation paths, a large number of antennas at both link ends still guarantees significant improvement of the system performance over the SISO case even with correlated spatial fading. While adding antennas at the base station has already been carried out both theoretically and commercially, integration of multiple antennas into the subscriber end is affected by the limited design volume, which results in significant system performance degradation [2], [5], [6].

The study of compact arrays at the receive end has drawn significant attention. In narrowband MIMO systems, it is widely agreed that the mutual coupling (MC) effect, which is induced by insufficient antenna element separation, can reduce the signal correlation by distorting the radiation patterns of each element [7]–[9]. However, it will also induce a mismatch between the characteristic impedance of the circuit and the antenna input, which is detrimental to the capacity performance [10]. This conflicting outcome of the MC effect is one important factor which contributes to different conclusions of its impact on MIMO capacity performance [8], [11]–[19].

Two methods in *n*-port theory are usually adopted to study compact MIMO systems. One is S-parameter analysis which reflects the wave transmission in an *n*-port electrical network; the other is Z-parameter analysis which expresses the voltage and current relations among all ports. The S-parameter framework has been well examined in [9], [16], [17], and recently improved by introducing the effect of amplifier networks to the coupled receive end [20]–[22]. The authors of [16] introduce various matching networks to improve the system performance, while more varieties of antenna matching networks are examined in [23]. It is proved in [9], [16] that the so-called *multiport-conjugate match* can realize zero output correlation and lossless power transfer from the antennas to the loads for any antenna spacing, and can thus offer significant capacity improvement for very small antenna spacings. Nevertheless, when the investigation is extended to wideband compact MIMO systems, it turns out that the optimum multiport-conjugate match can only be achieved for a small bandwidth [24], which does not fulfill the requirement for

large bandwidths in future broadband wireless communication networks. Apart from that, the multiport-conjugate match is not easy to implement as it involves multiple circuit components interconnected across the antenna ports [25]. Instead, the *single-port match* [10], [23], [24], [26] is a practical, if suboptimal solution, as it provides capacity improvement compared to the non-matched case and has a broader bandwidth than the *multiport-conjugate match*.

B. Contributions of the paper

In this paper, we present an analytical solution for the optimal *single-port match* for capacity maximization. Specifically, the contributions of this paper are summarized as follows:

- We develop a complete framework for $N \times N$ MIMO systems including the MC effect at both link ends using Z-parameters from a novel power transfer point of view, which is suitable for any kind of single-mode antennas at the link ends. The framework analysis also embraces a transmit power constraint corresponding to the S-parameter approach [16]. Moreover, a modified channel matrix including the MC effect is presented. Then we simplify the model to consider the MC effect at the receivers only, and show that the channel model used in [10], [26] is a special case of the general MIMO channel matrix presented in this paper.
- We state the derivation of the optimum single-port match for capacity maximization of a 2×2 MIMO system with MC at the receivers only, using an upper bound of the MIMO ergodic capacity. We note that the deviation holds for all single-mode antennas. The closed-form result of the optimum single-port match for capacity maximization in high signal-to-noise ratio (SNR) scenarios is also given and proved to be the *input impedance* of the receive antennas.
- We illustrate the above derivation flow using ideal dipole antennas. A perfect match is shown between analytical and simulation results. Moreover, we present the advantage of using the optimum single-port match compared to other single-port match cases for MIMO system performance. To demonstrate the practical value of our analytical study, an *experimental* monopole array is designed for MIMO capacity evaluation, which further confirms our findings in previous contributions.

C. Relation between previous and current work

Besides MIMO capacity improvement, some advantages of using the *single-port match* have been described in [10], [26]–[28]. Received power maximization or zero output correlation can be achieved by selecting proper matching impedances [27] for very close antenna spacing ($d = 0.05\lambda$), which has been confirmed by the experimental implementation in [29]. While the optimum received power and zero output correlation are very sensitive to the load variation [27], the maximum capacity is quite stable as the load changes [26]. However, it is observed in [26] that the optimum single-port matching impedance to maximize the capacity is different to the solutions that either maximize the received power or achieve zero correlation. The capacity evaluation of compact MIMO systems with matching networks using Z-parameters has partially been carried out in [10]–[12], [26]. In [11] multiple antennas of a fixed length are studied without consideration of the matching networks. Although compact MIMO receivers with various matching impedances are examined in [10], [26], no complete Z-parameter framework analysis and analytical result for the optimal single-port match are given. The author in [12] did present a Z-parameter MIMO system but with an inappropriate channel matrix expression, which will be further discussed in Section II, and no matching network was included in the study.

The remainder of this paper is organized as follows. Section II presents the analysis framework of the MIMO system model we adopt based on the Z-parameter approach. Section III provides the numerical deviation of the optimum single-port matching impedance for a 2×2 MIMO system, and gives closed-form results in high SNR regime. Section IV applies the analytical results in Section III to ideal dipole antennas, and compares the numerical and simulation results. Also the superiority of the optimum single-port match for compact MIMO arrays to other matching conditions is discussed. Results for experimental monopole antennas are provided in Section V to further support our analytical studies. Conclusions are given in Section VI.

In this paper, the superscripts ^{T}, *, and ^{H} represent matrix transpose, complex conjugate, and conjugate transpose operators, respectively. $\mathbf{I}_N$ denotes the $N \times N$ identity matrix. The notations $Tr(\mathbf{A})$, $E\{\mathbf{A}\}$, det($\mathbf{A}$) and $(\mathbf{A})_{ij}$ denote the trace, expectation, determinant and the (i, j)-th element of the matrix $\mathbf{A}$, respectively. The notation $\mathrm{Re}\{\cdot\}$ is used to denote the real part of a complex number/matrix.

II. MIMO System Analysis Based on Z-Parameters

A narrowband MIMO system with N transmit and N receive antennas is considered in this paper. For simplicity it is assumed that the channel $\mathbf{H}$ is frequency-flat, rich scattering, and without a line-of-sight propagation component. Also we assume the transmitter and receiver arrays are linear, the array elements are of identical polarization, the dimension of the arrays is negligible compared to the link distance, and initially the array elements of both ends are separated by over half-a-wavelength. Under all the above assumptions, the $N \times N$ channel matrix $\mathbf{H} = \mathbf{H}_{i.i.d.}$ is composed of i.i.d. random variables. Now we can focus on the impact of mutual coupling (MC) of the compact transmitter and/or receiver arrays on the original MIMO system excluding other possible factors which would affect the performance.

To continue our analysis in Section III, it is prerequisite to obtain the modified MIMO channel matrix expression utilizing Z-parameters. According to the *n*-port theory, the channel transfer function between the transmit and the receive arrays in Fig. 1 can be represented as [12]

$$\begin{bmatrix} \mathbf{v}_T \\ \mathbf{v}_R \end{bmatrix} = \begin{bmatrix} \mathbf{Z}_{TT} & \mathbf{Z}_{TR} \\ \mathbf{Z}_{RT} & \mathbf{Z}_{RR} \end{bmatrix} \begin{bmatrix} \mathbf{i}_T \\ \mathbf{i}_R \end{bmatrix} \tag{1}$$

where $\mathbf{v}_T = [V_{T1}, V_{T2}, ..., V_{TN}]^T$, $\mathbf{i}_T = [I_{T1}, I_{T2}, ..., I_{TN}]^T$ are the voltage and current vectors at the transmit end, respectively. Similarly, $\mathbf{v}_R = [V_{R1}, V_{R2}, ..., V_{RN}]^T$, $\mathbf{i}_R = [I_{R1}, I_{R2}, ..., I_{RN}]^T$ denote the voltages and currents at the receive end. The diagonal sub-block matrices $\mathbf{Z}_{TT}$ and $\mathbf{Z}_{RR}$ are both antenna impedance matrices containing the self and mutual impedances with dimension $N \times N$ for the transmit end and receive end, respectively. The $N \times N$ matrix $\mathbf{Z}_{RT}$ can be translated as the trans-impedance matrix [16] due to the impact of transmit end currents on the receive end voltages. We define $\mathbf{Z}_{TR} = 0$ to indicate that the transmitters are blind to the conditions (or currents) at the receivers.

In the compact receive subsystem of Fig. 1, an $N \times N$ impedance matching network $\mathbf{Z}_L$ is added after the receive antennas to compensate for the MC induced power reduction. Utilizing circuit theory at the receive subsystem it is easy to obtain

$$\mathbf{v}_R = -\mathbf{Z}_L \mathbf{i}_R. \tag{2}$$

Substituting (2) into (1) we find the receive voltage $\mathbf{v}_R$ as a function of the transmit voltage $\mathbf{v}_T$

$$\mathbf{v}_R = \left(\mathbf{I}_N + \mathbf{Z}_{RR}\mathbf{Z}_L^{-1}\right)^{-1} \mathbf{Z}_{RT}\mathbf{Z}_{TT}^{-1}\mathbf{v}_T. \tag{3}$$

Now we look back to the transmit subsystem. Usually, the transmit antennas are assumed to be spaced sufficiently far apart to ignore the impact of MC, but even then mismatches between antennas and corresponding sources still exists. As future wireless communication may involve peer-to-peer transmission between compact MIMO terminals (eg. mobile cooperation [30]), MC will be an issue for both link ends. Thus, a suitable source impedance network $\mathbf{Z}_S$ is inserted between the sources and transmit antennas to ensure an efficient power transmission. Similar to the receive subsystem, the relation between the source voltage $\mathbf{v}_S$ and transmit voltage $\mathbf{v}_T$ is

$$\mathbf{v}_T = \mathbf{Z}_{TT} \left(\mathbf{Z}_{TT} + \mathbf{Z}_S\right)^{-1} \mathbf{v}_S \tag{4}$$

where $\mathbf{v}_S = [V_{S1}, V_{S2}, ..., V_{SN}]^T$. Substituting (4) into (3) results in

$$\mathbf{v}_R = \overbrace{\mathbf{Z}_L \underbrace{\left(\mathbf{Z}_L + \mathbf{Z}_{RR}\right)^{-1} \mathbf{Z}_{RT} \left(\mathbf{Z}_{TT} + \mathbf{Z}_S\right)^{-1}}_{-\mathbf{i}_R} \mathbf{v}_S}^{\mathbf{H}_V} \tag{5}$$

where $\mathbf{H}_V$ is the channel/voltage transfer matrix [12]. However, because only the voltage across the resistance can be exploited by the receiver, $\mathbf{H}_V$ has to be modified to fulfill the power transfer requirement. We define $\mathbf{Z}_{L+R} = \mathbf{Z}_L + \mathbf{Z}_{RR}$, $\mathbf{Z}_{T+S} = \mathbf{Z}_{TT} + \mathbf{Z}_S$ and substitute $\mathbf{i}_R$ as defined in (5), then the total average received power of the MIMO system can be represented as

$$\begin{aligned} P_R &= E\left\{Tr\left(\mathrm{Re}\left\{\mathbf{Z}_L \mathbf{i}_R \mathbf{i}_R^H\right\}\right)\right\} \\ &= E\left\{Tr\left(\mathrm{Re}\left\{\mathbf{Z}_L\right\} \mathbf{Z}_{L+R}^{-1} \mathbf{Z}_{RT} \mathbf{Z}_{T+S}^{-1} \mathbf{v}_S \mathbf{v}_S^H \mathbf{Z}_{T+S}^{-H} \mathbf{Z}_{RT}^H \mathbf{Z}_{L+R}^{-H}\right)\right\} \\ &= E\left\{Tr\left(\mathbf{R}_L^{1/2} \mathbf{Z}_{L+R}^{-1} \mathbf{Z}_{RT} \mathbf{Z}_{T+S}^{-1} \mathbf{v}_S \mathbf{v}_S^H \mathbf{Z}_{T+S}^{-H} \mathbf{Z}_{RT}^H \mathbf{Z}_{L+R}^{-H} \mathbf{R}_L^{1/2(H)}\right)\right\} \end{aligned} \tag{6}$$

where $\mathbf{R}_L = \mathrm{Re}\left\{\mathbf{Z}_L\right\}$.

At the transmit end, the total average transmitted power is

$$P_T = E\left\{Tr\left(\mathrm{Re}\left\{\mathbf{Z}_{TT} \mathbf{i}_T \mathbf{i}_T^H\right\}\right)\right\} = E\left\{Tr\left(\mathbf{R}_T^{1/2} \mathbf{Z}_{T+S}^{-1} \mathbf{v}_S \mathbf{v}_S^H \mathbf{Z}_{T+S}^{-H} \mathbf{R}_T^{1/2(H)}\right)\right\} \tag{7}$$

where $\mathbf{R}_T = \mathrm{Re}\left\{\mathbf{Z}_{TT}\right\}$. If only the receiver knows the channel conditions, P_T can be evenly distributed across the antennas at the transmit end. Then (6) becomes

$$P_R = E\left\{Tr\left(\mathbf{H}_{mc} \frac{P_T}{N} \mathbf{I}_N \mathbf{H}_{mc}^H\right)\right\} \tag{8}$$

where $\mathbf{H}_{mc}$ is the channel transfer matrix between the source and the receiver load including the MC effect as represented in Fig. 1. We assume identical antenna elements are used in the whole

system model, as a result all the matrices in (7) are symmetric. Equation (7) can be substituted into (8) to give

$$P_R = \frac{1}{N} E\left\{ Tr\left(\mathbf{H}_{mc} \mathbf{R}_T^{1/2} \mathbf{Z}_{T+S}^{-1} \mathbf{v}_S \mathbf{v}_S^H \mathbf{Z}_{T+S}^{-H} \mathbf{R}_T^{(1/2)(H)} \mathbf{H}_{mc}^H \right) \right\}. \tag{9}$$

Comparing (6) and (9) we have

$$\mathbf{H}_{mc} = \mathbf{R}_L^{1/2} \mathbf{Z}_{L+R}^{-1} \mathbf{Z}_{RT} \mathbf{R}_T^{-1/2}. \tag{10}$$

From the definition of $\mathbf{Z}_{RT}$ and the expression in [16], it is apparent that $\mathbf{Z}_{RT}$ modifies the Rayleigh channel matrix $\mathbf{H}_{i.i.d.}$ by introducing far-field (FF) pattern distortion at the coupled link end(s). Hence, the matrix product $\mathbf{Z}_{RT}\mathbf{Z}_{RT}^H$ defines the correlation at both link ends

$$E\left\{ \mathbf{Z}_{RT} \mathbf{Z}_{RT}^H \right\} = c \mathbf{\Psi}_R \mathbf{\Psi}_T \tag{11}$$

where c is the average power gain of each channel branch (assuming the power gain of each branch is the same), $\mathbf{\Psi}_T$ and $\mathbf{\Psi}_R$ are $N \times N$ transmit and receive covariance matrices, respectively [4] with $\left|(\mathbf{\Psi}_T)_{ij}\right|$, $\left|(\mathbf{\Psi}_R)_{ij}\right| \leq 1$ and $(\mathbf{\Psi}_T)_{ii}$, $(\mathbf{\Psi}_R)_{ii} = 1$, $i, j = 1, 2, ..., N$. We assume $c = 1$ in the following analysis, then the MIMO channel should be normalized to the average channel gain of both link ends for the single antenna case. Consider a SISO system with both antennas self-conjugated matched, i.e. $z_L = z_{11}^*$, where z_L and z_{11} is the load and self impedance of the antenna, respectively. Utilizing (6) and (9) we obtain

$$E\left\{ h h^* \right\} = \frac{1}{4 r_{11}^2} E\left\{ z_{RT} z_{RT}^* \right\} \tag{12}$$

where h and z_{RT} are SISO channel and trans-impedance, respectively, and $r_{11} = \mathrm{Re}\{z_{11}\}$. To summarize, we have the following theorem:

Theorem 1: The general MIMO system channel transfer matrix including the MC effect at both link ends represented in Z-parameters is

$$\hat{\mathbf{H}}_{mc} = 2 r_{11} \mathbf{R}_L^{1/2} \mathbf{Z}_{L+R}^{-1} \mathbf{\Psi}_R^{1/2} \mathbf{H}_{i.i.d.} \mathbf{\Psi}_T^{1/2} \mathbf{R}_T^{-1/2}. \tag{13}$$

For the meaning of all the notation please refer to the above analysis.

Proof: The proof follows from normalizing (11) by (12), equation (10) is modified to (13).

Another method is available to prove (13) from the electromagnetic transmission point of view, which is also the theoretical preliminary of Section V. We return to (5) and define

$$\mathbf{v}_{RT} = \mathbf{Z}_{RT} \mathbf{i}_T = \mathbf{Z}_{RT} (\mathbf{Z}_{TT} + \mathbf{Z}_S)^{-1} \mathbf{v}_S, \tag{14}$$

where the voltage vector $\mathbf{v}_{RT}$ is recognized as the received voltages induced by the transmitter currents without the MC effect at the receivers [12]. In other words, the elements of $\mathbf{v}_{RT}$ are the open-circuit voltages caused by the incident electromagnetic field when other receive antennas are open-circuited [9], [12]. Utilizing (5) and (14), (6) can be rewritten as

$$\begin{aligned} P_R &= E\left\{Tr\left(\mathrm{Re}\left\{\mathbf{Z}_L^{-1}\mathbf{v}_R\mathbf{v}_R^H\right\}\right)\right\} = E\left\{Tr\left(\mathbf{R}_L\mathbf{Z}_{L+R}^{-1}\mathbf{v}_{RT}\mathbf{v}_{RT}^H\mathbf{Z}_{L+R}^{-H}\right)\right\} \\ &= Tr\left(\mathbf{R}_L\mathbf{Z}_{L+R}^{-1}E\left\{\mathbf{v}_{RT}\mathbf{v}_{RT}^H\right\}\mathbf{Z}_{L+R}^{-H}\right). \end{aligned} \tag{15}$$

Normalizing the term $E\left\{\mathbf{v}_{RT}\mathbf{v}_{RT}^H\right\}$ to the SISO case described before, we have

$$\frac{E\left\{\mathbf{v}_{RT}\mathbf{v}_{RT}^H\right\}}{\frac{1}{4r_{11}^2}E\left\{V_{RT}V_{RT}^H\right\}} = 4r_{11}^2\boldsymbol{\Psi}_{\mathbf{oc}} \tag{16}$$

where V_{RT} is the open-circuit voltage of the SISO system and $\boldsymbol{\Psi}_{\mathbf{oc}}$ is the so-called open-circuit correlation [27]. If both transmitters and receivers are coupled, $\boldsymbol{\Psi}_{\mathbf{oc}} = \boldsymbol{\Psi}_{\mathbf{R}}\boldsymbol{\Psi}_{\mathbf{T}}$; if the MC effect is assumed at the receivers only, $\boldsymbol{\Psi}_{\mathbf{oc}} = \boldsymbol{\Psi}_{\mathbf{R}}$. Combining (7), (8), (15) and (16), we find

$$E\left\{\hat{\mathbf{H}}_{mc}\hat{\mathbf{H}}_{mc}^H\right\} = 4r_{11}^2\mathbf{R}_L\mathrm{Re}\left\{\mathbf{Z}_{TT}^{-1}\right\}\mathbf{Z}_{L+R}^{-1}\boldsymbol{\Psi}_{oc}\mathbf{Z}_{L+R}^{-H}, \tag{17}$$

which is exactly the expectation of the total power gain of channel matrix in (13). ■

It is obvious in (13) that the source impedance network $\mathbf{Z}_S$ has no impact on the modified MIMO channel, as it has already affected the transmitted power in (7). If the transmitters are coupled, a new power constraint has to be defined for the channel-known-at-transmitter case, i.e. the waterfilling algorithm [16].

The maximum power transfer from the receive antennas to the load networks happens when $\mathbf{Z}_L = \mathbf{Z}_{RR}{}^H$, which is easily achieved in theory but difficult to implement in practice as an additional $N(N-1)/2$ load impedances are needed to decouple the MC among N receive antennas [25], [31]. Therefore, single-port matching is usually adopted where $\mathbf{Z}_L$ becomes diagonal. In the following sections we will concentrate on the compact receive end of the MIMO system with single-port matching. Thus, we have the following corollary,

Corollary 1: For the MC effect at the receive end only, the channel transfer matrix is

$$\tilde{\mathbf{H}}_{mc} = 2\sqrt{r_{11}r_L}\mathbf{Z}_{L+R}^{-1}\boldsymbol{\Psi}_R^{1/2}\mathbf{H}_{i.i.d.} \tag{18}$$

where $r_L = \mathrm{Re}\{z_L\}$. For the meaning of other notations please refer to the above analysis.

Proof: We further assume that the transmit antennas are sufficiently separated with no MC, rich scattering, i.e. $\mathbf{\Psi}_T = \mathbf{I}_N$, and self-conjugate match is used. Also when the receive antennas are matched with identical load impedance z_L, then (13) can be simplified as (18). ■

Equation (18) is identical to the channel matrix used in [10], [26], which demonstrates that the assumed channel model in [10], [26] is actually a special case of our general MIMO channel matrix in (13). Under the equally distributed transmit power assumption, the narrowband MIMO capacity for the channel matrix given by (18) is denoted as

$$C_{mc} = \log_2 \det \left(\mathbf{I}_N + \frac{\rho_r}{N} \tilde{\mathbf{H}}_{mc} \tilde{\mathbf{H}}_{mc}^H \right) \tag{19}$$

where ρ_r is the reference SNR.

III. Derivation of Optimal Single-Port Matching Impedance

In this section, we derive the optimal single-port matching impedance $z_{opt} = r_{opt} + jx_{opt}$ which maximizes the mean capacity $E\{C_{mc}\}$ for a 2×2 (N = 2) MIMO system model described in Section II. We replace the notations $\mathbf{Z}_{RR}$ and $\mathbf{\Psi}_R$ by $\mathbf{Z}$ and $\mathbf{\Psi}$ for simplicity.

As (19) contains a random channel matrix, it is difficult to carry out further analysis. Using Jensen's inequality and the concavity of $\log_2 \det$ [32], for any fixed antenna spacing d, the upper bound C_{up} [33] of the MIMO capacity is

$$E\left\{C_{mc}\right\} \leq C_{up} = \log_2 \det \left(\mathbf{I}_N + \frac{4\rho_r r_{11} r_L}{N} \mathbf{Z}_{L+R}^{-H} \mathbf{Z}_{L+R}^{-1} \mathbf{\Psi} \right). \tag{20}$$

We define the antenna self-impedance $z_{11} = r_{11} + jx_{11}$, mutual-impedance $z_{12} = r_{12} + jx_{12}$, load impedance $z_L = r_L + jx_L$, where r_{11}, r_{12}, $r_L \in \mathbb{R}^+$ as they are resistance components and the reactance components x_{11}, x_{12}, $x_L \in \mathbb{R}$. For identical antenna elements, we have $(\mathbf{Z})_{ij} = (\mathbf{Z})_{ji}$ based on the reciprocity theorem[1] [34]. Given a particular antenna spacing d and SNR ρ_r, (20) becomes a function of variables (r_L, x_L). As the matrix product $\mathbf{Z}_{L+R}^{-H} \mathbf{Z}_{L+R}^{-1}$ in (20) contains the variable pair (r_L, x_L), it has to be simplified.

$$\begin{aligned} \mathbf{Z}_{L+R}^{-H} \mathbf{Z}_{L+R}^{-1} &= \left(\left[\mathbf{Z} + \mathbf{Z}_L \right] \left[\mathbf{Z} + \mathbf{Z}_L \right]^H \right)^{-1} = \left(\left[\mathbf{Z} + z_L \mathbf{I}_N \right] \left[\mathbf{Z}^H + z_L^* \mathbf{I}_N \right] \right)^{-1} \\ &= \Big(\underbrace{|z_L|^2 \mathbf{I}_N}_{\mathbf{Z}_1} + \underbrace{z_L \mathbf{Z}^H + z_L^* \mathbf{Z}}_{\mathbf{Z}_2} + \underbrace{\mathbf{Z}\mathbf{Z}^H}_{\mathbf{Z}_3} \Big)^{-1}. \end{aligned} \tag{21}$$

[1]We note that the reciprocity theorem is independent of the assumptions about the transmission environment. The FF pattern of the array does change in different scenarios, i.e. according to variations of the mean angle-of-arrival and angular spread, and this effect is fully reflected in the correlation matrix $\mathbf{\Psi}$.

Expanding (21) we have

$$\begin{aligned}
\mathbf{Z}_1 &= \begin{bmatrix} r_L^2 + x_L^2 & 0 \\ 0 & r_L^2 + x_L^2 \end{bmatrix} \\
\mathbf{Z}_2 &= 2\left(r_L \cdot \begin{bmatrix} r_{11} & r_{12} \\ r_{12} & r_{11} \end{bmatrix} + x_L \cdot \begin{bmatrix} x_{11} & x_{12} \\ x_{12} & x_{11} \end{bmatrix} \right) \\
\mathbf{Z}_3 &= \begin{bmatrix} r_{11}^2 + x_{11}^2 + r_{12}^2 + x_{12}^2 & 2(r_{11}r_{12} + x_{11}x_{12}) \\ 2(r_{11}r_{12} + x_{11}x_{12}) & r_{11}^2 + x_{11}^2 + r_{12}^2 + x_{12}^2 \end{bmatrix}
\end{aligned} \tag{22}$$

Lemma 1: For any real symmetric Toeplitz matrix $\mathbf{A} = \begin{bmatrix} a_1 & a_2 \\ a_2 & a_1 \end{bmatrix}$, the singular value decomposition (SVD) of $\mathbf{A}$ can be written as $\mathbf{A} = \mathbf{U}\mathbf{D}\mathbf{U}^{\mathbf{T}} = \mathbf{U}\mathbf{D}\mathbf{U}$, where

$$\mathbf{U} = \frac{1}{\sqrt{2}} \begin{bmatrix} 1 & 1 \\ 1 & -1 \end{bmatrix}, \mathbf{D} = \begin{bmatrix} a_1 + a_2 & 0 \\ 0 & a_1 - a_2 \end{bmatrix}.$$

Proof: $\mathbf{A}$ is a 2×2 circulant matrix. Following [35], the eigenvalue solution of $\mathbf{A}$ is $\lambda_k = a_1 + a_2 r_k$, $k = 1, 2$, and r_k is the kth complex root of $r^2 = 1$. The corresponding eigenvector $u_k = 2^{-1/2}[1, r_k]^T$. Then $\mathbf{U}$ = $[u1, u2]$, and $\mathbf{U}$ is unitary. ■

Utilizing Lemma 1, the singular value decomposition (SVD) of (21) is given

$$\begin{aligned}
\mathbf{Z}_{L+R}^{-H}\mathbf{Z}_{L+R}^{-1} =& \left(\mathbf{U} \left(\begin{bmatrix} r_L^2 + x_L^2 & 0 \\ 0 & r_L^2 + x_L^2 \end{bmatrix} + 2r_L \cdot \begin{bmatrix} \mathfrak{R}_1 & 0 \\ 0 & \mathfrak{R}_2 \end{bmatrix} \right.\right. \\
& \left.\left. + 2x_L \cdot \begin{bmatrix} \mathfrak{X}_1 & 0 \\ 0 & \mathfrak{X}_2 \end{bmatrix} + \begin{bmatrix} \mathfrak{R}_1^2 + \mathfrak{X}_1^2 & 0 \\ 0 & \mathfrak{R}_2^2 + \mathfrak{X}_2^2 \end{bmatrix} \right) \mathbf{U} \right)^{-1} \\
=& \mathbf{U} \begin{bmatrix} (r_L + \mathfrak{R}_1)^2 + (x_L + \mathfrak{X}_1)^2 & 0 \\ 0 & (r_L + \mathfrak{R}_2)^2 + (x_L + \mathfrak{X}_2)^2 \end{bmatrix}^{-1} \mathbf{U} = \mathbf{U}\mathbf{\Lambda}^{-1}\mathbf{U}
\end{aligned} \tag{23}$$

where $\mathfrak{R}_1 = r_{11} + r_{12}$, $\mathfrak{X}_1 = x_{11} + x_{12}$, $\mathfrak{R}_2 = r_{11} - r_{12}$, $\mathfrak{X}_2 = x_{11} - x_{12}$. Using the property $\det(\mathbf{I} + \mathbf{AB}) = \det(\mathbf{I} + \mathbf{BA})$ [3], (20) can be rewritten as

$$C_{up} = \log_2 \det(\mathbf{I}_N + \kappa r_L \cdot \mathbf{U}\mathbf{\Lambda}^{-1}\mathbf{U}\mathbf{\Psi}) = \log_2 \det(\mathbf{I}_N + \kappa \mathbf{U}\mathbf{\Psi}\mathbf{U} r_L \mathbf{\Lambda}^{-1}) = \log_2 \det(\mathbf{Y}) \tag{24}$$

where $\kappa = \rho_r \cdot 4r_{11}/N$. According to the monotonically increasing characteristic of $\log(\cdot)$, the maximum point of $\det(\cdot)$ is the maximum point of $\log_2\det(\cdot)$. To derive the maximum point

(r_{opt}, x_{opt}) of $\det(\mathbf{Y})$, we evaluate the following derivatives

$$\frac{\partial \det(\mathbf{Y})}{\partial r_L} = \kappa \cdot \frac{(\mathfrak{R}_1^2 - r_L^2 + (x_L + \mathfrak{X}_1)^2) \cdot \Sigma_2 + (\mathfrak{R}_2^2 - r_L^2 + (x_L + \mathfrak{X}_2)^2) \cdot \Sigma_1}{\left(\left((r_L + \mathfrak{R}_1)^2 + (x_L + \mathfrak{X}_1)^2\right)\left((r_L + \mathfrak{R}_2)^2 + (x_L + \mathfrak{X}_2)^2\right)\right)^2} \tag{25a}$$

$$\frac{\partial \det(\mathbf{Y})}{\partial x_L} = -2\kappa r_L \cdot \frac{(x_L + \mathfrak{X}_1) \cdot \Sigma_2 + (x_L + \mathfrak{X}_2) \cdot \Sigma_1}{\left(\left((r_L + \mathfrak{R}_1)^2 + (x_L + \mathfrak{X}_1)^2\right)\left((r_L + \mathfrak{R}_2)^2 + (x_L + \mathfrak{X}_2)^2\right)\right)^2} \tag{25b}$$

where

$$\begin{aligned}
\Sigma_1 &= \big((r_L + \mathfrak{R}_1)^2 + (x_L + \mathfrak{X}_1)^2\big) \cdot \big((1 - \mathrm{Re}\{\alpha\})\big((r_L + \mathfrak{R}_1)^2 + (x_L + \mathfrak{X}_1)^2\big) + (1 - |\alpha|^2)\kappa r_L\big), \\
\Sigma_2 &= \big((r_L + \mathfrak{R}_2)^2 + (x_L + \mathfrak{X}_2)^2\big) \cdot \big((1 + \mathrm{Re}\{\alpha\})\big((r_L + \mathfrak{R}_2)^2 + (x_L + \mathfrak{X}_2)^2\big) + (1 - |\alpha|^2)\kappa r_L\big),
\end{aligned} \tag{26}$$

and $\alpha = (\mathbf{\Psi})_{12} = (\mathbf{\Psi})_{21}$ is the correlation coefficient between the two receivers. In (26) it can be shown that $\forall \Sigma_{1,2} > 0$. As the maximum point (r_{opt}, x_{opt}) makes (25) equal to zero, then from (25b) we can deduce

$$x_{opt} \in [\min(-\mathfrak{X}_1, -\mathfrak{X}_2), \max(-\mathfrak{X}_1, -\mathfrak{X}_2)]. \tag{27}$$

Substituting (27) into (25a) we have

$$r_{opt} \in [\min(\mathfrak{R}_1, \mathfrak{R}_2), \max(\sqrt{\mathfrak{R}_1^2 + (\mathfrak{X}_1 - \mathfrak{X}_2)^2}, \sqrt{\mathfrak{R}_2^2 + (\mathfrak{X}_1 - \mathfrak{X}_2)^2})]. \tag{28}$$

Solving (25a) and (25b) the simple relation between r_L and x_L can be obtained

$$r_L^2 + (x_L + \sigma)^2 = \Gamma. \tag{29}$$

Geometrically, (r_{opt}, x_{opt}) is a point on the circumference of a circle with the center at $(0, -\sigma)$ and radius $\sqrt{\Gamma}$, where $\sigma = x_{11} + \frac{r_{11}r_{12}}{x_{12}}, \Gamma = r_{11}^2 + r_{12}^2 + x_{12}^2 + \frac{r_{11}^2 r_{12}^2}{x_{12}^2}$. Combined with (27) and (28), (r_{opt}, x_{opt}) can be restricted to be located in an arc of the circle.

Substituting (29) into (25b), we can deduce a polynomial in x_L

$$\sum_{m=0}^{8} p_m x_L^m = \sum_{m=0}^{8} f_m(\mathfrak{R}_1, \mathfrak{X}_1, \mathfrak{R}_2, \mathfrak{X}_2, \sigma, \Gamma, \kappa) x_L^m = \sum_{m=0}^{8} g_m(r_{11}, x_{11}, r_{12}, x_{12}, \rho_r) x_L^m = 0 \tag{30}$$

where the coefficients p_m are determined by the high order polynomials $f_m(\mathfrak{R}_1, \mathfrak{X}_1, \mathfrak{R}_2, \mathfrak{X}_2, \sigma, \Gamma, \kappa)$ = $g_m(r_{11}, x_{11}, r_{12}, x_{12}, \rho_r)$. To summarize the calculation of z_{opt}, we present the following theorem,

Theorem 2: With fixed antenna spacing d and SNR ρ_r, the numerical result for the optimum single-port impedance z_{opt} for capacity maximization of a 2×2 MIMO system with compact receivers can be found as:

Step 1. Solving (30) to find all the roots of x_L;

Step 2. Filtering the results of **Step 1** by (27);

Step 3. Substituting the results of **Step 2** into (29) to get the corresponding roots of r_L;

Step 4. Filtering the results of **Step 3** by (28).

Proof: Please see the previous analysis in Section III. ■

In high SNR regime, we have the following corollary,

Corollary 2: The closed-form solution of the optimum single-port matching z_{opt} for capacity maximization of a 2×2 MIMO system with compact receivers is the input impedance of the receiver.

Proof: With high SNR, (24) can be simplified as

$$C_{up} = \log_2 \det(\kappa \mathbf{U}\mathbf{\Psi}\mathbf{U} r_L \mathbf{\Lambda^{-1}}) = \log_2 \det(\mathbf{Y}) \tag{31}$$

where $\det(\mathbf{Y}) = \frac{(\mathbf{1}-\alpha^{\mathbf{2}})}{\det(\mathbf{\Lambda})}$. The derivatives in (25) are modified by simplifying (26) as

$$\Sigma_i = (r_L + \mathfrak{R}_i)^2 + (x_L + \mathfrak{X}_i)^2, \qquad i = 1, 2. \tag{32}$$

Solving the equations we derive the closed-form of $z_{opt} = r_{opt} + j x_{opt}$, where

$$r_{opt} = \sqrt{\mathfrak{R}_1\mathfrak{R}_2\left(1 + \frac{(\mathfrak{X}_1 - \mathfrak{X}_2)^2}{(\mathfrak{R}_1 + \mathfrak{R}_2)^2}\right)} = \sqrt{r_{11}^2 - r_{12}^2 + x_{12}^2 - \frac{r_{12}^2 x_{12}^2}{r_{11}^2}} \tag{33a}$$

$$x_{opt} = -\frac{\mathfrak{R}_1\mathfrak{X}_2 + \mathfrak{R}_2\mathfrak{X}_1}{\mathfrak{R}_1 + \mathfrak{R}_2} = \frac{r_{12}x_{12}}{r_{11}} - x_{11} \tag{33b}$$

This solution of z_{opt} is exactly the input impedance (z_{in}) match in [24]. ■

The significance of this result is that for a high SNR scenario, z_{opt} is an exact solution which is only related to the array impedances and independent from the open-circuit correlation α, as well as any other channel correlation, which provides the possibility of practical implementation. It is not surprising to find out that z_{in} is the z_{opt} in high SNR case. This is because from circuit theory considerations it includes the MC effect into the matching network [36], which realizes the maximum power transfer between the corresponding source and receiver. Furthermore, it

gives low correlation for any antenna separation [24]. Although it is not the optimum single-port matching impedance for received power maximization, it the best candidate for capacity maximization.

IV. Simulation and Analysis

A MIMO system using $N = 2$ antennas with ideal half-wavelength ($\lambda/2$) dipoles [2] equipped at both ends is deployed in this work to demonstrate our analytical results in Section III. In the following paragraphs, we use the ideal $\lambda/2$ dipole case to evaluate numerically the analysis in Section III. Second, the optimal single-port impedances z_{opt} generated by Monte Carlo simulations of the same MIMO system model for both ergodic capacity C_m and upper bound of capacity C_{up} are compared to the numerical results. Last but most importantly, the superiority of z_{opt} compared to other matching networks to MIMO system performance will be discussed.

The self and mutual impedances of the ideal $\lambda/2$ dipoles are calculated numerically using the modified EMF method [3] [5] in Fig. 2. Choosing a specific reference SNR ρ_r and substituting the computed impedances data z_{11}, z_{12} into pre-calculated analytical polynomials g_m in (30), we can get multiple solutions of x_L for a given antenna spacing d. Then the selected values of x_L(s) are filtered by the range (27) which is also displayed in Fig. 3(a). Next the corresponding r_L(s) can be computed by (29). Fig. 4 depicts the arc of possible locations for (r_{opt}, x_{opt}) following from (29) of antenna spacing $d = 0.05\lambda$. The abscissa of Fig. 4 is determined by r_{Lmin} = min($\Re_2$) and r_{Lmax} = max($\sqrt{\Re_1^2 + (\mathfrak{X}_1 - \mathfrak{X}_2)^2}$) according to Fig. 3(b). In Fig. 4 it is obvious that x_{Lmax} = $-\mathfrak{X}_2$ = $-17.9\ \Omega$ and thus x_L(s) can not reach zero as shown in Fig. 3(a). Then the lower bound of x_L in Fig. 4 is accordingly modified to x_{Lmin} = $\min(-\mathfrak{X}_1)|_{-\mathfrak{X}_2 \leq -17.9}$ from Fig. 3(a). Then using (28) corresponding to Fig. 3(b), the correct solution pair (r_{opt}, x_{opt}) can be obtained. When

[2]Ideal half-wavelength dipoles are adopted because their self and mutual impedances are easily computed numerically, as well as being a reference case in the antenna field. The impedance matrices of other kinds of antennas obtained either analytically or experimentally can be applied in the system model in Section II as well. Hence, the analysis in Section II is general.

[3]Infinite thin dipoles are assumed for the EMF calculations . Usually the dipole diameter is far less than its length, thus EMF is still practicable. Similar self and mutual impedance results can be found for ideal dipoles in [5] and for practical dipole cases in [16], [37]. As our focus is on the relative ratio of the self and mutual impedances and not the absolute values, ideal dipoles are selected for simplicity.

d is fixed, the unique solution is a point on the arc, and the position of the point (r_{opt}, x_{opt}) on the arc depends on ρ_r.

To verify the accuracy of our numerical results (r_{opt}, x_{opt}), Monte Carlo simulations for the ergodic capacity and results for the upper bound in (20) are used. The transmit antennas are sufficiently spaced to avoid MC while the receive array is compact and consists of identical elements to the transmitters. As mentioned in Section II, a rich-scattering channel model with full angular spread is assumed, also the power azimuth spectrum (PAS) is uniform distributed around the receiver. Then $\alpha = J_0(2\pi d/\lambda)$ [38], where $J_0(\cdot)$ and d are the zeroth order Bessel function of the first kind and the antenna spacing, respectively. We concentrate on the system performance with $d < 0.5\lambda$ when the MC effect becomes severe. As the numerical z_{opt} is the maximum point of the upper bound C_{up} rather than the ergodic capacity C_m, the corresponding maximum points obtained by simulation for both cases are plotted in Fig. 5. The range of impedance points $\{z_L = r_L + jx_L : r_L \in [0, 150]\Omega, x_L \in [-100, 50]\Omega\}$ is chosen to get the maximum point of each C_{up}. The ergodic capacity C_m is simulated over 10000 random channel realizations for each impedance point at each selected antenna spacing d, thereby the range of z_L has to be shrunk to a few ohms around the maximum point of C_{up} in the same case to save computing time. In Fig. 5 it is apparent that the numerically derived z_{opt} agrees well with the corresponding results generated from simulations of C_{up}, and it matches the impedance where C_m reaches the maximum value as well. It is also clear that z_{opt} approaches the input impedance match z_{in} when the SNR increases, which is perfectly in accordance with our derivation in Section III. Another observation is that the reactance of z_{opt} is hardly affected by the value of SNR and the impact of SNR on the resistive part of z_{opt} diminishes when $d > 0.2\lambda$.

In the high SNR regime, r_{11}, x_{11} are constant in Fig. 2, then (33b) is dominated by $r_{12}x_{12}$. As r_{12} is monotonically decreasing and x_{12} is convex over $d \in [0.05, 0.5]\lambda$ in Fig. 2, the convexity of x_{opt} can be well explained in Fig. 5. (33a) can be further written as

$$r_{opt} = \frac{\sqrt{r_{11}^4 - r_{11}^2 r_{12}^2 + r_{11}^2 x_{12}^2 - r_{12}^2 x_{12}^2}}{r_{11}}.$$

Fig. 2 shows that $-r_{12}^2$ is monotonically increasing over $d \in [0.05, 0.4]\lambda$, and x_{12}^2 is monotonically increasing over $d \in [0.1, 0.5]\lambda$. Thus r_{opt} should be monotonically increasing over $d \in [0.1, 0.4]\lambda$, which agrees well with the r_{opt} curve in Fig. 5.

Because the numerical values of z_{opt} match very well to the simulation results of z_{opt} for both

C_{up} and C_m cases, we present the precise data of z_{opt} in Table I. For the resistive component r_{opt}, the numerical and both simulation results differ from each other for $d \leq 0.2\lambda$ with a maximum error of less than 1Ω. The errors decrease while ρ_r increases. When $d \geq 0.3\lambda$, the numerical and simulation r_{opt} of C_{up} are equal to each other with no error and the numerical resistance experiences an maximum error of 0.4Ω compared to the simulation r_{opt} of C_m for any value of ρ_r. For the reactive component x_{opt}, the numerical x_{opt} is equal to the simulation x_{opt} of C_{up} with no error for all values of ρ_r. The x_{opt} of C_m has an maximum error of 0.4Ω compared to the other two cases due to the limited number of realizations used for the Monte Carlo simulation. Both Fig. 5 and Table I confirm that our analytical study in Section III can yield z_{opt} corresponding to the maximum C_{up} accurately, and can further predict z_{opt} of the maximum C_m correctly and more efficiently than the Monte Carlo method. Values of the input impedance z_{in} of various d are also presented in Table I, and they agree well with the corresponding values of z_{opt} at $\rho = 20$dB. This again confirms our analytical finding for the high SNR regime in Section III.

Introducing various matching networks into compact MIMO terminals will improve the system performance. To illustrate how much we can benefit from the z_{opt} match, the mean capacity C_m and capacity upper bound C_{up} computed for antennas with the characteristic-impedance match for both no coupling (z_{0nc}) and MC (z_0) cases, self-conjugate match ($z_{11}{}^*$), input impedance match (z_{in}) and maximum capacity (z_{opt}) matching are depicted with different values of ρ_r in Fig. 6. Both C_{up} and C_m results are plotted to show the validity of using the capacity upper bound C_{up} to predict matching values for C_m. As illustrated in Fig. 6, using a matching network to optimize C_{up} also optimizes the value of C_m. When $\rho_r = 5$dB (Fig. 6(a)), the performance of the receivers without MC is always better than with MC. However, for $\rho_r = 20$dB case (Fig. 6(b)), the coupled compact array with any kind of matching networks outperforms that without MC at small spacing ($d < 0.2\lambda$). Meanwhile, the z_{opt} match surpasses other matching schemes when $d < 0.25\lambda$ and overlaps with the z_{11}^* match and z_{in} match as $d \geq 0.25\lambda$ in both low and high SNR scenarios. Moreover, in Fig. 6(a) the performance of the z_{opt} match deviates from that of the z_{in} match with better capacity results only at extremely close antenna spacings for $d < 0.1\lambda$. With increasing SNR, the performance of z_{opt} and z_{in} overlap with each other for all antenna spacings in Fig. 6(b), which again verifies our analysis. The relation between the trend of C_{up} and x_{opt} for the high SNR case cannot be clearly explained apparently from the analytical results. However, it is obvious that r_{opt} is the dominant factor that determines the

value of C_{up} as in Fig. 6 as C_{up} follows the monotonically increasing property of r_{opt} in Fig. 5 with all spacings. It can be understood physically that it is because r_{opt} is the load receiving the power which contains the mutual information.

V. Experimental Validation

As our analytical deviation in Section III is confirmed by the simulation analysis in Section IV, we further present measured antenna impedances and open-circuit correlation results to validate the generality of our numerical results.

The experimental setup of a compact receive array is shown in Fig. 7. Two quarter-wavelength monopoles with antenna spacings of $d = 0.05\lambda, 0.1\lambda, 0.15\lambda$ and a center frequency of 900MHz are mounted on a 330mm $\times$ 250mm ground plane. Both brass antennas of identical dimensions (diameter of 2mm) are directly soldered onto 50Ω matching network boards with the output ports of SMA connectors soldered onto the opposite end of the boards.

The self impedance of a single monopole and the self and mutual-impedances of the experimental monopole array are measured by a network analyzer. To calculate the open-circuit correlation addressed in Section II, the two-dimensional (2D) FF patterns of the monopole array for open-circuit terminations are obtained from an anechoic chamber at Perlos AB, Sweden[4]. An identical receive system model is simulated in SEMCAD [39] using full-wave finite-difference time-domain (FDTD) analysis. The simulation of the impedance matrix and coupled radiation patterns are compared with the measurement results.

There are no known analytical equations for the self and mutual impedances of monopoles on a finite ground plane. Hence, Fig. 8 displays the self and mutual impedances of the two-element monopole array from both simulation and measurement. The simulation results are derived from the open and short-circuit impedances [6] and identical elements are assumed. The experimental impedance results are transferred from the S-parameter data observed at the network analyzer. As in practice the monopoles cannot be exactly identical, the average values of the measured self and mutual impedances are shown in Fig. 8 as well. The close match of the measurement results of both monopoles ensures the validity of further experiment. Meanwhile, the simulation results

[4]Although the channel in the chamber is line-of-sight, the FF patterns are measured over 2π radians. This is consistent with a MIMO non-line-of-sight channel with uniformly distributed PAS and full angular spread. Thus the measured correlation can be used for the MIMO capacity evaluation.

and the average of the measurement results also shows great consistency. It is clear in Fig. 8 when the antenna spacing increases, the difference between the simulation and the average of the measurement results decreases. In the following measurement, we focus on the antenna spacing of $d = 0.05\lambda$, where the self and mutual impedances of the monopoles are $z_{11} = 47.5 + j10.9\Omega$, $z_{12} = 46.77 - j0.57\Omega$ in simulation, and $z_{11} = 46.72 + j9.39\Omega$, $z_{12} = 45.31 - j2.57\Omega$ on average in measurement. The corresponding open-circuit correlations of $d = 0.05\lambda$ are 0.9796 in SEMCAD and 0.959 in measurement calculated from the FF patterns.

Table II lists the ergodic capacity C_m calculated using antenna parameters generated from simulation and measurement of different impedances. The impedances z_A and z_B are selected from the area of optimum impedances for received power maximization, while z_C and z_D are picked from the approximately zero correlation circle [29]. The characteristic impedance is denoted by z_0. For the self-conjugate matching impedances z_{11}^*, the input matching impedances z_{in} and the optimum single-port matching impedances for capacity maximization z_{opt}, there are two sets of impedances shown based on the corresponding monopole impedances and open-circuit correlations obtained in simulation and measurement, respectively. The row of z_{opt}^n in Table II represents the numerical z_{opt} results using the method in Section III. We note that the same number of channel realizations and 20dB reference SNR ρ_r are used in generating C_m. Also the self impedances (the conjugate of z_{11}^* listed in Table II) are used for power normalization of the corresponding cases. It is obvious that z_{11} for a single monopole differs from that in the array, because in traditional simulations an approximate method is used to simulate the MC effect, where the same value z_{11} is assumed for both single antenna and antenna in array cases. However, z_{11} for isolated antennas does change when it is put in the array [16], [37].

Generally, the ergodic capacity using the antenna parameters in measurement are about 0.5 bits/s/Hz higher than the corresponding results computed from the simulation of each load point. However, the even gap reveals the consistency of both capacity results. Apparently, none of the impedances either maximizing the received power or achieving zero output correlation maximize the capacity, which confirms the finding in [10], [26]. Among these impedances, z_D offers the best performance as it is chosen to be the load with the highest received power along the zero correlation circle, and also because it is close to z_{opt}. The commonly used matching impedances z_0 and z_{11}^* also give inferior performance compared to the corresponding z_{in} match with an average capacity advantage of 0.5 bits/s/Hz. Again the numerical results of z_{opt} agree well with

the corresponding z_{opt} of the simulation, which shows the generality of our analytical study in Section III. The error between the corresponding numerical and simulation results of z_{opt} is within 1Ω, which is caused by the deviation between z_{11} for the single antenna and z_{11} used in the array. When a high SNR (ρ_r = 20dB) is assumed, both numerical and simulation results of z_{opt} show a great consistency to the corresponding z_{in}, especially for the measurement case. As shown in Table I, the errors between the numerical and simulation results of z_{opt} as well as z_{in} decrease when the antenna spacing increases, so we are confident of the validity of our derivation with larger antenna separations with this experimental setup of a monopole array.

VI. Conclusion

This paper has studied a complete MIMO system network model with compact arrays at both link ends containing arbitrary matching networks based on the Z-parameter approach. This model was used to derive the optimal single-port matching impedance (z_{opt}) for capacity maximization of a 2×2 MIMO system with coupled antenna elements at the receive end only. A general channel matrix including the MC effect expressed in Z-parameter form is also provided for future studies. Although the general closed-form solution of z_{opt} cannot be presented in this paper, an algorithm to obtain the exact solution is presented. Also, a precise closed-form of z_{opt} for the high SNR scenario is deduced and confirmed to be the input matching impedance of the receive end. The simulation of ideal dipoles are used to validate our analytical results, where we have shown that the analysis and simulation follow a great degree of consistency. By introducing z_{opt} into a compact MIMO receive subsystem, the ergodic capacity has an advantage of around 1 bit/s/Hz for antenna spacings less than 0.25λ compared to the the subsystem with characteristic match when the SNR is 20dB. An experimental setup of a monopole array is also described and the experiments verify the generality of our derivation. We demonstrate that a capacity benefit of 0.5 bits/s/Hz can be achieved over the commonly used self-conjugate match for an antenna element spacing 0.05λ at 20dB SNR.

We conclude that the MIMO system performance can be significantly improved by integrating z_{opt} into compact arrays. However, this advantage decreases with increasing antenna spacing. The z_{opt} we derived here is limited to the 2×2 MIMO system. Hence, more research has to be done for compact arrays with different sizes and configurations to explore the MC effect and the generality of z_{opt}. The general expression of the MIMO channel matrix in Z-parameters we

present in this paper offers a systematic framework for solving these problems. A measurement campaign involving direct MIMO channel measurements (including the effect of the matching network) and measured capacity evaluation is also an interesting aspect for future work.

ACKNOWLEDGMENT

The authors would like to thank Prof. Andreas Molisch of the Department of Electrical and Information Technology, Lund University for reviewing the paper and giving valuable feedback. Many thanks to Mr. Jie Ding of the Institute for Digital Communications, the University of Edinburgh for useful discussions. Also we thank Dr. Anders Sunesson of Perlos AB, Lund, Sweden for providing the facility and expertise to measure the antenna FF patterns, and Mr. Lars Hedenstjärna of the Department of Electrical and Information Technology, Lund University for technical advice and construction of the experimental hardware.

This work is supported by Scottish Funding Council for the Joint Research Institute with the Heriot-Watt University (a part of the Edinburgh Research Partnership), VINNOVA (grant no. 2007-01377), and partly conducted within the NEWCOM (Network of Excellence in Communications).

REFERENCES

[1] J. Winters, "On the capacity of radio communication systems with diversity in a rayleigh fading environment," *IEEE J. Select. Areas Commun.*, vol. 5, pp. 871–878, 1987.

[2] G. J. Foschini and M. J. Gans, "On limits of wireless communications in a fading environment when using multiple antennas," *Wireless Personal Communications*, vol. 6, pp. 311–335, Mar. 1998.

[3] I. E. Telatar, "Capacity of multi-antenna gaussian channels," *European Trans. Telecommun.*, vol. 10, pp. 585–595, 1999.

[4] A. Paulraj, R. Nabar, and D. Gore, *Introduction to space-time wireless communications*, 1st ed. Cambridge, UK: Cambridge University Press, 2003.

[5] C. A. Balanis, *Antenna theory*, 2nd ed., S. Elliot, Ed. USA: John Wiley & Sons, Inc, 1997.

[6] W. L. Stutzman and G. A. Thiele, *Antenna theory and design*, 2nd ed. New York, USA: John Wiley & Sons, Inc., 1998.

[7] R. G. Vaughan and J. B. Andersen, "Antenna diversity in mobile communications," *IEEE Trans. Veh. Technol.*, vol. VT-36, no. 4, pp. 149–172, Nov. 1987.

[8] T. Svantesson and A. Ranheim, "Mutual coupling effects on the capacity of multielement antenna systems," in *Proceedings of IEEE International Conference on Acoustics, Speech and Signal Processing (ICASSP'01)*, vol. 4, May 2001, pp. 2485–2488.

[9] J. W. Wallace and M. A. Jensen, "Termination-dependent diversity performance of coupled antennas: Network theory analysis," *IEEE Trans. Antennas Propagat.*, vol. 52, no. 1, pp. 98–105, January 2004.

[10] B. K. Lau, J. B. Andersen, G. Kristensson, and A. F. Molisch, "Antenna matching for capacity maximization in compact MIMO systems," in *Proceedings of 3rd International Symposium on Wireless Communications Systems (ISWCS)*, Valencia, Spain, Sept. 2006, (invited).

[11] R. Janaswamy, "Effect of element mutual coupling on the capacity of fixed length linear arrays," *IEEE Antennas Wireless Propagat. Lett.*, vol. 1, pp. 157–160, 2002.

[12] N. Chiurtu, B. Rimoldi, E. Telatar, and V. Pauli, "Impact of correlation and coupling on the capacity of MIMO systems," in *Proceedings of 3rd IEEE International Symposium on Signal Processing and Information Technology (ISSPIT'03)*, Dec. 2003, pp. 154–157.

[13] B. Clerckx, D. Vanhoenacker-Janvier, C. Oestges, and L. Vandendorpe, "Mutual coupling effects on the channel capacity and the space-time processing of MIMO communication systems," in *Proceedings of IEEE International Conference on Communications (ICC'03)*, vol. 4, May 2003, pp. 2638–2642.

[14] V. Jungnickel, V. Pohl, and C. V. Helmolt, "Capacity of MIMO systems with closely spaced antennas," *IEEE Commun. Lett.*, vol. 7, no. 8, pp. 361–363, August 2003.

[15] P. N. Fletcher, M. Dean, and A. R. Nix, "Mutual coupling in multi-element array antennas and its influence on MIMO channel capacity," *IEE Electronics Letters*, vol. 39, no. 4, pp. 342–344, February 2003.

[16] J. W. Wallace and M. A. Jensen, "Mutual coupling in MIMO wireless systems: a rigorous network theory analysis," *IEEE Trans. Wireless Commun.*, vol. 3, no. 4, pp. 1317–1325, July 2004.

[17] C. Waldschmidt, S. Schulteis, and W. Wiesbeck, "Complete RF system model for analysis of compact MIMO arrays," *IEEE Trans. Veh. Technol.*, vol. 53, no. 3, pp. 579–586, May 2004.

[18] E. A. Mehmet Kemal Özdemir and H. Arslan, "Dynamics of spatail correlation and implications on MIMO systems," *IEEE Commun. Mag.*, pp. 514–519, 2004.

[19] S. Wei, D. Goeckel, and R. Janaswamy, "On the asymptotic capacity of MIMO systems with antenna arrays of fixed length," *IEEE Trans. Wireless Commun.*, vol. 4, no. 4, pp. 1608–1621, 2005.

[20] M. L. Morris and M. A. Jensen, "Improved network analysis of coupled antenna dieversity performance," *IEEE Trans. Wireless Commun.*, vol. 4, no. 4, pp. 1928–1934, 2005.

[21] ——, "Network model for MIMO systems with coupled antennas and noisy amplifiers," *IEEE Trans. Antennas Propagat.*, vol. 53, no. 1, pp. 545–552, Jan. 2005.

[22] ——, "Impact of receive amplifier signal coupling on MIMO system performance," *IEEE Trans. Veh. Technol.*, vol. 54, no. 5, pp. 1678–1683, Sept. 2005.

[23] B. K. Lau, S. M. S. Ow, G. Kristensson, and A. F. Molisch, "Capacity analysis for compact MIMO systems," in *Proceedings of IEEE 61st Vihecular Technology Conference (VTC'05-Spring)*, vol. 1, May-June 2005, pp. 165–170.

[24] B. K. Lau, J. B. Andersen, G. Kristensson, and A. F. Molisch, "Impact of matching network on bandwidth of compact antenna arrays," *IEEE Trans. Antennas Propagat.*, vol. 54, no. 11, pp. 3225 – 3238, Nov. 2006.

[25] W. C.-Y. Lee, "Effect of mutual coupling on a mobile-radio maximum ratio diversity combiner with a large number of branches," *IEEE Trans. Commun.*, pp. 1188–1193, Dec. 1972.

[26] B. K. Lau and J. B. Andersen, "On closely coupled dipoles with load matching in a random field," in *Proceedings of IEEE 17th International Symposium on Personal, Indoor and Mobile Radio Communications (PIMRC'06)*, 2006.

[27] J. B. Andersen and B. K. Lau, "On closely coupled dipoles in a random field," *IEEE Antennas Wireless Propagat. Lett.*, vol. 5, pp. 73–75, 2006.

[28] Y. Fei and J. S. Thompson, "MIMO system sensitivity and coupled array design," in *Proceedings of IEEE 18th International Symposium on Personal, Indoor and Mobile Radio Communications (PIMRC'07)*, Sept. 2007.

[29] Y. Fei, B. K. Lau, A. Sunesson, A. J. Johansson, J. B. Andersen, and J. S. Thompson, "Experiments of closely coupled monopoles with load matching in a random field," in *Proceedings of 1st European Conference of Antenna and Propagation (EUCAP'06)*, Nov. 2006.

[30] Y. Fan and J. S. Thompson, "MIMO configurations for relay channels: Theory and practice," *IEEE Trans. Wireless Commun.*, vol. 6, no. 5, pp. 1774–1786, Mar. 2007.

[31] W. C. Y. Lee, "Mutual coupling effect on maximum-ratio diversity combiners and application to mobile radio," *IEEE Trans. Commun. Technol.*, vol. Com-18, no. 6, pp. 779–791, December 1970.

[32] T. M. Cover and J. A. Thomas, *Elements of information theory*, 2nd ed. USA: Jonh Wiley & Sons, Inc., 2006.

[33] S. Loyka and G. Tsoulos, "Estimating MIMO system performance using the correlation matrix approach," *IEEE Commun. Lett.*, vol. 6, no. 1, pp. 19–21, January 2002.

[34] J. D. Kraus, *Antennas*, 2nd ed. New York: McGraw-Hill, 1988.

[35] R. M. Gray, *Toeplitz and Circulant Matrices: A review*. USA: Now Publishers, Feb. 2006.

[36] K. Rosengren, J. Carlsson, and P.-S. Kildal, "Maximizing the effective diverstiy gain of two parallel dipoles by optimizing the source impedances," *Microwave and Optical Technology Letters*, vol. 48, no. 3, pp. 532–535, March 2006.

[37] S. M. S. Ow, "Impact of mutual coupling on compact MIMO systems," Master's thesis, Lund University, Lund, Sweden, March 2005.

[38] J. Salz and J. H. Winters, "Effect of fading correlation on adaptive arrays in digital mobile radio," *IEEE Trans. Veh. Technol.*, vol. 43, no. 4, pp. 1049–1057, November 1994.

[39] *SEMCAD*. [Online]. Available: http://www.semcad.com

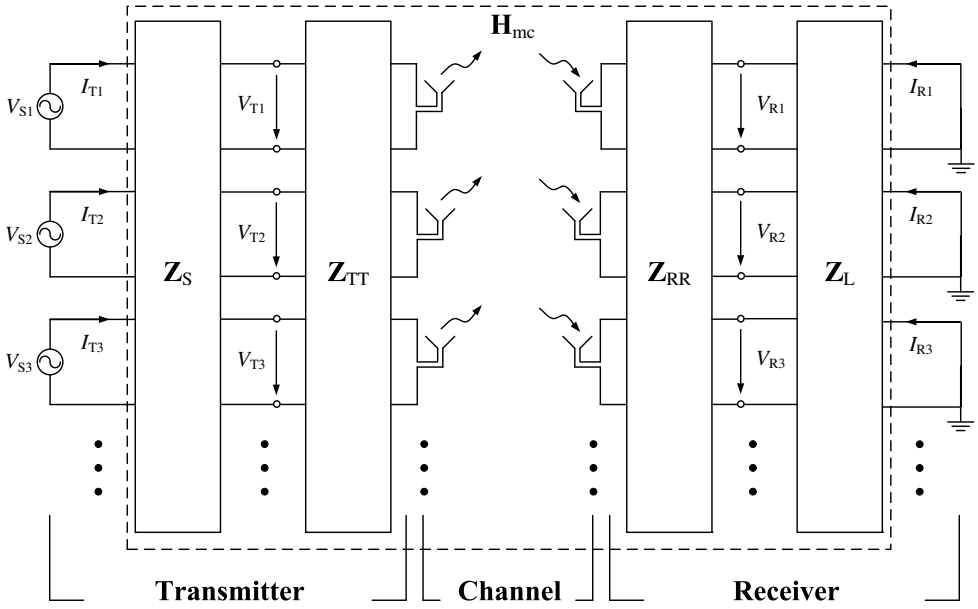

Fig. 1. Diagram of a MIMO system with antenna impedance matrices and matching networks at both link ends.

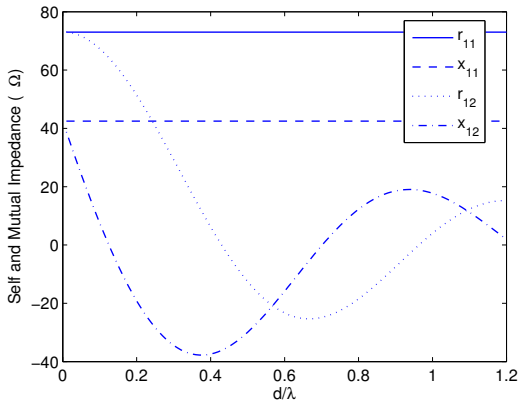

Fig. 2. The resistance and reactance components of self and mutual impedances with various antenna spacings.

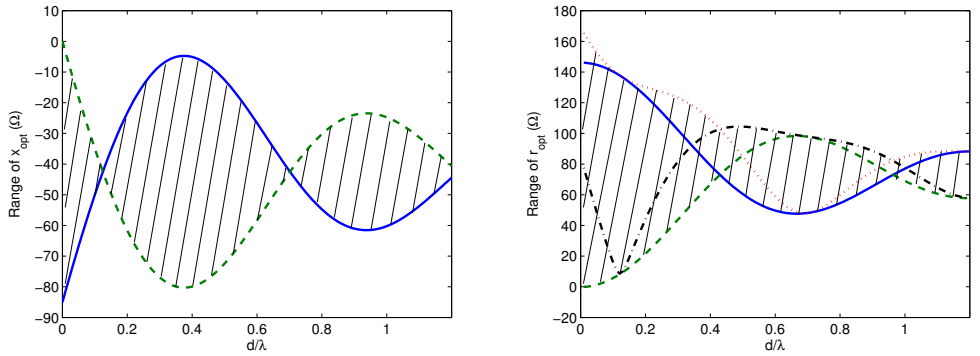

(a) (b)

Fig. 3. The possible range (shadow areas) of (r_{opt}, x_{opt}) of ideal $\lambda/2$ dipoles as a function of antenna spacing. In (a) x_{opt} varies between $-\mathfrak{X}_1$ (solid line) and $-\mathfrak{X}_2$ (dash line); in (b) r_{opt} moves among $\mathfrak{R}_1$ (solid line), $\mathfrak{R}_2$ (dash line), $\sqrt{\mathfrak{R}_1^2 + (\mathfrak{X}_1 - \mathfrak{X}_2)^2}$ (dot line) and $\sqrt{\mathfrak{R}_2^2 + (\mathfrak{X}_1 - \mathfrak{X}_2)^2}$ (dash-dot line).

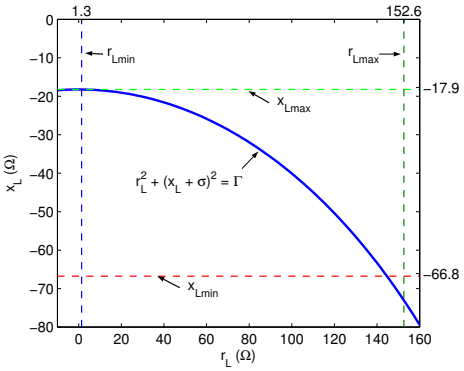

Fig. 4. Arc of the possible values of (r_{opt}, x_{opt}) for two compact ideal $\lambda/2$ dipoles of $d = 0.05\lambda$.

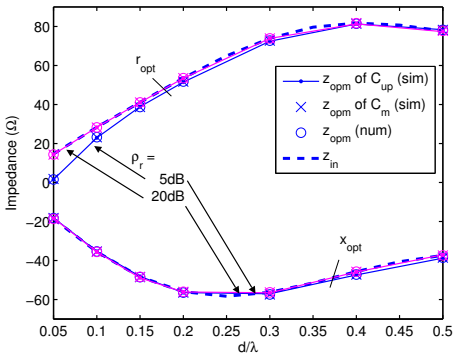

Fig. 5. The real and imaginary parts of numerical and simulation optimal single-port impedances compared to input impedance matching as a function of various antenna spacings with different ρ_r.

TABLE I

COMPARISON OF THE NUMERICAL AND SIMULATION RESISTANCE AND REACTANCE COMPONENTS OF THE OPTIMAL SINGLE-PORT IMPEDANCES WITH VARIOUS ANTENNA SPACINGS AND REFERENCE SNRS

d/λ	$r_{opt}(\Omega)$									$r_{in}(\Omega)$
	ρ_r = 5dB			ρ_r = 10dB			ρ_r = 20dB			
	num*	$\text{sim}^{\dagger}_{up}$	$\text{sim}^{\ddagger}_{m}$	num	sim_{up}	sim_{m}	num	sim_{up}	sim_{m}	
0.05	1.53	1.81	1.56	4.51	4.37	4.33	14.36	14.33	14.44	14.69
0.10	23.23	23.22	22.92	27.05	27.00	26.80	28.23	28.22	28.29	28.35
0.20	51.78	51.76	51.49	52.95	52.94	53.45	53.53	53.53	53.45	53.60
0.30	72.77	72.77	72.48	73.51	73.51	73.70	73.90	73.90	73.89	73.95
0.40	81.44	81.44	81.27	81.63	81.63	81.69	81.73	81.73	81.37	81.74
0.50	78.26	78.26	78.36	77.93	77.93	78.09	77.75	77.75	77.35	77.73
	$x_{opt}(\Omega)$									$x_{in}(\Omega)$
0.05	-18.23	-18.23	-18.16	-18.27	-18.27	-18.16	-18.66	-18.66	-18.26	-18.68
0.10	-35.35	-35.35	-35.30	-35.49	-35.49	-35.06	-35.54	-35.54	-35.62	-35.55
0.20	-56.46	-56.46	-56.44	-56.16	-56.17	-56.62	-56.02	-56.02	-56.12	-56.00
0.30	-57.44	-57.44	-57.05	-56.72	-56.73	-56.29	-56.35	-56.35	-56.57	-56.30
0.40	-47.21	-47.21	-47.39	-46.26	-46.26	-45.88	-45.75	-45.75	-45.88	-45.69
0.50	-38.54	-38.55	-38.77	-37.81	-37.81	-38.16	-37.41	-37.41	-37.07	-37.36

*numerical results †simulation results based on C_{up} ‡simulation results based on C_m

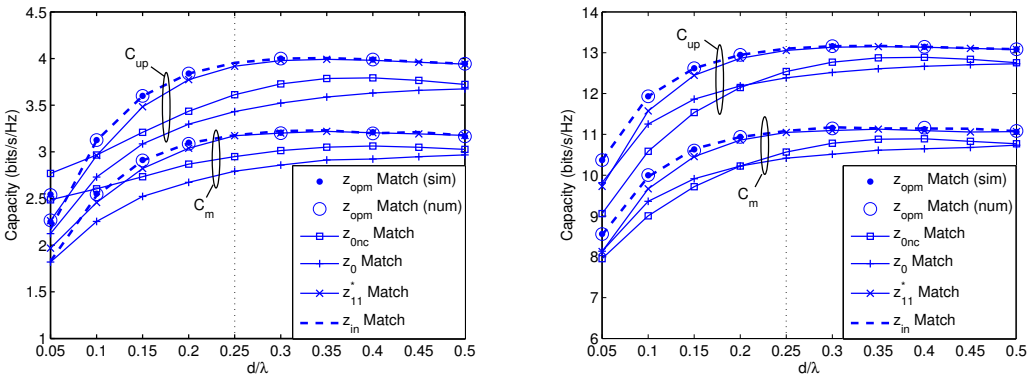

(a) $\rho_r = 5dB$ (b) $\rho_r = 20dB$

Fig. 6. The mean capacity and upper bound capacity with various matching networks as a function of d with different ρ_r.

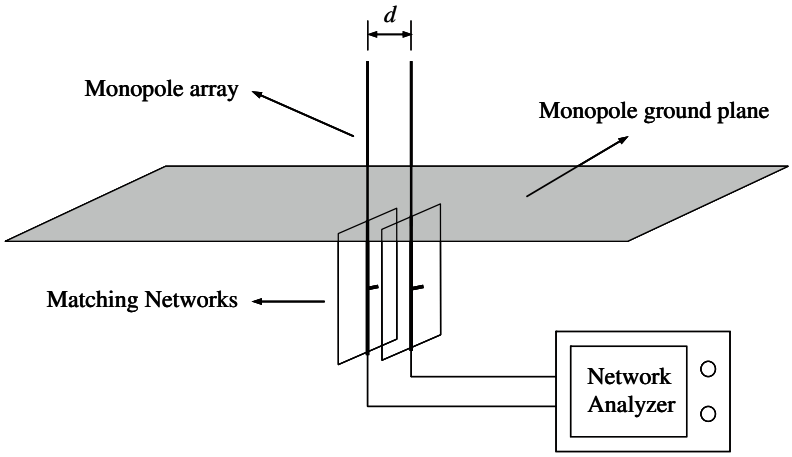

Fig. 7. Experimental setup of two $\lambda/4$ monopoles mounted on a ground plane and connected to matching networks.

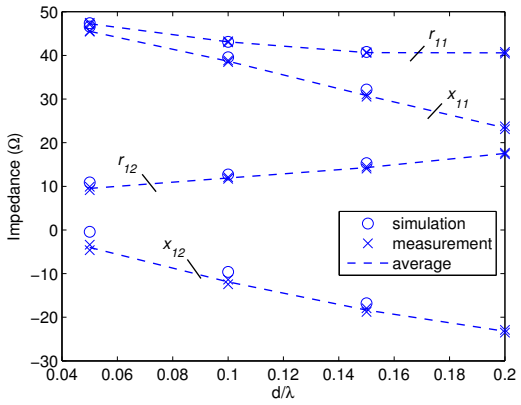

Fig. 8. Simulation and measurement results of the self and mutual impedances for a two-$\lambda/4$-monopole array with various antenna spacings.

TABLE II

COMPARISON OF THE ERGODIC CAPACITY BETWEEN CHOSEN LOADS WITH ANTENNA PARAMETERS FROM SIMULATION AND MEASUREMENT & CONTRAST BETWEEN NUMERICAL AND SIMULATION RESULTS OF OPTIMUM SINGLE-PORT IMPEDANCE.

	$Impedances\ (\Omega)$	$C_m\ (bits/s/Hz)$	
		sim†	mea‡
z_A	70.69 - j9	7.8572	8.4699
z_B	1.5 - j12.8	7.8150	8.3154
z_C	4.06 + j3	5.6516	6.2921
z_D	16.5 - j12	8.4068	9.1431
z_0	50	7.9810	8.6913
z_{11}^*	45.6 - j20.5 (sim)	8.0201	/
	45.5 - j19.22 (mea)	/	8.7579
z_{in}	8.29 - j11.46 (sim)	8.4517	/
	11.41 - j11.88 (mea)	/	9.2046
z_{opt}	8.67 - j11.85 (sim)	8.5313	/
	11.23 - j11.6 (mea)	/	9.2688
z_{opt}^n	9.09 - j11.46 (sim)	8.4558	/
	11.23 - j11.89 (mea)	/	9.2353

†results based on antenna parameters in simulation
‡results based on antenna parameters in measurement
^{n}numerical results

Optimal Single-Port Impedance Matching for Compact MIMO Arrays

Yuanyuan Fei, Yijia Fan and John S. Thompson
Institute for Digital Communications, Joint Research Institute for Signal & Image Processing
School of Engineering & Electronics, the University of Edinburgh
Edinburgh, EH9 3JL, UK
Email: {y.fei, y.fan, john.thompson}@ed.ac.uk

***Abstract*— Recent theoretical and simulation studies reveal that closely coupled antennas with appropriately chosen impedance matching loads can yield the desired characteristic of high MIMO capacity. Because of the practical infeasibility of multiport-conjugate matching, the single-port matching impedance (Z_{opt}) which maximizes the capacity of a 2×2 MIMO system with coupled half-wavelength dipoles is derived in this paper. We derive Z_{opt} for an ergodic capacity upper bound including the mutual coupling and matching networks effect. We show that the closed-form of Z_{opt} in the high SNR regime is identical to the input impedance. The analytical results are validated by numerical simulations.**

I. Introduction

Multiple-input multiple-output (MIMO) systems where multiple antennas are deployed at both link ends promise significant gains in spectrum efficiency and link reliability [1], [2]. Nevertheless, it has been mentioned [1] that the integration of MIMO technique into compact devices is restricted if the antenna spacing is below half a wavelength. This because strong mutual coupling (MC) between closely spaced antenna elements results in changes in antenna patterns (antenna correlation) and loss of antenna efficiency [3]. In [4], MC is claimed as a detriment to MIMO systems. However, MC can also be a positive factor to increase the MIMO performance under some circumstances. Recently, [5] clarified that the capacity of coupled antennas can be greatly improved by introducing proper matching networks into the multiple antenna system using S-parameter network theory. It turns out that the multiport-conjugate match is the optimal matching technique to improve the performance of capacity for compact MIMO arrays. Nevertheless, it is not feasible to integrate this solution into MIMO systems as multi-loads has to be introduced to each receive port [6]. Although the design of multiport-conjugate matching network has been reported in [7], the authors do not know of any experimental results being presented in the literature. As a result, the single-port match is still an attractive if suboptimal solution [8]. Actually, some experimental implementations have already tried to demonstrate maximum power collection by introducing single-port matching [9] according to the theory developed in [10]. In [11], the 'single maximum' characteristic of capacity as a function of matching impedances has already been discovered for antenna spacing $d = 0.05, 0.1\lambda$ based on numerical simulation. In our study we extend the investigation to different antenna spacings, and derive the the single-port matching impedance that maximizes the Shannon capacity. Also we prove that the optimal single-port matching impedance is equal to the input impedance [12] in the high SNR case. All the results are validated by numerical simulations which show excellent agreement.

The remainder of this paper is organized as follows. Section II gives the MIMO system model we adopt. Section III discribes the motivation of this work. Section IV presents the numerical deviation of the optimal single-port matching impedance. Section V compares the numerical and simulation results. Conclusions are given in Section VI.

II. MIMO System Model

An $N \times N$ MIMO system model is used in this paper. We assume the channel is frequency-flat fading, and the total average energy at the transmitter over one symbol period is P. The input-output relation is [13]

$$\mathbf{y} = \sqrt{P/N}\mathbf{H}\mathbf{x} + \mathbf{v} \tag{1}$$

where $\mathbf{y} = [y_1, ..., y_N]^T$, $\mathbf{x} = [x_1, ..., x_N]^T$ are the received signal vector and the transmitted signal vector, respectively. $\mathbf{H}$ represents the MIMO channel with dimension $N \times N$, and the additive Gaussian noise vector is $\mathbf{v} = [v_1, ..., v_N]^T$ with the covariance matrix $E\{\mathbf{v}\mathbf{v}^\dagger\} = N_0\mathbf{I}$. The superscript † means the conjugate transposition while $E\{\cdot\}$ denotes the expectation operator. Finally, $\mathbf{I}$ is an $N \times N$ identity matrix.

A. Capacity of MIMO channels

We assume the optimum transmit signals to maximize capacity are independent and equal-powered at the transmit antennas [13]. The narrowband MIMO Shannon capacity can be denoted as [1]

$$C = \log_2 \det\left(\mathbf{I} + \frac{P}{N \cdot N_0}\mathbf{H}\mathbf{H}^\dagger\right). \tag{2}$$

Moreover, the channel fading is considered to be independent across the transmit antennas but correlated at the receive antennas. $\mathbf{H}$ can be expressed by the modified Kronecker model

$$\mathbf{H} = \mathbf{\Psi}^{1/2}\mathbf{H}_{i.i.d.} \tag{3}$$

If the uniformly distributed arriving signal model in space is assumed, the receive end correlation matrix $\mathbf{\Psi}$ has elements

$\psi_{ii} = 1$ and $\psi_{ij} = J_0(2\pi d/\lambda)(i,j = 1,...,N, i \neq j)$ [14], where $J_0(\cdot)$, d, and λ are the zeroth Bessel function, the antenna spacing and the received signal wavelength respectively. $\mathbf{H}_{i.i.d.}$ is an $N \times N$ classical independent and identically Rayleigh distributed (i.i.d.) channel matrix.

B. Mutual Coupling Coefficient

In n-port theory, the mutual impedance matrix $\mathbf{Z}$ is defined as:

$$\mathbf{Z} = \begin{bmatrix} Z_{11} & Z_{12} & Z_{13} & \cdots \\ Z_{12} & Z_{22} & Z_{23} & \cdots \\ Z_{13} & Z_{23} & Z_{33} & \cdots \\ \vdots & \vdots & \vdots & \ddots \end{bmatrix} \tag{4}$$

where Z_{ii} is the self-impedance of the ith element and Z_{ij} means the mutual-impedance between the ith and jth elements. Here $Z_{ij} = Z_{ji}$ is based on the reciprocity theorem [15]. The matching-impedance matrix $\mathbf{Z_L}$ is given by

$$\mathbf{Z_L} = \begin{bmatrix} Z_{L_1} & 0 & 0 & \cdots \\ 0 & Z_{L_2} & 0 & \cdots \\ 0 & 0 & Z_{L_3} & \cdots \\ \vdots & \vdots & \vdots & \ddots \end{bmatrix} \tag{5}$$

with element Z_{L_i} indicating the matching impedance in the ith antenna branch. We assume there is no coupling between the matching impedances, so that all the non-diagonal elements of $\mathbf{Z_L}$ are zero. All the antenna elements are considered identical in the remainder of the paper, thus we define $Z_{ii} = Z_{11}$, $Z_{L_i} = Z_L$. By utilizing the voltage-current relations [16], the MC coefficient matrix is

$$\mathfrak{C}_{mc} = (\mathbf{Z} + \mathbf{Z_L})^{-1} = (\mathbf{Z} + Z_L \cdot \mathbf{I})^{-1} \tag{6}$$

C. MIMO Capacity with Mutual Coupling

The MC effect at the receiver end can be easily included into the MIMO system [17] by

$$\mathbf{H}_{mc} = \mathfrak{C}_{mc}\mathbf{H} \tag{7}$$

where $\mathbf{H}_{mc}$ is the modified MIMO channel with MC[1]. Suppose that the matching networks are perfectly lossless and each transmitter is self-conjugate ($Z_{11}{}^*$) matched. Without the MC effect $f(Z_L, Z_{11}, Z_{12})$, the MIMO system has an antenna power gain $\mathcal{G}_r = 4\mathrm{Re}\{Z_{11}\}\mathrm{Re}\{Z_L\}$ normalized to the self-conjugate matched single antenna case [10] for a 2×2 system,

$$P_r \propto \mathcal{G}_r \cdot f(Z_L, Z_{11}, Z_{12}) \tag{8}$$

which should be included in the MIMO system evaluation as well. P_r represents the normalized total received power. The modified MIMO capacity expression according to (2) is

$$C_m = \log_2 \det\left(\mathbf{I} + \frac{\rho_r \cdot \mathcal{G}_r}{N}\mathbf{H}_{mc} \cdot \mathbf{H}_{mc}{}^{\dagger}\right) \tag{9}$$

where $\rho_r = P/N_0$ is the reference SNR. An identical result has been derived in [11] though obtained from a different perspective.

[1]We note that the MC coefficient (6) in our paper is different from that in [17] but the way to obtain (7) is the same. In our system model, (6) should be used and the same results can be found in [8], [11].

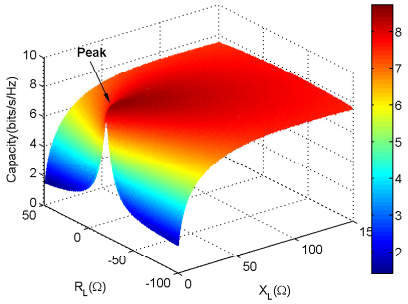

Fig. 1. Ergodic capacity vs. the real and imaginary parts of Z_L at $d = 0.05\lambda$.

D. Upper bound of MIMO Capacity

Define the ergodic capacity as $E\{C_m\}$. Using Jensen's inequality and the concavity of $\log_2\det(\cdot)$ [18], for any fixed antenna spacing d, we obtain the upper bound C_{up} [19] of the MIMO capacity at each impedance matching load point Z_{L_0} as

$$E\{C_m(\mathbf{X})|_{Z_{L_0}}\} \leq C_{up} \tag{10}$$

where $\mathbf{X} = \mathbf{H}_{mc} \cdot \mathbf{H}_{mc}{}^{\dagger}$,

$$\begin{aligned} C_{up} &= C_m(E\{\mathbf{X}\})|_{Z_{L_0}} \\ &= \log_2 \det\left(\mathbf{I} + \rho_r \cdot \mathcal{G}_r|_{\mathrm{Re}\{Z_{L_0}\}} \cdot \mathfrak{C}_{mc}{}^{\dagger}\mathfrak{C}_{mc}\mathbf{\Psi}\right) \end{aligned} \tag{11}$$

III. Problem Derivation

A 2×2 MIMO system is simulated under the assumptions presented in Section II. Identical ideal half-wavelength dipoles with infinite thin wire diameter are used at both ends. We focus on the coupled receive end. With ideal conditions, the self-impedance $Z_{11} = 73 + j42.5\Omega$ is constant, and the mutual-impedance $Z_{12} = Z_{21}$ can be deduced using the modified EMF method [16]. For each load point Z_{L_0}, 10000 random channel realizations are deployed to estimate the MIMO system performance. All the simulation parameters are valid through the remainder of the paper.

As shown in Fig. 1, the 3-dimensional ergodic capacity surface is plotted with various matched impedances points $\{Z_{L_0} = R_{L_0} + jX_{L_0} : R_{L_0} \in R_L, X_{L_0} \in X_L\}$, where $R_L \in [0, 150]\Omega$, $X_L \in [-100, 50]\Omega$. We take the $d = 0.05\lambda$ case as an example to demonstrate that the capacity performance is concave and resembles the received power characteristic in [10] except only one peak is observed with the changing of matching networks for one fixed d. For other antenna spacings less than 0.5λ, the surface of C_m has the similar properties. This observation implies that there should be a maximum point for C_m, and it will be derived in Section IV.

IV. Optimal Single-Port Matching Impedance

As (9) contains a random channel matrix, it is difficult to deduce the optimal single-port matching impedance (Z_{opt})

$$\mathfrak{C}_{mc}{}^{\dagger}\mathfrak{C}_{mc} = \left(\mathbf{U}\left(\begin{bmatrix} r_L^2+x_L^2 & 0 \\ 0 & r_L^2+x_L^2 \end{bmatrix} + 2r_L\cdot\begin{bmatrix} \mathfrak{R}_1 & 0 \\ 0 & \mathfrak{R}_2 \end{bmatrix} + 2x_L\cdot\begin{bmatrix} \mathfrak{X}_1 & 0 \\ 0 & \mathfrak{X}_2 \end{bmatrix} + \begin{bmatrix} \mathfrak{R}_1^2+\mathfrak{X}_1^2 & 0 \\ 0 & \mathfrak{R}_2^2+\mathfrak{X}_2^2 \end{bmatrix}\right)\mathbf{U}\right)^{-1}$$
$$= \mathbf{U}\begin{bmatrix} (r_L+\mathfrak{R}_1)^2+(x_L+\mathfrak{X}_1)^2 & 0 \\ 0 & (r_L+\mathfrak{R}_2)^2+(x_L+\mathfrak{X}_2)^2 \end{bmatrix}^{-1}\mathbf{U} = \mathbf{U}\mathbf{\Lambda^{-1}}\mathbf{U} \quad (14)$$

from C_m. Therefore, we focus on (11) to derive Z_{opt} by calculating the maximum value of C_{up}. We define $Z_{11} = r_{11} + jx_{11}$, $Z_{12} = r_{12} + jx_{12}$, $Z_L = r_L + jx_L$, where r_{11}, r_{12}, $r_L \in \mathbb{R}^+$ as they are resistances and reactances x_{11}, x_{12}, $x_L \in \mathbb{R}$. Given a fixed reference SNR ρ_r and antenna spacing d, the self and mutual impedances Z_{11}, Z_{12} become constant, then (11) is only a function of variables (r_L, x_L). Besides $\mathcal{G}_r$, $\mathfrak{C}_{mc}{}^{\dagger}\mathfrak{C}_{mc}$ contains both variables (r_L, x_L) and has to be simplified. From (6) we obtain

$$\mathfrak{C}_{mc}{}^{\dagger}\mathfrak{C}_{mc} = \left(\left[\mathbf{Z} + Z_L\cdot\mathbf{I}\right]\left[\mathbf{Z}^* + Z_L^*\cdot\mathbf{I}\right]\right)^{-1}$$
$$= \left(\underbrace{|Z_L|^2\cdot\mathbf{I}}_{\mathbf{Z_1}} + \underbrace{Z_L\cdot\mathbf{Z}^* + Z_L^*\cdot\mathbf{Z}}_{\mathbf{Z_2}} + \underbrace{\mathbf{Z}\mathbf{Z}^*}_{\mathbf{Z_3}}\right)^{-1}. \quad (12)$$

Expanding (12) we have

$$\mathbf{Z_1} = \begin{bmatrix} r_L^2+x_L^2 & 0 \\ 0 & r_L^2+x_L^2 \end{bmatrix}$$
$$\mathbf{Z_2} = 2\left(r_L\cdot\begin{bmatrix} r_{11} & r_{12} \\ r_{12} & r_{11} \end{bmatrix} + x_L\cdot\begin{bmatrix} x_{11} & x_{12} \\ x_{12} & x_{11} \end{bmatrix}\right)$$
$$\mathbf{Z_3} = \begin{bmatrix} r_{11}^2+x_{11}^2+r_{12}^2+x_{12}^2 & 2(r_{11}r_{12}+x_{11}x_{12}) \\ 2(r_{11}r_{12}+x_{11}x_{12}) & r_{11}^2+x_{11}^2+r_{12}^2+x_{12}^2 \end{bmatrix} \quad (13)$$

where $\mathbf{Z_1}$, $\mathbf{Z_2}$ and $\mathbf{Z_3}$ are all real symmetric Toeplitz matrices. By utilizing the following theorem, $\mathbf{Z_2}$ and $\mathbf{Z_3}$ can be decomposed and further simplified.

Theorem : For any real symmetric Toeplitz matrix

$$\mathbf{A} = \begin{bmatrix} a_1 & a_2 \\ a_2 & a_1 \end{bmatrix}, \qquad a_1 \in \mathbb{R}^+,\ a_2 \in \mathbb{R},\ a_1 > a_2$$

the singular value decomposition (SVD) of $\mathbf{A}$ can be written as

$$\mathbf{A} = \mathbf{U}\mathbf{D}\mathbf{U}' = \mathbf{U}\mathbf{D}\mathbf{U}$$

where

$$\mathbf{U} = \frac{1}{\sqrt{2}}\begin{bmatrix} 1 & 1 \\ 1 & -1 \end{bmatrix}, \mathbf{D} = \begin{bmatrix} a_1+a_2 & 0 \\ 0 & a_1-a_2 \end{bmatrix}$$

and the superscript $'$ is the matrix transpose.

Proof: See Appendix. ∎

In Fig. 2 it is obvious that $r_{11} > r_{12}$ and $x_{11} > x_{12}$. We can easily deduce $\mathbf{Z_3}$ also fulfills the constraints of *Theorem 1*. Utilizing *Theorem 1*, the SVD of (12) is (14) at the top of the page, where $\mathfrak{R}_1 = r_{11}+r_{12}$, $\mathfrak{X}_1 = x_{11}+x_{12}$, $\mathfrak{R}_2 = r_{11}-r_{12}$, $\mathfrak{X}_2 = x_{11}-x_{12}$. Using the property $\det(\mathbf{I}+\mathbf{AB}) = \det(\mathbf{I}+\mathbf{BA})$ [2], (11) can be rewritten as

$$C_{up} = \log_2\det(\mathbf{I} + \kappa r_L\cdot\mathbf{U}\mathbf{\Lambda^{-1}}\mathbf{U}\mathbf{\Psi})$$
$$= \log_2\det(\mathbf{I} + \kappa\mathbf{U}\mathbf{\Psi}\mathbf{U}r_L\mathbf{\Lambda^{-1}}) = \log_2\det(\mathbf{Y}) \quad (15)$$

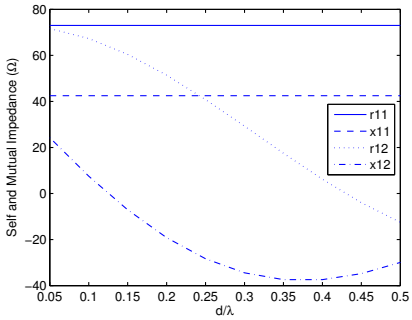

Fig. 2. The real and imaginary parts of self and mutual impedances with various antenna spacings.

where $\kappa = \rho_r\cdot 4\mathrm{Re}\{Z_{11}\}/N$. According to the monotonically increasing characteristic of $\log(\cdot)$, the maximum point of $\det(\cdot)$ is the maximum point of $\log_2\det(\cdot)$. To derive the maximum point of $\det(\mathbf{Y})$, we deduce the following derivatives

$$\frac{\partial\det(\mathbf{Y})}{\partial r_L} = \left(\mathfrak{R}_1^2 - r_L^2 + (x_L+\mathfrak{X}_1)^2\right)\cdot\Sigma_2 + \left(\mathfrak{R}_2^2 - r_L^2 + (x_L+\mathfrak{X}_2)^2\right)\cdot\Sigma_1 \quad (16a)$$
$$\frac{\partial\det(\mathbf{Y})}{\partial x_L} = (x_L+\mathfrak{X}_1)\cdot\Sigma_2 + (x_L+\mathfrak{X}_2)\cdot\Sigma_1 \quad (16b)$$

where

$$\Sigma_i = \left((r_L+\mathfrak{R}_i)^2+(x_L+\mathfrak{X}_i)^2\right)\cdot\left((1+\alpha)\left((r_L+\mathfrak{R}_i)^2 + (x_L+\mathfrak{X}_i)^2\right) + (1-\alpha^2)\kappa r_L\right), \qquad i = 1,2 \quad (17)$$

and $\alpha = \psi_{12}$ in (3) is the correlation between the two receiver antennas. As the maximum point, Z_{opt} must be a stationary point to make (16) equal to zero. Utilizing (16a) and (16b) it is easily to obtain the simple relation between r_L and x_L

$$r_L^2 + (x_L+\sigma)^2 = \Gamma \quad (18)$$

where

$$\sigma = x_{11} + \frac{r_{11}r_{12}}{x_{12}}, \qquad \Gamma = r_{11}^2 + r_{12}^2 + x_{12}^2 + \frac{r_{11}^2 r_{12}^2}{x_{12}^2}.$$

Substituting (18) into (16b), we can deduce a polynomial in x_L. The closed form solution for x_L is unknown in general and has to be calculated numerically.

If a high SNR condition is assumed, a closed form solution can be obtained. Equation (15) can be rewritten as

$$C_{up} = \log_2\det(\kappa\mathbf{U}\mathbf{\Psi}\mathbf{U}r_L\mathbf{\Lambda^{-1}}) \quad (19)$$

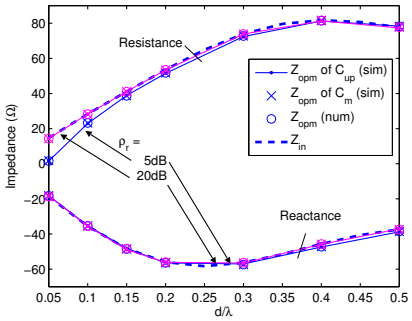

Fig. 3. The real and imaginary parts of numerical and simulation optimal single-port impedances compared to input impedance matching as a function of various antenna spacings with different ρ_r.

then

$$\det(\mathbf{Y}) = \frac{(\mathbf{1} - \alpha^{\mathbf{2}})}{\det(\mathbf{\Lambda})}. \tag{20}$$

The derivatives in (16) are modified by simplifying (17) as

$$\Sigma_i = (r_L + \Re_i)^2 + (x_L + \mathfrak{X}_i)^2, \qquad i = 1, 2. \tag{21}$$

Solving the equations we derive the closed-form of $Z_{opt} = r_{opt} + jx_{opt}$, where

$$r_{opt} = \sqrt{\Re_1\Re_2\left(1 + \frac{(\mathfrak{X}_1 - \mathfrak{X}_2)^2}{(\Re_1 + \Re_2)^2}\right)} = \sqrt{r_{11}^2 - r_{12}^2 + x_{12}^2 - \frac{r_{12}^2 x_{12}^2}{r_{11}^2}} \tag{22a}$$

$$x_{opt} = -\frac{\Re_1\mathfrak{X}_2 + \Re_2\mathfrak{X}_1}{\Re_1 + \Re_2} = \frac{r_{12}x_{12}}{r_{11}} - x_{11} \tag{22b}$$

This solution of Z_{opt} is exactly the input impedance match in [12].

V. Simulation Results and Analysis

Fig. 3 illuminates that the numerically derived Z_{opt} agrees well with that generated from simulations of C_{up}. The numerical Z_{opt} matches to the impedance where C_m reaches the maximum value as well[2]. It is also clear that Z_{opt} approaches the input impedance match (Z_{in}) when the SNR increases, which is perfectly in accord with our derivation in Section IV. Another phenomenon is that the reactance of Z_{opt} is hardly affected by the SNR and the impact of SNR on the resistance of Z_{opt} diminishes when $d > 0.2\lambda$. In the high SNR regime, r_{11}, x_{11} are constant (Fig. 2), then (22b) is dominated by $r_{12}x_{12}$. As r_{12} is monotonically decreasing and x_{12} is convex

[2]We note that the numerical Z_{opt}, Z_{opt} from simulation of C_{up}, and Z_{opt} from simulation of C_m match to each other with the error less than 1 Ω. Thus, the differences are hard to tell from Fig. 3.

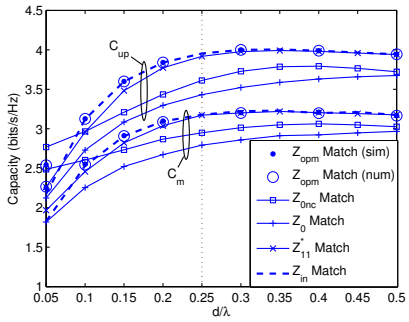

(a) $\rho_r = 5dB$

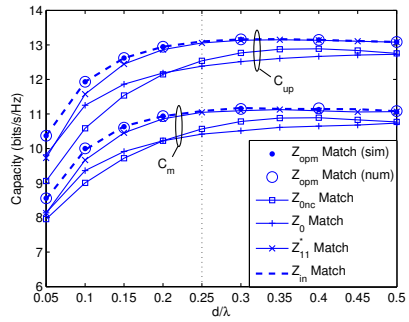

(b) $\rho_r = 20dB$

Fig. 4. The mean capacity and upper bound capacity with various matching networks as a function of antenna spacing with different ρ_r.

over $d \in [0.05, 0.5]\lambda$ in Fig. 2, the convexity of x_{opt} can be well explained in Fig. 3. (22a) can be further written as

$$r_{opt} = \frac{\sqrt{r_{11}^4 - r_{11}^2 r_{12}^2 + r_{11}^2 x_{12}^2 - r_{12}^2 x_{12}^2}}{r_{11}}.$$

Fig. 2 shows that $-r_{12}^2$ is monotonically increasing over $d \in [0.05, 0.4]\lambda$, and x_{12}^2 is monotonically increasing over $d \in [0.1, 0.5]\lambda$. Thus r_{opt} should be monotonically increasing over $d \in [0.1, 0.4]\lambda$, which agrees well with the r_{opt} curve in Fig. 3.

To illustrate how much we can benefit from Z_{opt} match, the mean capacity (C_m) and capacity upper bound (C_{up}) computed for antennas with characteristic-impedance match of both no coupling (Z_{0nc}) and MC (Z_0) cases, self-conjugate match ($Z_{11}{}^*$), input impedance match (Z_{in}) and maximum capacity (Z_{opt}) match are depicted with different SNRs in Fig. 4. The coupled compact array with matching networks outperforms the array without MC at small spacing ($d < 0.2\lambda$). Meanwhile, Z_{opt} matching surpasses other matching schemes when $d < 0.25\lambda$. In Fig. 4(a), the performance of the Z_{opt} match deviates from that of the Z_{in} match with better capacity results only at extremely close antenna spacings $d < 0.1\lambda$. Fig.

4 also illustrates C_{up} preserves the characteristic of C_m. With increasing SNR, the performance of Z_{opt} and Z_{in} overlap with each other in Fig. 4(b), which again verifies our analysis. The relation between the trend of C_{up} and the variation of Z_{opt}, Z_{11}, Z_{12} for the high SNR case can not be explained easily from the analytical results. However, it is obvious that r_{opt} is important in deriving C_{up} as in Fig. 4 C_{up} follows the monotonically increasing property of r_{opt} in Fig. 3 with all spacings. It can be understood physically that it is because r_{opt} is the load receiving the power which contains the mutual information.

VI. Conclusion

The optimal single-port matching impedance (Z_{opt}) of a 2×2 MIMO system with coupled half-wavelength dipoles is studied in this paper. We present a novel method to derive the numerical Z_{opt} from the upper bound capacity including the mutual coupling and matching network effect. We also prove that Z_{opt} is identical to the input impedance in the high SNR regime. The numerical results are validated by the simulation and in perfect agreement. The capacity results for the Z_{opt} match for various antenna spacings is found and it outperforms other matching networks for small antenna spacings ($d < 0.25\lambda$).

Acknowledgment

The authors would like to thank Dr. Buon Kiong (Vincent) Lau, Radio Systems Group & Electromagnetic Theory Group Department of Electroscience, Lund University, Sweden for motivating this work and for many useful discussions. The project is supported by Scottish Funding Council for the Joint Research Institute with the Heriot-Watt University (a part of the Edinburgh Research Partnership).

Appendix
Proof of *Theorem*

From the SVD definition we know that $\mathbf{U}$ is the matrix of the eigenvectors of $\mathbf{AA'} = \mathbf{A'A}$ as $\mathbf{A}$ is symmetric. To obtain the eigenvalues of

$$\mathbf{\Delta} = \mathbf{AA'} = \begin{bmatrix} \delta_1 & \delta_2 \\ \delta_2 & \delta_1 \end{bmatrix} = \begin{bmatrix} a_1^2 + a_2^2 & 2a_1a_2 \\ 2a_1a_2 & a_1^2 + a_2^2 \end{bmatrix}, \quad (23)$$

the determinant and trace of $\mathbf{\Delta}$ are given as $\det(\mathbf{\Delta}) = (a_1^2 - a_2^2)^2$, $\mathrm{Tr}(\mathbf{\Delta}) = 2(a_1^2 + a_2^2)$. Then the eigenvalues of $\mathbf{\Delta}$ can be denote as [20]

$$\begin{aligned} \lambda_i &= \frac{\mathrm{Tr}(\mathbf{\Delta}) \pm \sqrt{\mathrm{Tr}(\mathbf{\Delta})^2 - 4\det(\mathbf{\Delta})}}{2} \\ &= (a_1 \pm a_2)^2, \qquad i = 1, 2. \end{aligned} \quad (24)$$

We obtain

$$\mathbf{D} = \begin{bmatrix} \sqrt{\lambda_1} & 0 \\ 0 & \sqrt{\lambda_2} \end{bmatrix} = \begin{bmatrix} |a_1 + a_2| & 0 \\ 0 & |a_1 - a_2| \end{bmatrix}. \quad (25)$$

With our constrains, it is easy to get $a_1 + a_2 > 0$ and $a_1 - a_2 > 0$, then $\mathbf{D}$ can be further reduced to

$$\mathbf{D} = \begin{bmatrix} a_1 + a_2 & 0 \\ 0 & a_1 - a_2 \end{bmatrix}. \quad (26)$$

Next we derive the eigenvectors $\mathbf{u_1}$, $\mathbf{u_2}$ of $\mathbf{\Delta}$. Using the definition in [20], we write

$$\begin{aligned} \mathbf{u_1} &\propto \begin{bmatrix} \delta_2 \\ \lambda_1 - \delta_1 \end{bmatrix} = \begin{bmatrix} 2a_1a_2 \\ 2a_1a_2 \end{bmatrix} \propto \begin{bmatrix} 1 \\ 1 \end{bmatrix} \\ \mathbf{u_2} &\propto \begin{bmatrix} \delta_2 \\ \lambda_2 - \delta_1 \end{bmatrix} = \begin{bmatrix} 2a_1a_2 \\ -2a_1a_2 \end{bmatrix} \propto \begin{bmatrix} 1 \\ -1 \end{bmatrix}. \end{aligned} \quad (27)$$

Now we assume that $\mathbf{U} = [\ \mathbf{u_1} \quad \mathbf{u_2}\ ] = \begin{bmatrix} 1 & 1 \\ 1 & -1 \end{bmatrix}$,

$$\mathbf{UDU'} = \mathbf{UDU} = \begin{bmatrix} 2a_1 & 2a_2 \\ 2a_2 & 2a_1 \end{bmatrix} = 2\mathbf{A}. \quad (28)$$

We modify $\mathbf{U} = \frac{1}{\sqrt{2}} \begin{bmatrix} 1 & 1 \\ 1 & -1 \end{bmatrix}$ to fulfill $\mathbf{A} = \mathbf{UDU}$.

References

[1] G. J. Foschini and M. J. Gans, "On limits of wireless communications in a fading environment when using multiple antennas," *Wireless Personal Communications*, vol. 6, pp. 311–335, Mar. 1998.
[2] I. E. Telatar, "Capacity of multi-antenna gaussian channels," *European Trans. Telecommun.*, vol. 10, pp. 585–595, 1999.
[3] P.-S. Kildal and K. Rosengren, "Electromagnetic analysis of effective and apparent diversity gain of two parallel dipoles," *IEEE Antennas Wireless Propagat. Lett.*, vol. 2, pp. 9–13, 2003.
[4] E. A. Mehmet Kemal Özdemir and H. Arslan, "Dynamics of spatail correlation and implications on MIMO systems," *IEEE Commun. Mag.*, pp. 514–519, 2004.
[5] J. W. Wallace and M. A. Jensen, "Mutual coupling in MIMO wireless systems: a rigorous network theory analysis," *IEEE Trans. Wireless Commun.*, vol. 3, no. 4, pp. 1317–1325, 2004.
[6] W. C.-Y. Lee, "Effect of mutual coupling on a mobile-radio maximum ratio diversity combiner with a large number of branches," *IEEE Trans. Commun.*, pp. 1188–1193, Dec. 1972.
[7] S. Dossche, S. Blanch, and J. Romeu, "Optimum antenna matching to minimise signal correlation on a two-port antenna diversity system," *IEE Electronics Letters*, vol. 40, no. 19, pp. 1164–1165, September 2004.
[8] B. K. Lau, J. B. Andersen, G. Kristensson, and A. F. Molisch, "Antenna matching for capacity maximization in compact MIMO systems," in *Proceedings of 3rd International Symposium on Wireless Communications Systems (ISWCS)*, Valencia, Spain, Sept. 2006, (invited).
[9] Y. Fei, B. K. Lau, A. Sunesson, A. J. Johansson, J. B. Andersen, and J. S. Thompson, "Experiments of closely coupled monopoles with load matching in a random field," in *Proceedings of EUCAP'06*, Nov. 2006.
[10] J. B. Andersen and B. K. Lau, "On closely coupled dipoles in a random field," *IEEE Antennas Wireless Propagat. Lett.*, vol. 5, pp. 73–75, 2006.
[11] B. K. Lau and J. B. Andersen, "On closely coupled dipoles with load matching in a random field," in *Proceedings of IEEE PIMRC'06*, 2006.
[12] B. K. Lau, J. B. Andersen, G. Kristensson, and A. F. Molisch, "Impact of matching network on bandwidth of compact antenna arrays," *IEEE Trans. Antennas Propagat.*, vol. 54, no. 11, pp. 3225 – 3238, Nov. 2006.
[13] A. Paulraj, R. Nabar, and D. Gore, *Introduction to space-time wireless communications*, 1st ed. Cambridge, UK: Cambridge University, 2003.
[14] J. Salz and J. H. Winters, "Effect of fading correlation on adaptive arrays in digital mobile radio," *IEEE Trans. Veh. Technol.*, vol. 43, no. 4, pp. 1049–1057, Nov. 1994.
[15] J. D. Kraus, *Antennas*, 2nd ed. New York: McGraw-Hill, 1988.
[16] C. A. Balanis, *Antenna theory*, 2nd ed., S. Elliot, Ed. USA: John Wiley & Sons, Inc, 1997.
[17] B. Clerckx, D. Vanhoenacker-Janvier, C. Oestges, and L. Vandendorpe, "Mutual coupling effects on the channel capacity and the space-time processing of MIMO communication systems," in *Proceedings of IEEE ICC'03*, vol. 4, May 2003, pp. 2638–2642.
[18] T. M. Cover and J. A. Thomas, *Elements of information theory*, 2nd ed. USA: Jonh Wiley & Sons, Inc., 2006.
[19] S. Loyka and G. Tsoulos, "Estimating MIMO system performance using the correlation matrix approach," *IEEE Commun. Lett.*, vol. 6, no. 1, pp. 19–21, January 2002.
[20] K. B. Petersen and M. S. Pedersen, *The Matrix Cookbook*, Feb. 2006. [Online]. Available: http://matrixcookbook.com/

CONTINUOUS STUDY OF CLOSELY COUPLED DIPOLES WITH MATCHING NETWORKS

Yuanyuan Fei and John S. Thompson

Institute for Digital Communications, Joint Research Institute for Signal & Image Processing
School fo Engineering & Electronics, the Univeristy of Edinburgh
Edinburgh, EH9 3JL, UK
Email: y.fei@ed.ac.uk, john.thompson@ed.ac.uk
Fax: +44-131-6506554

Keywords: MIMO, received power, power difference.

Abstract

Power collection at the receive end in a multi-input multi-output (MIMO) system is critical to information recovery, especially for compact receive arrays. In this work we discuss the correct analytical received power expression with various matching impedances which maximize the received power of compact antenna array. The power differences and power collection ability of the optimum impedance match compared to the self-conjugate match for a two-element dipole array is also studied.

1 Introduction

Multiple-input multiple-output (MIMO) systems where multiple antennas are deployed at both link ends have been comprehensively explored in the past decade due to their significant gains in spectrum efficiency and link reliability [1],[2],[3]. It is widely accepted that antenna spacings of less than half a wavelength will cause significant degradation of MIMO system performance [3]. In practice, due to the limitation of the space at the receiver end (mobile, PDA etc.), it is not easy to achieve the required half-wavelength spacing when multi-antennas are implemented.

When the antenna spacing is smaller than half a wavelength, each antenna element will induce currents on other adjacent elements introducing interference and distorting the array pattern via the so-called mutual coupling (MC) effect. However, we can mitigate the impact of MC by introducing appropriate matching networks into MIMO systems [4]. The matching networks can be properly chosen to increase the received power and decrease the output correlation of the receive end [5],[6] to turn MC into an advantage of the system. The received power and correlation of a coupled two-element half-wavelength dipole array has been investigated analytical- ly in both [6] and [7], though from different points of view. Reference [6] uses the circuit theory point of view, while [7] is based on the MC coefficient combined with the steering vector of the antenna array. Reference [6] also directly includes the impact of the matching networks on the received power and correlation, and is verified experimentally in [8]. We prefer the results in [6] because it explored the impedances maximizing the received power. However, [7] only assumed the receive antennas to be self-conjugate matched. In theory, [6] and [7] should give identical answers for uniform matching networks and antenna spacing. Interestingly, we find the received power expression in [7] gives totally different results compared to [6].

In this paper, we will investigate the difference between [6] and [7] analytically, and conclude the method in [6] is correct. Moreover, the matching loads maximizing the received power mentioned in [6] will be studied for various antenna spacings as functions of power difference [7]. The maximum received power [6] will be compared to the received power utilizing the self-conjugate match of various antenna spacings as the authors only focused on single antenna spacing of 0.05 wavelength in [6]. We will see significant benefits by adopting the optimum impedances maximizing the received power.

The reminder of the paper is organized as follows. Section 2 describes the coupled receiver model we use. Section 3 provides the analytical study of the two methods. Simulation results are given in Section 4. Conclusions are presented in Section 5.

2 Receiver model with mutual coupling

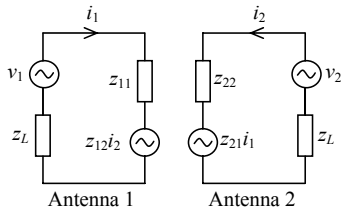

Fig. 1 Equivalent circuit of two coupled receive antennas

When the compact receive array is under consideration, mutual coupling is a severe influence as we mentioned in Section 1.
Fig. 1 shows the analytical equivalent circuit for two coupled receivers with matching networks. The scalars z_{11}, z_{22} and z_{12}, z_{21} are the self and mutual impedances of antenna 1 and 2, respectively. An identical matching impedance z_L is applied to

both antennas. The voltages v1 and v2 are open-circuit voltages which are correlated and determined by the surrounding propagation environment. In both circuits, we have the induced currents i_1 and i_2, respectively. Under the assumption of identical antennas, $z_{11} = z_{22}$ and $z_{12} = z_{21,}$ and the theoretical expressions of mean received power and output correlation have been derived in [6].

3 Analytical study of the received power

3.1 From the circuit theory point of view

The received power of antenna 1 after normalizing to the received power of the conjugate-matched single antenna case $P_0 = E\{r_{11}|i_0|^2\}$ is [6]

$$P_1 = \frac{4r_L r_{11}\left(\left|z_{11}+z_L\right|^2 + \left|z_{12}\right|^2 - 2\mathrm{Re}\left\{\alpha\left(z_{11}+z_L\right)z_{12}^*\right\}\right)}{\left|\left(z_{11}+z_L\right)^2 - z_{12}^2\right|^2} \quad (1)$$

where r_L and r_{11} are the resistance components of z_L and z_{11}, respectively. The notation $\mathrm{Re}\{\cdot\}$ and * represent the real part and conjugate of a complex number. Moreover, α is the open-circuit correlation as discussed in [6]. Let us define

$$\mathrm{A} = 2\mathrm{Re}\left\{\alpha\left(z_{11}+z_L\right)z_{12}^*\right\} \quad (2)$$

Also we can expand $\alpha = R_{xx} + jR_{xy}$, $z_{11} = r_{11} + jx_{11}$, $z_{12} = r_{12} + jx_{12}$, and $z_L = r_L + jx_L$, then (2) can be expanded as

$$\begin{aligned}\mathrm{A} &= 2\cdot\mathrm{Re}\left\{\left(R_{xx}+jR_{xy}\right)\left[\left(r_{11}+r_L\right)+j\left(x_{11}+x_L\right)\right]\left(r_{12}-jx_{12}\right)\right\}\\ &= 2\cdot\mathrm{Re}\left\{\left(R_{xx}+jR_{xy}\right)\left\{\left[r_{12}\left(r_{11}+r_L\right)+x_{12}\left(x_{11}+x_L\right)\right]\right.\right.\\ &\quad \left.\left.+\,j\left[r_{12}\left(x_{11}+x_L\right)-x_{12}\left(r_{11}+r_L\right)\right]\right\}\right\}\\ &= 2\left\{R_{xx}\left[r_{12}\left(r_L+r_{11}\right)+x_{12}\left(x_L+x_{11}\right)\right]\right.\\ &\quad \left.+\,R_{xy}\left[x_{12}\left(r_L+r_{11}\right)-r_{12}\left(x_L+x_{11}\right)\right]\right\}\end{aligned} \quad (3)$$

We will use (3) for future comparison.

3.2 Based on the mutual coupling coefficient and steering vector

As observed from
Fig. 1, the mutual coupling (MC) coefficient of a two-identical-antenna-element array is given by [9],[10]

$$\mathbf{C} = z_L\cdot\left(z_L\mathbf{I}+\mathbf{Z}\right)^{-1} = \begin{bmatrix} c & d \\ d & c \end{bmatrix} \quad (4)$$

where $\mathbf{I}$ is the 2 dimensional identity matrix and $\mathbf{Z}$ is the mutual impedance matrix with elements z_{11} and z_{12}. We note that in [7],[11], $\mathbf{C} = (z_L + z_{11})(z_L\mathbf{I} + \mathbf{Z})^{-1}$ has been used. However, if we refer back to [9], (4) should be used for the system model described in Section 2. Referring to the expression of received power presented in [7], the validity of $\mathbf{C}$ will directly affect the power evaluation as we will see in the following derivation.

The 2 dimensional steering vector of a two antenna array with identical and omni-directional elements but without MC is

$$\mathbf{a}_{nc}(\varphi) = \begin{bmatrix}1 & e^{j\tau}\end{bmatrix}^T \quad (5)$$

where $\tau = 2\pi d\sin(\varphi)/\lambda$ and ^{T} represents transpose of a matrix /vector. Then the modified steering vector with MC of the same system is

$$\begin{aligned}\mathbf{a}_{mc}(\varphi) &= \begin{bmatrix} a_{mc}^1(\varphi) \\ a_{mc}^2(\varphi)\end{bmatrix} = \mathbf{C}\times\mathbf{a}_{nc}(\varphi) = \begin{bmatrix} c & d \\ d & c\end{bmatrix}\times\begin{bmatrix}1 \\ e^{j\tau}\end{bmatrix}\\ &= \begin{bmatrix} c+d\cdot e^{j\tau} \\ c\cdot e^{j\tau}+d\end{bmatrix} = \begin{bmatrix} c+d\cdot e^{j\tau} \\ \left(c+d\cdot e^{-j\tau}\right)\cdot e^{j\tau}\end{bmatrix}\end{aligned} \quad (6)$$

Also (6) can be seen as a distortion of the far-field pattern

$$\begin{bmatrix} f_{mc}^1(\varphi) \\ f_{mc}^2(\varphi)\end{bmatrix} = \begin{bmatrix} c+d\cdot e^{j\tau} \\ c+d\cdot e^{-j\tau}\end{bmatrix} \quad (7)$$

Referring to [12], the mean received power is defined as

$$P_i = \int_{\pi+\varphi_0}^{\pi+\varphi_0}\left|f_i(\varphi)\right|^2 p(\varphi)d\varphi \quad (8)$$

where $p(\varphi)$ is the power azimuth spectrum of the incoming waves, and φ_0 is the mean angle-of-arrival. Substituting (6) into (8) we obtain

$$\begin{aligned}\mathrm{P}_1 &= \int_{\pi+\varphi_0}^{\pi+\varphi_0}\left|f_{\mathrm{mc}}^1(\varphi)\right|^2 p(\varphi)d\varphi\\ &= \int_{\pi+\varphi_0}^{\pi+\varphi_0}\left(|c|^2+|d|^2+c\cdot e^{-j\tau}\cdot d^*+c^*\cdot d\cdot e^{j\tau}\right)p(\varphi)d\varphi\\ &= |c|^2\cdot\int_{\pi+\varphi_0}^{\pi+\varphi_0}\left(1+|g|^2+g^*\cdot e^{-j\tau}+g\cdot e^{j\tau}\right)p(\varphi)d\varphi\\ &= |c|^2\cdot\left(1+|g|^2+2\cdot\int_{\pi+\varphi_0}^{\pi+\varphi_0}\mathrm{Re}\left\{g\cdot e^{j\tau}\right\}p(\varphi)d\varphi\right)\\ &= |c|^2\cdot\left(1+|g|^2+2\cdot\int_{\pi+\varphi_0}^{\pi+\varphi_0}\left[\mathrm{Re}\{g\}\cos(\tau)-\mathrm{Im}\{g\}\sin(\tau)\right]p(\varphi)d\varphi\right)\end{aligned} \quad (9)$$

where $g = d/c$ and $\mathrm{Im}\{\cdot\}$ denotes the imaginary part of a complex. Without the MC effect, the signal correlation α can be further expressed as

$$\begin{aligned}\alpha = R_{xx}+jR_{xy} &= \int_{\pi+\varphi_0}^{\pi+\varphi_0} -e^{j\tau}p(\varphi)d\varphi\\ &= \int_{\pi+\varphi_0}^{\pi+\varphi_0}\left[\cos(\tau)-j\sin(\tau)\right]p(\varphi)d\varphi\end{aligned} \quad (10)$$

The received power of antenna 1 is given in [7]

$$P_1' = |c|^2\cdot[1+|g|^2+\underbrace{2\cdot\mathrm{Re}\{g\}\cdot R_{xx}+2\cdot\mathrm{Im}\{g\}\cdot R_{xy}}_{\mathrm{B}}] \quad (11)$$

Calculated in Maple [13], variables c, d, and g can be obtained from the load and antenna impedances as follows:

$$c = \frac{z_L\left(z_L+z_{11}\right)}{\left(z_L+z_{11}\right)^2-z_{12}^2},\ d = \frac{z_L z_{12}}{\left(z_L+z_{11}\right)^2-z_{12}^2},\ g = d/c = \frac{z_{12}}{z_L+z_{11}} \quad (12)$$

We are interested in the underbraced part B in (11) to check if its numerator equals A in (3). First, g can be expanded as

$$\mathrm{B} = 2 \cdot \frac{R_{xx} \cdot \left[r_{12}\left(r_L + r_{11}\right) + x_{12}\left(x_L + x_{11}\right)\right] + R_{xy} \cdot \left[x_{12}\left(r_L + r_{11}\right) - r_{12}\left(x_L + x_{11}\right)\right]}{\left(z_L + z_{11}\right)^2} \tag{13}$$

$$P_1' = \left|\frac{z_L\left(z_L + z_{11}\right)}{\left(z_L + z_{11}\right)^2 - z_{12}^2}\right|^2 \cdot \left[1 + \left|\frac{z_{12}}{z_L + z_{11}}\right|^2 + 2 \cdot \frac{R_{xx} \cdot \left[r_{12}\left(r_L + r_{11}\right) + x_{12}\left(x_L + x_{11}\right)\right] + R_{xy} \cdot \left[x_{12}\left(r_L + r_{11}\right) - r_{12}\left(x_L + x_{11}\right)\right]}{\left(z_L + z_{11}\right)^2}\right]$$

$$= \frac{\left|z_L\right|^2 \cdot \left(\left|z_L + z_{11}\right|^2 + \left|z_{12}\right|^2 - 2\,\mathrm{Re}\left\{\alpha\left(z_L + z_{11}\right)z_{12}^*\right\}\right)}{\left|\left(z_L + z_{11}\right)^2 - z_{12}^2\right|^2} \tag{14}$$

$$g = \frac{z_{12}}{z_L + z_{11}}$$

$$= \frac{\left[r_{12}\left(r_L + r_{11}\right) + x_{12}\left(x_L + x_{11}\right)\right] + j\left[x_{12}\left(r_L + r_{11}\right) - r_{12}\left(x_L + x_{11}\right)\right]}{\left(z_L + z_{11}\right)^2} \tag{15}$$

Next, we substitute (13) into part B of (11) at the top of this page. We can see the numerator of (14) is exactly the same as A in (3). Now we plug (12) and (14) into (11), then the received power P_1' is simplified to (15) at the top of this page.

The difference between (1) and (15) is obvious that (1) is multiplied with factor $4r_{11}r_L$, while (15) with factor $|z_L|^2$. Which one is correct? We will compare the simulation results in the next Section and give further discussion.

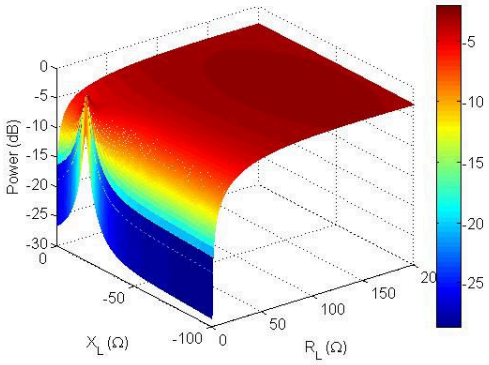

Fig. 2 3D received power of antenna 1 vs. load impedances using equation (1).

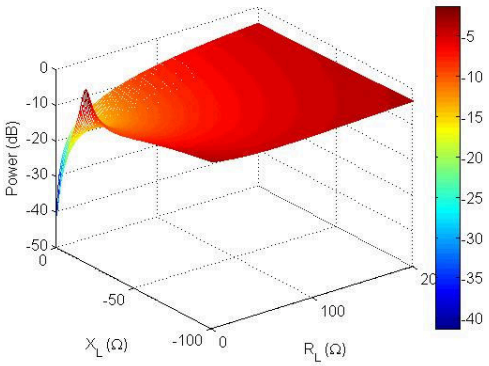

Fig. 3 3D received power of antenna 1 vs. load impedances using equation (15).

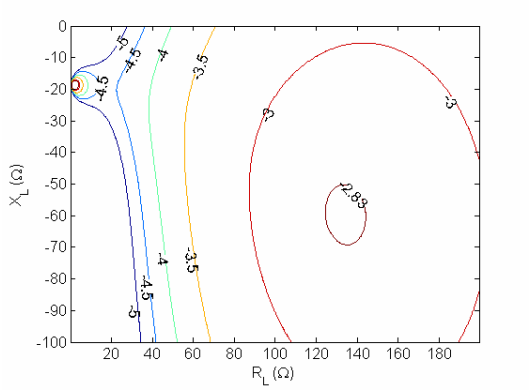

Fig. 4 The contour plot of received power of antenna 1 vs. load impedances using equation (1).

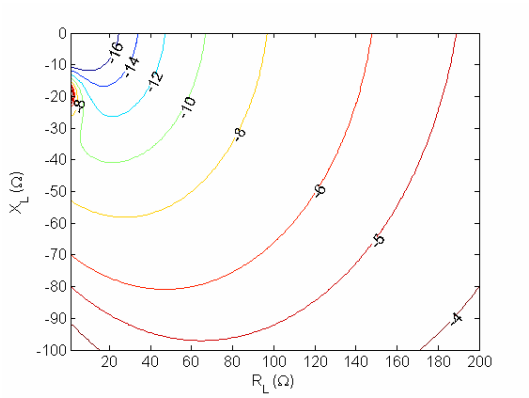

Fig. 5 The contour plot of received power of antenna 1 vs. load impedances using equation (15).

4 Simulation results and discussions

The differences of the simulation results between the receive power equations (1) and (15) are quite obvious in Fig. 2 and Fig. 3, even more clear in Fig. 4 and Fig. 5. In Fig. 2 and Fig. 4, the 'two maxima' phenomenon has already been proved experimentally in [8]. However as shown in Fig. 3 and Fig. 5, the two maxima in Fig. 4 are substituted by only one maximum point around (R_L, X_L) = (0, -18) Ω (one of the maximum points in Fig. 4). Another incorrect phenomenon in Fig. 3 and Fig. 5 is that when the resistance R_L approaches zero and the reactance X_L deviates from the matched point (-20 Ω), the received power should decrease as in Fig. 2 rather than increase in Fig. 3 because the power is stored not received from the circuit theory point of view.

The incorrectness of (15) is not due to the fact that it has not been normalized to the single antenna case, otherwise the output correlation α can not be in the range [0,1]. It is because when the matching networks are considered, the calculation of received power should only count in the voltage span over the resistance rather than that over the whole impedance. If we modify equation (15) by multiplying by the correction factor $4r_{11}r_L / |z_L|^2$, Fig. 3 and Fig. 5 will display exactly as Fig. 2 and Fig. 4. The output correlation computed using both methods in Section 3 will be identical as the factors $4r_{11}r_L$ and $|z_L|^2$ can be eliminated by the division operation.

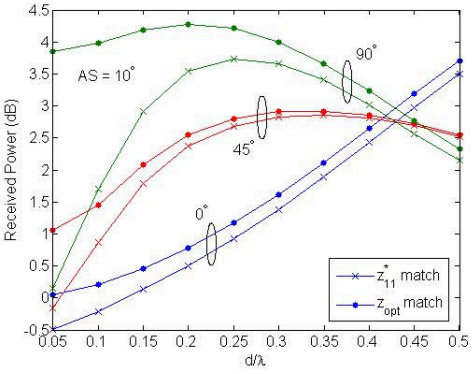

Fig. 6 The total received power as a function of antenna spacings with fixed angular spread and various angle of arrivals.

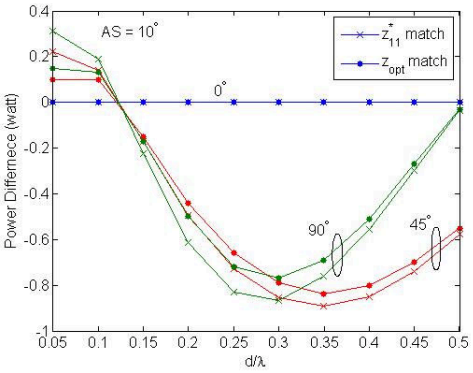

Fig. 7 The power difference as a function of antenna spacings with fixed angular spread and various angle-of-arrivals.

Next the advantage of using the impedance to maximize the received power (z_{opt}) rather than the self-conjugate match (z_{11}^*) is presented (note that the z_{opt} for each scenario is different). We assume the angle-of-arrival (AOA) at the receive end is Laplacian distributed as often assumed, e.g. [14]. In our simulation, we fix the angular spread AS = 10°, and the AOA is chosen as 0°, 45°, 90°. Only compact receive arrays are considered, so $d < 0.5\lambda$. Both the total received power using z_{opt} and z_{11}^* of each scenario are plotted in Fig. 6. Generally, for antenna spacing $d < 0.42\lambda$ and AOA = 90°, the receive array gets the highest power compared to other incident directions of AOA. The received power for AOA = 0° increases approximately linearly as d increases to 0.5λ on account of the mutual coupling (MC) effect. For AOA = 45° the highest received power is obtained at $d = 0.3\lambda$ due to MC and afterwards starts to decrease due to the lesser effect of MC. The same phenomenon is found for AOA = 90° and the highest received power happens at $d = 0.2\lambda$ for the z_{opt} case and $d = 0.26\lambda$ for the z_{11}^* case. For each AOA scenario, the z_{opt} match always offers higher received power compared to the z_{11}^* match at identical d of about 0.5dB for AOA = 0°, 1.1dB for AOA = 45°, 3.9dB for AOA = 90°, and even for $d > 0.5\lambda$ for AOA = 0° and 45°.

As good diversity performance requires the total received power to be distributed evenly at each receive branch, the power difference between the two antennas is depicted in Fig. 7. In general, the power difference of AOA = 0° is always zero as the receive model is symmetric. For AOA = 45° and 90°, the power differences first drop before $d < 0.12\lambda$, and then increase till $d = 0.35\lambda$ for AOA = 45°, $d = 0.3\lambda$ for AOA = 90°, then drop again till $d = 0.5\lambda$. Interestingly, we find the power difference of AOA = 90° is much smaller than that of AOA = 45° for $d \in [0.35\lambda, 0.5\lambda]$ (similar as in [7]). For each AOA scenario, the z_{opt} match always provides lower power difference compared to the z_{11}^* match at identical d.

Comparing Fig. 6 and Fig. 7 we can observe that although higher total received power is achieved at $d \in [0.2\lambda, 0.3\lambda]$ for AOA = 45° and 90°, the power differences are very large at that range, which can not be accepted for good diversity requirements in MIMO systems. Moreover, the power difference is nigligible for AOA = 0°, but the received power is very low for small antenna spacings. However, as we can see from Fig. 6 and Fig. 7, at $d \in [0.1\lambda, 0.2\lambda]$, the received power increases significantly when AOA departs from 0°, and also the power difference is small within that range. This is the desirable range of d for the two-element compact receive array especially in MIMO systems with no line-of-sight components.

5 Conclusion

In this paper we examined the correct received power expression with various matching impedances analytically and numerically for a compact two-element half-wavelength dipole receive array. The total received power and power difference of different antenna spacings and angles-of-arrival have been explored as well. We conclude that utilizing the matching impedances which maximize the total received power for compact receive arrays promises higher power collection and lower power difference with any antenna spacing and angle-of-arrival. The values [0.1λ, 0.2λ] are the range of the desirable antenna spacings to fulfil a good diversity performance in MIMO systems with no line-of-sight components. The optimum antenna spacing for receive arrays with more antenna elements can be studied for future work.

Acknowledgements

The authors would like to thank Dr. Buon Kiong (Vincent) Lau, Radio Systems Group & Electromagnetic Theory Group, Department of Electroscience, Lund University, Sweden for motivating this work and for many useful discussions.

The project is supported by Scottish Funding Council for the Joint Research Institute with the Heriot-Watt University (a part of the Edinburgh Research Partnership).

References

[1] J. Winters, "On the Capacity of Radio Communication Systems with Diversity in a Rayleigh Fading Environment," *IEEE Journal on Selected Areas in Communications*, vol. 5, pp. 871-878, Jun. 1987.

[2] I. E. Telatar, "Capacity of multi-antenna Gaussian channels," *European Transactions on Telecommunications*, vol. 10, pp. 585-595, 1999.

[3] G. J. Foschini and M. J. Gans, "On limits of wireless communications in a fading environment when using multiple antennas," *Wireless Personal Communications*, vol. 6, pp. 311-335, Mar. 1998.

[4] B. K. Lau, S. M. S. Ow, G. Kristensson, and A. F. Molisch, "Capacity analysis for compact MIMO systems," in *Proceedings of IEEE 61st Vehicular Technology Conference (VTC05'-Spring)*, vol. 1, pp. 165-170, 2 May-1 Jun. 2005.

[5] J. W. Wallace and M. A. Jensen, "Termination-dependent diversity performance of coupled antennas: network theory analysis," *IEEE Transactions on Antennas and Propagation*, vol. 52, no. 1, pp. 98-105, Jan. 2004.

[6] J. B. Andersen and B. K. Lau, "On closely coupled dipoles in a random field," *IEEE Antennas and Wireless Propagation Letters*, vol. 5, no. 1, pp. 73-75, 2006.

[7] X. Li and Z.-P. Nie, "Mutual coupling effects on the performance of MIMO wireless channels," *IEEE Antennas and Wireless Propagation Letters*, vol. 3, pp. 344-347, 2004.

[8] Y. Fei, B. K. Lau, A. Sunesson, A. J. Johansson, J. B. Andersen, and J. S. Thompson, "Experiments of closely coupled monopoles with load matching in a random field," in *Proceedings of 1st European Conference of Antenna and Propagation (EUCAP'06)*, Nov. 2006.

[9] I. J. Gupta and A. A. Ksienski, "Effect of mutual coupling on the performance of adaptive arrays," *IEEE Transactions on Antennas and Propagation*, vol. AP-31, no. 5, pp. 785-791, Sept. 1983.

[10] S.-K. Yong, "Compact antenna arrays for mobile communications," Ph.D. dissertation, the University of Edinburgh, Dec. 2003.

[11] T. Svantesson and A. Rnheim, "Mutual coupling effects on the performance of MIMO wireless channels," *IEEE International Conference on Acoustics, Speech, and Signal Processing (ICASSP01')*, pp. 2485-2488, 2001.

[12] W. L. Stutzman and G. A. Thiele, *Antenna Theory and Design*, 2nd ed. New York: Wiley, 1998..

[13] Maple. [Online]. Available: www.maplesoft.com

[14] A. Forenza, D. J. Love and R. W. Heath, "Simplified spatial correlation models for clustered MIMO channels with different array configurations," *IEEE Transactions on Vehicular Technology*, in press.

THE CAPACITY OF MATCHED COMPACT LINEAR ANTENNA ARRAYS

Yuanyuan Fei and John S. Thompson

Institute for Digital Communications, Joint Research Institute for Signal & Image Processing
School fo Engineering & Electronics, the Univeristy of Edinburgh
Edinburgh, EH9 3JL, UK
Email: y.fei@ed.ac.uk, john.thompson@ed.ac.uk
Fax: +44-131-6506554

Keywords: MIMO, Z-parameter, ergodic capacity.

Abstract

Measuring the performance of compact MIMO receive antennas is always a critical issue in wireless communication studies. Plenty of work has been done to improve the system performance including introducing proper matching networks at the receive end. In this paper, we derive a network MIMO system model from Z-parameter point of view containing arbitrary matching networks. It is the first time that system level simulations of MIMO capacity of $N\times N$ ($N\geq 2$) configuration with various matching networks have been examined. The MIMO performance can always be improved for large system configurations by introducing suitable matching networks for compact antenna arrays.

1 Introduction

The comprehensively studied multiple-input multiple-output (MIMO) systems promise significant gains in spectrum efficiency and link reliability by deploying multiple antennas at both ends of a wireless link [1],[2],[3]. The more antenna elements are packed at both link ends, the better performance we can obtain from MIMO systems [4]. It is easy to add multiple antennas at the base station end to promise better performance according to MIMO constructions. However, integrating multi-antenna elements at the subscriber end is hard to realize as when the antenna spacing less than half wavelength, performance degradation will occur due to the mutual coupling (MC) effect [3]. This is important since the space is limited in palm-size devices. If the performance of the compact arrays (antenna spacing less than half wavelength) can be improved, it is possible to increase the number of transmit antennas at the base station end as well. Then higher link performance can be achieved.

Plenty of research has been done on both compact receive arrays and MIMO system performance. Some claim that MC plays an active part in MIMO systems [5],[6], while some believe that MC is detrimental to MIMO performance [7],[8]. These conflicing conclusions are mainly due to either different MIMO system models being assumed or that the channel models were normalized in different ways. Two major publications [9],[10] present the relations between compact receive arrays and MIMO performance using S-parameters in n-port theory [11]. In [10] the authors emphasize that introducing matching networks to compact receive arrays can improve the MIMO capacity significantly for very close antenna spacing which has attracted a lot of attention [12],[13]. Similar studies of compact receive arrays in MIMO systems with matching networks using the intuitive Z-parameter have also been carried out in [7],[14],[15]. However, none of them give a system-level study or a precise channel matrix with MC effect or the results of MIMO capacity studies containing a compact receive array of more than two elements.

In this paper, a complete study of compact receive arrays with various matching networks using Z-parameters in MIMO systems is presented. The precise modified MIMO channel matrix including the MC effect is provided. Also MIMO capacities of configuration $N\times N$ ($N\geq 2$) with various matching loads as a function of different antenna spacings and/or with different signal-to-noise ratio (SNR) level are explored.

The reminder of the paper is organized as follows. Section 2 describes the MIMO system model we assume. Section 3 gives the network model and the derivation of the channel matrix with the MC effect included. Simulation results of capacities for different MIMO configurations with matching networks are discussed in Section 4. Conclusions are presented in Section 5.

2 MIMO system model

A narrowband MIMO system with an antenna array of size N at both ends is considered in this paper. We assume the channel is flat, rich scattering, and without a line-of-sight propagation component. The total average energy at the transmitter over one symbol period is P. Then the input-output relation for a symbol period is [4]

$$\mathbf{y} = \sqrt{P/N}\mathbf{H}\mathbf{x} + \mathbf{v} \tag{1}$$

where $\mathbf{y} = [y_1, \ldots, y_N]^T$, $\mathbf{x} = [x_1, \ldots, x_N]^T$ are the received signal vector and the transmitted signal vector, respectively. The notation ^{T} is the vector transpose operator. $\mathbf{H}$ represents the MIMO channel with dimension $N\times N$. Under all the above assumptions, $\mathbf{H}$ is composed of independent zero mean circularly symmetric complex Gaussian random variables [4].

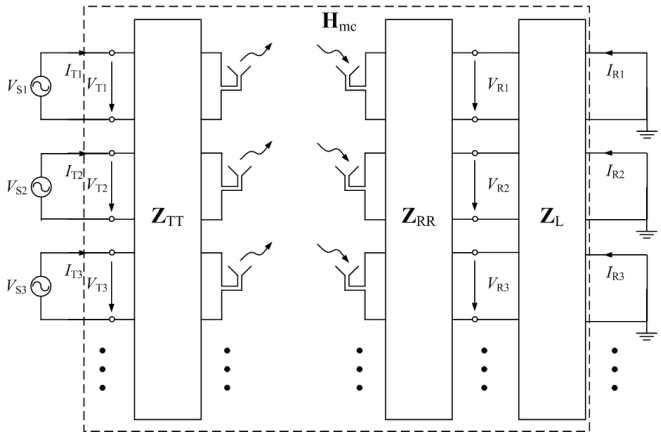

Fig. 1 Diagram of a MIMO system with antenna impedance matrices and matching networks at the receive end.

The additive Gaussian noise vector is $\mathbf{v} = [v_1, \ldots, v_N]^T$ with the covariance matrix $E\{\mathbf{v}\mathbf{v}^H\} = N_0\mathbf{I}$. The superscript ^{H} is the conjugate transposition while $E\{\cdot\}$ denotes the expectation operator. $\mathbf{I}$ is an $N\times N$ identity matrix. Now we can focus on the direct impact of mutual coupling (MC) of the compact receive end on the MIMO channel $\mathbf{H}$ excluding other possible factors which would affect the channel performance.

3 Z-parameter network analysis

We further assume that the transmit antennas are spaced far apart with no MC, rich scattering and self-conjugate matching, which indicate that there is no correlation at the transmit end. However, the receive end is extremely compact with element spacings less than half wavelength but with various matching networks used. According to the *n*-port theory, the channel transfer function between transmit and receive arrays as shown in Fig. 1 can be represented by the Z-parameter matrix as [14]

$$\begin{bmatrix}\mathbf{v}_T\\ \mathbf{v}_R\end{bmatrix} = \begin{bmatrix}\mathbf{Z}_{TT} & \mathbf{Z}_{TR}\\ \mathbf{Z}_{RT} & \mathbf{Z}_{RR}\end{bmatrix}\begin{bmatrix}\mathbf{i}_T\\ \mathbf{i}_R\end{bmatrix} \tag{2}$$

where $\mathbf{v}_T = [V_{T1}, \ldots, V_{TN}]^T$, $\mathbf{i}_T = [I_{T1}, \ldots, I_{TN}]^T$ are the voltage and current vectors at the transmit end, respectively. Similarly, $\mathbf{v}_R = [V_{R1}, \ldots, V_{RN}]^T$, $\mathbf{i}_R = [I_{R1}, \ldots, I_{RN}]^T$ denote the voltages and currents at the receive end. The $N\times N$ diagonal matrices $\mathbf{Z}_{TT}$ and $\mathbf{Z}_{RR}$ are both antenna impedance matrices containing the self and mutual impedances of the transmit end and receive end, respectively. The $N\times N$ matrix $\mathbf{Z}_{RT}$ can be translated as the trans-impedance matrix [10] due to the impact of transmit end currents on the receive end voltages. We assume $\mathbf{Z}_{TR} = 0$ to imply that the transmitters have no knowledge about the channel conditions to the receivers.

In the compact receive subsystem of Fig. 1, an $N\times N$ impedance matching network $\mathbf{Z}_L$ is added after the receive antennas to compensate the MC induced power deduction. Based on the circuit theory, it is easy to obtain

$$\mathbf{v}_R = -\mathbf{Z}_L\mathbf{i}_R \tag{3}$$

at the receive subsystem. Substituting (3) into (2) we get the receive voltage $\mathbf{v}_R$ as a function of the transmit voltage $\mathbf{v}_T$

$$\mathbf{v}_R = \underbrace{\left(\mathbf{I} + \mathbf{Z}_{RR}\mathbf{Z}_L^{-1}\right)^{-1}\mathbf{Z}_{RT}\mathbf{Z}_{TT}^{-1}}_{\mathbf{H}_v}\mathbf{v}_T = \mathbf{Z}_L\underbrace{\left(\mathbf{Z}_L + \mathbf{Z}_{RR}\right)^{-1}\mathbf{Z}_{RT}\mathbf{Z}_{TT}^{-1}}_{-\mathbf{i}_R}\mathbf{v}_T\,. \tag{4}$$

where $\mathbf{H}_v$ is the channel/voltage transfer matrix [14]. Because only the voltage across the resistance can be exploited by the receiver, $\mathbf{H}_v$ has to be modified to fulfil the power transfer requirement. We define $\mathbf{Z}_{L+R} = \mathbf{Z}_L + \mathbf{Z}_{RR}$, and substitute $\mathbf{i}_R$ of (4), then the average total received power of the MIMO system is

$$\begin{aligned} P_R &= E\left\{Tr\left(\mathrm{Re}\left\{\mathbf{Z}_L\mathbf{i}_R\mathbf{i}_R^H\right\}\right)\right\}\\ &= E\left\{Tr\left(\mathrm{Re}\left\{\mathbf{Z}_L\right\}\mathbf{Z}_{L+R}^{-1}\mathbf{Z}_{RT}\mathbf{Z}_{TT}^{-1}\mathbf{v}_T\mathbf{v}_T^H\mathbf{Z}_{TT}^{-H}\mathbf{Z}_{RT}^H\mathbf{Z}_{L+R}^{-H}\right)\right\}\\ &= E\left\{Tr\left(\mathbf{Y}_L\mathbf{Z}_{L+R}^{-1}\mathbf{Z}_{RT}\mathbf{Z}_{TT}^{-1}\mathbf{v}_T\mathbf{v}_T^H\mathbf{Z}_{TT}^{-H}\mathbf{Z}_{RT}^H\mathbf{Z}_{L+R}^{-H}\mathbf{Y}_L^H\right)\right\} \end{aligned} \tag{5}$$

where $\mathbf{Y}_L = (\mathbf{Z}_L + \mathbf{Z}_L^H)^{1/2} \;/\; \sqrt{2}$.

The average total transmitted power will be

$$P_T = E\left\{Tr\left(\mathrm{Re}\left\{\mathbf{Z}_{TT}\mathbf{i}_T\mathbf{i}_T^H\right\}\right)\right\} = E\left\{Tr\left(\mathbf{Y}_T\mathbf{Z}_{TT}^{-1}\mathbf{v}_T\mathbf{v}_T^H\mathbf{Z}_{TT}^{-H}\mathbf{Y}_T^H\right)\right\} \tag{6}$$

where $\mathbf{Y}_T = (\mathbf{Z}_{TT} + \mathbf{Z}_{TT}^H)^{1/2} \;/\; \sqrt{2}$. If only the receiver knows the channel conditions, P_T can be evenly distributed at the transmit end. Then (5) becomes

$$P_R = E\left\{Tr\left(\mathbf{H}_{mc}\frac{P_T}{N}\mathbf{I}\mathbf{H}_{mc}^H\right)\right\} \tag{7}$$

where $\mathbf{H}_{mc}$ is the channel transfer matrix between the transmitter and the receiver load including the MC effect as shown in Fig. 1. We assume identical antenna elements are

used in the whole system model, thereby all the matrices in (6) are symmetric. Equation (6) can be substituted into (7)

$$P_R = \frac{1}{N} E\left\{Tr\left(\mathbf{H}_{mc}\mathbf{Y}_T\mathbf{Z}_{TT}^{-1}\mathbf{v}_T\mathbf{v}_T^H\mathbf{Z}_{TT}^{-H}\mathbf{Y}_T^H\mathbf{H}_{mc}^H\right)\right\} \quad (8)$$

Comparing (5) and (8) we have

$$\mathbf{H}_{mc} = \mathbf{Y}_L\mathbf{Z}_{L+R}^{-1}\mathbf{Z}_{RT}\mathbf{Y}_T^{-1} \quad (9)$$

From the definition of $\mathbf{Z}_{RT}$ and the expression in [10], it is apparent that $\mathbf{Z}_{RT}$ modifies the identical, independently distributed channel matrix $\mathbf{H}$ by introducing far-field pattern distortion at the coupled receive end. Hence, the matrix product $\mathbf{Z}_{RT}\mathbf{Z}_{RT}^H$ defines the MC induced correlation

$$E\left\{\mathbf{Z}_{RT}\mathbf{Z}_{RT}^H\right\} = c\mathbf{\Psi}_R \quad (10)$$

where c is the average power gain of each channel branch (assuming the power gain of each branch is the same), $\mathbf{\Psi}_R$ is the $N\times N$ covariance matrix of the receive end [4] with $|(\mathbf{\Psi}_R)_{ij}| \le 1$, $|(\mathbf{\Psi}_R)_{ii}| = 1$, $i,j = 1,2,\ldots,N$. We assume $c = 1$ in this paper, then the MIMO channel should be normalized to the average channel gain of both link ends for the single antenna case. Consider a single-input single-output (SISO) system with both ends self-conjugate matched ($z_L = z_{11}^*$, where z_L and z_{11} is the load and self impedance of the antenna, respectively). Utilizing (5) and (8) we obtain

$$E\left\{hh^*\right\} = \frac{1}{4r_{11}^2} E\left\{z_{RT}z_{RT}^*\right\} \quad (11)$$

where h and z_{RT} are SISO channel and trans-impedance, respectively, and $r_{11} = \mathrm{Re}\{z_{11}\}$. The notation * denotes the conjugate operation for a complex number. After normalizing (10) by (11), (9) is modified to

$$\mathbf{H}_{mc} = 2\sqrt{r_{11}}\mathbf{Y}_L\mathbf{Z}_{L+R}^{-1}\mathbf{\Psi}_R^{1/2}\mathbf{H} \quad (12)$$

Under the equally distributed transmit power assumption, the narrowband MIMO capacity for the channel matrix given by (12) is denoted as

$$\begin{aligned} C_{mc} &= \log_2\det\left(\mathbf{I} + \frac{\rho_r}{N}\mathbf{H}_{mc}\mathbf{H}_{mc}^H\right) \\ &= \log_2\det\left(\mathbf{I} + \frac{4r_{11}\rho_r}{N}\mathrm{Re}\{\mathbf{Z}_L\}\mathbf{Z}_{L+R}^{-1}\mathbf{\Psi}_R^{1/2}\mathbf{H}\mathbf{H}^H\mathbf{\Psi}_R^{H/2}\mathbf{Z}_{L+R}^{-H}\right) \end{aligned} \quad (13)$$

where ρ_r is the reference SNR.

4 Simulation results and discussion

Several interesting simulation results have been obtained based on equation (13). For simplicity ideal half-wavelength dipoles are used in the model, and the self and mutual impedances are calculated by EMF method [16]. Note that the impedances of practical dipoles have been studied in [10],[12], and similar results have been obtained compared to the ideal case. Hence, the ideal dipole assumption will not affect the validity of our study. We also assume the uniform angle-of-arrive distribution, as a result the elements of the receive end correlation matrix $(\mathbf{\Psi})_{ij}$ can be computed by the zeroth Bessel Function [17]. The capacity performance of 2×2, 4×4, and 8×8 MIMO configurations are simulated with other parameters, e.g. reference SNR and antenna spacings. 5000 random channel realizations are deployed for each capacity result.

Fig. 2 plots the cumulative density function of the capacity performance of different MIMO configurations with matching networks. The antenna spacing is assumed to be 0.2 wavelengths and the SNR is 5dB. It is obvious that introducing matching networks into the compact receiver will definitely improve the system performance. Under fixed antenna spacing and SNR, the larger the MIMO system is, the more it can benefit from the matching networks. Interestingly, the system performance with full coupling performs better than with no coupling in this scenario for 4×4 MIMO configuration according to Fig. 2. It is true that the capacity performance of both cases overlaps with each other at some antenna spacings [12]. Shown to be the most efficient matching network, the multiport-conjugate match offers an impressive system improvement for 10% outage capacity of about 0.5 bits for 2×2 and 3 bits for 4×4 MIMO configurations over full coupling case. The widely used selfconjugate match also provides a better performance for 10% outage capacity of around 0.2 bits 0.2 bits for 2×2 and 1 bit for 4×4 MIMO configurations when compared to the system with full coupling. As a result, the multiport-conjugate match performs better than the self-conjugate match by about 0.3 bits for 2×2 and 2 bits for 4×4 case when measuring 10% outage capacity.

The ergodic capacity of various MIMO systems in different SNR scenarios is depicted in Fig. 3. Generally speaking, the MIMO performance for larger receive arrays without MC effect is better than the system with MC. With fixed antenna

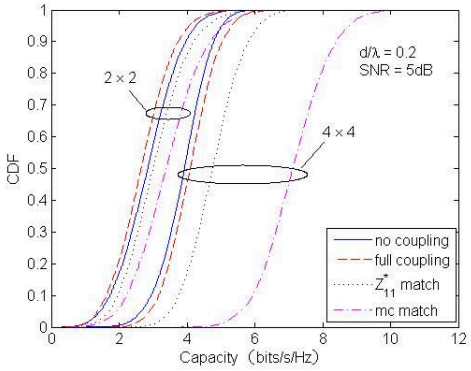

Fig. 2 The cumulative density function (CDF) of MIMO capacity with different configurations and matching networks. (The 'mc match' means multiport-conjugate match.)

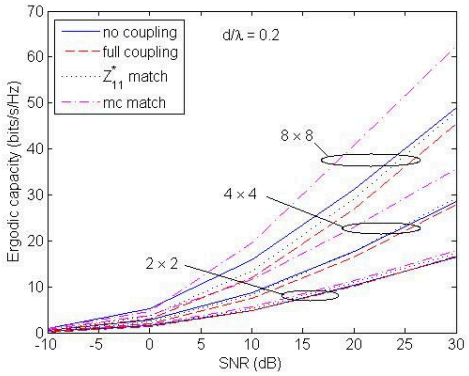

Fig. 3 Ergodic capacity as a function of signal-to-noise ratio of different MIMO configurations with matching networks.

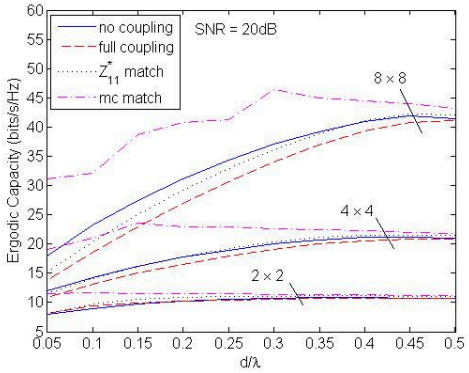

Fig. 4 Ergodic capacity of different configurations with matching networks vs. antenna spacings

spacing at $d = 0.2\lambda$, the matching network impact is much more effective in high SNR scenarios, while in low SNR scenarios improvements are still guaranteed by using matching networks. Among each MIMO configuration, the multiport-conjugate match gives more than 2 bits gain for 2×2, 7 bits for 4×4, and 15 bits for the 8×8 MIMO case at 30dB SNR when compared to the corresponding fully coupled systems. Meanwhile, the ergodic capacity of the self-conjugate matched systems performs better with higher SNRs as well by offering 1 bit benefit for 2×2, 2 bits for 4×4, and 4 bits for 8×8 MIMO configurations at 30dB SNR over the coupled cases.

In Fig. 4 we explore the MIMO performance with changing antenna spacing at 20dB SNR. We notice that it is harder to reach the full capacity performance except with the multiport-conjugate match due to the compact array size of larger system configuration. For example, although the 2×2 system capacity is much lower than the 8×8 system, it approaches the full capacity around $d = 0.2\lambda$, while for 8×8 system it does not happen until $d = 0.45\lambda$. However, the self-conjugate match still promises a significant performance advantage over the full coupling case within the whole spacing range of about 1 bit for 2×2, 2 bits for 4×4 and 3 bits for 8×8 MIMO configurations. The multiport-conjugate match does not either increase smoothly or has the same increasing trend of other matching conditions with the MIMO configuration growing up. Similar phenomenon has been found in [10] even for the 2×2 case, which can be explained by the super-directivity characteristics of the array [18]. However, the multiport-conjugate match achieves the full capacity performance much quicker than other matching cases, e.g. $d = 0.05\lambda$ for 2×2 case, $d = 0.15\lambda$ for 4×4 case, and $d = 0.3\lambda$ for 8×8 case. It also indicates that the multiport-conjugate match performs much better than other matching conditions. For example, in Fig. 4 at $d = 0.1\lambda$, the ergodic capacity with multiport-conjugate match is 3 bits higher for 2×2, 7 bits for 4×4, and 14 bits for 8×8 cases compared to the full coupling systems.

As it is shown in all the simulation results, the multiport-conjugate match performs much better than the self-conjugate match for larger antenna configuration when antenna spacing and SNR are fixed, for higher SNR with the same antenna configuration and SNR, and for smaller antenna spacing of each antenna configuration and fixed SNR. It is proved to have the lossless power transfer from the receivers to the loads [10]. However, it is difficult to realize due to multiple matching loads have to be implemented into each receive circuit [19]. Although in [12],[20] the authors have reported the design of the multiport-conjugate match in theory, they also confirmed multiple loads have to be added to achieve the optimum performance, and no experimental setup has backed up to the theoretical studies. In this case, the self-conjugate match is a good candidate for practical implementation as they are able to offer a stable improvement of MIMO performance compared to fully coupled case and easier to achieve in practice than the multiport-conjugate match.

5 Conclusion

In this paper, a network model for MIMO systems with a compact receiver is presented using Z-parameters. Both mutual coupling effect and matching network components are included. The precise channel transfer matrix is given and is backed up with simulation analysis. Adding matching networks into compact MIMO receivers always enhances the system performance. The larger the system configuration using the matching networks, the higher system improvement would be, especially in high SNR scenarios. The multiport-conjugate match significant performance improvements in all cases examined here. Compared to the fully coupled receiver, the self-conjugate match also offers performance improvements under any circumstances and it is easier to achieve in practice than the multiport-conjugate match. Experimental setups can be implemented to support the theoretical study.

Acknowledgements

The authors would like to thank Dr. Buon Kiong (Vincent) Lau, Radio Systems Group & Electromagnetic Theory Group, Department of Electroscience, Lund University, Sweden for motivating this work and for many useful discussions.

The project is supported by Scottish Funding Council for the Joint Research Institute with the Heriot-Watt University (a part of the Edinburgh Research Partnership).

References

[1] J. Winters, "On the Capacity of Radio Communication Systems with Diversity in a Rayleigh Fading Environment," *IEEE Journal on Selected Areas in Communications*, vol. 5, pp. 871-878, Jun. 1987.

[2] I. E. Telatar, "Capacity of multi-antenna Gaussian channels," *European Transactions on Telecommunications*, vol. 10, pp. 585-595, 1999.

[3] G. J. Foschini and M. J. Gans, "On limits of wireless communications in a fading environment when using multiple antennas," *Wireless Personal Communications*, vol. 6, pp. 311-335, Mar. 1998.

[4] A. Paulraj, R. Nabar, and D. Gore, *Introduction to space-time wireless communications*, 1st ed. Cambridge, UK: Cambridge University Press, 2003.

[5] T. Svantesson and A. Tanheim, "Mutual coupling effects on the capacity of multielement antenna systems," in *Proceedings of IEEE International Conference on Acoustics, Speech, and Signal Processing (ICASSP01')*, vol. 4, pp. 2485-2488, 7-11 May 2001.

[6] V. Jungnickel, V. Pohl, and C. von Helmolt, "Capacity of MIMO systems with closely spaced antennas," *IEEE Communications Letters*, vol. 7, no. 8, pp. 361-363, August 2003.

[7] R. Janaswamy, "Effect of element mutual coupling on the capacity of fixed length linear arrays," *Antennas and Wireless Propagation Letters*, vol. 1, no. 8, pp. 157-160, 2002.

[8] M. K. Ozdemir, E. Arvas, and H. Arslan, "Dynamics of spatial correlation and implications on MIMO systems," *IEEE Communications Magazine*, vol. 42, no. 6, pp. S-14-S19, June 2004.

[9] C. Waldschmidt, S. Schulteis, and W. Wiesbeck, "Complete RF system model for analysis of compact MIMO arrays," *IEEE Transactions on Vehicular Technology*, vol. 53, no. 3, pp. 579-586, May 2004.

[10] J. W. Wallace and M. A. Jensen, "Mutual coupling in MIMO wireless systems: a rigorous network theory analysis," *IEEE Transactions on Wireless Communications*, vol. 3, no. 4, pp. 1317-1325, July 2004.

[11] C. Waldschmidt, C. Kuhnert, M. Pauli, and W. Wiesbeck, "Handy MIMO," *IEE Communications Engineer*, pp. 22-23, February/March 2005.

[12] S. Ow, "Impact of mutual coupling on compact MIMO systems," Master's thesis, Lund University, Lund, Sweden, March 2005.

[13] B. K. Lau, S. Ow, G. Kristensson, and A. F. Molisch, "Capacity analysis for compact MIMO systems," in *Proceedings of IEEE 61st Vihecular Technology Conference (VTC'05-Spring),* vol. 1, pp. 165-170, May-June 2005.

[14] N. Chiurtu, B. Rimoldi, E. Telatar, and V. Pauli, "Impact of correlation and coupling on the capacity of MIMO systems," in *Proceedings of 3rd IEEE International Symposium on Signal Processing and Information Technology (ISSPIT'03),* pp. 154-157, 2003.

[15] B. K. Lau and J. B. Andersen, "On closely coupled dipoles with matching networks in a random field," in *Proceedings of 17th IEEE International Symposium on Personal, Indoor and Mobile Radio Communications (PIMRC06')*, pp. 1-5, September 2006.

[16] C. A. Balanis, *Antennas theory*, 2nd ed., S. Eliot, Ed. USA: John Wiley & Sons, Inc, 1997.

[17] J. Salz and J. H. Winters, "Effect of fading correlation on adaptive arrays in digital mobile radio," *IEEE Transactions on Vehicular Technology*, vol. 43, no. 4, pp. 1049-1057, November 1994.

[18] R. Harrington, "Antenna excitation for maximum gain," IEEE Transactions on Antennas and Propagation, vol. AP-13, pp. 896-903, November 1965.

[19] W. C.-Y. Lee, "Mutual coupling effect on maximum-ratio diversity combiners and application to mobile radio, *IEEE Transactions on Communications Technology*, vol. Com-18, no. 6, pp. 779-791, December 1970.

[20] S. Dossche, J. Romeu and S. Blanch, "Optimum antenna matching to minimise signal correlation on a two-port antenna diversity system," *Electronics Letters*, vol. 40, pp. 1164-1165, 2004.

The 18th Annual IEEE International Symposium on Personal, Indoor and Mobile Radio Communications (PIMRC'07)

MIMO SYSTEM SENSITIVITY AND COUPLED ARRAY DESIGN

Yuanyuan Fei and John S. Thompson
Institute for Digital Communications
Joint Research Institute for Signal & Image Processing
School of Engineering & Electronics
the University of Edinburgh
Edinburgh, EH9 3JL, UK

ABSTRACT

Recent theoretical and simulation studies reveal that closely coupled antennas with appropriately chosen impedance matching loads can yield desirable MIMO capacity. The performance sensitivity of a 2×2 MIMO system with coupled half-wavelength dipoles and single-port decoupling matching networks is presented in this paper. We show that the optimal single-port matching impedance in the sense of maximizing capacity exists for various small antenna spacings. It is a promising approach to improve the compact array performance. The sensitivities of MIMO capacity with matching networks to antenna spacing and antenna structures are also discussed.

I INTRODUCTION

Multiple-input multiple-output (MIMO) systems received worldwide attention in the past ten years due to their ability to increase system efficiency significantly by using multi-antennas at both ends of a wireless communication link [1], [2]. Nevertheless, as early as in [1], it has already been mentioned that the integration of MIMO technique into compact devices is restricted if the antenna spacing is below half a wavelength. Strong mutual coupling (MC) between closely spaced antenna elements also results in changes in antenna patterns (thus antenna correlation) and loss of antenna efficiency [3].

Intuitively, MC has a detrimental effect on MIMO systems [4]. However, it is claimed in [5, 6] that MC can increase the MIMO performance under some circumstances. Recent studies [7, 8] showed that the capacity of coupled antennas can be greatly improved by introducing proper matching networks into the multiple antenna system using S-parameter network theory and clarified that the multiport-conjugate match is the optimal matching technique to improve the performance of power/capacity for compact MIMO arrays. Nevertheless, it is not feasible to integrate this solution into MIMO systems as N loads are needed at each port for N coupled antennas, which increases the design volume and the chance of mismatch. As a result, the single-port match is still an attractive if suboptimal solution. Actually, some experimental implementation has already tried to demonstrate the maximum power collection by introducing the single-port matching [9] based on [10]. In [11], the relationship between various load impedances and MIMO capacity is investigated for antenna spacing $d = 0.05\lambda$, and the 'single maximum' characteristic of capacity as a function of matching impedances has already been discovered. In our study we will expand the investigation to different antenna spacings, and explore the sensitivity of MIMO system performance to the coupled array design with single-port matching networks.

The remainder of this paper is organized as follows. Section II gives the MIMO system model. Section III provides simulation results, and focuses on MIMO system sensitivity analysis with antenna spacing, optimal single-port matching and antenna structure. Conclusions are given in Section IV.

The project is supported by Scottish Funding Council for the Joint Research Institute with the Heriot-Watt University (a part of the Edinburgh Research Partnership).

II MIMO SYSTEM MODEL

A MIMO system with N transmit and N receive antennas is considered in this paper. For simplicity it is assumed that the channel is frequency-flat fading, and the total average energy at the transmitter over one symbol period is P. The input-output relation for a symbol period is [12]

$$\mathbf{y} = \sqrt{P/N}\mathbf{H}\mathbf{x} + \mathbf{v} \tag{1}$$

where $\mathbf{y} = [y_1, ..., y_N]^T$, $\mathbf{x} = [x_1, ..., x_N]^T$ are the received signal vector, the transmitted signal vector, respectively. $\mathbf{H}$ represents the MIMO channel with dimension $N \times N$, and the additive Gaussian noise vector is $\mathbf{v} = [v_1, ..., v_N]^T$ with the covariance matrix $E\{\mathbf{v}\mathbf{v}^\dagger\} = N_0\mathbf{I}$. The superscript † means the conjugate transposition while $E\{\cdot\}$ denotes the expectation operator. Finally, $\mathbf{I}$ is an $N \times N$ identity matrix.

A Capacity of MIMO channels

We assume that $\mathbf{H}$ has no preferred transmit direction, and is perfectly knowThis implies the optimum transmit signals to maximize capacity are independent and equal-powered at the transmit antennas [12]. In information theory, we can calculate the narrowband MIMO Shannon capacity as [1]

$$C = \log_2 \left| \mathbf{I} + \frac{\rho}{N}\mathbf{H}\mathbf{H}^\dagger \right| \tag{2}$$

where ρ is the signal-to-noise (SNR) ratio. Moreover, we assume the channel is rich-scattering at both ends, as well as the transmitters are far apart, $\mathbf{H}$ can be expressed by the semicorrelated Kronecker model [13]

$$\mathbf{H} = \mathbf{R}^{1/2}\mathbf{H}_{i.i.d.} \tag{3}$$

If the uniformly distributed arriving signal model in space is assumed, the receive end correlation matrix $\mathbf{R}$ has elements $r_{ii} = 1$ and $r_{ij} = J_0(2\pi d/\lambda)(i, j = 1, ..., N, i \neq j)$ [14],

The 18th Annual IEEE International Symposium on Personal, Indoor and Mobile Radio Communications (PIMRC'07)

where $J_0(\cdot)$, d, and λ are the zeroth Bessel function, the antenna spacing and the received signal wavelength respectively. $\mathbf{H}_{i.i.d.}$ is an $N \times N$ independent and identically Rayleigh distributed (i.i.d.) channel matrix.

B Mutual Coupling Coefficient

As compact receive antennas are considered with spacing $d < 0.5\lambda$, the MC effect becomes a crucial one to model. MC can be explained as an interaction caused by neighboring elements inducing extra voltages between each other. In port theory, the mutual impedance matrix $\mathbf{Z}$ is defined as

$$\mathbf{Z} = \begin{bmatrix} Z_{11} & Z_{12} & Z_{13} & \cdots \\ Z_{12} & Z_{22} & Z_{23} & \cdots \\ Z_{13} & Z_{23} & Z_{33} & \cdots \\ \vdots & \vdots & \vdots & \ddots \end{bmatrix} \quad (4)$$

where Z_{ii} is the self-impedance of the ith element and Z_{ij} means the mutual-impedance between the ith and jth elements. Here $Z_{ij} = Z_{ji}$ is based on the reciprocity theorem [15]. As previously published [7, 8], introducing specific load impedances into the antenna circuit can significantly increase the performance of MIMO systems. The matching-impedance matrix $\mathbf{Z_L}$ is given

$$\mathbf{Z_L} = \begin{bmatrix} Z_{L_1} & 0 & 0 & \cdots \\ 0 & Z_{L_2} & 0 & \cdots \\ 0 & 0 & Z_{L_3} & \cdots \\ \vdots & \vdots & \vdots & \ddots \end{bmatrix} \quad (5)$$

with element Z_{L_i} indicating the matching impedance in the ith antenna branch. If there is no MC between the matching impedances, the non-diagonal elements of $\mathbf{Z_L}$ are zero. The antenna elements are considered identical in the remainder of the paper, thus $Z_{ii} = Z_{11}$, $Z_{L_i} = Z_L$. By utilizing the voltage-current relations [16], the MC coefficient matrix is

$$\mathfrak{C}_{mc} = (\mathbf{Z} + \mathbf{Z_L})^{-1} = (\mathbf{Z} + Z_L \cdot \mathbf{I})^{-1} \quad (6)$$

C MIMO Capacity with Mutual Coupling

The MC effect at the receiver end can be easily included into the MIMO system [17] by

$$\mathbf{H}_{mc} = \mathfrak{C}_{mc}\mathbf{H} \quad (7)$$

where $\mathbf{H}_{mc}$ is the modified MIMO channel with MC. Suppose that the matching networks are perfectly lossless and the each transmitter is self-conjugate ($Z_{11}{}^*$) matched. Without the MC effect, the MIMO system will always have an antenna power gain of $4R_{11}R_L$ normalized to the self-conjugate matched single antenna case [10] for a 2×2 system, which should be included in the system evaluation as well. R_{11} and R_L are the resistances (real parts) of Z_{11} and Z_L, respectively. The modified MIMO capacity expression according to (2) is

$$C_m = \log_2 \left| \mathbf{I} + \frac{\rho_r \cdot 4R_{11}R_L}{N} \mathbf{H}_{mc}\mathbf{H}_{mc}{}^{\dagger} \right| \quad (8)$$

where ρ_r is the reference SNR of the system depending on N_0. Identical result has been derived in [11] though illuminated from a different perspective.

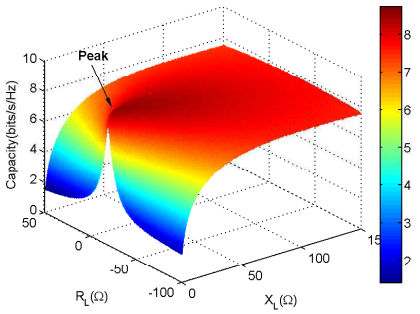

Figure 1: Ergodic capacity vs. the real and imaginary parts of Z_L at $d = 0.05\lambda$.

D Upper bound of MIMO Capacity

Define the ergodic capacity as $E\{C_m\}$. Using Jensen's inequality and the concavity of $\log|\cdot|$ [18], we obtain the upper bound C_{up} of the MIMO capacity at each impedance matching load point Z_{L_0} as

$$E\{C_m(\mathbf{X})|_{Z_L=Z_{L_0}}\} \leq C_{up} \quad (9)$$

where $\mathbf{X} = \mathbf{H}_{mc} \cdot \mathbf{H}_{mc}{}^{\dagger}$,

$$\begin{aligned} C_{up} &= C_m(E\{\mathbf{X}\})|_{Z_L=Z_{L_0}} \\ &= \log_2 \left| \mathbf{I} + \rho_r \cdot 4R_{11}R_{L_0} \cdot \mathfrak{C}_{mc}{}^{\dagger}\mathfrak{C}_{mc}\mathbf{R} \right| \end{aligned} \quad (10)$$

and R_{L_0} is the real part of Z_{L_0}. As we will see in Section III, C_{up} is very helpful for simplifying the evaluation of sensitivity of MIMO capacity to non-ideal impedance matching.

III Simulation and Analysis

To illustrate the impact of MC on MIMO systems, a basic 2×2 system configuration is simulated under the conditions presented in Section II. Identical ideal half-wavelength dipoles with infinite thin wire diameter are used at both ends since they are comprehensively studied and taken as references in the antenna field. Now we focus on the coupled receive end. Under the ideal assumption, the self-impedance $Z_{11} = 73 + j42.5\Omega$ is constant, and the mutual-impedance $Z_{12} = Z_{21}$ is calculated using the modified EMF method [1] [16]. For each load point Z_{L_0}, 10000 random channel realizations are deployed to estimate the MIMO system performance with $\rho_r = 20dB$.

A Capacity of Various Impedance Matching

As shown in Fig. 1, the 3-dimensional ergodic capacity surface is plotted with various matched impedances points $\{Z_{L_0} = R_{L_0} + jX_{L_0} : R_{L_0} \in R_L, X_{L_0} \in X_L\}$, where $R_L \in [0, 150]\Omega$,

[1] Infinite thin dipoles are assumed in EMF. Usually the dipole diameter is far less than its length, thus EMF is still practicable. Identical capacity results are given compared to real dipole cases in [7, 8].

The 18th Annual IEEE International Symposium on Personal, Indoor and Mobile Radio Communications (PIMRC'07)

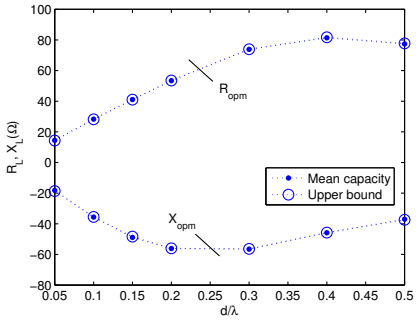

Figure 2: The optimal matching impedances $Z_{opm} = R_{opm} + jX_{opm}$ versus various antenna spacing for the mean capacity and upper bound capacity of the system with SNR $\rho_r = 20dB$.

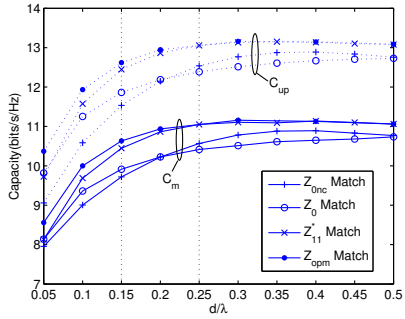

Figure 3: The mean capacity (dash line) and upper bound capacity (solid line) with various matching networks as a function of antenna spacing with SNR $\rho_r = 20dB$.

$X_L \in [-100, 50]\Omega$, and the physical meaning of X_{L_0} is the reactance of impedance Z_{L_0}. We take the $d = 0.05\lambda$ case as an example to demonstrate that the capacity performance is concave and resembles the received power characteristic in [10] except only one peak is observed with the changing of matching networks at one fixed d. For other antenna spacings less than 0.5λ, the surface of C_m has the similar properties.

B Optimal Single-Port Matching and Antenna Spacing

Although the multiport-conjuate matching is quite attractive to improve the compact array performance in MIMO systems [7], it is difficult to implement in practice given the current state of the art. Therefore, The single-port impedance matching which gives the best MIMO performance for a specific antenna spacing is worthwhile to investigate as a simpler alternative. Fig. 2 plots the optimal matching impedances Z_{opm} (the peak coordinates of Fig. 1) of various antenna spacings d for the mean capacity and the capacity upper bound of the system. As far as compact arrays are concerned, antenna spacings $d > 0.5$ are not considered due to the negligible MC effect. It is obvious that the simulation results agree very well for C_m and C_{up} cases as each dot is almost in the center of the circle it corresponds to. To illuminate how much we can benefit from the Z_{opm} matching, the mean capacity and upper bound capacity computed for ideal antennas with characteristic-impedance matching both with no coupling (Z_{0nc}) and with MC (Z_0), self-conjugate matching ($Z_{11}{}^*$), and Z_{opm} matching are depicted in Fig. 3. The coupled compact array with matching networks outperforms the array without MC at small spacing ($d < 0.2\lambda$). Meanwhile, Z_{opm} matching surpasses other matching schemes when $d < 0.25\lambda$. Another interesting phenomenon is the increasing trend/slope of C_m and C_{up} are nearly the same for different matching pairs with $d > 0.15\lambda$, which is very useful for the analysis of next step. We look back to Fig. 2. Despite of the superiority of Z_{opm} matching, we need to consider its sensitivity to small changes in receiver configuration for practical implementation.

C Capacity Sensitivity and Impedance Matching

The sensitivity of the matching network is important as it varies easily with the environment (temperature, humidity, etc.) besides the design accuracy. To evaluate the sensitivity reasonably, we define the performance efficiency of C_m with each single d

$$\eta_{C_m}|_{Z_L=Z_{L_0}} = \frac{C_m|_{Z_L=Z_{L_0}}}{\max(C_m|_{Z_L=Z_{L_0}})} = \frac{C_m|_{Z_L=Z_{L_0}}}{C_m|_{Z_L=Z_{opm}}} \quad (11)$$

$\eta_{c_{up}}$ is defined in the same way for C_{up} as well. Next, the precision error of the matching network is defined as

$$\Delta R = \frac{R_L - R_{opm}}{Z_0}, \Delta X = \frac{X_L - X_{opm}}{Z_0} \quad (12)$$

where $Z_0 = 50\Omega$ is the reference of calibration. It is obvious that Z_{opm} locates at the origin of the Cartesian coordinates under the definition of (12). Also, we assume that the matching networks of both receivers have the same precision error simultaneously. In Fig. 4 the smooth solid curve is the contour plot

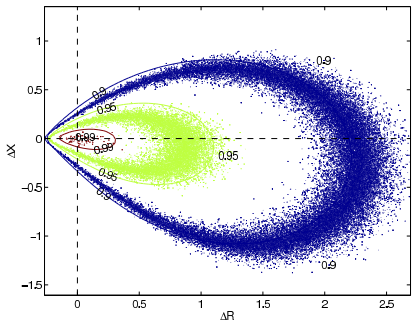

Figure 4: The capacity efficiency $\eta_{c_m}, \eta_{c_{up}} = 0.9, 0.95, 0.99$ as a function of $(\Delta R, \Delta X)$ with $d = 0.05\lambda$.

The 18th Annual IEEE International Symposium on Personal, Indoor and Mobile Radio Communications (PIMRC'07)

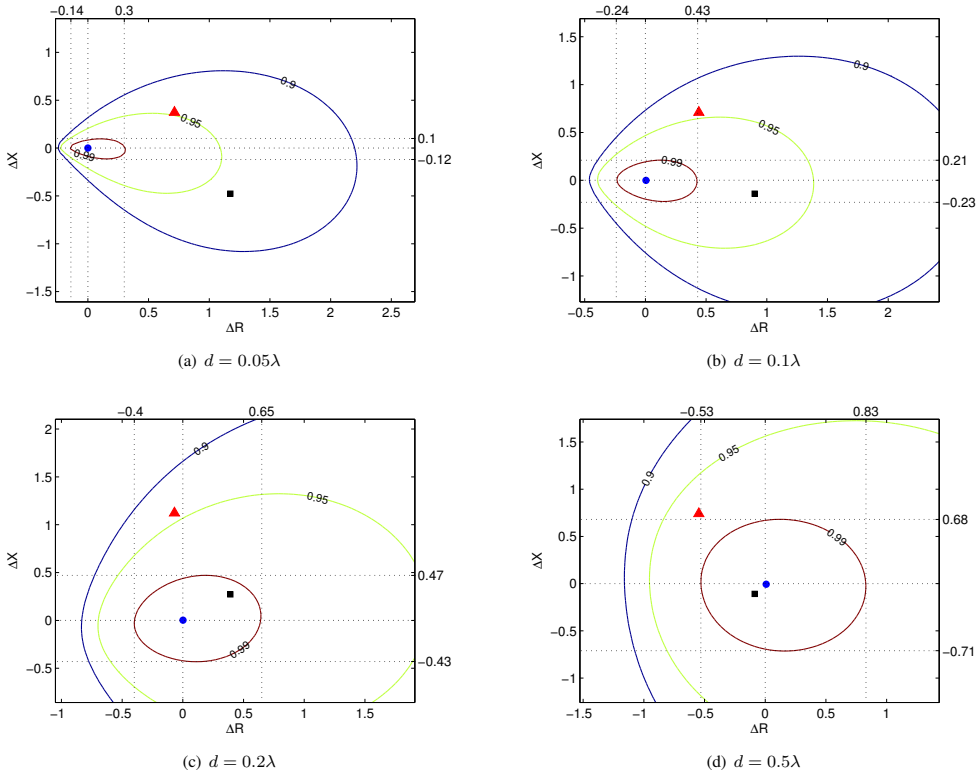

Figure 5: The upper bound capacity efficiency $\eta_{c_{up}} = 0.9, 0.95, 0.99$ as a function of $(\Delta R, \Delta X)$ with various d. Special impedances Z_{opm} (dots), Z_0 (triangles), and ${Z_{11}}^*$ (squares) are also marked in different cases.

of $\eta_{c_{up}}$, while the clusters of dots are the distribution of η_{C_m}. It is coarse because of the random channels to generate C_m. However, Fig. 4 also shows that

$$E\left\{(\Delta R, \Delta X)\right\}|_{\eta_{C_m}=\eta_0} \approx (\Delta R_0, \Delta X_0)|_{\eta_{C_{up}}=\eta_0} \qquad (13)$$

where $\eta_0 \in [0.9, 1]$. The scalars $\eta_{c_{up}}$ and η_{C_m} will be more similar with larger antenna spacing. Therefore, $\eta_{c_{up}}$ is generated for different d to estimate the capacity sensitivity, which avoids extensive simulations to evaluate η_{C_m}.

Fig. 5 give us a clear demonstration of the MIMO performance disturbance due to the optimal matching impedance deviation and its trend with increasing antenna spacing as well. For example, Fig. 5(a) tells us that the system has to sacrifice 1% performance degradation if the matching impedances in the system were offset from Z_{opm} with a maximal range of $\Delta R \in [-0.14, 0.3]$, $\Delta X \in [-0.12, 0.1]$. It also shows that both Z_0 and ${Z_{11}}^*$ matching can offer the capacity about 95% of the maximum at $d = 0.05\lambda$, which is consistent with in Fig. 3.

When d is fixed, the maximal range of ΔX is always smaller than the range of ΔR at $\eta_{C_{up}} = 0.99$, which indicates that the system's performance is more sensitive to the matching reactance variance X_L. When d is increasing, the maximal precision error area of 99% capacity efficiency gets larger, which is an encouraging phenomenon for the practical implementation. Meanwhile, the Z_{opm} point is approaching ${Z_{11}}^*$, which explains why the capacity of both matching systems converges in Fig. 3 with increasing antenna spacing. Generally, the MIMO system performance is not sensitive to Z_{opm} mismatch even at very small antenna spacings ($d = 0.05\lambda$), which makes single-port matching a promising approach to decouple the compact arrays.

D Capacity Sensitivity for Antenna Structure

Besides antenna spacing and matching networks, the accuracy of antenna structure is another factor which can affect the MIMO systems performance directly by changing the self and mutual impedances. The self and mutual impedances are simulated based in [19]. As in Fig. 6(a), with a very close antenna spacing, although Z_{opm} matching is better compared to other matching networks at half-wavelength ($l = 0.5\lambda$), its performance drops quickly if l is not precisely 0.5λ. The highest

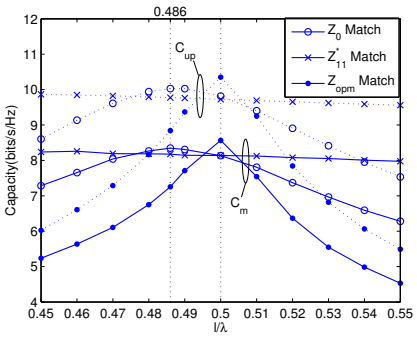

(a) $d = 0.05\lambda$

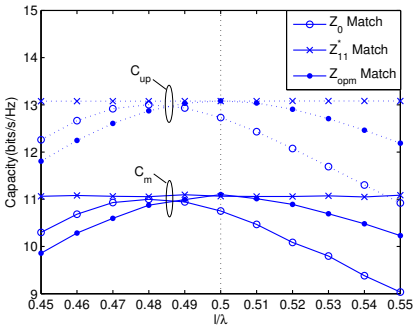

(b) $d = 0.5\lambda$

Figure 6: The mean capacity (dash line) and upper bound capacity (solid line) with various matching networks as a function of dipole lengths.

capacity of Z_0 matching is attained at $l = 0.486\lambda$, which is the first resonant length ($Z_{11} = R_{11}$) of a dipole antenna. ${Z_{11}}^*$ matching gives the most stable performance of the three methods. When d is increased to 0.5λ (Fig. 6(b)), Z_{opm} matching verses dipole length becomes flat, but the performance of ${Z_{11}}^*$ matching is catches up with Z_{opm} matching, and even surpasses Z_{opm} matching except for the $l = 0.5\lambda$ case. Therefore, ${Z_{11}}^*$ matching is the best matching network for large antenna spacings with imprecisely known dipole length.

IV Conclusion

The performance sensitivity of a 2×2 MIMO system with coupled half-wavelength dipoles and decoupling matching networks is presented in this paper. By utilizing the modified MIMO capacity and upper bound capacity including the mutual coupling and matching networks effect, the optimal single-port matching for various antenna spacing is found and it outperforms other matching networks for small antenna spacing ($d < 0.25\lambda$). When antenna spacing and dipole lengths are fixed, MIMO capacity is not sensitive to optimal impedance mismatch; when the optimal matching network is precise, the MIMO system is relatively sensitive to antenna structure mismatch. In general, optimal single-port matching is a feasible technique to improve the compact array performance.

References

[1] G. J. Foschini and M. J. Gans, "On limits of wireless communications in a fading environment when using multiple antennas," *Wireless Personal Communications*, vol. 6, pp. 311–335, Mar. 1998.

[2] I. E. Telatar, "Capacity of multi-antenna gaussian channels," *European Trans. Telecommun.*, vol. 10, pp. 585–595, 1999.

[3] P.-S. Kildal and K. Rosengren, "Electromagnetic analysis of effective and apparent diversity gain of two parallel dipoles," *IEEE Antennas Wireless Propagat. Lett.*, vol. 2, pp. 9–13, 2003.

[4] E. A. Mehmet Kemal Özdemir and H. Arslan, "Dynamics of spatial correlation and implications on MIMO systems," *IEEE Commun. Mag.*, pp. 514–519, 2004.

[5] T. Svantesson and A. Ranheim, "Mutual coupling effects on the capacity of multielement antenna systems," in *Proceedings of IEEE International Conference on Acoustics, Speech and Signal Processing (ICASSP'01)*, vol. 4, May 2001, pp. 2485–2488.

[6] V. Jungnickel, V. Pohl, and C. V. Helmolt, "Capacity of MIMO systems with closely spaced antennas," *IEEE Commun. Lett.*, vol. 7, no. 8, pp. 361–363, Aug. 2003.

[7] J. W. Wallace and M. A. Jensen, "Mutual coupling in MIMO wireless systems: a rigorous network theory analysis," *IEEE Trans. Wireless Commun.*, vol. 3, no. 4, pp. 1317–1325, 2004.

[8] B. K. Lau, S. M. S. Ow, G. Kristensson, and A. F. Molisch, "Capacity analysis for compact MIMO systems," in *Proceedings of IEEE 61st Vehicular Technology Conference (VTC'05-Spring)*, vol. 1, May- 2005, pp. 165–170.

[9] Y. Fei, B. K. Lau, A. Sunesson, A. J. Johansson, J. B. Andersen, and J. S. Thompson, "Experiments of closely coupled monopoles with load matching in a random field," in *Proceedings of 1st European Conference of Antenna and Propagation (EUCAP'06)*, Nov. 2006.

[10] J. B. Andersen and B. K. Lau, "On closely coupled dipoles in a random field," *IEEE Antennas Wireless Propagat. Lett.*, vol. 5, pp. 73–75, 2006.

[11] B. K. Lau and J. B. Andersen, "On closely coupled dipoles with load matching in a random field," in *Proceedings of IEEE 17th International Symposium on Personal, Indoor and Mobile Radio Communications (PIMRC'06)*, 2006.

[12] A. Paulraj, R. Nabar, and D. Gore, *Introduction to space-time wireless communications*, 1st ed. Cambridge, UK: Cambridge University, 2003.

[13] P. J. Smith, S. Roy, and M. Shafi, "Capacity of MIMO systems with semicorrelated flat fading," *IEEE Trans. Inform. Theory*, vol. 49, no. 10, pp. 2781–2788, Oct. 2003.

[14] J. Salz and J. H. Winters, "Effect of fading correlation on adaptive arrays in digital mobile radio," *IEEE Trans. Veh. Technol.*, vol. 43, no. 4, pp. 1049–1057, Nov. 1994.

[15] J. D. Kraus, *Antennas*, 2nd ed. New York: McGraw-Hill, 1988.

[16] C. A. Balanis, *Antenna theory*, 2nd ed., S. Elliot, Ed. USA: John Wiley & Sons, Inc, 1997.

[17] B. Clerckx, D. Vanhoenacker-Janvier, C. Oestges, and L. Vandendorpe, "Mutual coupling effects on the channel capacity and the space-time processing of MIMO communication systems," in *Proceedings of IEEE International Conference on Communications (ICC'03)*, vol. 4, May 2003, pp. 2638–2642.

[18] T. M. Cover and J. A. Thomas, *Elements of information theory*, 2nd ed. USA: Jonh Wiley & Sons, Inc., 2006.

[19] S. J. Orfanidis, *Electromagnetic waves and antennas*, USA, 2004. [Online]. Available: http://www.ece.rutgers.edu/˜orfanidi/ewa/

EXPERIMENTS OF CLOSELY COUPLED MONOPOLES WITH LOAD MATCHING IN A RANDOM FIELD

Yuanyuan Fei [1], Buon Kiong Lau [2], Anders Sunesson [3], Anders J Johansson [2], Jørgen Bach Andersen [4], and John S. Thompson [1]

[1] Institute for Digital Communications, Joint Research Institute for Signal & Image Processing, University of Edinburgh, UK. Email: y.fei@ed.ac.uk, john.thompson@ed.ac.uk

[2] Department of Electroscience, Lund University, Sweden. Email: bklau@ieee.org, anders.j.johansson@es.lth.se

[3] Perlos AB, Sweden, Email: anders.sunesson@perlos.com

[4] Department of Communications Technology, Aalborg University, Denmark. Email: jba@kom.aau.dk

ABSTRACT

Recent theoretical and simulation studies reveal that closely coupled antennas with appropriately chosen impedance matching loads can yield desired characteristics of small antenna correlation coefficients and/or high received power levels. However, no experiment has been performed to verify these claims. Here, we describe an experimental setup used to investigate the correlation and received power of closely coupled antennas with impedance matching. Specifically, a two-monopole array with a small antenna spacing 0.05 wavelength and five different matching networks are constructed and measured. Whereas our experimental results largely confirm theoretical predictions, some discrepancies due to simplifications made in the theoretical models are observed.

1. INTRODUCTION

Multiple-input multiple-output (MIMO) systems received worldwide attention in the past ten years due to their ability to significantly increase system efficiency by using multi-antennas at both ends of a wireless communication link [1]-[3]. Nevertheless, as early as in [3], it has already been mentioned the integration of MIMO technique into compact devices is restricted if the antenna spacing is below half a wavelength. This is because small antenna spacing leads to high antenna correlation and thus degradation in MIMO capacity. Moreover, strong mutual coupling (MC) between closely spaced antenna elements also results in changes in antenna patterns (thus antenna correlation) and loss of antenna efficiency [4].

Intuitively, MC is a detrimental ingredient to MIMO systems [5]. However, it is claimed in [6], [7] that MC can also be a positive factor to increase the MIMO performance under some circumstances. Recent studies [8]-[10] showed that correlation and capacity of coupled antennas can be greatly improved by introducing proper matching loads into the multiple antenna system. In [11] and [12], the relationship between various load impedances and received power/antenna correlation is carefully investigated but no measurement has been implemented to confirm the presented numerical results. On the other hand, while the S-parameters of a two-monopole array were measured and used in a related study [13], the matching networks were modeled numerically.

In this paper, a compact two- (quarter-wavelength $\lambda/4$) monopole array and five different matching networks are realized in order to experimentally verify the observed phenomena in [12]. Practical insights are presented on the role of impedance matching in the closely coupled antenna array. The paper is organized

The project is supported by VINNOVA (grant no. P24843-3), Scottish Funding Council for the Joint Research Institute with the Heriot-Watt University (a part of the Edinburgh Research Partnership), and partly conducted within the NEWCOM (Network of Excellence in Communications).

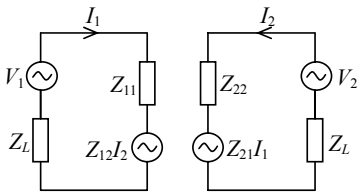

Figure 1. Equivalent circuit of two coupled antennas.

as follows. Section 2 provides the theoretical preliminaries. Section 3 focuses on the design of the overall experimental setup as well as the design of matching networks using transmission lines and open-circuit stubs. In Section 4, the simulation and experimental results are presented and discussed. Conclusions are given in Section 5.

2. THEORETICAL PRELIMINARIES

The analytical equivalent circuit for two coupled antennas is showed in Fig. 1. An identical (matching) load impedance Z_L is applied to both antennas. Z_{11}, Z_{22} and Z_{12}, Z_{21} are the self and mutual impedances of antenna 1 and 2, respectively. Meanwhile, V_1 and V_2 are open-circuit voltages as determined by the surrounding propagation environment, and they are correlated due to the small antenna spacing. Under the assumption of identical antennas, the theoretical expressions of mean received power and output correlation are derived in [12]. In practice, the relative mean received power of antenna 1 P_1 for a uniform 2D angular power spectrum (APS) can be defined by far-field antenna patterns as in Eq. 1

$$P_1 = \frac{P_{L1}}{P_0} = \frac{\int_0^{2\pi} \left|E_{L1}(\phi)\right|^2 d\phi}{\int_0^{2\pi} \left|E_0(\phi)\right|^2 d\phi}, \quad (1)$$

where P_{L1} is the power gathered by antenna 1 with load Z_L when antenna 2 is terminated with load Z_L, P_0 is the power received by a reference conjugate-matched single antenna, and $E_{L1}(\phi)$ and $E_0(\phi)$ represent the 2D far-field radiation patterns for the loaded and reference antenna cases, respectively. P_2 can be derived similarly. Eq. 2. gives the expression of the output correlation ρ, assuming uniform 2D APS where V_{L1} and V_{L2} are load voltages of antennas 1 and 2, respectively.

$$\rho = \frac{E\{V_{L1}V_{L2}^*\}}{E\{\left|V_{L1}\right|^2\}E\{\left|V_{L2}\right|^2\}} = \frac{\int_0^{2\pi} E_1(\phi)E_2^*(\phi)d\phi}{\sqrt{\int_0^{2\pi}\left|E_1(\phi)\right|^2 d\phi \int_0^{2\pi}\left|E_2(\phi)\right|^2 d\phi}}, \quad (2)$$

3. EXPERIMENTAL SETUP

3.1. System setup

The experimental setup is shown in Fig. 2. Two quarter-wavelength monopoles with antenna spacing of d = 0.05λ and 900MHz center frequency are mounted on a 330mm × 250mm ground plane. For convenience, the brass antennas of identical dimensions (thickness of 2mm) are directly soldered onto different matching network boards. The output ports are SMA connectors soldered onto the opposite end of the boards.

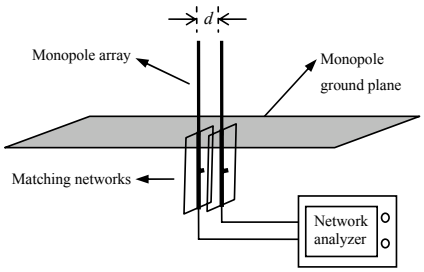

Figure 2. Experimental setup of two λ/4 monopoles mounted on a ground plane and connected to matching networks.

The self impedance of a single monopole and the self and mutual-impedances of the above monopole array are measured by a network analyzer. The network analyzer is also used for tuning the antennas with different matching boards. The 2D far-field radiation patterns of the monopole array for terminations with open-circuit and different matching networks are obtained from an anechoic chamber at Perlos AB, Sweden.

3.2. Matching network design

The design of matching networks is the vital step in the project. We apply the well established single-stub

matching technique in [14], [15]. For simplicity, the configuration of transmission line and parallel open-circuited stub based on a 50Ω transmission line is adopted.

Practically, the impedance matching networks are realized by making the appropriate microstrip transmission lines using double-side PCB boards. The width of the microstrip line is determined by the relative permittivity (ε_r) and the height (h) of the substrate layer, while the actual length design depends on the wavelength in the substrate dielectric $\lambda_e = \lambda_0/\sqrt{\varepsilon_e}$, where λ_0 is the wavelength in the free space and ε_e is defined as the effective permittivity of the dielectric interface, which can be deduced from ε_r and the width-to-height ratio w/h. A number of empirical formulas exist for w and ε_e, e.g. [14], [15], and we use those in [15].

4. MEASUREMENT AND SIMULATION RESULTS

The monopoles and ground plane are modeled in SEMCAD [16] using full-wave FDTD analysis. The impedance matrix and coupled radiation patterns are simulated for comparisons with the measurement.

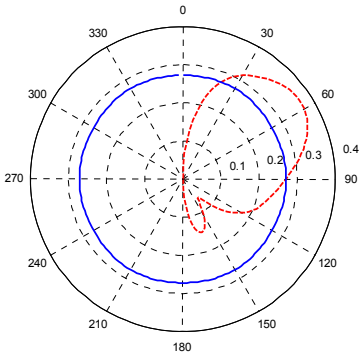

Figure 3. 2D far-field radiation patterns of single monopole. x-y plane(solid); y-z plane(dashed).

The single monopole antenna 2D far-field pattern cuts of *x-y* and *y-z* planes exported from SEMCAD are plotted in Fig. 3. As can be seen, the pattern of the azimuth plane (*x-y*) is almost omnidirectional, which agrees with analytical predictions. Referring to the elevation plane (*y-z*), an unexpected small backlobe appears under the ground plane. However, since only the pattern above the ground plane is important and the backlobe is relatively small, the backlobe has negligible impact on antenna performance. The simulated self-impedance of a single monopole Z_0 = 45.6 + j20.5 Ω agrees well with the measured impedance Z_0 = 45.5 + j19.22Ω.

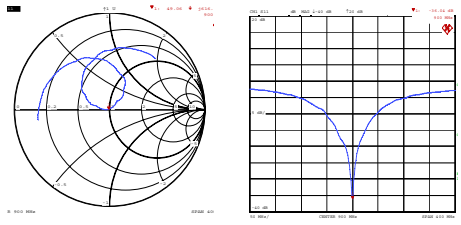

(a) (b)

Figure 4. (a). The matched impedance in Smith Chart (b). The return loss (S_{11}) of the matched monopole

To confirm the single-stub matching technique, conjugate matching for a single antenna has been attempted. From the impedance matching point of view, the input impedance of the matched antenna should be exactly 50Ω at 900MHz, i.e. the resonant frequency is tuned to 900MHz. Due to limitations in the accuracy of empirical formulas, the designed network has a resonant frequency of 897MHz. This can be easily rectified by a very small adjustment in the stub length. After a minor adjustment, the impedance (in Smith chart) and return loss read from the network analyzer are displayed in Figs. 4. In Fig. 4(b), the bandwidth is about 100MHz at -10dB return loss (or 11% fractional bandwidth).

The impedance matrix of the coupled antenna array is the most straightforward parameter to reflect the MC effect since the mutual-impedance is the outcome of the interaction between the antennas. As there are no analytical expressions for Z_{11} and Z_{12} of monopoles with finite/rectangular ground plane, both simulation and measurement results are generated. The simulated Z_{11} and Z_{12} are equal to 47.5 + j10.9Ω, 46.77 – j0.57Ω, while the measured average values are (Z_{11} + Z_{22}) /2 =

46.72 + *j*9.39Ω, $(Z_{12} + Z_{21})/2$ = 45.31 – *j*2.57Ω, since ideally $Z_{11} = Z_{22}$ and $Z_{21} = Z_{12}$ for the given setup.

Besides the impedance matrix, the open-circuit correlation (ρ_{oc}) is also required to obtain the received power and output correlation from load impedances [12]. Using the open-circuit patterns from SEMCAD and Eq. 2, we obtain ρ_{oc}= 0.9796. This is close to the theoretical value for uniform 2D APS (i.e. Clarkes' model) of $\rho_{oc} = J_0(kd) = 0.9755$, where $k = 2\pi/\lambda$. Experimentally, the 2D ρ_{oc} is a complex value of 0.9473 + *j*0.0033. The imaginary part of ρ_{oc} approaches zero if the phases of the radiation patterns of the coupled antennas are symmetric about array broadside. However, it is very difficult to achieve this exactly in practice. In the case of complex valued ρ_{oc}, the total mean received power of the array should be considered instead of the mean received power of either antenna 1 or 2 as they will differ [17]. Figs. 5 and 7 display the contour plot of the total received power and output correlation utilizing the measured antenna impedances and 2D ρ_{oc} (as in [12]). Corresponding results are plotted in Figs. 6 and 8, but with the SEMCAD simulated impedances and ρ_{oc} = 0.9796. The interesting 'two maxima' phenomenon of the received power and the concentric zero output correlation contours [12] are visible in both sets of figures.

To experimentally verify the received power and correlation results in these plots, five matching load impedances (A to E) were selected from Fig. 5 and 7 (the same points are also labeled in Figs 6 and 8). The expected values at these points, as extracted from Fig. 5-8, are summarized in Tab. 1 and Tab. 2. Results from measurements performed based on the actual imple-

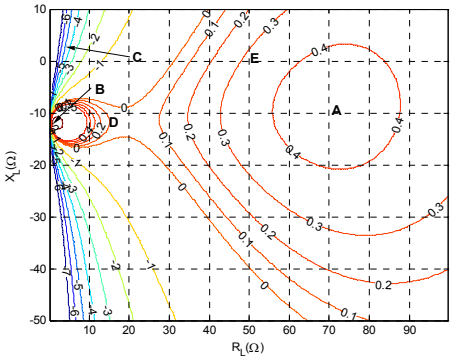

Figure 5. Numerical total power in dB as a function of Z_L with $d = 0.05\lambda$, $\rho_{oc} = 0.9473 + j0.0033$.

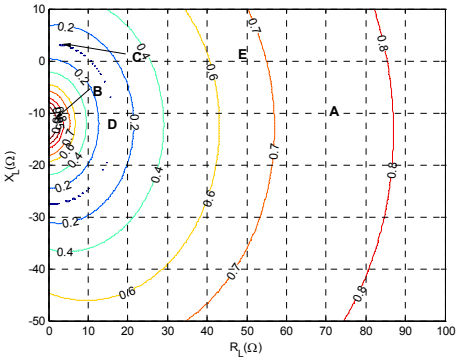

Figure 7. The output signal correlation as a function of Z_L $\rho_{oc} = 0.9473 + j0.0033$.

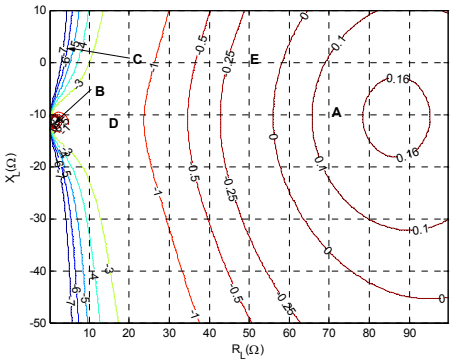

Figure 6. Numerical total power in dB vs. real and imaginary parts of Z_L with $d = 0.05\lambda$, $\rho_{oc} = 0.9796$.

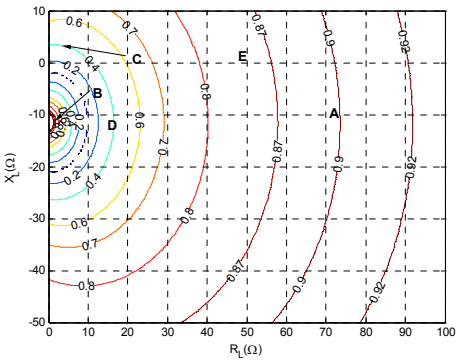

Figure 8. The output signal correlation vs. real and imaginary parts of Z_L $\rho_{oc} = 0.9796$.

mentations of the selected matching impedance loads are summarized in Tab. 3.

First, we note that points A and B are chosen close to the two maxima of total received power (Fig. 5); C and D are picked from the approximately zero correlation circle (where D has the highest received power along this circle and C has a low received power of -5dB) (Figs. 5 and 7); while E is the simple 50Ω load matching as a general case.

Comparing predicted results based on measured ρ_{oc} and antenna impedances (and ideal load impedances) in Tab. 1 against directly measured results in Tab. 3, it is apparent that the measured total powers of different matching impedances generally suffer a degradation of 0.8 ~ 2.4dB except at point **B** where the gap is as large as 5.5dB. Regarding the output correlations, they are 10% higher than in Tab. 1 for most cases: at point **B** 10% lower and point **C** 30% more.

On the other hand, comparing predicted results based on simulation in Tab. 2 against directly measured results in Tab. 3, we note that the measured results agree better with the simulated results in Tab. 2 than the corresponding results in Tab. 1, except for the correlation of point D.

Moreover, it is found that the values in Tab. 2 remain almost unchanged if the measured antenna impedances (and simulated ρ_{oc}) are used instead of the simulated impedances. Taking this into consideration, and noting the some results differ considerably between Tabs. 1 and 2, we deduce that both the received power and correlation of the compact antenna array are sensitive to ρ_{oc}. Thus, the accuracy in determining ρ_{oc} (from simulated and measured open-circuit patterns) can contribute significantly to the differences between Tabs. 1 to 3, as discussed above. However, as we have seen in Figs. 5 to 8 and Tabs. 1 to 3, the two performance metrics (especially the trend) are still in general agreement between the simulated and measured cases.

The additional power loss of the directly measured case (Tab. 3) as compared to the other cases (Tabs. 1 and 2) can be partially accounted for by ohmic losses in the antennas and the matching networks. The ohmic loss is particularly severe in the case of point **B** where the predicted supergain is eliminated by high current flow. Other reasons for the discrepancies between the results (in Tabs. 1 to 3) include: (1) the sensitivity of the location of the narrow supergain peak to ρ_{oc} (see Figs. 5

Table 1. Selected load impedance for measurement with numerical total received power and correlation

	Impedances(Ω)	P_{total} (dB)	Correlation
A	70.69 - *j*9	0.4340	0.7581
B	1.5 – *j*12.8	2.5591	0.9310
C	4.06 + *j*3	-5.0000	0.0052
D	16.5 – *j*12	0.0654	0.0105
E	50 + *j*0	0.3208	0.6717

Table 2. Selected load impedance for measurement with simulated total received power and correlation

	Impedances(Ω)	P_{total} (dB)	Correlation
A	70.69 - *j*9	0.1310	0.8960
B	1.5 – *j*12.8	-0.3479	0.8668
C	4.06 + *j*3	-6.5213	0.3923
D	16.5 – *j*12	-1.4224	0.4032
E	50 + *j*0	-0.1300	0.8525

Table3. Total received power and correlation data of various load impedances in experiment

	Impedances(Ω)	P_{total} (dB)	Correlation
A	70.69 - *j*9	-0.2870	0.8541
B	1.5 – *j*12.8	-3.9977	0.7910
C	4.06 + *j*3	-7.3498	0.3681
D	16.5 – *j*12	-1.7685	0.1674
E	50 + *j*0	-0.9154	0.7800

and 6); (2) the non-ideal implementation of the matching impedance loads (even though fine-tuning was performed); (3) the accuracy of the measured complex-valued radiation patterns.

Contrasting among points **A**-**E** in Tab. 1, high received power and correlation exist for both points **A** and **B**, while **C** has the lowest correlation but also the lowest received power (or efficiency). Only point **D** provides a low correlation and a relatively high received power simultaneously. Experimentally in Tab. 3 (and likewise through simulation in Tab. 2) it is confirmed that point **D** is the preferred matching point compared to points **B** and **C** which are located in the steep gradient region for the power in Fig. 5.

5. CONCLUSION

The relative total received power and output signal correlation have been investigated numerically and experimentally by constructing a highly compact (spaced by 0.05λ) two-element $\lambda/4$ monopole array with different matching terminations. We showed that, despite some discrepancies, the measured results are generally in agreement with previous numerical analyses. The study confirms that load values could be optimized to combat performance degradation due to MC in compact antenna arrays, which improves the feasibility of incorporating MIMO techniques into small platforms.

ACKNOWLEDGEMENTS

We thank Mr. Lars Hedenstjärna of the Department of Electroscience, Lund University for technical advice and clever constructions of the experimental hardware.

6. REFERENCES

[1] J. Winters, "On the Capacity of Radio Communication Systems with Diversity in a Rayleigh Fading Environment," *IEEE J. Select. Areas Commun.*, vol. 5, pp. 871-878, Jun. 1987.

[2] I. E. Telatar, "Capacity of multi-antenna Gaussian channels," *European Trans. Telecommun*., vol. 10, pp. 585-595, 1999.

[3] G. J. Foschini and M. J. Gans, "On limits of wireless communications in a fading environment when using multiple antennas," *Wireless Personal Commun.*, vol. 6, pp. 311-335, Mar. 1998.

[4] P. S. Kildal and K. Rosengren, "Electromagnetic analysis of effective and apparent diversity gain of two parallel dipoles," *IEEE Antennas and Wireless Propagat. Lett*. , vol. 2, no. 1, pp. 9-13, 2003.

[5] M. K. Ozdemir, E. Arvas, and H. Arslan, "Dynamics of spatial correlation and implications on MIMO systems," *IEEE Commun. Magazine*, vol. 42, no. 6, pp. S14-S19, Jun. 2004.

[6] T. Svantesson, and A. Tanheim, "Mutual coupling effects on the capacity of multielement antenna systems," in *Proc. IEEE International Conference on Acoustics, Speech, and Signal Processing* (ICASSP´2001), vol. 4, pp. 2485-2488, 7-11 May 2001.

[7] V. Jungnickel, V. Pohl, and C. von Helmolt, "Capacity of MIMO systems with closely spaced antennas," *IEEE Commun. Lett.*, vol. 7, no. 8, pp. 361-363, Aug. 2003.

[8] J. W. Wallace and M. A. Jensen, "Termination-dependent diversity performance of coupled antennas: network theory analysis," *IEEE Trans. Antennas Propag*., vol. 52, no. 1, pp. 98-105, Jan. 2004.

[9] ——, "Mutual coupling in MIMO wireless systems: A rigorous network theory analysis," *IEEE Trans. Wireless Commun*., vol. 3, no. 4, pp. 1317-1325, Jul. 2004.

[10] B. K. Lau, S. M. S. Ow, G. Kristensson, and A. F. Molisch, "Capacity analysis for compact MIMO systems," in *Proc. IEEE 61st VTC Spring*, vol. 1, pp. 165-170, 2 May-1 Jun. 2005.

[11] R. G. Vaughan and J. B. Andersen, "Antenna diversity in mobile communications," *IEEE Trans. Vehic. Technol*., vol. VT-36, no. 4, pp. 149-172, Nov. 1987.

[12] J. B. Andersen and B. K. Lau, "On closely coupled dipoles in a random field," *IEEE Antennas and Wireless Propag. Lett.*, vol. 5, no. 1, pp. 73-75, 2006.

[13] S. Dossche, J. Romeu and S. Blanch, "Matching network for a spatial diversity antenna system," in *Proc. IEEE Symp. Personal Indoor and Mobile Radio Communication* (PIMRC'2004), vol. 1, pp. 427-431, 5-8 Sep. 2004.

[14] D. M. Pozar, *Microwave Engineering*, John Wiley, 1998.

[15] S. J. Orfanidis, *Electromagnetic Waves and Antennas*, http://www.ece.rutgers.edu/~orfanidi/ewa, Jun. 2004.

[16] *SEMCAD*, http://www.semcad.com.

[17] B. K. Lau and J. B. Andersen, "On closely coupled dipoles with load matching in a random field," in *Proc. IEEE Symp. Personal Indoor and Mobile Radio Communication* (PIMRC'2006), in press.

References

[1] J. Winters, "On the capacity of radio communication systems with diversity in a rayleigh fading environment," *IEEE Journal on Selected Areas in Communications*, vol. 5, pp. 871–878, 1987.

[2] G. J. Foschini and M. J. Gans, "On limits of wireless communications in a fading environment when using multiple antennas," *Wireless Personal Communications*, vol. 6, pp. 311–335, Mar. 1998.

[3] I. E. Telatar, "Capacity of multi-antenna gaussian channels," *European Trans. Telecommun.*, vol. 10, pp. 585–595, 1999.

[4] D. Gesbert, M. Shafi, D. shan Shiu, P. J. Smith, and A. Naguib, "From theory to practice: an overview of MIMO space-time coded wireless systems," *IEEE Journal on Selected Areas in Communications*, vol. 21, no. 3, pp. 281–302, Apr. 2003.

[5] M. A. Jensen and J. W. Wallace, "A review of antennas and propagation for MIMO wireless communications," *IEEE Transactions on Antennas and Propagation*, vol. 52, no. 11, pp. 2810–2824, Nov. 2004.

[6] A. J. Paulraj, D. A. Gore, R. U. Nabar, and H. Bolcskei, "An overview of MIMO communications–a key to gigabit wireless," *Proceedings of the IEEE*, vol. 92, no. 2, pp. 198–218, Feb. 2004.

[7] C. A. Balanis, *Antenna theory analysis and design*, 2nd ed., S. Elliot, Ed. USA: John Wiley & Sons, Inc, 1997.

[8] W. L. Stutzman and G. A. Thiele, *Antenna theory and design*, 2nd ed. New York, USA: John Wiley & Sons, Inc., 1998.

[9] R. G. Vaughan and J. B. Andersen, "Antenna diversity in mobile communications," *IEEE Transactions on Vehicular Technology*, vol. VT-36, no. 4, pp. 149–172, Nov. 1987.

[10] T. Svantesson and A. Ranheim, "Mutual coupling effects on the capacity of multielement antenna systems," in *Proceedings of IEEE International Conference on Acoustics, Speech and Signal Processing (ICASSP'01)*, vol. 4, May 2001, pp. 2485–2488.

[11] J. W. Wallace and M. A. Jensen, "Termination-dependent diversity performance of coupled antennas: Network theory analysis," *IEEE Transactions on Antennas and Propagation*, vol. 52, no. 1, pp. 98–105, Jan. 2004.

[12] B. K. Lau, J. B. Andersen, G. Kristensson, and A. F. Molisch, "Antenna matching for capacity maximization in compact MIMO systems," in *Proceedings of 3rd International Symposium on Wireless Communications Systems (ISWCS)*, Valencia, Spain, Sept. 2006, (invited).

[13] R. Janaswamy, "Effect of element mutual coupling on the capacity of fixed length linear arrays," *IEEE Antennas and Wireless Propagation Letters*, vol. 1, pp. 157–160, 2002.

[14] N. Chiurtu, B. Rimoldi, E. Telatar, and V. Pauli, "Impact of correlation and coupling on the capacity of MIMO systems," in *Proceedings of 3rd IEEE International Symposium on Signal Processing and Information Technology (ISSPIT'03)*, Dec. 2003, pp. 154–157.

[15] B. Clerckx, D. Vanhoenacker-Janvier, C. Oestges, and L. Vandendorpe, "Mutual coupling effects on the channel capacity and the space-time processing of MIMO communication systems," in *Proceedings of IEEE International Conference on Communications (ICC'03)*, vol. 4, May 2003, pp. 2638–2642.

[16] V. Jungnickel, V. Pohl, and C. V. Helmolt, "Capacity of MIMO systems with closely spaced antennas," *IEEE Communications Letters*, vol. 7, no. 8, pp. 361–363, Aug. 2003.

[17] P. N. Fletcher, M. Dean, and A. R. Nix, "Mutual coupling in multi-element array antennas and its influence on MIMO channel capacity," *IEE Electronics Letters*, vol. 39, no. 4, pp. 342–344, Feb. 2003.

[18] J. W. Wallace and M. A. Jensen, "Mutual coupling in MIMO wireless systems: a rigorous network theory analysis," *IEEE Transactions on Wireless Communications*, vol. 3, no. 4, pp. 1317–1325, July 2004.

[19] C. Waldschmidt, S. Schulteis, and W. Wiesbeck, "Complete RF system model for analysis of compact MIMO arrays," *IEEE Transactions on Vehicular Technology*, vol. 53, no. 3, pp. 579–586, May 2004.

[20] M. K. Özdemir, E. Arvas, and H. Arslan, "Dynamics of spatail correlation and implications on MIMO systems," *IEEE Communications Magazine*, pp. 514–519, 2004.

[21] S. Wei, D. Goeckel, and R. Janaswamy, "On the asymptotic capacity of MIMO systems with antenna arrays of fixed length," *IEEE Transactions on Wireless Communications*, vol. 4, no. 4, pp. 1608–1621, 2005.

[22] J. B. Andersen and B. K. Lau, "On closely coupled dipoles in a random field," *IEEE Antennas and Wireless Propagation Letters*, vol. 5, pp. 73–75, 2006.

[23] B. K. Lau and J. B. Andersen, "On closely coupled dipoles with load matching in a random field," in *Proceedings of IEEE 17th International Symposium on Personal, Indoor and Mobile Radio Communications (PIMRC'06)*, 2006.

[24] Y. Fei and J. S. Thompson, "MIMO system sensitivity and coupled array design," in *Proceedings of IEEE 18th International Symposium on Personal, Indoor and Mobile Radio Communications (PIMRC'07)*, Sept. 2007.

[25] Y. Fei, B. K. Lau, A. Sunesson, A. J. Johansson, J. B. Andersen, and J. S. Thompson, "Experiments of closely coupled monopoles with load matching in a random field," in *Proceedings of 1st European Conference of Antenna and Propagation (EUCAP'06)*, Nice, France, Nov. 2006.

[26] M. L. Morris and M. A. Jensen, "Improved network analysis of coupled antenna diversity performance," *IEEE Transactions on Wireless Communications*, vol. 4, no. 4, pp. 1928–1934, 2005.

[27] ——, "Network model for MIMO systems with coupled antennas and noisy amplifiers," *IEEE Transactions on Antennas and Propagation*, vol. 53, no. 1, pp. 545–552, Jan. 2005.

[28] ——, "Impact of receive amplifier signal coupling on MIMO system performance," *IEEE Transactions on Vehicular Technology*, vol. 54, no. 5, pp. 1678–1683, Sept. 2005.

[29] B. K. Lau, S. M. S. Ow, G. Kristensson, and A. F. Molisch, "Capacity analysis for compact MIMO systems," in *Proceedings of IEEE 61st Vihecular Technology Conference (VTC'05-Spring)*, vol. 1, May- 2005, pp. 165–170.

[30] B. K. Lau, J. B. Andersen, G. Kristensson, and A. F. Molisch, "Impact of matching network on bandwidth of compact antenna arrays," *IEEE Transactions on Antennas and Propagation*, vol. 54, no. 11, pp. 3225 – 3238, Nov. 2006.

[31] W. C.-Y. Lee, "Effect of mutual coupling on a mobile-radio maximum ratio diversity combiner with a large number of branches," *IEEE Transactions on Communications*, pp. 1188–1193, Dec. 1972.

[32] Y. Fei and J. S. Thompson, "Continuous study of closely coupled dipoles with matching networks," in *Proceedings of 2nd European Conference of Antenna and Propagation (EUCAP'07)*, Edinburgh, UK, Nov. 2007.

[33] Y. Fei, Y. Fan, B. K. Lau, and J. S. Thompson, "Optimal single-port matching impedance for capacity maximization in compact MIMO arrays," *IEEE Transactions on Antennas and Propagation*, Oct. 2007.

[34] Y. Fei and J. S. Thompson, "The capacity of matched compact linear antenna arrays," in *Proceedings of 2nd European Conference of Antenna and Propagation (EUCAP'07)*, Edinburgh, UK, Nov. 2007.

[35] ——, "Optimal single-port impedance matching for compact MIMO arrays," in *Proceedings of 50th IEEE Global Telecommunications Conference (GLOBECOM'07)*, Washington D.C., USA, Nov. 2007.

[36] ——, *4G Mobile & Wireless Communications Technologies*. River Publishers, Nov. 2007, ch. Design of Compact Antenna Arrays for MIMO Wireless Communications.

[37] D. Tse and P. Viswanath, *Foundamentals of wireless communications*. USA, New York: Cambridge University Press, 2005.

[38] A. Goldsmith, *Wireless communications*. Cambridge: Cambridge University Press, 2005.

[39] T. S. Rappaport, *Wireless communications: principles and practice*. Upper Saddle River, NJ: Prentice Hall PTR, 1996.

[40] A. Paulraj, R. Nabar, and D. Gore, *Introduction to space-time wireless communications*, 1st ed. Cambridge, UK: Cambridge University Press, 2003.

[41] B. Sklar, "Rayleigh fading channels in mobile digital communication systems part 1: Characterization," *IEEE Communications Magazine*, pp. 136–146, Sept. 1997.

[42] W. C. Jakes, *Microwave Mobile Communications*. New Jersey, USA: IEEE Press, 1974.

[43] S. R. Saunders, *Antennas and propagation for wireless communication systems*. University of Surrey, Guildford, UK: John Wiley & Sons, Inc., Dec. 1999.

[44] C. Oestges and A. J. Paulraj, "Beneficial impact of channel correlations on MIMO capacity," *IEE Electronics Letters*, vol. 40, no. 10, May 2004.

[45] D.-S. Shiu, G. J. Foschini, M. J. Gans, and J. M. Kahn, "Fading correlation and its effect on the capacity of multielement antenna systems," *IEEE Transactions on Communications*, vol. 48, no. 3, pp. 502–513, Mar. 2000.

[46] C.-N. Chuah, D. N. C. Tse, J. M. Kahn, and R. A. Valenzuela, "Capacity scaling in MIMO wireless systems under correlated fading," *IEEE Transactions on Information Theory*, vol. 48, no. 3, pp. 637–650, Mar. 2002.

[47] W. Weichselberger, M. Herdin, H. Özcelik, and E. Bonek, "A stochastic MIMO channel model with joint correlation of both link ends," *IEEE Transactions on Wireless Communications*, vol. 5, no. 1, pp. 90–100, Jan. 2006.

[48] J. P. Kermoal, L. Schumacher, K. I. Pedersen, P. E. Mogensen, and F. Frederiksen, "A stochastic MIMO radio channel model with experimental validation," *IEEE Journal on Selected Areas in Communications*, vol. 20, no. 6, pp. 1211–1226, Aug. 2002.

[49] H. Özcelik, M. Herdin, W. Weichselberger, J. Wallace, and E. Bonek, "Deficiencies of the kronecker MIMO radio channel model," *Electronic Letters*, vol. 39, pp. 1209–1210, Aug. 2003.

[50] K. Yu, M. Bengtsson, B. Ottersten, D. McNamara, P. Karlsson, and M. Beach, "A wideband statistical model for NLOS indoor MIMO channels," in *Proceedings of IEEE 55th Vihecular Technology Conference (VTC'02-Spring)*, vol. 1, Birmingham, AL, May 2002, pp. 370–374.

[51] T. M. Cover and J. A. Thomas, *Elements of information theory*, 2nd ed. USA: Jonh Wiley & Sons, Inc., 2006.

[52] R. A. Horn and C. R. Johnson, *Matrix analysis*. USA: Cambridge University Press, 1999.

[53] G. Raleigh and J. M. Cioffi, "Spatial-temporal coding for wireless communications," *IEEE Transactions on Communications*, vol. 46, pp. 357–366, 1998.

[54] P. J. Smith and M. Shafi, "On a gaussian approximation to the capacity of wireless MIMO systems," in *Proceedings of IEEE International Conference on Communications (ICC'02)*, 2002, pp. 406–410.

[55] *IEEE Standard Definitions of Terms for Antennas*, IEEE Std 154-183, 1983.

[56] J. D. Kraus, *Antennas*, 2nd ed. New York: McGraw-Hill, 1988.

[57] T. Svantesson, M. A. Jensen, and J. W. Wallace, "Analysis of electromagnetic field polarizations in multi-antenna systems," *IEEE Transactions on Wireless Communications*, vol. 3, Mar. 2004.

[58] R. U. Nabar, H. Bölcskei, V. Erceg, D. Gesbert, and A. J. Paulraj, "Performance of multiantenna signal techniques in the presence of polarization diversity," *IEEE Transactions on Signal Processing*, vol. 50, no. 10, pp. 2553–2562, Oct. 2002.

[59] K. Rosengren, "Characterization of terminal antennas for diversity and MIMO systems by theory, simulations and measurements in reverberation chamber," Ph.D. dissertation, Chalmers University of Technology, Göteborg, Sweden, 2005.

[60] S. M. S. Ow, "Impact of mutual coupling on compact MIMO systems," Master's thesis, Lund University, Lund, Sweden, Mar. 2005.

[61] S. J. Orfanidis, *Electromagnetic waves and antennas*, USA, 2004. [Online]. Available: http://www.ece.rutgers.edu/ orfanidi/ewa/

[62] M. Abramowitz and I. A. Stegun, *Handbook of Mathematical Functions: with formulas, graphs and mathematical tables*. New York: Dover Publications, 1973.

[63] X. Li and Z.-P. Nie, "Mutual coupling effects on the performance of MIMO wireless channels," *IEEE Antennas and Wireless Propagation Letters*, vol. 3, pp. 344–347, 2004.

[64] I. J. Gupta and A. A. Ksienski, "Effect of mutual coupling on the performance of adaptive arrays," *IEEE Transactions on Antennas and Propagation*, vol. AP-31, no. 5, pp. 785–791, Sept. 1983.

[65] *FEKO*. [Online]. Available: http://www.feko.info/

[66] *Sonnet Lite*. [Online]. Available: http://www.sonnetusa.com/products/lite/

[67] *SEMCAD*. [Online]. Available: http://www.semcad.com

[68] D. M. Pozar, *Microwave engineering*, 2nd ed., C. Robey, Ed. USA: John Wiley & Sons, Inc, 1998.

[69] R. G. Vaughan and N. L. Scott, "Closely spaced monopoles for mobile communications," *Radio Science*, vol. 28, pp. 1259–1266, Nov.-Dec. 1993.

[70] O. Nørklit, P. D. Teal, and R. G. Vaughan, "Measurement and evaluation of multiantenna handsets in indoor mobile communication," *IEEE Transactions on Antennas and Propagation*, vol. 49, pp. 429–437, Mar. 2001.

[71] C. Waldschmidt, J. V. Hagen, and W. Wiesbeck, "Influence and modeling of mutual coupling in MIMO and diversity systems," in *Proceedings of IEEE Antennas and Propagation Society International Symposium*, vol. 3, San Antonio, TX, 2002, pp. 190–193.

[72] A. Forenza, D. J. Love, and R. W. H. Jr., "Simplified spatial correlation models for clustered MIMO channels with different array configurations," *IEEE Transactions on Vehicular Technology*, 2007, to appear.

[73] T. Kurner, D. J. Cichon, and W. Wiesbeck, "Concepts and results for 3D digital terrain-based wave propagation models: An overview," *IEEE Journal on Selected Areas in Communications*, vol. 11, no. 11, pp. 1002–1012, Sept. 1993.

[74] S. Y. Seidel and T. S. Rappaport, "Site-specific propagation prediction for wireless in-building personal communication system design," in *Proceedings of IEEE 40nd Vihecular Technology Conference (VTC'94-Spring)*, vol. 43, 1994, pp. 879–891.

[75] G. E. Athanasiadou, A. R. Nix, and J. P. McGeehan, "A microcellular ray-tracing propagation model and evaluation of its narrow-band and wide-band predictions," *IEEE Journal on Selected Areas in Communications*, vol. 18, pp. 322–335, Mar. 2000.

[76] M. Stege, J. Jelitto, M. Bronzel, and G. Fettweis, "A multiple input-multiple output channel model for simulation of tx- and rx-diversity wireless systems," in *Proceedings of IEEE 52nd Vihecular Technology Conference (VTC'00-Fall)*, vol. 2, Sept. 2000, pp. 833–839.

[77] A. F. Molisch, "A generic model for MIMO wireless propagation channels in macro- and micorcells," *IEEE Transactions on Signal Processing*, vol. 52, pp. 61–71, Jan. 2004.

[78] K. Yu, "Multiple-input multiple-output radio propagation channels: characteristics and models," Ph.D. dissertation, Signal Sensor and Systems, KTH, Sweden, 2005.

[79] P.-S. Kildal and K. Rosengren, "Electromagnetic analysis of effective and apparent diversity gain of two parallel dipoles," *IEEE Antennas and Wireless Propagation Letters*, vol. 2, pp. 9–13, 2003.

[80] L. M. Correia, *Wireless flexible personalised communications: COST 259, European co-operation in mobile radio research*. Chichester, UK: John Wiley & Sons, Inc, 2001.

[81] A. Derneryd and G. Kristensson, "Signal correlation including antenna coupling," *IEE Electronics Letters*, vol. 40, no. 3, pp. 157–159, Feb. 2004.

[82] J. Salz and J. H. Winters, "Effect of fading correlation on adaptive arrays in digital mobile radio," *IEEE Transactions on Vehicular Technology*, vol. 43, no. 4, pp. 1049–1057, Nov. 1994.

[83] M. T. Feeney and J. D. Parsons, "Cross-correlation between 900 mhz signal received on vertically separated antennas in small-cell radio systems," *IEE Proceedings I*, vol. 138, no. 2, pp. 81–86, Apr. 1991.

[84] K. I. Pedersen, P. E. Mogensen, and B. H. Fleury, "A stochastic model of the temporal and azimuthal dispersion seen at the base station in outdoor propagation environments," *IEEE Transactions on Vehicular Technology*, vol. 49, no. 2, pp. 437–447, Mar. 2000.

[85] Q. H. Spencer, B. D. Jeffs, M. A. Jensen, and A. L. Swindlehurst, "Modeling the statistical time and angle of arrival characteristics of an indoor multipath channel," *IEEE Journal on Selected Areas in Communications*, vol. 18, no. 3, pp. 347–360, Mar. 2000.

[86] G. German, Q. Spencer, L. Swindlehust, and R. Valenzuela, "Wireless indoor channel modeling: statistical agreement of ray tracing simulations and channel sounding measurements," in *Proceedings of IEEE International Conference on Acoustics, Speech and Signal Processing (ICASSP'01)*, vol. 4, May 2001, pp. 2501–2504.

[87] A. S. Y. Poon and M. Ho, "Indoor multiple-antenna channel characterization from 2 to 8 ghz," *Proceedings of IEEE International Conference on Communications (ICC'03)*, vol. 5, pp. 3519–3523, May 2003.

[88] L. Schumacher, J. P. Kermoal, F. Frederiksen, K. I. Pedersen, A. Algans, and P. E. Mogensen, "MIMO channel characterisation," IST METRA, Aalborg, Denmark, IST-1999-11719/AAU-WP2-D2-V1.1, Feb. 2001.

[89] G. T. S. Group, "Spatial channel model, SCM-134 text V6.0," Spatial Channel Model AHG (Combined ad-hoc from 3GPP and 3GPP2), Tech. Rep., Apr. 2003.

[90] V. Erceg et al., "TGn channel models," IEEE 8.02.11-03/940r4, Tech. Rep., May 2004.

[91] L. Schumacher, K. I. Pedersen, and P. Mogensen, "From antenna spacings to theoretical capacities - guidelines for simulating MIMO systems," in *Proceedings of IEEE 17th International Symposium on Personal, Indoor and Mobile Radio Communications (PIMRC'02)*, 2002.

[92] H. J. Chaloupka and X. Wang, "On the properties of small arrays with closely spaced antenna elements," in *Proceedings of IEEE Antennas and Propagation Sociery International Symposium*, vol. 3, June 2004, pp. 2699–2702.

[93] S. Dossche, S. Blanch, and J. Romeu, "Optimum antenna matching to minimise signal correlation on a two-port antenna diversity system," *IEE Electronics Letters*, vol. 40, no. 19, pp. 1164–1165, Sept. 2004.

[94] W. C. Y. Lee, "Mutual coupling effect on maximum-ratio diversity combiners and application to mobile radio," *IEEE Transactions on Communication Technology*, vol. Com-18, no. 6, pp. 779–791, Dec. 1970.

[95] P.-S. Kildal, K. Rosengren, J. Byun, and J. Lee, "Definition of effective diverstiy gain and how to measure it in a reverberation chamber," *Microwave and Optical Technology Letters*, vol. 34, no. 1, pp. 56–59, 2002.

[96] *Maple*. [Online]. Available: http://www.maplesoft.com

[97] R. P. Haviland, "Supergain antennas: possibilities and problems," *IEEE Antennas and Propagation Magazine*, vol. 37, pp. 13–26, Aug. 1995.

[98] M. L. Morris, M. A. Jensen, and J. Wallace, "Superdirectivity in mimo systems," *IEEE Transactions on Antennas and Propagation*, vol. 53, pp. 2850–2857, 2005.

[99] J. W. Wallace and M. A. Jensen, "The capacity of MIMO wireless systems with mutual coupling," in *Proceedings of IEEE 56th Vihecular Technology Conference (VTC'02-Fall)*, vol. 2, Sept. 2002, pp. 696–700.

[100] B. Lindmark, "Capacity of a 2 x 2 MIMO antenna system with mutual coupling losses," in *Proceedings of IEEE Antennas and Propagation Society International Symposium*, vol. 2, 2004, pp. 1720–1723.

[101] K. Rosengren, J. Carlsson, and P.-S. Kildal, "Maximizing the effective diverstiy gain of two parallel dipoles by optimizing the source impedances," *Microwave and Optical Technology Letters*, vol. 48, no. 3, pp. 532–535, Mar. 2006.

[102] P.-S. Kildal and K. Rosengren, "Correlation and capacity of MIMO systems and mutual coupling, radiation efficiency, and diversity gain of their antennas- simulations and measurements in a reverberation chamber," *IEEE Communications Magazine*, vol. 42, pp. 104–112, Dec. 2004.

[103] S. Dossche, J. Romeu, and S. Blanch, "Matching network for a spatial diversity antenna system," in *Proceedings of IEEE 15th International Symposium on Personal, Indoor and Mobile Radio Communications (PIMRC'04)*, vol. 1, Sept. 2004, pp. 427–431.

[104] Y. Fan and J. S. Thompson, "MIMO configurations for relay channels: Theory and practice," *IEEE Transactions on Wireless Communications*, vol. 6, no. 5, pp. 1774–1786, Mar. 2007.

[105] S. Loyka and G. Tsoulos, "Estimating MIMO system performance using the correlation matrix approach," *IEEE Communications Letters*, vol. 6, no. 1, pp. 19–21, Jan. 2002.

[106] R. M. Gray, *Toeplitz and Circulant Matrices: A review*. USA: Now Publishers, Feb. 2006.

[107] I. Kneppo and J. Fabian, *Microwave Integrated Circuits*. Springer, 1994.

[108] J. B. Fraleigh, *A First Course in Abstract Algebra*, 5th ed. Addison-Wesley, 1994.

[109] *Matlab 7 Getting Started Guide*. [Online]. Available: http://www.mathworks.com/